UNIVERSIDAD AUTÓNOMA DE MADRID

FACULTAD DE CIENCIAS

DEPARTAMENTO DE BIOLOGÍA

DEEP REFACTORING OF CENTRAL CARBON METABOLISM IN THE SOIL BACTERIUM *PSEUDOMONAS PUTIDA*

TESIS DOCTORAL

Memoria presentada para optar al título de Doctor en Microbiología

Alberto Sánchez-Pascuala Jerez

DIRECTORES DE TESIS

Dr. Víctor de Lorenzo Prieto

Dr. Pablo Iván Nikel

Consejo Superior de Investigaciones Científicas (CSIC)

Centro Nacional de Biotecnología (CNB)

Madrid, 2017

Víctor de Lorenzo Prieto, Profesor de Investigación del Consejo Superior de Investigaciones Científicas en el Centro Nacional de Biotecnología (CNB-CSIC) de Madrid (España) y

Pablo Iván Nikel, Investigador Senior de Novo Nordisk Foundation Center for Biosustainability (DTU BIOSUSTAIN) de Copenhague (Dinamarca),

CERTIFICAN que

Don Alberto Sánchez-Pascuala Jerez, Licenciado en Biología por la Universidad de Alcalá (Madrid), ha realizado bajo su dirección el trabajo de investigación titulado:

"DEEP REFACTORING OF CENTRAL CARBON METABOLISM IN THE SOIL BACTERIUM *PSEUDOMONAS PUTIDA*"

y consideran que el trabajo realizado reúne todas las condiciones requeridas por la legislación vigente, así como la originalidad y calidad científica necesarias, para poder ser presentado y defendido con el fin de optar al grado de Doctor por la Universidad Autónoma de Madrid.

Y para que así conste y surta los efectos oportunos, firman el presente certificado en Madrid a 1 de junio de 2017.

Firman Directores de la Tesis Doctoral:

Dr. Víctor de Lorenzo Prieto
Prof. de Investigación del CSIC

Dr. Pablo Iván Nikel
Inv. Senior DTU BIOSUSTAIN

To my guiding stars… My aunt Maribel, and grandparents Simo and Maxi.
We have not been able to share this way, but I know that you are always with me.

A las estrellas que me guían… Mi tía Maribel, y mis abuelos Simo y Maxi.
No hemos podido compartir este camino, pero siempre estaréis a mi lado.

ACKNOWLEDGMENTS

This work would not have been possible without the support of many people.

I would like to express my sincere gratitude and admiration to my advisor, Prof. Víctor de Lorenzo. Since I arrived to your laboratory, you have taught me the importance to carry out excellent science with ethic, passion and humility. At the same time, your personal and professional qualities transform the daily life in the laboratory in a wonderful experience. I will take your research lessons as an inspiration to conduct my future path. *¡Muchas gracias por darme la oportunidad de disfrutar de esta experiencia!*

I cannot forget the full support provided by my co-advisor, Dr. Pablo Iván Nikel. Your help during the creation of this Thesis has been crucial for its achievement. Your scientific and personal support have made the present manuscript possible, and at the same time, you have taught me all the necessary elements to face the future with confidence. You are a model to follow and encourage others to make science of quality. *¡Eternamente agradecido por todo Doc!*

Thanks to Rafael Rivilla for being my tutor and helping me with all the bureaucratic problems. I have particularly appreciated the moments in which we forgot the paperwork and discussed about science. You should be proud of the wonderful educational work developed in your Master and PhD program. *¡Gracias!*

Thanks to Tobias Fuhrer at IMSB (ETH, Zürich) to make possible the ^{13}C-based fluxomic analyses displayed in this Thesis.

Thanks to Stefano Donati to provide the necessary knowledge in order to work with Flux Balance Analysis (FBA). You are an excellence person and you will be an excellent scientist.

Thanks to my ex-labmates Chu, Ilaria, Aleyo and Ángel. I started my science adventure with your help and finished it with an amazing friendship!

I am eternally grateful for the support and good times provided for the people that comprise the laboratory:
A Sofía tengo que agradecerle gran parte del profesional que soy ahora. Desde el momento que llegué al laboratorio no he parado de aprender, y estaré siempre orgulloso de poder transmitir a quien me sea posible todo lo básico para ser un buen microbiólogo. ¡Gracias por tantos cafés y buenos momentos amiga!
A Belén, mi eterna compañera de pasillo, le debo mucho del conocimiento que ahora tengo sobre Biología Molecular (enzimas, polimerasas, …). ¡Muchas gracias por todo!
A Ángeles, mi compañera de poyata, un placer haber compartido estos años las penas predoctorales. ¡Tu tesis será genial!

A Elena, gracias por toda la ayuda prestada en este poco tiempo. Serás una gran científica, pero ya eres una gran persona.

A mis queridísimos compañeros de café, Esteban y Tomás. Sois unos grandes profesionales y unas grandísimas personas. Gracias por todas las conversaciones compartidas. ¡De mayor quiero ser como vosotros!

A David, muchas gracias por esas charlas "gamers" y no. Siempre pensaré que eres un cerebro y una buenísima persona.

A Yamal, mi compañero en el mundo de las carreras, gracias por siempre llevar puesta una sonrisa y compartir toda tu energía con los demás. ¡Trabajar contigo es un placer!

To Pavel and Huseyin, thanks a lot for your help in the laboratory. The chance to share the time with people from other country enrich the mind, and for sure, help me to write this enormous Thesis in English. *¡Gracias chicos!*

A Inés, muchísimas gracias por la ayuda administrativa. En ocasiones la burocracia es más compleja que la ciencia y siempre has podido solventar cualquier situación. Junto a ello, siempre has sabido escuchar cualquier penuria y tener unas palabras de ayuda. ¡Muchas gracias!

A toda la gente que compone la familia del CNB: Carol, Santa, Lola, Inés, Ramón, Dani… Hacéis que ir a trabajar diariamente sea un placer. ¡Gracias a todos!

A "los de la Uni": Peli, Vir, Jesús, Majalí, Pablo, Rubén y Patri. Vuestra amistad es tan importante como el título que conseguimos en la universidad. Siempre habéis sabido añadir una nota de felicidad a mi vida. ¡Gracias por vuestra amistad!

A mis "cuñados" favoritos (y únicos) Carmen y Javi. Hemos generado una pequeña familia maravillosa. El apoyo que nos hemos dado diariamente me ha permitido llegar a donde estoy. ¡Gracias por esas pizzas y sushis!

A mis "suegros" Carmen y Agustín, gracias por todos los buenos momentos vividos. Junto a ello, mi más eterna gratitud por haber traído al mundo a la persona que me hace ser feliz todos los días. ¡Gracias!

A los "del barrio": Alex, Carlos, Pablo, Víctor, Luis, Sergi y Jesús. Es una fortuna poder seguir contando con vuestra amistad después de tantos años. Siempre estáis cuando se os necesita, y hacéis revivir los maravillosos momentos que hemos vivido desde que íbamos al colegio. ¡Gracias amigos!

A Sergio (mi sensei), el cual me ha demostrado que cuidar tu cuerpo es tan importante como tu mente. Eres un ejemplo de superación a la hora de afrontar las dificultades que plantea la vida. ¡Gracias!

A Alfredo, toda mi gratitud y cariño. Eres un ejemplo a seguir en lo profesional y lo personal. ¡Gracias por todos los consejos que me has dado!

A mi tío Santi, una de las personas más inteligentes e íntegras que conozco. Siempre orgulloso de oír en ocasiones la frase: "como te pareces a tu tío".

A mis padres, Conchi y José. Es imposible recoger en estas líneas el amor y admiración que siento por vosotros. Soy lo que soy gracias a vuestra ayuda y cada día que pasa no hago más que agradecer la fantástica familia que me ha tocado disfrutar. ¡Gracias padres!

A mi pareja, compañera, amiga, … María. La presente Tesis es en gran parte tuya, el apoyo que me has ofrecido desde que nos conocemos me ha hecho alcanzar todas las metas marcadas. Te admiro y quiero a partes iguales. ¡Gracias por compartir la maravillosa persona que eres conmigo!

GENERAL INDEX

INDEX OF FIGURES

INDEX OF TABLES

ABBREVIATIONS

2-KG	2-Ketoglutarate
2-OX	2-Oxoglutarate
2K6PG	2-Ketogluconate-6-*P*
2KG	2-Ketogluconate
2PG	Glycerate-2-*P*
3-*m*B	3-Methylbenzoate
3PG	Glycerate-3-*P*
6PG	6-Phosphogluconate
A	Absorbance
ABC	ATP-binding cassette
Acetyl-CoA	Acetyl-coenzyme A
Ap	Ampicillin
ATP	Adenosine triphosphate
BPG	Glycerate-1,3-P_2
CDS	Coding sequences
CDW	Cell dry weight
Cm	Chloramphenicol
DCPIP	Dichlorophenolindophenol
DHAP	Dihydroxyacetone-*P*
DNA	Deoxyribonucleic acid
ED pathway	Entner-Doudoroff pathway
Eda	2-Keto-3-deoxy-6-phosphogluconate aldolase
Edd	6-Phosphogluconate dehydratase
EMP pathway	Embden-Meyerhof-Parnas pathway
EPS	Extracellular polymeric substances
F6P	Fructose-6-*P*
FAD	Flavin adenine dinucleotide
FBA	Flux balance analysis
FBP	Fructose-1,6-P_2
Fbp	Fructose-1,6-bisphospatase
Fda	Fructose-1,6-P_2 aldolase
G6P	Glucose-6-*P*
GA3P	Glyceraldehyde-3-*P*
Gad	Gluconate 2-dehydrogenase
Gap	GA3P dehydrogenase
GC-MS	Gas chromatography coupled to mass spectrometry
Gcd	Glucose dehydrogenase
Glk	Glucokinase
Gm	Gentamicin
GntZ	6-Phosphogluconate dehydrogenase
GnuK	Gluconate kinase
GRAS	Generally recognized as safe
HPLC	High-performance liquid chromatography
IM	Inner membrane
IPTG	Isopropyl-1-thio-β-galactopyranoside

kb	1,000 base pairs
KDPG	2-Keto-3-deoxy-6-phosphogluconate
Km	Kanamycin
LB	Lysogeny Broth (Luria-Bertani) medium
LC-MS	Liquid chromatography coupled to mass spectrometry
NAD^+	Nicotinamide adenine dinucleotide
NADH	Nicotinamide adenine dinucleotide reduced form
$NADP^+$	Nicotinamide adenine dinucleotide phosphate
NADPH	Nicotinamide adenine dinucleotide phosphate reduced form
OAA	Oxaloacetate
OD	Optical density
OM	Outer membrane
ORF	Open reading frame
PCR	Polymerase chain reaction
PEP	Phosphoenolpyruvate
Pfk	6-Phosphofructo-1-kinase
Pgi	Glucose-6-*P* isomerase
Pgl	6-Phosphogluconolactonase
PHB	Poly(3-hydroxybutyrate)
PP pathway	Pentose phosphate pathway
PQQ	Pyrroloquinoline quinone
PS	Periplasmic space
PTS	Phosphoenolpyruvate (PEP):carbohydrate phosphotransferase system
PtxD	2-Ketogluconate-6-*P*
Pyk	Pyruvate kinases
Pyr	Pyruvate
R5P	Ribose-5-*P*
RBS	Ribosome binding site
Ri5P	Ribulose-5-*P*
RNA	Ribonucleic acid
S7P	Sedoheptulose-7-*P*
Sm	Streptomycin
Tc	Tetracyclin
TCA cycle	Tricarboxylic acid cycle
Tpi	Triose-*P* isomerase
WT	Wild-type
X5P	Xylulose-5-*P*
Zwf	Glucose-6-*P* 1-dehydrogenase

ABSTRACT

Pseudomonas putida KT2440 is currently one of the most appealing microorganisms to be used as a cell platform in biotechnological applications. Its high metabolic versatility, increased resistance to oxidative stress, and amenability to genetic manipulations, are some of the main reasons for which *P. putida* is gaining attention as a *chassis* for bioproduction. This soil bacterium displays an atypical structure in its very central carbon metabolism when growing on glucose as the carbon source, in which the supply of reducing power (*i.e.*, NADPH) prevails over the formation of ATP. Strain KT2440 operates a glycolytic cycle based on the Entner-Doudoroff (ED) route, as opposed to a linear glycolysis (that prevails in Enterobacteria). Such a metabolic architecture enables growth and survival of *P. putida* KT2440 under stressful conditions, in which catabolic overproduction of NADPH would be advantageous (*e.g.*, the natural environments this bacterium thrives in). However, the low energy efficiency limits the widespread use of *P. putida* in biotechnological processes that require a high level of ATP generation.

The present Thesis aims at setting the basis to modify this state of affairs by undertaking a complete metabolic refactoring of *P. putida* KT2440 in order to increase its glucose-dependent energetic performance by *de novo* engineering of the bacterial metabolic lifestyle. The achievement of such goal comprised different steps in which Synthetic Biology approaches have been thoroughly incorporated. First, a powerful genetic tool for *à la carte* engineering of glycolytic activities in different Gram-negative bacteria (*i.e.*, the GlucoBrick platform) has been designed and constructed. The adoption of this standardized tool allowed for the rational implementation of a functional Embden-Meyerhof-Parnas (EMP) pathway in *P. putida* KT2440, which substituted the native, less energy-efficient ED route. Furthermore, the central carbon metabolism of *P. putida* KT2440 was streamlined by introducing several mutations in key glycolytic steps to facilitate the accommodation of novel biochemical capacities; this approach resulted in the generation of a set of *P. putida glycolytic chassis*. Simultaneously, the impact generated by the disruption of the native metabolic regime was studied by eliminating the glucose-6-*P* isomerase (Pgi) activities of strain KT2440, that resulted in an overall perturbation of the response to exogenous oxidative stress. The physiological and metabolic characterization of the glycolytic mutants developed in this study has thereby increased the fundamental knowledge on central carbon metabolism in *P. putida* KT2440.

Finally, the *P. putida glycolytic chassis* obtained in this Thesis, devoid of all the glycolytic steps in the upper catabolism along with the native glucose transport system, served as the biological container for hosting a functional, energy-efficient linear EMP pathway. This study tackles a novel aspect in terms of Metabolic Engineering, serving as a case example of network-wide metabolic refactoring of an environmental bacterium to increase its catalytic potential. As an evidence of this achievement, a complete ^{13}C-based fluxomic analysis was conducted in the engineered strain, in which the itinerary followed by carbon skeletons derived from glucose were exhaustively mapped throughout the novel metabolic network.

This approach demonstrated that the linear glycolytic pathway grafted into *P. putida* is functional, and that its ATP output was higher than that mediated by the native biochemical network.

RESUMEN

En la actualidad, *Pseudomonas putida* KT2440 se considera como uno de los microorganismos más atractivos para su utilización como plataforma biológica en aplicaciones biotecnológicas. Su gran versatilidad metabólica, elevada resistencia a estrés oxidativo, y la facilidad a la hora de ser manipulada genéticamente, son algunas de las características que han propiciado el interés en *P. putida* KT2440 y su aplicación como *chassis* en bio-producción. Esta bacteria del suelo presenta una estructura atípica en su metabolismo central cuando se cultiva en glucosa como fuente de carbono, favoreciéndose la generación de poder reductor (es decir, NADPH) en detrimento de la formación de ATP. La cepa KT2440 lleva a cabo una glicólisis cíclica basada en la ruta de Entner-Doudoroff (ED), a diferencia de la glicólisis lineal típica (prevalente en Enterobacterias). Esta arquitectura metabólica ha permitido que *P. putida* KT2440 pueda sobrevivir y crecer bajo condiciones de estrés, en las cuales una sobre-producción catabólica de NADPH resulta ventajosa para incrementar la supervivencia en el medio ambiente natural. Sin embargo, el bajo rendimiento energético de esta bacteria repercute negativamente en su potencial biotecnológico en aquellos procesos que requieren de una demanda de ATP elevada.

La presente Tesis Doctoral pretende asentar las bases para revertir esta situación, llevando a cabo una completa refactorización metabólica de *P. putida* KT2440 con el fin de incrementar el rendimiento energético de esta bacteria a partir de glucosa. Con el fin de alcanzar este objetivo, el presente estudio hace uso de un abordaje basado en la Biología Sintética. Primeramente, se creó y diseñó una potente herramienta genética (denominada *sistema GlucoBrick*) con la cual se pueden implementar actividades glicolíticas en diferentes bacterias Gram-negativas *a la carta*. La utilización de esta herramienta estandarizada permitió la implementación funcional de la ruta de Embden-Meyerhof-Parnas (EMP) en *P. putida* KT2440, sustituyendo de esta forma la ruta nativa ED, menos favorable energéticamente. Dicho proceso ha sido posible mediante la reducción genómica de *P. putida* KT2440, que facilitó la introducción de nuevas capacidades metabólicas mediante la eliminación de diversos elementos glicolíticos endógenos. Como resultado de esta operación, se ha generado un conjunto de *chassis glicolíticos* derivados de esta bacteria. Paralelamente, en este estudio se ha evaluado el impacto metabólico de interrumpir el funcionamiento normal del metabolismo de la cepa KT2440, mediante la eliminación de la actividad glucosa-6-*P* isomerasa (Pgi). Dicha manipulación resultó en una disminución significativa de la respuesta de esta bacteria al estrés oxidativo exógeno. En conjunto, la obtención de un gran número de mutantes glicolíticos de *P. putida* KT2440 permitió incrementar el conocimiento sobre el metabolismo central de carbono en este microorganismo.

Finalmente, el *chassis glicolítico* basado en *P. putida* KT2440 construido en esta Tesis Doctoral, en el cual las vías nativas de transporte y utilización de glucosa han sido inhabilitadas, ha sido utilizado como el hospedador funcional de una ruta linear de EMP. El trabajo desarrollado en este estudio se enmarca en el

campo de la Ingeniería Metabólica, siendo un ejemplo en el que se ha modificado racional y completamente la utilización de glucosa como fuente de carbono en un microorganismo ambiental. A la hora de demostrar la eficacia de dicha reconversión metabólica, en el presente trabajo se planteó el análisis de flujos de carbono mediante sustratos que contienen ^{13}C, con el que ha sido posible mapear el recorrido de los esqueletos de carbono a través de toda la red metabólica. Este enfoque experimental demostró que la ruta glicolítica lineal es funcional y activa, y que la generación de ATP en la cepa de *P*. *putida* modificada es mayor que el generado por las rutas metabólicas nativas.

I. INTRODUCTION

«*Not to know what happened before you were born is to be a child forever*»
Marcus Tullius Cicero
(106 BC-43 BC)

INTRODUCTION

1. Conspectus of *Pseudomonas putida*

1.1. *Pseudomonas* in perspective: a bit of history. *Pseudomonas putida* KT2440 is the bacterium that has been selected in this study for a deep refactoring of its central carbon metabolism, thereby bestowing a new *metabolic identity* onto it. The history of this microorganism is closely linked to the metabolic versatility displayed by the entire genus to which it belongs, that has prompted the biotechnological interest on this group of bacteria.

The name *Pseudomonas* was coined in 1894 by Prof. Migula. Back then, the genus was described as a group of cells with polar organs of motility and formation of spores in some special cases (Migula, 1894; Migula, 1900). This description was obviously short and inaccurate, but at the end of the XIX century, it was accepted for publication. This unclear description transformed the genus *Pseudomonas* in an authentic jumble until the publication of the doctoral thesis defended by L. E. den Dooren de Jong in 1926. This publication revealed one of the features that would define (and classify) the entire genus more accurately: its remarkable ability to degrade a large variety of organic compounds (including relevant toxic substances) as a part of the process of carbon mineralization (den Dooren de Jong, 1926). The den Dooren de Jong's thesis was however not widely used by contemporary scientists, given that the thesis was written in Dutch, but held out an inspirational vision for Stanier and collaborators, who went on creating the first accurate description of the *Pseudomonas* genus some forty years later (Stanier *et al.*, 1966). The Stanier's study proposed a set of differential tables based on nutritional characteristics, and occasionally on some morphological details, to classify the most relevant *Pseudomonas* species (including *P. putida*). This work provided a unifying definition of *Pseudomonas* that is currently valid for the most characteristic members of the group: «*Unicellular rods, with the long axis straight or curved, but not helical. Motile by means of one or more polar flagella. Gram-negative. Do not form spores, stalks, or sheaths. The energy-yielding metabolism is respiratory, never fermentative or photosynthetic. All use molecular oxygen as a terminal oxidant; and some can use denitrification as an alternative, anaerobic respiratory mechanism. All are chemoorganotrophs; some are facultative chemolithotrophs that use H_2 as an energy source*» (Stanier *et al.*, 1966).

The confusing panorama became clearer thanks to new methodologies and technical approaches, based on the studies of macromolecular identifiers. The DNA/DNA and RNAr/DNA hybridization techniques (Doi & Igarashi, 1965; Johnson & Ordal, 1968; Palleroni *et al.*, 1973) enabled the division of *Pseudomonas* species into five taxonomic groups (*i.e.*, RNA-I to RNA-V). This was the key step towards the final phylogeny and taxonomy classification, which was possible upon obtaining the sequence of the 16S rRNA gene

(Palleroni *et al.*, 1973). Based on this seminal publication, still valid at the present time, the genus *Pseudomonas* was limited to the previously described RNA-I group within the subclass of Gram-negative, aerobic γ-Proteobacteria (Palleroni, 2003).

Currently, the number of species assigned to the *Pseudomonas* genus encompasses a large number of members [>200 and still growing (Euzeby, 1997)]. These bacteria have been isolated from a large number of environments [*e.g.*, plant rhizosphere, soil, and water (Jensen *et al.*, 2004)], reflecting the enormous metabolic versatility that is characteristic of this group of microorganisms. The *Genomic Era* allowed to access the technologies needed for sequencing the entire genome of different bacteria of this group, thereby discovering an extensive collection of enzymes and metabolic pathways that can degrade a large number of organic compounds, including xenobiotic pollutants (Winsor *et al.*, 2016). In order to be able to consume such variety of structurally unrelated carbon sources, bacteria of the *Pseudomonas* genus display a large set of diverse metabolic pathways. These features also indicate that *Pseudomonas* is a robust group of microorganisms with a great potential for biotechnological applications. This is the case of the subject of study in this Thesis, *P. putida* KT2440, a microorganism that has been largely employed in different areas of bioremediation and biocatalysis (Nikel *et al.*, 2014b; Poblete-Castro *et al.*, 2012; 2017) since its isolation and identification in the 70s. The biotechnological interest on this bacterium has served as an inspiration for the present Thesis, by proposing the possibility of refactoring its central carbon metabolism capacities and taking advantage of the physiological characteristics displayed by the genus.

1.2. *Pseudomonas putida* KT2440. This bacterium is the best characterized saprophytic member of the Pseudomonads group. This situation partially stems from the fact that it has retained its ability to survive and function in the environment (Bagdasarian *et al.*, 1981; Regenhardt *et al.*, 2002). This bacterial strain is the plasmid-free derivative of a toluene-degrading bacterium, originally termed *Pseudomonas arvilla* strain mt-2 (Kojima *et al.*, 1967), and subsequently re-classified as *P. putida* mt-2 (Williams & Murray, 1974). The biotechnological applicability of *P. putida* KT2440 is backed by its certification as a safety strain by the Recombinant DNA Advisory Committee (Federal Register. Appendix E, 1982). On top of that, this bacterium has been extensively used as a host for cloning and gene expression, considering its capability to degrade aromatic compounds (*e.g.*, toluene or *m*-xylene), which makes it a promising microbial platform for biodegradation approaches (Jiménez *et al.*, 2002; Martins dos Santos *et al.*, 2004; Timmis, 2002).

In terms of genomic knowledge, *P. putida* KT2440 has been the subject of a progressive updating over the last years. The first attempt to completely sequence its single chromosome was published in 2002 (Nelson *et al.*, 2002), and was recently updated by Belda and collaborators in 2016 (Belda *et al.*, 2016). The revised genome of *P. putida* KT2440 is 6,181,873 bp long, with a G+C content of 61.5%. The updated genome profile encompasses 5,592 coding sequences (CDS), 1,151 of which encode hypothetical proteins, and 28 encode pseudogenes. This high level of knowledge allowed to predict 1,485 CDSs associated to

actual biochemical reactions, configuring a rather diverse biochemical map of the metabolism in this bacterium (Udaondo *et al.*, 2016).

1.3. Biotechnological potential of *P. putida* KT2440. The general description of *P. putida* KT2440 exposed in the last section provides clues of its biotechnological potential. Taking into account that the main goal of this Thesis has been to increase the catalytic capability of strain KT2440 *via* refactoring of its central carbon metabolism, this section compiles and summarizes the metabolic and physiological features that served as source of inspiration for the present study.

The fundamental knowledge gathered from genome analysis of *P. putida* has allowed to predict its biocatalytic potential. For example, strain mt-2 has a remarkable capacity to degrade aromatic compounds [*e.g.*, toluene or *m*-xylene (Jiménez *et al.*, 2002)], and displays high levels of solvent tolerance (Ramos *et al.*, 2015). These features allow for the utilization of this bacterium as an agent in different bioremediation and bioproduction approaches (Loeschcke & Thies, 2015; Poblete-Castro *et al.*, 2012). Additionally to these specific examples of physiological and metabolic robustness, the particular structure of its central carbon metabolism confers *P. putida* KT2440 a high tolerance to oxidative stress (Kim & Park, 2014), which is of interest for several biotechnological applications [*e.g.*, biofuels production (Liao *et al.*, 2016)]. This bacterial strain is also a well-established microbial host for cloning and heterologous gene expression, empowered by a steadily increasing number of genetic tools tailored for molecular manipulations (Durante-Rodríguez *et al.*, 2014; Lieder *et al.*, 2015; Martínez-García & de Lorenzo, 2011; Martínez-García *et al.*, 2011; 2014a,b; Silva-Rocha *et al.*, 2013). These advantageous traits are not limited to *wet* laboratory applications, as indicated by the availability of four genome-scale constraint-based metabolic models for *in silico* studies (Belda *et al.*, 2016; Nogales *et al.*, 2008; Puchałka *et al.*, 2008; Sohn *et al.*, 2010).

In summary, the wide applicability of this soil bacterium in industrial bioprocesses [*e.g.*, for the production of biopolymers (Linger *et al.*, 2014; Prieto *et al.*, 2016), natural products (Klein *et al.*, 2017; Loeschcke & Thies, 2015), and metabolic *building blocks* such as adipic acid (Okamura-Abe *et al.*, 2016; Vardon *et al.*, 2015)] supports the scope of the present study to improve its central carbon metabolism in terms of energetic balance. In this regard, the glucose metabolism of *P. putida* KT2440 is an excellent example of a biochemical network evolutionary adapted to the environmental conditions (Chavarría *et al.*, 2013). Such metabolic organization enables this bacterium to obtain a high level of reducing power (in the form of NADPH), used not only in anabolism (Spaans *et al.*, 2015), but also important to counteract oxidative stress (Kim & Park, 2014; Singh *et al.*, 2007). This metabolic operation of the biochemical network of *P. putida* does not prioritize energy production (in terms of ATP) when the cells grow on hexose substrates, and thus somewhat limits the feasibility of this bacterium in applications for which this requirement is essential (Hara & Kondo, 2015; Schuster, 2000). For this reason, the entire transformation of the central carbon metabolism of *P. putida* KT2440 [based on the Entner-Doudoroff (ED) pathway] into an energy-

efficient glucose catabolic network inspired in the Embden-Meyerhof-Parnas (EMP) pathway was systematically tackled as indicated below.

2. Central carbon metabolism in *P. putida* KT2440

Historically, the majority of Metabolic Engineering efforts have been focused on what could be considered *peripheral aspects* (Ajikumar *et al.*, 2010; Raab *et al.*, 2005; Stephanopoulos, 2012; Wu *et al.*, 2016); *e.g.*, the elimination of competing endogenous pathways, the fine-tuning of gene expression and substrate transport, and the rerouting of small molecules at given nodes of the target biochemical network. Approaches that target central carbon metabolism, which fuels microbial cell factories to obtain the energy and precursors needed for growth and bioproduction, are scarce (Jojima & Inui, 2015; Kern *et al.*, 2007; Nikel *et al.*, 2016a). This may be partially due to the difficulties of manipulating the *core* metabolism (Papagianni, 2012), which is extremely interconnected with the rest of the biochemical network. As indicated in **Table 1**, the literature reflects some of these partial attempts to carry out a deep metabolic transformation of industrially-relevant microorganisms (*e.g.*, by replacing their main glycolytic pathways). Against this background, the present Thesis evaluates the possibility of refactoring the central carbon metabolism of *P. putida* KT2440 in terms of glucose utilization pathways as an attempt to improve its overall energy balance. As an introduction to this specific issue, an overall vision of the native glucose metabolism of *P. putida* KT2440 is discussed in the section below.

Table 1 | **Previous attempts to refactor the central carbon metabolism of different microorganisms.**

Microorganism	Pathway[a]		Phenotype on glucose[b]	Reference
	Targeted	Added		
Saccharomyces cerevisiae	EMP	ED	N.G.	Benisch & Boles (2014)
P. putida KT2440	ED	EMP	N.G.	Chavarría *et al.* (2013)
Zymomonas mobilis	ED	EMP	40% lower μ	Chen *et al.* (2013)

[a] In the case of *Z. mobilis*, the participation of the target pathway was not removed completely (*i.e.*, by employing antisense inhibition). In the other examples, the target pathway was totally blocked (*i.e.*, by deletion of the cognate genes). Abbreviations are as follows: EMP, Embden-Meyerhof-Parnas pathway; and ED, Entner-Doudoroff pathway.

[b] General description of the growth phenotype under glycolytic conditions. Abbreviations are as follows: N.G., no growth; and μ, specific growth rate.

2.1. The energy-dependent glucose uptake system of *P. putida* KT2440. One of the critical steps in the optimization of microbial cell factories using Metabolic Engineering approaches is the uptake of substrate(s). *P. putida* KT2440 is able to enter glucose in its central carbon metabolism by means of two different routes (**Fig. 1**): (i) phosphorylation of the hexose in the cytoplasm by glucokinase (Glk), or (ii) oxidation in the

periplasm to gluconate and/or 2-ketogluconate (2KG) through the activity of glucose dehydrogenase (Gcd) and gluconate 2-dehydrogenase, collectively referred to as Gad (del Castillo *et al.*, 2007; 2008; Fuhrer *et al.*, 2005; Latrach-Tlemçani *et al.*, 2008). The transport of hexoses from the extracellular medium to the bacterial cytoplasm, crossing the outer and inner membrane, is carried out by an ATP-binding cassette (ABC) transport system coupled to the action of the OprB porins (**Fig. 1a**). The OprB porins [OprB-1 (PP_1019) and OprB-2 (PP_1445)] facilitate the diffusion of glucose across the outer membrane (del Castillo *et al.*, 2007; Wylie & Worobec, 1995). Then, the ABC transport system captures glucose from the periplasmic space with the aid of the periplasmic sugar-binding protein encoded by the *gtsA* gene (*PP_1015*). This complex, composed by the sugar and the periplasmic-binding protein, interacts with the *core* of the ABC transporter system encoded by the *gtsB* (*PP_1016*), *gtsC* (*PP_1017*), and *gtsD* (*PP_1018*) genes to finally introduce the carbohydrate into the cytoplasm (Schneider, 2001). This type of glucose transport systems is widely distributed in Gram-negative bacteria, in which the periplasmic-binding protein has a very high affinity for the specific substrate, *i.e.*, glucose (Jensen *et al.*, 2002). For example, the hexose transport system of *Thermococcus litoralis*, that exhibits a binding protein similar to that of strain KT2440, has a K_m of approximately 20 nM, whereas the K_m of the native glucose uptake system of *Escherichia coli* is around 1 μM (Xavier *et al.*, 1996). The high affinity of these transport systems come along with the investment of ATP, allowing for the efficient uptake of glucose even when the sugar concentrations are very low, as it is often the case in natural environments (Davidson & Chen, 2004). In terms of Metabolic Engineering purposes, however, such transport systems are to be avoided as they would use ATP that could be otherwise funneled into other biochemical processes.

2.2. The atypical glucose metabolism in *P. putida* KT2440. As hinted above, the central carbon metabolism of *P. putida* KT2440 is an example of a biochemical network adapted to ensure bacterial survival under stressful conditions (Chavarría *et al.*, 2013; Nikel *et al.*, 2015a). In order to meet this environmental challenge, the genome of *P. putida* KT2440 contains all the genes encoding enzymes of the three prominent catabolic pathways for sugars in bacteria: the ED pathway, the EMP pathway, and the pentose phosphate (PP) pathway (**Fig. 1b**). An enzyme remarkably absent in the biochemical network of *P. putida* KT2440 is 6-phosphofructo-1-kinase (Pfk), that enables the transformation of fructose-6-*P* (F6P) into fructose-1,6-P_2 (FBP) in many microorganisms (Chavarría *et al.*, 2013). The absence of Pfk results in the inability of strain KT2440 to degrade glucose *via* the linear, downwards EMP pathway, a phenomenon recognized in other environmental microorganisms as well [*e.g.*, *Shewanella oneidensis* (Tang *et al.*, 2009)].

After being transported into the periplasmic space, glucose is transformed into 6-phosphogluconate (6PG) through a series of peripheral reactions (Daddaoua *et al.*, 2009; del Castillo *et al.*, 2007), and this metabolite is processed almost exclusively (96%) through the 6-phosphogluconate dehydratase (Edd) and 2-keto-3-deoxy-6-phosphogluconate aldolase (Eda) enzymes (*i.e.*, the ED pathway proper) with only a very small fraction (*ca*. 4%), entering the PP pathway. Edd transforms 6PG to 2-keto-3-deoxy-6-

phosphogluconate (KDPG), and this metabolic intermediate is then split by Eda into pyruvate (Pyr) and glyceraldehyde-3-*P* (GA3P). Interestingly, the ED-based metabolism is far more distributed in Nature than previously thought (Bar-Even *et al.*, 2012); the two ED enzymes being highly conserved among bacterial and even archaeal species.

By adopting a multi-omic approach in cells grown on glucose, it was recently demonstrated that *P. putida* KT2440 operates a cyclic glycolysis (Nikel *et al.*, 2015a). This particular architecture in central carbon metabolism was termed *EDEMP cycle*. The functionality of this biochemical device is based on the prevalent participation of the ED pathway, supported by the incomplete EMP pathway [operating as a gluconeogenic route (Nikel *et al.*, 2014a; 2015b)], and the first two elements of the PP pathway (Nikel *et al.*, 2014a; 2015b). By using this atypical metabolic configuration, *P. putida* KT2440 recycles part of the trioses-*P* pool back to glucose-6-*P* (G6P), as indicated in **Fig. 1b**. Under balanced growth conditions with glucose as the only carbon source, the EDEMP cycle recycles *ca*. 10-15% of the trioses-*P* generated by the ED pathway back to hexoses-*P*. The rest of carbon skeletons in the form of trioses-*P* is further metabolized into acetyl-coenzyme A (acetyl-CoA) to enter into the tricarboxylic acid (TCA) cycle in order to produce biomass precursors and reducing equivalents. The study of mutants blocked at different steps of the EDEMP cycle highlighted the relevance of this sub-network for the survival and robustness of *P. putida* KT2440. For example, interrupting the cycle has proved to affect the overall redox balance of this bacterium, despite the fact that the *core* metabolism of strain KT2440 has been demonstrated to be quite robust to both redox and energy perturbations (Ebert *et al.*, 2011). At the same time, the disruption of this metabolic cycle can compromise the synthesis of different precursors coming from the recycling of trioses-*P* [*i.e.*, generation of FBP, which could not be obtained otherwise (Portais & Delort, 2002)].

The operation of the glycolytic cycle also results in a high endurance of *P. putida* to oxidative stress. This is one of the most important characteristic features displayed by this environmental bacterium, reflected in its capacity to inhabit polluted environments (Kim & Park, 2014). The activity of the major dehydrogenases in the EDEMP cycle of *P. putida* KT2440, such as glucose-6-*P* 1-dehydrogenase (Zwf), is directly coupled to the formation of NADPH (Nikel & Chavarría, 2016), with a relatively small degree of promiscuity in cofactor selectivity (Nikel *et al.*, 2015a). In the case of the linear ED pathway, one NADPH molecule is generated per molecule of G6P entering the process through Zwf. In the EDEMP cycle, in contrast, the yield of NADPH can increase significantly depending on the extent of recycling (**Fig. 1b**). This is possible due to the formation of additional G6P from F6P *via* the glucose-6-*P* isomerase (Pgi) activity, feeding the Zwf activity with extra substrate molecules. The relevance of this network to *P. putida* KT2440 has been exposed by the material impossibility to obtain a complete Zwf mutant. At the same time, the essentiality of Zwf is hinted by the presence of three isoenzymes for the same biochemical reaction [*i.e.*, Zwf (PP_5351), ZwfA (PP_1022), and ZwfB (PP_4042)], an example of redundancy associated to environmental adaptation (Bratlie *et al.*, 2010; Maleki *et al.*, 2015).

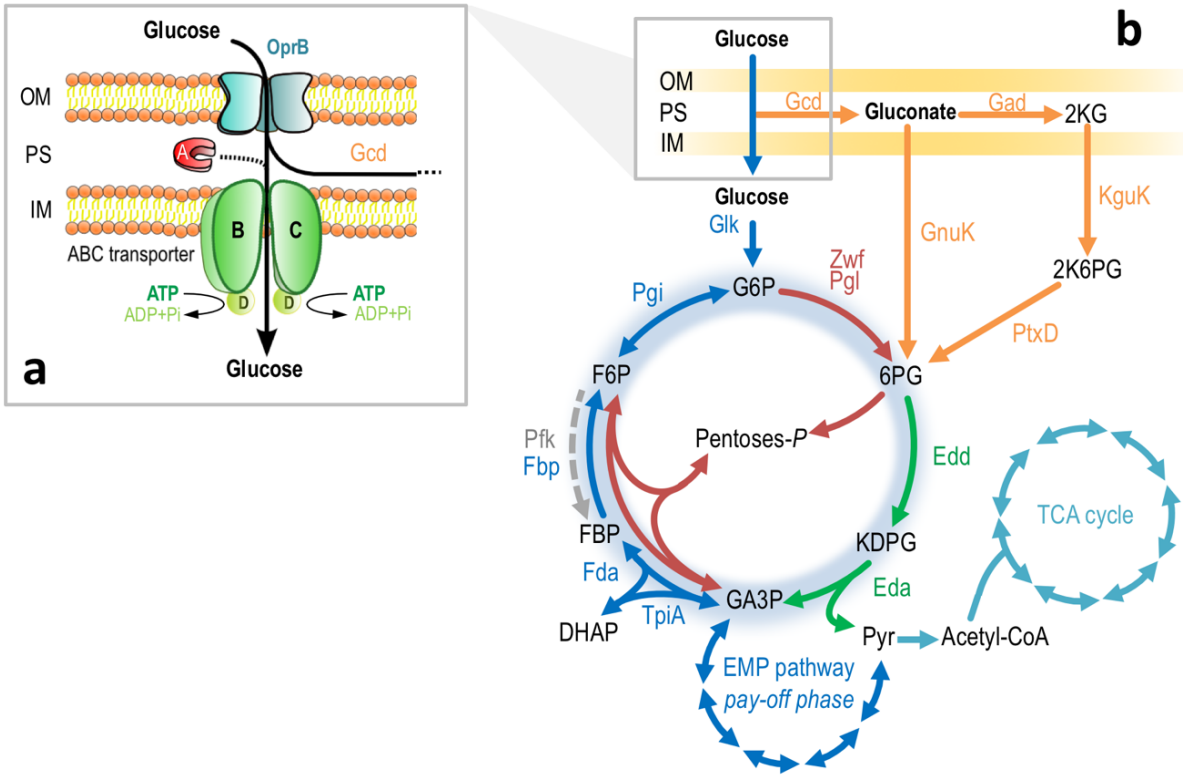

Figure 1 | **Glucose metabolism of *P. putida* KT2440.** (**a**) Schematic representation depicting the glucose uptake system of *P. putida* KT2440. The capital letters shown in the picture indicate the functional subunits of the ABC transporter. (**b**) Simplified representation of central carbon metabolism in *P. putida* KT2440. Glucose catabolism occurs mainly through the activity of the Entner-Doudoroff (ED) pathway, and part of the trioses-*P* thereby generated are recycled back to hexoses-*P* by means of the *EDEMP cycle*, that also encompasses activities from the (gluconeogenic) Embden-Meyerhof-Parnas (EMP) and pentose phosphate (PP) pathways. The scheme also depicts the conversion of pyruvate into acetyl-coenzyme A, that enters in the tricarboxylic acid (TCA) cycle. A set of *peripheral reactions* can oxidize glucose to gluconate and/or 2-ketogluconate (2KG) before any phosphorylation of the intermediates occurs. Each metabolic block is indicated with different colours, and the EDEMP cycle is shaded in blue in the diagram. Note that 6-phosphofructo-1-kinase (Pfk) activity is absent and this reaction is indicated as a dashed grey row. The abbreviations used in this picture are as follows: G6P, glucose-6-*P*; F6P, fructose-6-*P*; FBP, fructose-1,6-P_2; DHAP, dihydroxyacetone-*P*; GA3P, glyceraldehyde-3-*P*; Pyr, pyruvate; 6PG, 6-phosphogluconate; KDPG, 2-keto-3-deoxy-6-phosphogluconate; acetyl-CoA, acetyl-coenzyme A; 2K6PG, 2-ketogluconate-6-*P*; OM, outer membrane; PS, periplasmic space; and IM, inner membrane.

2.3. ED pathway *vs.* EMP pathway: reducing power *vs.* energy yield. As indicated above, the metabolic lifestyle of *P. putida* KT2440 enables this bacterium to survive under adverse environmental conditions (Chavarría *et al.*, 2013), but at the same time it somewhat limits the use of this microorganism in biotechnological applications that require high rates of ATP formation (Hara & Kondo, 2015; Schuster, 2000). Taking into account this operational limitation, the objective of this Thesis is focused on the transformation of the native EDEMP cycle-based metabolism of *P. putida* KT2440 into an energy-efficient EMP-based biochemical network. Yet, what are the main differences of each catabolic lifestyle?

Microbial cells need to expend a great deal of energy to maintain their functional organization. The EMP and ED catabolic pathways satisfy this energy demand with the generation of ATP during glucose metabolism (Stettner & Segrè, 2013). However, the ATP yield in either pathway is certainly not the same. The stoichiometry of reactants and products in each case (**Fig. 2**) indicates that the EMP pathway produces twice as much ATP per glucose than the ED pathway does (Bar-Even *et al.*, 2012). The first part of glycolysis is based on the investment of ATP to phosphorylate hexose sugars (*i.e.*, the so-called *preparatory phase*). These phosphorylated intermediaries are then cleaved to generate two trioses intermediates. The investment in ATP is recovered in the second phase of glycolysis (termed *pay-off phase*), where the oxidation of trioses-*P* drives the generation of ATP. Despite that the two glycolytic pathways overlap in some reactions (**Fig. 2**), they differ in the number of three carbon intermediates in the *pay-off* phase. In the case of the EMP pathway, 2 ATP equivalents are consumed to phosphorylate glucose twice, and both trioses-*P* intermediates (*i.e.*, GA3P) enter the *pay-off* phase to produce two ATP each (**Fig. 2a**). On the other hand, the ED pathway consumes one ATP to phosphorylate glucose once (as it was indicated in the previous section, see **Fig. 1b**), obtaining a unique GA3P molecule to be entered in the *pay-off* phase (**Fig. 2b**). This approach results in the production of 1 ATP equivalent per molecule of glucose. In summary, while the EMP pathway extracts two ATP molecules per glucose, the ED pathway only yields one.

Why is the ED pathway so widely distributed in bacteria despite its low energy yield? Phylogenetic analysis indicate that the ED pathway predated the EMP pathway (which is rather common in eukaryotes) in the evolutionary timeline (Romano & Conway, 1996). This theory considered the EMP route to be a fine-tuned adaptation of the ED-based biochemistry in order to optimize energy efficiency. However, a more recent study suggested a different scenario, in which the ED pathway should be considered as a thermodynamically favored network (Flamholz *et al.*, 2013). In this case, the low ATP from the ED pathway yield is compensated by the low cost of the machinery employed in this route (*i.e.*, just two enzymes needed to operate the ED route as opposed to the ten enzymes that compose the EMP pathway). In any case, it seems plausible that the evolutionary choice of one route over the other is based on the particular adaptations to the environment, a feature that is unique for each biological entity.

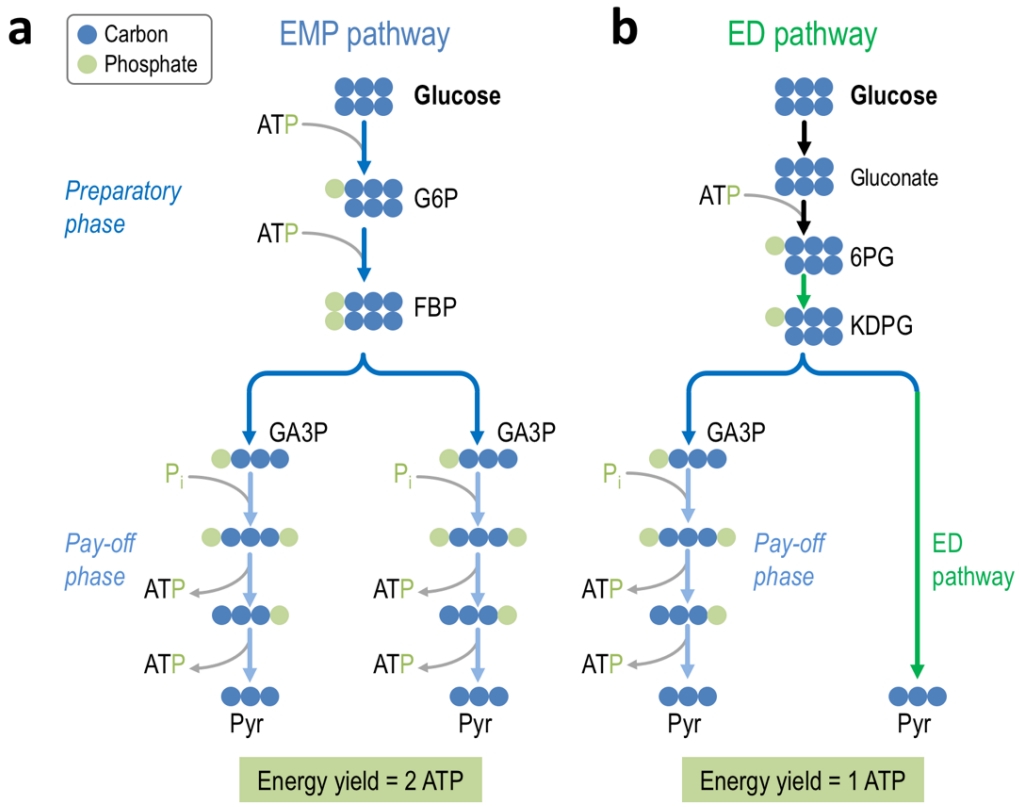

Figure 2 | **Structural differences and similarities between the ED and EMP catabolic routes.** The scheme depicts the key aspects of (**a**) the Embden-Meyerhof-Parnas (EMP) pathway and (**b**) the Entner-Doudoroff (ED) pathway. The EMP and ED reactions are indicated by colored arrows (blue and green, respectively). The carbon atoms and phosphate groups are shown in different colors to highlight the organization of the ATP consuming and producing steps. Other features (*e.g.*, the stoichiometry of reducing cofactors, such as NADH and NADPH) have been removed to simplify the scheme. The abbreviations used in this scheme are as follows: G6P, glucose-6-*P*; FBP, fructose-1,6-P_2; GA3P, glyceraldehyde-3-*P*; Pyr, pyruvate; 6PG, 6-phosphogluconate; and KDPG, 2-keto-3-deoxy-6-phosphogluconate.

3. Synthetic Biology and Metabolic Engineering for refactoring the central carbon metabolism of *P. putida* KT2440

Metabolic Engineering emerged as a discipline which employs the existing knowledge about living systems to generate biological entities that can be used as biofactories for the production of value-added products (Breitling & Takano, 2015; King *et al.*, 2016; Nielsen & Keasling, 2016; Schuster *et al.*, 2000). Currently, Synthetic Biology provides a large number of strategies and tools for the rational creation of predictable DNA circuits to be used in Metabolic Engineering (Stephanopoulos, 2012). DNA synthesis has been optimized during the last years by the use of automated instruments, allowing for the significant reduction in the operational prizes (*i.e.*, 50 USD/bp some 20 years ago *vs.* <0.2 USD/bp nowadays). DNA *democratization* has enabled bottom-up approaches that facilitate the reconstruction of entire metabolic

networks *à la carte* (Jullesson *et al.*, 2015). DNA synthesis is as important as the biological machinery that expresses and contains these nucleic acids. This basic idea of *biological container* leads to the important concept of *chassis*, which can be defined as the live platform able to host and sustain the molecular transactions necessary for expressing the information encoded in any DNA design (Danchin, 2012). In the present Thesis, both notions are exploited under the form of two key elements: (i) a set of standardized DNA elements (designed as a genetic tool), that encode the whole of the reactions needed to implement the linear EMP glycolytic pathway in virtually any Gram-negative host, and (ii) a deeply streamlined *P. putida* KT2440-based *chassis*, that allows for deep refactoring of central carbon metabolism. In the next sections, the principles at the basis of these key elements are discussed in detail (**Fig. 3**).

3.1. Genetic tools in Metabolic Engineering. The *post-Genomic Era* we are living nowadays has changed the angle from which Metabolic Engineering endeavors are approached. The enormous volume of data on genes, proteins, and metabolites that has been accumulated thus far, together with the decrease in DNA synthesis costs, has made rational engineering attempts easier. Users are now able to design and quickly synthetize DNA constructs encoding practically any desired metabolic pathway. This situation has, in turn, gradually shifted away the focus of Metabolic Engineering from manipulating individual pathways to purposedly perturbing the entire biochemical network in the host cell (Lee & Kim, 2015; Park & Lee, 2008; Stafford & Stephanopoulos, 2001). Synthetic Biology devices are an essential part of the repertoire of tools currently available to reach such a purpose.

The concept of *tool* is directly correlated with the term of *portability* (**Fig. 3a**). As it was mentioned before, the type of genetic tool designed in this Thesis is meant to be compatible with a wide variety of Gram-negative bacteria (including, but certainly not limited to, *P. putida*). This situation is relevant since many of the available tools used nowadays for manipulating microbial metabolism are not universally applicable. Usually, these tools are specific to only certain pathways or products. This lack of transferability of a majority of tools and techniques between hosts, in turn, can be attributed to an incomplete understanding of regulatory mechanisms in the cell (Yadav *et al.*, 2012). Thus, the development of genetic tools should also consider an up-to-date knowledge of regulatory elements both in the DNA sequences employed for their construction and the regulatory network in the host.

Furthermore, the feasibility of cheaply synthetizing DNA *à la carte* allows for the introduction of another key notion in the process of genetic tool design: *modularity*, an important principle for the standardization sough after by Synthetic Biology approaches (**Fig. 3a**). A well-designed genetic tool must facilitate the manipulation of its basic component elements; *e.g.*, with the introduction of a logic pattern of enzyme restriction sites (Yadav & Stephanopoulos, 2010). Modularization, especially in the form of *one module-one source* strategy, enables faster construction, testing, and identification of expression configurations that maximize product formation in different scenarios.

At the same time that the genetic tool is generated by sticking to the principle of modularity, functional components should be designed by taking into account the genomic containment that is going to host them. A versatile genetic tool must be easy to be *cut-and-pasted* into standardized plasmid vector/transposon systems, making the assembly of DNA both facile and affordable (Biggs *et al.*, 2014). The Synthetic Biology community is constantly providing standards to follow during the implementation of these practices (**Fig. 3a**); *e.g.*, the SEVA (*Standard European Vector Architecture*) plasmid collection (Silva-Rocha *et al.*, 2013), and the pBAM1/pBAMDs transposon platform (Martínez-García *et al.*, 2011; 2014a). This set of plasmids appears as a promising asset to deploy Metabolic Engineering designs in Gram-negative bacteria. However, the use of plasmids should be considered as a *beta*-phase testing in terms of stable metabolic manipulations: plasmid segregation, imprecise control of plasmid-based gene expression, and metabolic burden are just a few drawbacks of adopting plasmid-based heterologous gene expression (Anthony *et al.*, 2009; Bentley *et al.*, 1990; Jones *et al.*, 2000). For this reason, stable chromosome-based expression *via* transposition events are an alternative to circumvent these challenging issues. This strategy avoids (or, at least, alleviates the effect of) some of the above-mentioned problems, such as asymmetric segregation and problems with plasmid maintenance, the associated metabolic stress, and the need of antibiotic supplementation (Tyo *et al.*, 2009). Taking into account the principles detailed in this section (including the concepts of *portability*, *modularity*, and *composable DNA assembly*), a promising genetic tool for *à la carte* implementation of a flawless EMP glycolytic pathway in different Gram-negative bacteria is thoroughly presented in this Thesis.

3.2. Bacterial *chassis* design in Metabolic Engineering. Once the coding DNA modules have been designed and generated, the next step comprises the selection (and, if necessary, the engineering) of an appealing biological container for the construct(s). The many qualities of *P. putida*, which have been already indicated in the first part of the *Introduction*, served as an inspiration to unleash the full catalytic potential of this bacterium as a case example of deep refactoring of the entire carbon metabolism. This task is, however, a rather challenging venture. As a first step, it is necessary to generate a well-designed *chassis* amenable to host the novel metabolic capacities to be implanted.

The design of a hefty bacterial *chassis* needs to follow rules as strict as the ones indicated above for standard genetic tools (Kim *et al.*, 2016a). An appealing microbial *chassis* must hold the minimal information (i) to operate autonomously, (ii) to complete the basic biological functions of growth and maintenance, and (iii) to properly run the necessary cellular machinery to withstand stressful conditions that can appear during catalytic processes (Danchin, 2012). Taking into account all this information, the *chassis* construction process often encompasses the removal of genes that encode non-essential functions for survival under specific conditions (Choe *et al.*, 2016). The concept of a *minimal bacterial genome* needs to be discussed in the context in which it is meant to be applied, adapting the type and extent of genetic manipulations to

the main goal of the entire project (in our case, refactoring of central carbon metabolism using glucose as the carbon source).

The idea of a minimal genomic *chassis* has been already exploited in the past in several industrially-relevant microorganisms (Choe *et al.*, 2016; Martínez-García & de Lorenzo, 2016). Genome reduction seems to be a promising approach to make bacterial hosts more predictable and easily controllable (Lieder *et al.*, 2015; Martínez-García *et al.*, 2014c). At the same time, the functional simplification of biochemical pathways and metabolic nodes in the engineered cells minimizes the interactions between the cellular machinery and the genetic construct(s) implanted (**Fig. 3b**), which can otherwise result in the appearance of undesired side reactions and difficult-to-predict phenotypes (Kim & Copley, 2012; Nielsen *et al.*, 2013). In our particular case, the implementation of novel metabolic capacities in a complex biochemical network poses an additional issue to solve, *i.e.*, the competition of extant pathways for the substrate (**Fig. 3b**). The elements involved in the *core* bacterial metabolism are highly interconnected through a large number of essential biochemical reactions (*e.g.*, glycolysis, anabolic reactions, and TCA cycle, to mention just a few examples). The refactoring and manipulation of these central biochemical routes calls for a detailed knowledge of the substrate's itineraries. The overall success of these approaches largely depends on the elimination of competing reactions diverting carbon intermediates from the pathway(s) of interest (Tepper & Shlomi, 2010; Wendisch *et al.*, 2016).

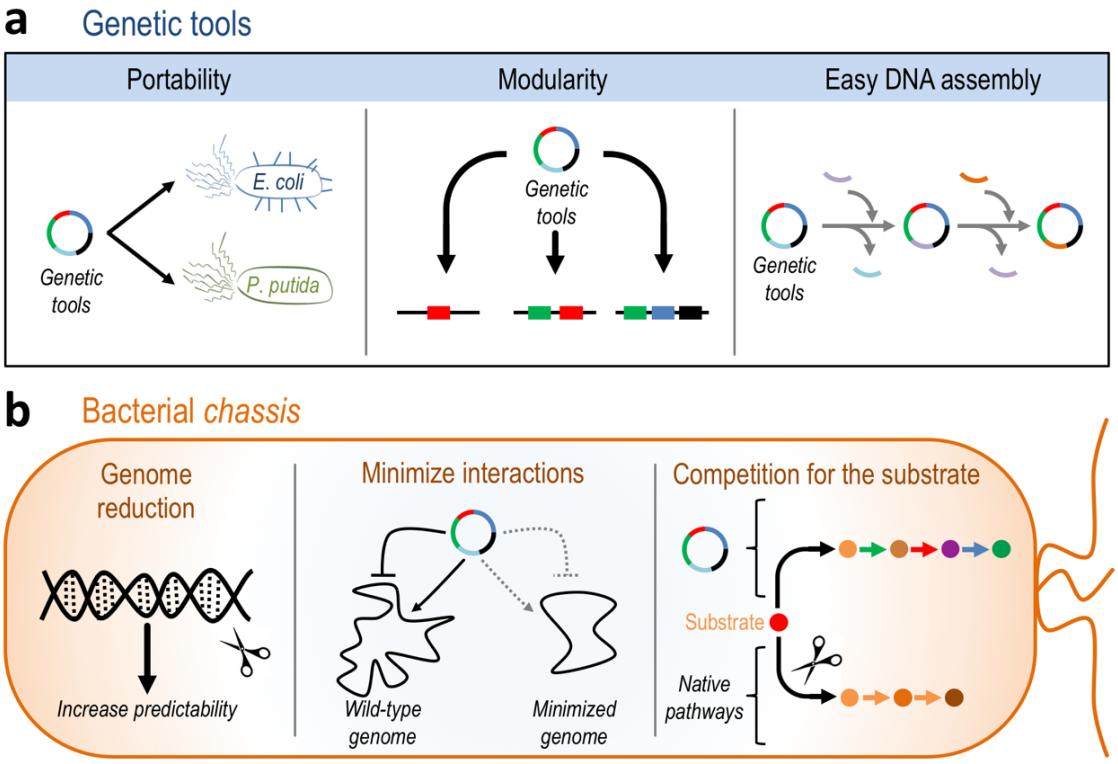

Figure 3 | **Key concepts in Synthetic Biology-guided Metabolic Engineering.** The large number of works developed under the discipline of Metabolic Engineering have allowed to identify the relevant elements in most endeavors: (**a**) the generation of standard genetic tools, and (**b**) the design and construction of a suitable bacterial *chassis*. (**a**) A well-designed genetic tool is characterized by its *portability* (*i.e.*, allowing the user to be employ the tool in different, often unrelated, biological entities), *modularity* (*i.e.*, facilitating the manipulation of its constituent components), and the facility to be *assembled* (*i.e.*, making the assemblage of DNA comfortable). (**b**) The biological container for these constructs (*chassis*) must be streamlined to increase its predictability, minimizing the potential interactions between the cellular machinery and the implanted genetic construct, and removing the native pathways that can compete for the substrate of the desired reaction(s).

4. The issue at stake: *de novo* engineering of central carbon metabolism in *P. putida* KT2440

P. putida KT2440 displays a remarkable endurance to different types of exogenous stressors, holding the promise to outcompete other microbial cell platforms in specific biotechnological applications. These advantageous properties stem from an atypical central carbon metabolism, which is geared to obtain reducing power (*i.e.*, NADPH). However, the central carbon metabolism of this bacterium does not prioritize the generation of ATP, an important requirement in a large number of biotechnological process. Taking into account this challenging scenario, the present work seeks to engineer the catabolic lifestyle of *P. putida* to unleash its catalytic potential in applications in which a high yield of ATP on substrate is desirable. For this reason, a complete refactoring of the central carbon metabolism of this bacterium was undertaken by adhering to the Synthetic Biology principles enumerated in the previous sections. This Synthetic Biology-guided metabolic transformation is based on the substitution of the highly redox-efficient ED pathway by a synthetic ATP-generating EMP route transplanted into a heavily engineered *P. putida chassis*. The whole process is divided into individual steps, driven by independent objectives. Firstly, the design and creation of the *GlucoBrick platform*, a standard genetic tool capable of implementing the EMP pathway glycolytic activities into virtually any Gram-negative bacterium, is discussed in **Chapter 1**. The genomic streamlining process conducted to generate an appropriate *P. putida glycolytic chassis* is explained in **Chapter 2**. The native metabolic wiring of the EDEMP cycle is explored by interrupting the step catalyzed by Pgi in **Chapter 3**. Finally, **Chapter 4** discloses the results of combining the GlucoBrick platform into the final version of the *P. putida* glycolytic *chassis*, analyzing the physiological effects of such network-wide metabolic manipulation by means of a fluxomic strategy.

II. OBJECTIVES

«*No one knows what he can do till he tries*»
Publilius Syrus
(85 BC-43 BC)

OBJECTIVES

The **general objective** of this Thesis is:

The *de novo* refactoring of the central carbon metabolism of *Pseudomonas putida* KT2440 to implement a functional linear glycolysis, based on the Embden-Meyerhof-Parnas (EMP) pathway, for enhanced energy balance from glucose.

This general objective is implemented trough the execution of the following **specific objectives**:

1. To design a broad-host-range genetic tool for *à la carte* implementation of the EMP pathway-based glycolytic activities in different Gram-negative bacteria.

2. To construct a useful *P. putida* KT2440 *glycolytic chassis*, capable of accommodating novel catabolic pathways in its central carbon metabolism.

3. To understand the metabolic wiring of native glycolytic pathways in strain KT2440, through the interruption of the biochemical step catalyzed by glucose-6-*P* isomerase (Pgi).

4. To implement a flawless linear EMP pathway in a *P. putida glycolytic chassis* as the only way to process glucose, increasing, at the same time, the ATP output from hexoses as the carbon source.

III. MATERIALS & METHODS

«*Help me to do it myself*»
Maria Tecla Artemisia Montessori
(1870 AC-1952 AC)

MATERIALS & METHODS

1. General procedures

1.1. Bacterial strains

The bacterial strains used in this Thesis are described in **Table 2**.

Table 2 | **Bacterial strains used in this Thesis.**

Strain	Relevant characteristics[a]	Reference or source
Escherichia coli		
CC118	Cloning host; Δ(*ara-leu*) *araD* Δ*lacX174 galE galK phoA thiE1 rpsE rpoB*(Rif^R) *argE*(Am) *recA1*	Manoil & Beckwith (1985)
CC118 λ*pir*	Cloning host for plasmids containing an R6K origin of replication; Δ(*ara-leu*) *ara*D Δ*lac*X174 *galE galK phoA20 thi-1 rpsE rpoB argE* (Am) *recA1*, λ*pir* lysogen	Herrero *et al.* (1990)
DH5α λ*pir*	Cloning host for plasmids containing an R6K origin of replication; F$^-$ λ$^-$ *endA1 glnX44*(AS) *thiE1 recA1 relA1 spoT1 gyrA96*(Nal^R) *rfbC1 deoR nupG* Φ80(*lacZ*Δ*M15*) Δ(*argF-lac*)*U169 hsdR17*(r_K^- m_K^+), λ*pir* lysogen	Hanahan & Meselson (1983)
HB101	Mating helper strain; F$^-$ λ$^-$ *hsdS20*(rB^- mB^-) *recA13 leuB6*(Am) *araC14* Δ(*gpt-proA*)*62 lacY1 galK2*(Oc) *xyl-5 mtl-1 thiE1 rpsL20 glnX44*^{B}(AS)^B	Boyer & Roulland-Dussoix (1969)
BW25113[b]	Wild-type strain; F$^-$ λ$^-$ Δ(*araD-araB*)*567* Δ*lacZ4787*(::*rrnB-3*) *rph-1* Δ(*rhaD-rhaB*)*568 hsdR514*	Datsenko & Wanner (2000)
JW3887-1[b]	Same as BW25113, but Δ*pfkA775*::*aphA*; Km^R	Baba *et al.* (2006)
JW5280-1[b]	Same as BW25113, but Δ*pfkB722*::*aphA*; Km^R	Baba *et al.* (2006)
BPfkAB	Same as BW25113, but Δ*pfkA775*::*FRT* Δ*pfkB722*::*aphA*; Km^R	This study
JW2385-1[b]	Same as BW25113, but Δ*glk-726*::*aphA*; Km^R	Baba *et al.* (2006)
JW2409-1[b]	Same as BW25113, but Δ*ptsI745*::*aphA*; Km^R	Baba *et al.* (2006)
BPG	Same as BW25113, but Δ*glk-726*::*FRT* Δ*ptsI745*::*aphA*; Km^R	Nikel & de Lorenzo (2013b)
JW3890-2[b]	Same as BW25113, but Δ*tpiA778*::*aphA*; Km^R	Baba *et al.* (2006)
W3110	Wild-type strain; F$^-$ λ$^-$ *IN*(*rrnD-rrnE*)*1 rph-1*	Jensen (1993), Bachmann (1972)

DS121[b]	Same as W3110, but Δ*epd-11*::*erm*; Ery^R	Seta *et al.* (1997)
DS122[b]	Same as W3110, but Δ*gapA12*::*cat*; Cm^R	Seta *et al.* (1997)
DS123[b]	Same as W3110, but Δ*gapA12*::*cat* Δ*epd-11*::*erm*; Cm^R Ery^R	Seta *et al.* (1997)
DS123PK	Same as W3110, but Δ*gapA12*::*cat* Δ*epd-11*::*erm* Δ*ptsI745*::*aphA*; Cm^R Ery^R Km^R	This study
DS123P	Same as W3110, but Δ*gapA12*::*cat* Δ*epd-11*::*erm* Δ*ptsI745*::*FRT*; Cm^R Ery^R	This study
DF575[b]	F^- λ^- *glnX44*(AS) *relA1 eno-2 rpsL104 malA malT1*(λ^R) *xyl-7 mtlA2 thiE1*	Thomson *et al.* (1979)
DF576[b]	F^- λ^- *glnX44*(AS) *relA1 pgk-2 rpsL104 malA malT1*(λ^R) *xyl-7 mtlA2 thiE1*	Thomson *et al.* (1979)

Strain	**Relevant characteristics[a]**	**Reference or source**
Pseudomonas putida		
KT2440	Wild-type strain, derived from *P. putida* mt-2 (Worsey & Williams, 1975) cured of the TOL plasmid pWW0	Bagdasarian *et al.* (1981)
KT2440 Δ*glk*	Same as KT2440, but with an in-frame deletion of the *glk* gene (*PP_1011*)	This study
KT2440 Δ*gcd*	Same as KT2440, but with an in-frame deletion of the *gcd* gene (*PP_1444*)	This study
KT2440 Δ*PP_3382-4*	Same as KT2440, but with an in-frame deletion of the genes *PP_3382*, *PP_3383* and *PP_3384* by a single deletion event	This study
KT2440 Δ*PP_3623*	Same as KT2440, but with an in-frame deletion of the *PP_3623* gene	This study
KT2440 Δ*PP_4232*	Same as KT2440, but with an in-frame deletion of the *PP_4232* gene	This study
KT2440 Δ*gad*	Same as KT2440 Δ*PP_3382-4*, but with an in-frame deletion of the genes *PP_3623* and *PP_4232*	This study
KT2440 Δ*glk* Δ*gcd*	Same as KT2440 Δ*glk*, but with an in-frame deletion of the *gcd* gene (*PP_1444*)	This study
KT2440 Δ*edd*	Same as KT2440, but with an in-frame deletion of the *edd* gene (*PP_1010*)	This study
KT2440 Δ*eda*	Same as KT2440, but with an in-frame deletion of the *eda* gene (*PP_1024*)	This study
KT2440 Δ*gts*	Same as KT2440, but with an in-frame deletion of the genes that encode the sugar ABC transporter [Δ*gtsA* (*PP_1015*), Δ*gtsB* (*PP_1016*), Δ*gtsC* (*PP_1017*) and Δ*gtsD* (*PP_1018*)]	This study

KT2440 Δ*gts* Δ*gcd*	Same as KT2440 Δ*gts*, but with an in-frame deletion of the *gcd* gene (*PP_1444*)	This study
KT2440 Δ*gts* Δ*gcd*·T	Same as KT2440 Δ*gts* Δ*gcd* but *PP_5SE*::mini-Tn*5*(*glf*); (chromosomal insertion of the gene encoding the Glf glucose transporter from *Zymomonas mobilis*); Km^R	This study
GC1	Glycolytic *chassis* I; derivative of *P. putida* KT2440 with the deletions described for the mutants Δ*glk,* Δ*gcd,* Δ*gad* and Δ*edd*	This study
GC2	Glycolytic *chassis* II; derivative of *P. putida* GC1 with the deletions described for the mutants Δ*gts* and Δ*eda*	This study
GC2·T·GBI	Same as *P. putida* GC2 but *PP_0841*::mini-Tn*5*(*glf*); chromosomal insertion of the gene encoding the Glf glucose transporter from *Zymomonas mobilis* and genome coordinate 6,005,012:mini-Tn*5*(GBI); chromosomal insertion of the genes of Module I of the GlucoBrick platform; Km^R Sm^R	This study
GC2·T·GBI·GBII	Same as *P. putida* GC2·T·GBI but *PP_0806*:mini-Tn*5*(GBII); chromosomal insertion of the Module II of the GlucoBrick platform; Km^R Sm^R Gm^R	This study
KT2440 Δ*pgi-I*	Same as KT2440, but with an in-frame deletion of the *pgi-I* gene (*PP_1808*)	This study
KT2440 Δ*pgi-II*	Same as KT2440, but with an in-frame deletion of the *pgi-II* gene (*PP_4701*)	This study
KT2440 Δ*pgi-I* Δ*pgi-II*	Same as KT2440 Δ*pgi-I*, but with an in-frame deletion of the *pgi-II* gene (*PP_4701*)	This study
KT2440 Δ*gntZ*	Same as KT2440, but with an in-frame deletion of the *gntZ* gene (*PP_4043*)	This study
KT2440 Δ*pgi-I* Δ*pgi-II* Δ*gntZ*	Same as KT2440 Δ*pgi-I* Δ*pgi-II*, but with an in-frame deletion of the *gntZ* gene (*PP_4043*)	This study
Pseudomonas aeruginosa		
PAO1	Wild-type strain (PAO1001), original stock conserved by P. V. Phibbs	Stover *et al.* (2000)

[a] Antibiotic markers: *Ap*, ampicillin; *Cm*, chloramphenicol; *Ery*, erythromycin; *Gm*, gentamicin; *Km*, kanamycin; *Nal*, nalidixic acid; *Rif*, rifampicin; *Sm*, streptomycin; *Sp*, spectinomycin; and *Tc*, tetracycline.

[b] Strain obtained from the *E. coli* Genetic Stock Center (Yale University, New Haven, CT, USA).

1.2. Plasmids

The plasmids used in this study are described in **Table 3**.

Table 3 | **Plasmids used in this study.**

Plasmids	Relevant characteristics[a]	Reference or source
pKD46	Ap^R; helper plasmid expressing the λ-Red recombination functions	Datsenko & Wanner (2000)
pCP20	Ap^R Cm^R; helper plasmid used for excision of *FRT-aphA-FRT* (Km^R), *Saccharomyces cerevisiae FLP* λcI857 λP_R *repA*(Ts)	Cherepanov & Wackernagel (1995)
pRK600	Cm^R; Helper plasmid used for conjugation, *oriV*(ColE1), RK2(*mob*$^+$ *tra*$^+$); derivative of plasmid pRK2013 (Ditta *et al.*, 1980)	Kessler *et al.* (1992)
pEMG	Km^R; *oriV*(R6K), vector used for deletions, *lacZ*α with two flanking I-*Sce*I target sites	Martínez-García & de Lorenzo (2011)
pEMGΔ*glk*	Km^R; pEMG derivative bearing a 1.0-kb TS1-TS2 *Eco*RI-*Bam*HI insert for deletion of the *glk* gene of *P. putida* KT2440	This study
pEMGΔ*gcd*	Km^R; pEMG derivative bearing a 1.0-kb TS1-TS2 *Eco*RI-*Bam*HI insert for deletion of the *gcd* gene of *P. putida* KT2440	This study
pEMGΔ *PP_3382-4*	Km^R; pEMG derivative bearing a 1.0-kb TS1-TS2 *Eco*RI-*Bam*HI insert for deletion of the group of genes *PP_3382*, *PP_3383* and *PP_3384* of *P. putida* KT2440	This study
pEMGΔ *PP_3623*	Km^R; pEMG derivative bearing a 1.0-kb TS1-TS2 *Eco*RI-*Bam*HI insert for deletion of the *PP_3623* gene of *P. putida* KT2440	This study
pEMGΔ *PP_4232*	Km^R; pEMG derivative bearing a 1.0-kb TS1-TS2 *Sac*I-*Bam*HI insert for deletion of the *PP_4232* gene of *P. putida* KT2440	This study
pEMGΔ*edd*	Km^R; pEMG derivative bearing a 1.0-kb TS1-TS2 *Eco*RI-*Bam*HI insert for deletion of the *edd* gene of *P. putida* KT2440	This study
pEMGΔ*eddΔglk*	Km^R; pEMG derivative bearing a 1.0-kb TS1-TS2 *Eco*RI-*Bam*HI insert for deletion of the *edd* gene of *P. putida* KT2440 Δ*glk*	This study
pEMGΔ*eda*	Km^R; pEMG derivative bearing a 1.0-kb TS1-TS2 *Eco*RI-*Bam*HI insert for deletion of the *eda* gene of *P. putida* KT2440	This study
pEMGΔ*gts*	Km^R; pEMG derivative bearing a 1.0-kb TS1-TS2 *Eco*RI-*Bam*HI insert for deletion of the genes that encoded the sugar ABC transporter by a single deletion event: Δ*gtsA* (*PP_1015*), Δ*gtsB* (*PP_1016*), Δ*gtsC* (*PP_1017*) and Δ*gtsD* (*PP_1018*)	This study
pEMGΔ*pgi-I*	Km^R; pEMG derivative bearing a 1.2-kb TS1-TS2 *Eco*RI-*Bam*HI insert for deletion of the *pgi-I* gene of *P. putida* KT2440	This study

pEMGΔ*pgi-II*	Km^R; pEMG derivative bearing a 1.1-kb TS1-TS2 *Eco*RI-*Bam*HI insert for deletion of the *pgi-II* gene of *P. putida* KT2440	This study
pEMGΔ*gntZ*	Km^R; pEMG derivative bearing a 1.0-kb TS1-TS2 *Sac*I-*Bam*HI insert for deletion of the *gntZ* gene of *P. putida* KT2440	This study
pSW-I^b	Ap^R; *oriV*(RK2), *xylS*, *Pm*→I-*Sce*I, transcriptional fusion of the gene encoding I-*Sce*I to the *Pm* promoter	Wong & Mekalanos (2000)
pAeT41	Ap^R; derivative of cloning vector pUC18 bearing a *ca*. 5-kb *Sma*I/*Eco*RI DNA fragment spanning the *phaC1AB1* gene cluster from *Cupriavidus necator*	Peoples & Sinskey (1989)
pSEVA224	Km^R; standard SEVA expression vector, *oriV*(RK2) *lacI^Q*, P_{trc}	Silva-Rocha *et al.* (2013)
pS224·GPG	Km^R; pSEVA224 derivative bearing *glk* and *pfkA* from Module I, and *gapA* from Module II	This study
pS224·GBI	Km^R; pSEVA224 derivative bearing Module I as an *Avr*II-*Bam*HI insert	This study
pS224·GBII	Km^R; pSEVA224 derivative bearing Module II as a *Bam*HI-*Hin*dIII insert	This study
pSEVA234	Km^R; standard SEVA expression vector, *oriV*(pBBR1) *lacI^Q*, P_{trc}	Silva-Rocha *et al.* (2013)
pS234·GBI	Km^R; pSEVA234 derivative bearing Module I as an *Avr*II-*Bam*HI insert	This study
pSEVA434	Sm^R/Sp^R; standard SEVA expression vector, *oriV*(pBBR1) *lacI^Q*, P_{trc}	Silva-Rocha *et al.* (2013)
pS434·GBI	Sm^R/Sp^R; pSEVA434 derivative bearing Module I as an *Avr*II-*Bam*HI insert	This study
pSEVA424	Sm^R/Sp^R; standard SEVA expression vector, *oriV*(RK2) *lacI^Q*, P_{trc}	Silva-Rocha *et al.* (2013)
pS424·*gapA*	Sm^R/Sp^R; pSEVA424 bearing *gapA* from Module II	This study
pS424·GBI	Sm^R/Sp^R; pSEVA424 derivative bearing Module I as an *Avr*II-*Bam*HI insert	This study
pSEVA438	Sm^R/Sp^R; standard SEVA expression vector, *oriV*(pBBR1) *xylS*, *Pm*	Silva-Rocha *et al.* (2013)
pS438·GBI	Sm^R/Sp^R; pSEVA438 derivative bearing Module I as an *Avr*II-*Bam*HI insert	This study
pS438·*glf*	Sm^R/Sp^R; pSEVA438 derivative bearing *glf* (glucose facilitator) gene from *Zymomonas mobilis* as an *Eco*RI-*Kpn*I insert	This study
pRK600	Helper plasmid used for conjugation; *ori*(ColE1), RK2(*mob$^+$ tra$^+$*); Cm^R	Kessler *et al.* (1992)
pBAMD1-2	Mini-Tn*5* delivery plasmid; *ori*(R6K); Ap^R Km^R	Martínez-García *et al.* (2014a)
pBAMD1-2·*glf*	Derivative of pBAMD1-2; delivery plasmid used to insert *glf* (glucose facilitator) gene from *Zymomonas mobilis* as an *Eco*RI-*Kpn*I insert in the chromosome of recipient *P. putida* strains; Ap^R Km^R	This study

pBAMD1-4	Mini-Tn*5* delivery plasmid; *ori*(R6K); Ap^R Sm^R/Sp^R	Martínez-García *et al.* (2014a)
pBAMD1-4·GBI	Derivative of pBAMD1-4; delivery plasmid used to insert GlucoBrick Module I as an *Avr*II-*Bam*HI insert in the chromosome of recipient *P. putida* strains; Ap^R Sm^R/Sp^R	This study
pBAMD1-6	Mini-Tn*5* delivery plasmid; *ori*(R6K); Ap^R Gm^R	Martínez-García *et al.* (2014a)
pBAMD1-6·GBII	Derivative of pBAMD1-2; delivery plasmid used to insert GlucoBrick Module II as a *Bam*HI-*Hin*dIII insert in the chromosome of recipient *P. putida* strains; Ap^R Gm^R	This study

[a] Antibiotic markers: *Ap*, ampicillin; *Cm*, chloramphenicol; *Km*, kanamycin; *Sm*, streptomycin; *Sp*, spectinomycin; and *Gm*, gentamicin. Ts, temperature-sensitive origin of replication.

[b] This plasmid is the same as pSW(I-*Sce*I) (Wong & Mekalanos, 2000), renamed here as pSW-I for simplicity.

1.3. Culture conditions. *P. putida* cultures were incubated at 30ºC; *E. coli* and *Pseudomonas aeruginosa* were grown at 37ºC. In order to obtain cultures for the propagation and construction of plasmids, *E. coli* strains CC118 and DH5α λ*pir* were grown in Lysogeny Broth (LB) medium (Green & Sambrook, 2012; Martínez-García *et al.*, 2017). For physiology experiments and to obtain cell-free extracts for enzyme activity assays, bacterial cells were grown with rotatory shaking at 170 r.p.m. in 250-ml Erlenmeyer flasks filled with 50 ml of M9 minimal medium, containing 6 g l^{-1} Na_2HPO_4, 3 g l^{-1} KH_2PO_4, 1.4 g l^{-1} $(NH_4)_2SO_4$, 0.5 g l^{-1} NaCl, 0.2 g l^{-1} $MgSO_4·7H_2O$, and 2.5 ml l^{-1} of a trace elements solution (Nikel & de Lorenzo, 2013a). In the case of *E. coli* strains grown in minimal media cultures, $CaCl_2$ was added at 0.1 mM and vitamin B1 was added at 0.05% (w/v). Unless otherwise indicated, minimal medium cultures were added with glucose at 20 mM. In some cultures, isopropyl-1-thio-β-galactopyranoside (IPTG) was added at 1 mM. Some glycolytic mutants of *E. coli* are affected in their growth even in rich LB medium (Thomson *et al.*, 1979); these mutants were grown in M9GCM semi-synthetic medium. This culture medium contains the same salts as M9 minimal medium, but also 0.75% (w/v) amino acids from casein hydrolyzate (Becton-Dickinson Diagnostics Co., Sparks, MD, USA), 10 mM glucose, 20 mM glycerol, 15 mM sodium malate, and 0.05% (w/v) vitamin B1. In the case of *E. coli* Δ*gapA* Δ*epd* and Δ*gapA* Δ*epd* Δ*ptsI* mutants (*i.e.*, deficient in the *epd*-encoded erythrose-4-*P* dehydrogenase), pyridoxine hydrochloride was added to the culture medium at 5 μM (Yang *et al.*, 1998). In order to adapt the cells to growth on glucose from rich LB medium, pre-inocula were prepared with a few isolated colonies from LB medium plates. Those pre-inocula were grown overnight (with the exception of the strains with a lower growth rate, where the pre-inocula were prepared well in advance to provide enough amount of cells) in 10 ml of M9 minimal medium with glucose or M9GCM semi-synthetic medium with the corresponding antibiotics in 100-ml Erlenmeyer flasks. In the case of solid media cultures needed to streak cells, the composition was the same than those applicable in liquid medium with the addition of 15 g l^{-1} of agar. The antibiotics employed for selection were added to the media when needed at the following final

concentrations: ampicillin (Ap), 150 μg ml^{-1} for *E. coli* strains or 500 μg ml^{-1} for *P. putida* strains; streptomycin (Sm), 50 μg ml^{-1} or 80 μg ml^{-1} for *P. putida* strains; gentamicin (Gm), 10 μg ml^{-1}; and kanamycin (Km), 50 μg ml^{-1} with the exception of *P. aeruginosa*, for which 300 μg ml^{-1} Km was needed to select colonies after transformation of plasmids by electroporation. For the construction of *P. putida* mutants, 3-methylbenzoate (3-*m*B) was used at 15 mM to induce the XylS-dependent *Pm* promoter. Experiments for poly(3-hydroxybutyrate) (PHB) accumulation were carried out in LB medium added with glucose at 10 g l^{-1} and the antibiotics and inducers described in the text (in these experiments, 3-*m*B was used at 0.5 mM to induce the expression of the genes in Module II). In order to check the capability of some cultures to grow in gluconeogenic conditions, minimal medium cultures were added with succinate at 30 mM. This concentration was selected for the purpose of obtaining the same concentration of carbon atoms (120 mM) when the cultures were inoculated in glycolytic (glucose) or glunoneogenic (succinate) conditions. For long-term preservation, bacteria (previously grown in LB medium plates) were frozen in LB medium containing 20% (v/v) glycerol and kept at –80ºC.

1.4. Bacterial transformation. The transformation of *E. coli* strains was carried out (i) chemically, by following the RbCl method (Green & Sambrook, 2012) to obtain competent cells, or (ii) by electroporation (Wirth *et al.*, 1989), by following the method described by Datsenko and Wanner (Datsenko & Wanner, 2000). In the case of *P. putida* transformation, electrocompetent cells were obtained by subsequent washings at room temperature with 300 mM sucrose (Choi *et al.*, 2006). For all strains, when appropriate, the electroporation was performed in a Gene Pulser/Pulse Controller (Bio-Rad) system configured as follows: 2.5 kV, 25 μF, 200 Ω.

1.5. DNA manipulation and sequencing. DNA manipulations were carried out following routine laboratory techniques (Green & Sambrook, 2012). Plasmid DNA purification was accomplished with the QIAprep Spin Miniprep kit (Qiagen Inc., Valencia, CA, USA) according to the manufacturer's instructions. Restriction and DNA modification enzymes employed in this study were purchased from New England Biolabs (Ipswich, MA, USA). Isolate colonies from fresh LB plates were the starting material for colony polymerase chain reaction (PCR) amplification in order to check the presence of plasmid or gene deletions/insertion. PCR products were purified with the NucleoSpin Extract II kit (Macherey-Nagel, Düren, Germany). Agarose gel visualization was possible with the use of VersaDoc™ apparatus (Bio-Rad Corp., Hercules, CA, USA). Sanger sequencing (Secugen SL, Madrid, Spain) was used in order to check the accuracy of all the DNA constructs.

1.6. Design of oligonucleotides. Oligonucleotides employed in PCR reactions were designed from the DNA sequence of interest using the software DNASTAR Lasergene Suite v14 (DNASTAR, Inc. Madison, WI, USA). The oligonucleotides used in this study were obtained from Sigma-Aldrich Co. (St. Louis, MO, USA) and are described in **Table 4**.

Table 4 | **Oligonucleotides employed in PCR reactions.**

Name	**Sequence** (5' → 3')	**Tm** (ºC)	**Use**
PP_1011-TS1F-*Eco*RI	G**GA ATT C**GA GGC CCC GGC GCG GGT GTT CCA GGA CCA G	88	Construction of *P. putida* Δ*glk*
PP_1011-TS1R	*CAT CGG GGC CGC AAA GCG CCC CCC TCA GTG* GTG CTT CAT TTG AGG TGC TCC AGG GCC GAG	92	
PP_1011-TS2F	*CAC TGA GGG GGG CGC TTT GCG GCC CCG ATG*	86	
PP_1011-TS2R-*Bam*HI	CG**G GAT CC**C GCC AGT CGT CGA AGG CCA GCA CGG CGT TG	88	
PP_1444-TS1F-*Eco*RI	G**GA ATT C**GC GGC AGT GCC GAG GTG TCG AAG TGG CGG TGG	86	Construction of *P. putida*Δ*gcd*
PP_1444-TS1R	*GGC CTG AAG ATC CAG AGC AGT TTC TAA CCC* GCG ACA CCG CTC CCG CAG GCT CAA CCC TGA GG	89	
PP_1444-TS2F	*GGG TTA GAA ACT GCT CTG GAT CTT CAG GCC*	74	
PP_1444-TS2R-*Bam*HI	CG**G GAT CC**G TCA GCC GGC CGC CCT CAG CGG CGC CGC CT	95	
PP_3382-4-TS1F-*Eco*RI	G**GA ATT C**GT CGT CAG TAA AGG ACG TGA ACG ACT GGA C	76	Construction of *P. putida* Δ*PP_3382-4*
PP_3382-4-TS1R	*CAA GGC CGC CCC ACA GCC GAT GAG GAT TCG* CGT GTT TTT CAG CGC CCT CGC CCG TAG GAG	91	
PP_3382-4-TS2F	*GGG TTA GAA ACT GCT CTG GAT CTT CAG GCC*	74	
PP_3382-4-TS2R-*Bam*HI	CG**G GAT CC**G TCA GCC GGC CGC CCT CAG CGG CGC CGC CT	95	
PP_3623-TS1F-*Eco*RI	G**GA ATT C**TT GTC CGG CGG CTG GAA GCG CGG ACC GTT C	85	Construction of *P. putida* Δ*PP_3623*
PP_3623-TS1R	*CAG CCT CGC GTC GGT ACA TGT GCC ACT CCA* AGG CGT CCC TTG TGC GAT CAG CTG AAG GTG	89	
PP_3623-TS2F	*TGG AGT GGC ACA TGT ACC GAC GCG AGG CTG*	81	
PP_3623-TS2R-*Bam*HI	CG**G GAT CC**T CAT CTG GGT GCG CCA GGA CAA TGC CTT TG	83	
PP_4232-TS1F-*Sac*I	C**GA GCT C**GC CGA CAC GCA AGC GCA CCC GGG CAT TTT C	87	Construction of *P. putida* Δ*PP_4232*
PP_4232-TS1R	*CGA TCT CGG CCT GGT CAA GGA GGG TTG AAC* AGC GTG CAG CAT CTC GAT CTA CAG GTG ATC	85	
PP_4232-TS2F	*GTT CAA CCC TCC TTG ACC AGG CCG AGA TCG*	78	
PP_4232-TS2R-*Bam*HI	CG**G GAT CC**C CGG TCG GGC CGG TCG AGG TTC CCG CGG AC	92	

PP_1010-TS1F-*Ecor*RI	G**GA ATT C**GC ACT GAC CGC GAT ACG GTC	75	Construction of *P. putida* Δ*edd*
PP_1010-TS1R	*CAC CAA CCA GCA GGT GCT TCA T*GT ACT GGA CTC CAG GCT AAT TG	80	
PP_1010-TS2F	*ATG AAG CAC CTG CTG GTT GGT G*	71	
PP_1010-TS2R-*Bam*HI	CG**G GAT CC**C CTA CCG GCA GGT CAA CAT G	79	
PP_1010(Δ*glk*)-TS1R	*GCA AAG CGC CCC CCT CAG TG*G TAC TGG ACT CCA GGC TAA TTG	83	In combination with *PP_1010*-TS1F-*Ecor*RI and *PP_1010*-TS2R-*Bam*HI to remove *edd* gene in *P. putida* Δ*glk*
PP_1010(Δ*glk*)-TS2F	*CAC TGA GGG GGG CGC TTT GC*	75	
PP_1024-TS1F-*Eco*RI	G**GA ATT C**GT CAC TGT CAG CCT GGC TGA	75	Construction of *P. putida* Δ*eda*
PP_1024-TS1R	*CGT AAA GCA CAC AAC TGT TT*T CAT GGG CAC CAG TAG ATG T	76	
PP_1024-TS2F	*AAA CAG TTG TGT GCT TTA CG*	61	
PP_1024-TS2R-*Bam*HI	CG**G GAT CC**C AAG GGC AAC GGC GCC CTG G	86	
PP_1015-8-TS1F-*Eco*RI	G**GA ATT C**GC ATT GTT CGA CAC AGC CTG	72	Construction of *P. putida* ΔGts
PP_1015-8-TS1R	*TTA TTG ATG GTG TAG ACG AG*C GGA GCA CCT TTC TTG TTG T	76	
PP_1015-8-TS2F	*CTC GTC TAC ACC ATC AAT AA*	58	
PP_1015-8-TS2R-*Bam*HI	CG**G GAT CC**G TCG AAG TAC TTC TGC TTG A	74	
PP_1808-TS1F-*Eco*RI	ATT T**GA ATT C**AC ATC GAC GAC TTC CGC CAC	64	Construction of *P. putida* Δ*pgi-I*
PP_1808-TS1R	*AAG ATC CTT GAT ACG GGT AAA GCC AG*	64	
PP_1808-TS2F	*CTG GCT TTA CCC GTA TCA AGG ATC TT*C CCT GCT TGA TAC TGG CCC G	66	
PP_1808-TS2R-*Bam*HI	ATT T**GG ATC C**CT CAG AGG GGT CTC GGC AGG	65	
PP_4701-TS1F-*Eco*RI	ATT T**GA ATT C**AC CTG AAT ATG CCG ATC CAG ATC ATC	65	Construction of *P. putida* Δ*pgi-II*
PP_4701-TS1R	*GTG CGT GGT GAG GGC TTG G*	66	

PP_4701-TS2F	*CCA AGC CCT CAC CAC GCA C*TC GCG GGT AAA CCC GCC TAC	67	
PP_4701-TS2R-*Bam*HI	ATT T**GG ATC C**CG CCT TTC TTC ACA CCG CG	66	
PP_4043-TS1F-*Sac*I	C**GA GCT C**CT GGC CAG GTC GGT GCC GAA	83	Construction of *P. putida* Δ*gntZ*
PP_4043-TS1R	*CGA AAA GGG AGC ATT GGC TC*A TGA CTA AAC AGA CCC TTG C	78	
PP_4043-TS2F	*GAG CCA ATG CTC CCT TTT CG*	67	
PP_4043-TS2R-*Bam*HI	CG**G GAT CC**G ATG AAG GAC AGC CGC TTG C	79	
pSW-F	GGA CGC TTC GCT GAA AAC TA	65	Presence of pSW-I
pSW-R	AAC GTC GTG ACT GGG AAA AC	65	

Bold letters indicate recognition site for the restriction enzymes and the complementary sequences used in splicing-by-overlap extension (*SOEing*; Horton, 1995; Nikel & de Lorenzo, 2013b) PCR amplifications are shown in italics.

1.7. Construction of *P. putida* mutant strains. Clean *P. putida* knock-out mutants were obtained following the protocol described by Martínez-García & de Lorenzo (2011). These mutants are listed and described in **Table 2**. The method is based on the use of the suicide pEMG vector, where long flanking regions are cloned upstream and downstream of the target gene(s) by PCR, using chromosomal DNA from strain KT2440 as the template. The oligonucleotides employed to amplify these *ca*. 500-bp long flanking regions (TS1, upstream; and TS2, downstream) are described in **Table 4**. A 1-kbp amplification product (*i.e.*, spanning the TS1-TS2 regions flanking target gene or group of genes, indicated with "*x*") were obtained using the two 500-bp amplicons mentioned above as the template and the external oligonucleotides (*i.e.*, *x*-TS1F and *x*-TS2R) by splicing-by-overlap extension (*SOEing*) PCR (Horton, 1995; Nikel & de Lorenzo, 2013b). The TS1-TS2 DNA fragments were digested with *Eco*RI and *Bam*HI (except in the cases indicated in **Table 3**), cloned into the I-*Sce*I–bearing pEMG vector digested with the same enzymes (giving rise to plasmid pEMGΔ*x*) and verified by enzyme restriction and Sanger DNA sequencing. The resulting pEMGΔ*x* vectors were electroporated in *P. putida* KT2440 in order to force cointegration events (this plasmid lacks a compatible origin of replication for *Pseudomonas* species). Merodiploids were selected by plating bacteria in LB medium plates containing Km and subsequently isolating to check by PCR reaction using oligonucleotides *x*-TS1F and *x*-TS2R. Once a suitable cointegration event was obtained, the selected bacterial clone was transformed with plasmid pSW-I and selected in LB medium plates containing Ap. In order to facilitate the recombination process (mediated by the I-*Sce*I endonuclease) that allows the deletion event, the mentioned strains were incubated for 6 h in 5 ml of LB medium containing 500 μg ml^{-1} Ap and 15 mM 3-*m*B. The resulting cultures were plated onto LB medium plates to obtain individual colonies, that were

restreaked onto LB medium with or without Km to check for the loss of the cointegrated plasmid. The Km-sensitive clones were analyzed by colony PCR (using the pair of oligonucleotides *x*-TS1F and *x*-TS2R) to distinguish between deletion or revertant [*i.e.*, wild-type (WT)] events. As a final step, the pSW-I plasmid was eliminated from the treated strains after several consecutive passes in liquid LB medium. In order to verify the elimination of the plasmid pSW-I, all the candidates were plated onto LB medium plates with 500 μg ml^{-1} Ap and checked by PCR using the oligonucleotides pSW-F and pSW-R, which hybridize in the sequence of the pSW-I plasmid (Martínez-García & de Lorenzo, 2011).

1.8. Construction of *E. coli* mutant strains. Mutations in glycolytic genes were accumulated in *E. coli* derivatives *via* sequential transduction of individual alleles with bacteriophage P1 (Godoy *et al.*, 2015; Nikel & de Lorenzo, 2013b) using individual mutants from the KEIO collection (Baba *et al.*, 2006) as donors, followed by elimination of the antibiotic resistance marker using plasmid pCP20 (Cherepanov & Wackernagel, 1995).

1.9. DNA delivering using mini-Tn*5* transposons. The stable insertion of foreign DNA into the chromosome of different *P. putida* mutants was carried out with the mini-Tn*5* transposon borne by the synthetic pBAMD plasmids (Martínez-García *et al.*, 2014a). The method to deliver DNA between different strains involved tripartite conjugative mating. *E. coli* CC118 λ*pir* (carrying the pBAMD construct) was used as the donor strain, along with the mating-helper strain *E. coli* HB101 (carrying pRK600), and the appropriate *P. putida* mutants as the recipients. The conjugative mating was conducted as described elsewhere (Martínez-García & de Lorenzo, 2012). Briefly, bacteria were grown in LB medium overnight with the appropriate combination of antibiotics, then the cells were diluted to obtain an optical density at 600 nm (OD_{600}) of 1. These cultures were washed twice with 10 mM $MgSO_4$ in order to remove the antibiotics from the culture medium, and each cell suspension was added to a 10-ml plastic tube with 5 ml of 10 mM $MgSO_4$ to obtain a final OD_{600} of *ca*. 0.03. After mixing these suspensions gently, the content of the tube was concentrated by filtration and the cells were laid onto a filter disk (0.45 μm pore-size, 23 mm diameter, EMD Millipore Corp., Billerica, MA, USA). The filter disks were placed onto a LB medium plate and the plates were incubated at 30ºC for 6 h. The filters were placed separately in 10-ml plastic tubes with 5 ml of 10 mM $MgSO_4$, and the biomass was suspended by vortexing the contents 10 s. The suspensions were diluted appropriately and plated onto M9 minimal medium plates with 0.2% (w/v) citrate and the appropriate antibiotics to select *P. putida* over *E. coli*.

1.10. *In silico* prediction of gene functions. In order to hypothesize about the function of genes without previous experimental validation, an *in silico* approach was employed based on the use of different well-implemented genome databases. The web resources used in this Thesis were the MicroScope platform (Genoscope, Evry, France; http://www.genoscope.cns.fr/agc/microscope) and the *Pseudomonas* Genome

Database (Simon Fraser University, British Columbia, Canada; http://www.pseudomonas.com) (Vallenet *et al.*, 2017; Winsor *et al.*, 2016).

1.11. Statistical Analysis. All the experiments reported were independently repeated at least twice (as indicated in the corresponding figure or table legend), and the mean value of the corresponding parameter ± standard deviation is presented. In some cases, the level of significance of the differences when comparing results was evaluated by means of the Student's *t* test with $\alpha = 0.05$.

2. Biochemical characterization

2.1. Preparation of bacterial cell-free extracts. Cell-free extracts of *E. coli*, *P. putida*, and *P. aeruginosa* were obtained by a modification of published protocols (Chavarría *et al.*, 2016; Nikel *et al.*, 2014a). Enzyme activity determinations were carried out in cell-free extracts obtained from bacterial cultures harvested during the mid-exponential phase of growth (corresponding to an OD_{600} of 0.5) or, in some specific experiments, after 24 h of incubation. Cell-free extracts were obtained from 50 ml of culture broth (in 250-ml Erlenmeyer flasks). Biomass was collected by centrifuging the cultures at 4,000 r.p.m. for 15 min at 4ºC. Cell pellets were washed twice with 25 ml of pre-cooled 67 mM potassium phosphate buffer (pH = 7.1) at 4ºC. From this step onwards, the protocol followed to obtain the cell-free extract was modified depending on the location of the enzyme (*i.e.*, membrane-bound or cytoplasm). In the case of enzymes located or associated with the cell membrane (*e.g.*, Gcd and Gad activities), the resulting pellets were suspended in 2-ml Eppendorf tubes with the appropriate volume of pre-cooled 60 mM glycylglycine buffer (pH = 7.1) to obtain a cell density of 0.2 g of cells (wet weight) per milliliter of buffer. The suspensions were sonicated in seven 30-s intervals separated by 1.5 min rests in ice to avoid heating of the sample (18-20 kHz, 1.0-1.5 A). At this point, the mixtures were centrifuged at 13,000 r.p.m for 30 min at 4ºC to remove the insoluble cell debris. Cell-free extracts were stored at –20ºC until use.

In the case of cytoplasmic enzymes, pellets were washed with 67 mM potassium phosphate buffer obtained as explained above, and bacteria were resuspended in 1 ml of the same buffer and centrifuged in 2-ml Eppendorf tubes at 8,000 r.p.m. for 10 min at 4ºC. After carefully removing the supernatant, the cell wet weight was obtained for each pellet in order to calculate the volume of reagents needed for protein extraction using the Novagen BugBuster™ protocol (EMD Millipore Corp., Billerica, MA, USA). Pellets and cell-free extracts were kept on ice throughout the whole procedure. Bacterial lysis was achieved by using 5 ml of BugBuster™ Protein Extraction Reagent per gram of cell paste. Afterwards, 1 µl of Lysonase™ Bioprocessing Reagent was added per 1 ml of BugBuster™ Protein Extraction Reagent used for re-suspension of the cells. Bacteria were lysed by shaking for 20 min at room temperature in a Rotamax 120 orbital shaker (Heidolph Instruments GmbH & Co. KG, Schwabach, Germany) at 150 r.p.m. The insoluble

cell debris was removed by centrifugation at 13,000 r.p.m. for 20 min at 4ºC and the supernatants (*i.e.*, cell-free extracts) were stored at –20ºC until use.

2.2. *In vitro* enzymatic assay. In order to determine the activity of three key glycolytic enzymes (Glk, Pfk, and GA3P dehydrogenase), the *in vitro* assays were carried out at 30ºC when using cell-free extracts from *P. putida* or at 37ºC when using cell-free extracts from *P. aeruginosa* and *E. coli*. The remaining activities were measured at 25ºC as indicated by Sigma-Aldrich Co. (St. Louis, MO, USA) in the corresponding enzymatic assay protocols or by following previously described protocols (Ng & Dawes, 1973; Nikel *et al.*, 2014a). All the enzymes were assessed under the optimal reported conditions for pH, substrate, and cofactor concentration (Chavarría *et al.*, 2013; Nikel & Chavarría, 2016; Nikel *et al.*, 2014a; 2015a). *In vitro* assays were conducted in Nunc™ MicroWell™ 96-well microplates (Thermo Fisher Scientific Inc., Waltham, MA, USA) in a SpectraMax™ M2e multi-mode microplate reader (Molecular Devices LLC, Sunnyvale, CA, USA). All the specific enzyme activities are reported as nmol substrate converted min^{-1} mg of $protein^{-1}$. Protein concentration in cell-free extracts was assessed using the Bradford (Bradford, 1976) Protein Assay (Bio-Rad Laboratories Inc., Hercules, CA, USA). All the accessory enzymes (with the exceptions indicated below) were from *Saccharomyces cerevisiae* and they were purchased from Sigma-Aldrich Co. An extinction coefficient ($\varepsilon_{NADP/H}$) of 6.22 mM^{-1} cm^{-1}, representing the difference between the extinction coefficients of NAD(P)H and $NAD(P)^+$. In the case of dichlorophenolindophenol (DCPIP) the extinction coefficients were determined as 4.1 mM^{-1} cm^{-1} at 600 nm (pH = 5.5) and 9.1 mM^{-1} cm^{-1} at 576 nm (pH = 5.5). The limit of detection for all the enzymatic assays was consistently below 2-5 nmol min^{-1} $mg_{protein}^{-1}$. The specific protocols used for the determinations are detailed below.

Aldolase. *Fructose-1,6-P_2 aldolase* (EC 4.1.2.13). The reaction mixture contained 17.3 μl of 1 M Tris·HCl buffer (pH = 7.4), 6.7 μl of 58 mM fructose-1,6-P_2, 1.9 μl of 14 mM NADH, 6.7 μl of α-glycerophosphate dehydrogenase/triosephosphate isomerase from rabbit muscle (50 units ml^{-1} each), 165.4 μl of water, and 2 μl of cell-free extract (or an appropriate dilution in 67 mM potassium phosphate buffer, pH = 7.1). The decrease in absorbance at 340 nm (A_{340}) was measured during the assay.

Edd. *6-Phosphogluconate dehydratase* (EC 4.2.1.12). The Edd activity was assayed in a two-step reaction protocol obtained by modification of previously published methods (Baumann & Baumann, 1975; Ponce *et al.*, 2005; Vicente & Cánovas, 1973a). The assay mixture contained in a final volume of 0.1 ml: 50 mM Tris·HCl buffer (pH = 7.5), 10 mM $MgCl_2$, 10 μM gluconate-6-*P*, and an appropriate dilution of cell-free extract. This mixture was incubated for 5 min at room temperature and diluted with the same reaction buffer up to 2 ml. The mixture was heated for 2 min at 95ºC and centrifuged at 14,000 r.p.m. during 10 min at room temperature. The supernatant solution was assayed for pyruvate formation by using a mixture that contained 20 μl of the supernatant and 180 μl of a solution containing 50 mM Tris·HCl buffer (pH = 7.5), 10 mM $MgCl_2$,

1mM EDTA, 0.1 mM NADH, and 0.5 U L-lactate dehydrogenase from bovine heart. The decrease in A_{340} was measured during the assay at 37ºC.

Gad. *Gluconate 2-dehydrogenase* (EC 1.1.99.3). The reaction mixture contained 40 μl of 100 mM sodium acetate buffer (pH = 5.5), 16.7 μl of 75 mM sodium gluconate, 6.7 μl of 15 mM KCN, 33.2 μl of DCPIP (0.5 mg l^{-1}), 96.7 μl of water, and 6.7 μl of cell-free extract (or an appropriate dilution in 100 mM sodium acetate buffer pH = 5.5). The decrease in absorbance at 576 nm (A_{576}) was measured during the assay.

Gcd. *Glucose dehydrogenase* (EC 1.1.1.47). The reaction mixture contained 66.7 μl of 100 mM sodium acetate buffer (pH = 5.5), 36.7 μl of 75 mM glucose, 6.7 μl of 15 mM KCN, 13.2 μl of DCPIP (0.5 mg l^{-1}), 70 μl of water, and 6.7 μl of cell-free extract (or an appropriate dilution in 100 mM sodium acetate buffer pH = 5.5). The decrease in absorbance at 600 nm (A_{600}) was measured during the assay.

Glk. *ATP–D-Hexose 6-phosphotransferase* or *glucokinase* (EC 2.7.1.1). The reaction mixture contained 67 μl of 120 mM Tris·HCl buffer (pH = 8.2), 26 μl of 500 mM glucose, 8 μl of 250 mM $MgCl_2$, 53 μl of 36 mM ATP, 10 μl of 20 mM $NADP^+$, 13 μl of glucose-6-*P* dehydrogenase (15 units ml^{-1}), 18 μl of water, and 5 μl of cell-free extract (or an appropriate dilution in 67 mM potassium phosphate buffer, pH = 7.1). The increase in A_{340} was measured during the assay.

GntZ. *6-Phosphogluconate dehydrogenase* (EC 1.1.1.44). The reaction mixture contained 188.4 μl of 100 mM glycylglycine buffer (pH = 7.5), 3.4 μl of 100 mM 6-phosphogluconate, 6.9 μl of 60 mM NAD^+, and 1.3 μl of cell-free extract (or an appropriate dilution in 100 mM glycylglycine buffer, pH = 7.5). The increase in A_{340} was measured during the assay.

Pgi. *Glucose-6-P isomerase* (EC 5.3.1.9). The reaction mixture contained 33.3 μl of 240 mM glycylglycine buffer (pH = 7.1), 6.7 μl of 100 mM D-fructose-6-*P*, 6.7 μl of 20 mM $NADP^+$, 6.7 μl of 100 mM $MgCl_2$, 6.7 μl of glucose-6-*P* dehydrogenase (50 units ml^{-1}), 133.2 μl of water, and 6.7 μl of cell-free extract (or an appropriate dilution in 67 mM potassium phosphate buffer, pH = 7.1). The increase in A_{340} was measured during the assay.

Pfk. *6-Phosphofructo-1-kinase* (EC 2.7.1.11). The reaction mixture contained 20 μl of 1 M Tris·HCl buffer (pH = 7.5), 2 μl of 100 mM fructose-6-*P*, 8 μl of 250 mM $MgCl_2$, 4 μl of 100 mM NH_4Cl, 4 μl of 10 mM NADH, 6 μl of 36 mM ATP, 4 μl of fructose-1,6-P_2 aldolase (50 units ml^{-1}), 1.5 μl of triosephosphate isomerase (500 units ml^{-1}), 1.5 μl of glycerol-3-*P* dehydrogenase from rabbit muscle (170 units ml^{-1}), 144 μl

of water, and 5 μl of cell-free extract (or an appropriate dilution in 67 mM potassium phosphate buffer, pH = 7.1). The decrease in A_{340} was measured during the assay.

Tpi. *Triose-P isomerase* (EC 5.3.1.1). The reaction mixture contained 20 μl of 1 M triethanolamine buffer (pH = 7.9), 2 μl of 0.5 M EDTA, 4 μl of glycerol-3-*P* dehydrogenase from rabbit muscle (17 units ml^{-1}), 2 μl of 40 mM D,L-glyceraldehyde-3-*P*, 2 μl of 14 mM NADH, 168 μl of water, and 2 μl of cell-free extract (or an appropriate dilution in 67 mM potassium phosphate buffer, pH = 7.1). The decrease in A_{340} was measured during the assay.

3. Analytical determinations

3.1. Measurement of poly(3-hydroxybutyrate) (PHB) content. The amount of PHB was obtained by means of gas chromatography following protocols described in the literature (Nikel *et al.*, 2006). Approximately 10 mg of freeze-dried biomass (0.01 mPa; 8 h) was weighed and deposited in Teflon-stoppered vials. Methanolysis was carried out by addition of 2 ml of CH_3OH/H_2SO_4 (85:15 [v/v]) and 2 ml of $CHCl_3$. These samples were heated at 100ºC for 150 min, cooled at room temperature, and mixed with 2 ml of 1 M $NaHCO_3$. Then, the aqueous phase was discarded, and the organic phase was extracted twice with the use of deionized water. Once the sample settled all the layers, the lower phase was removed drying with anhydrous Na_2SO_4. The methyl esters of 3-hydroxybutyrate were quantified in a Hewlett Packard HP 5890 gas chromatograph equipped with a Hewlett Packard FFAP column. Pure PHB (Sigma Aldrich Co.) was used as a standard for the calibration, and the PHB content was defined as the ratio of grams of PHB per grams of cell dry weight (CDW).

3.2. Determination of intracellular concentration of acetyl-coenzyme A. The intracellular concentration of acetyl-coenzyme A (CoA) was determined by liquid chromatography coupled to mass spectrometry (LC-MS) as previously described (Pflüger-Grau *et al.*, 2011). To this end, the biomass content in 2 ml of cultures was harvested by fast centrifugation at 14,000 r.p.m. during 20 s and the pellets were immediately frozen in liquid N_2 to quench the cell metabolome (Hajjaj *et al.*, 1998). Acetyl-CoA was then extracted from biomass with 0.5 ml of 60% (v/v) ethanol buffered with 25 mM ammonium acetate (pH = 7.2) at 70ºC for 1 min (Fuhrer & Sauer, 2009). The liquid extracts were pooled in a new tube and dried at 120 μbar to obtain a dried sample which was resuspended in 100 μl of MilliQ water. Acetyl-CoA was measured in an Agilent model 1200 SL high-performance liquid chromatograph (HPLC) coupled with a hybrid triple-quadrupole/linear ion trap mass spectrometer, model 4000 Q TRAP™ (Applied Biosystems) equipped with a turbo ion spray source. The chromatographic interpretation was made possible by adopting the Gao's method (Gao *et al.*, 2007), and normalizing the results with a 1 μg ml^{-1} acetyl-CoA (Sigma Aldrich Co.) standard.

3.3. Glucose concentration. All the experiments requiring measurement of glucose concentration were performed by adapting a protocol based on the glucose (GO) assay kit (Sigma-Aldrich Co.). This method was used to quantify residual glucose in culture supernatants in 96-well microtiter plates (Nunclon™Δ Surface; Nunc A/S, Roskilde, Denmark). The assay reagent was prepared as indicated in the technical bulletin; the final mix per well contained 80 μl of the assay reagent, 40 μl of the sample (diluted with water to approximately 20-80 μg glucose ml^{-1}), and 80 μl of 12 N H_2SO_4. The amount of the final pink-colored product (oxidized *o*-dianisidine) was quantified at 540 nm using a SpectraMax M2e plate reader (Molecular Devices, LLC., Sunnyvale, CA, USA).

4. Determination of phenotypic parameters

4.1. Phenotypic MicroArray™ technology. The Phenotypic MicroArray™ (PM) technology provided by Biolog Inc. (Biolog, Hayward, CA, USA) was used to obtain a global view of the physiological consequences of eliminating the Pgi activity in *P. putida* KT2440 (Bochner, 2009; Bochner *et al.*, 2001). The set-up for this PM analysis was the *full array*, which evaluates a set of 20 different plates (*i.e.* PM1-PM20) to index metabolic and stress-related differences between the mutant and the WT strain. This approach allowed to test the influence of different carbon, nitrogen, phosphorous and sulphur sources, extreme pH conditions, nutrient supplements, osmolytes, and the sensitivity to a collection of stressors. PM registered the kinetics of bacterial respiration using the reduction of tetrazolium dye as a general physiological indicator. Respiration ratios, either negative or positive, depending on whether the mutant respiration decreased or increased with respect to the WT strain, were used to quantify the phenotypes of the Pgi mutant strain.

4.2. Stress resistance determination. Paraquat was employed as an oxidative stressor agent. This molecule catalyzes the formation of reactive oxygen species and decreases the NADPH cellular pool (Bus & Gibson, 1984), allowing us to determine the amount of available reducing power in different strains. This stressor was use in two different experimental approaches: (i) quantitative, obtaining a *survival ratio*, or (ii) qualitative, determining the *zone of inhibition in agar diffusion tests*. The approach used to obtain survival ratios is based on a previously published method (Martínez-García *et al.*, 2014d) and was performed in liquid cultures. Pre-inocula were grown overnight in M9 minimal medium containing glucose and subsequently diluted to an OD_{600} of 0.05 in the same medium with and without paraquat at 10 μM. Then, bacterial growth was monitored by measuring the OD_{600} in 96-well microtiter plates (Nunclon™Δ Surface; Nunc A/S, Roskilde, Denmark) for 24 h in a SpectraMax™ M2e multi-mode microplate reader (Molecular Devices LLC, Sunnyvale, CA, USA). Finally, the survival ratio was calculated as the OD_{600} in cultures containing paraquat *vs*. the OD_{600} in cultures without the stressor. The second approach (*i.e.*, qualitative) is based on zones of inhibition in agar diffusion test. These zones of inhibition were assessed by using the top-agar approach. To this end, M9 minimal medium plates, containing glucose as the carbon source, were

prepared as indicated in the section *Culture conditions*. On the other hand, 5 ml of M9 minimal medium containing glucose and 7 g l^{-1} of agar was prepared in a pool of tubes pre-heated at 40ºC. Cultures of the strains to be tested were diluted in these tubes to an OD_{600} of 0.05, and the suspensions were subsequently spread homogeneously in the surface of the previously prepared plates. When the two layers were completely solidified, a porous paper disc, soaked with a 10 μl of 100 μM paraquat, was placed in the middle of the plate. Inhibition zones were determined after incubation of the plates at 30°C during 24 h.

4.3. Biofilm formation assay. Biofilm formation was measured by means of a crystal violet assay (Nikel *et al.*, 2013; O'Toole & Kolter, 1998). The different strains were grown in 96-well microtiter plates (Nunclon™Δ Surface; Nunc A/S, Roskilde, Denmark) with M9 minimal medium containing glucose for 24 h at 30ºC without shaking. Then, the culture was removed from the wells and transferred in a new 96-well microtiter plate to calculate the OD_{600} for the planktonic amount of cells using a SpectraMax™ M2e multi-mode microplate reader (Molecular Devices LLC, Sunnyvale, CA, USA). After washing the initial wells three times with H_2O, 200 μl of 0.1% (w/v) crystal violet was added to the plates, which were then incubated 30 min at room temperature. Once the solution was discarded, the crystal violet associated with the biofilm was dissolved by addition of 150 μl of 33% (v/v) acetic acid and gentle shaking during 1 h at room temperature. The amount of crystal violet associated to biofilm was measured in a SpectraMax™ M2e multi-mode microplate reader at 560 nm, and the obtained data were normalized to the OD_{600} of each culture to obtain the biofilm indexes.

5. Metabolic flux analysis and LC-MS/MS

5.1. Quantitative physiology. Physiological parameters for metabolic flux analysis were calculated as previously indicated in the literature (Nikel & Chavarría, 2016). The strains under study were grown in 1000-ml Erlenmeyer flasks with 200 ml of M9 minimal medium with glucose as the carbon source. Cell growth was monitored spectrophotometrically by measuring the OD_{600} and the concentration of glucose was obtained with the glucose (GO) assay kit (Sigma-Aldrich Co.) as indicated in the supplier's manual. The following physiological parameters were determined by regression analysis during the exponential growth phase in batch cultures (Nikel & Chavarría, 2016): biomass yield on glucose ($Y_{x/s}$), maximum specific growth rate (μ), and specific rate of glucose consumption (q_S). The correlation factor (k) between OD_{600} and CDW were obtained from batch cultures of each strain. CDW concentration was calculated from at least four parallel 10-ml cell suspension by centrifugation at 4,000 r.p.m at 4 ºC for 10 min. Bacterial pellets were freeze-dried for 24 h and weighed.

5.2. Determination of metabolite concentration by LC-MS/MS. Bacterial cultures were grown until they reached mid-exponential phase (*i.e.* OD_{600} of *ca*. 0.5), at which point the biomass corresponding to 0.5-0.6 mg of CDW was collected in triplicates by fast centrifugation (13,000 r.p.m., 30 s, –4 ºC). Cultures were grown on either 100% [1-^{13}C]-glucose (Cambridge Isotope Laboratories, Inc.) or 100% [6-^{13}C]-glucose (Cambridge Isotope Laboratories, Inc.) as the sole carbon source, harvested, and processed as described above. The ^{13}C labelling patterns of free intracellular metabolites were determined on the system mentioned above for dihydroxyacetone-*P* (DHAP), F6P, FBP, G6P, 6PG, phosphoenolpyruvate (PEP), ribose-5-*P* (R5P), ribulose-5-*P* (Ri5P), sedoheptulose-7-*P* (S7P), xylulose-5-*P* (X5P), and Pyr as described previously (Rühl *et al.*, 2012). Bacterial pellets were immediately frozen in liquid N_2. Samples were extracted three times with 0.5 ml of 60% (v/v) ethanol buffered with 10 mM ammonium acetate (pH = 7.2) at 78ºC for 1 min. After each extraction step, the biomass was separated by centrifugation at 13,000 r.p.m. for 1 min. The three liquid extracts were pooled in a new tube and dried at 120 μbar, and finally stored at –80ºC. Samples were resuspended in 20 μl of Milli-Q water and injected into a Waters Acquity UPLC system (Waters Corp., Mildford, MA, USA) with a Waters Acquity T3 column (150 mm × 2.1 mm × 1.8 μm, Waters Corp.) coupled to a Thermo TSQ Quantum Ultra triple quadrupole instrument (Thermo Fisher Scientific Inc., Wattham, MA, USA) with electrospray ionization. The quantitative analysis of raw metabolic data and the normalization procedure were conducted as explained by Nikel *et al.* (2015a) and van der Werf *et al.* (2008).

5.3. Metabolic flux ratio analysis by gas chromatography coupled to mass spectrometry (GC-MS). Either 100% [1-^{13}C]-glucose (Cambridge Isotope Laboratories, Inc.), or a mixture of 20% (w/w) [U-^{13}C]-glucose (Cambridge Isotope Laboratories, Inc.) and 80% (w/w) natural glucose were added to the cultures used for metabolic flux ratio analysis. Culture aliquots of 5 ml were harvested in mid-exponential growth by centrifugation at 4,000 r.p.m at 4 ºC for 10 min. Bacterial pellets were washed twice with 1 ml of 0.9% (w/v) NaCl, then hydrolyzed in 1 ml of 6 M HCl for 24 h at 110 ºC in sealed 2-ml Eppendorf tubes, and desiccated overnight in a heating block at 85ºC under a constant air stream. The hydrolysate was dissolved in 50 μl of 99.8% (w/v) dimethyl formamide and subsequently transferred into a new tube. For derivatization, 30 μl of *N*-methyl-N-(*tert*-butyldimethylsilyl)-trifluoroacetamide was added and the mixture was incubated at 85 ºC for 60 min. The ^{13}C labelling patterns of proteinogenic amino acids were determined injecting 1 μl of the derivatized sample into a 6890N Network GC apparatus (Agilent Technologies) combined with a 5875 inert XL mass selective detector (Agilent Technologies) and analyzed as described previously (Dauner & Sauer, 2000; Fischer & Sauer, 2003). The corrected mass distributions were correlated to the *in vivo* metabolic activities obtained by the previously described measured of physiological parameters and statistical-data treatment of metabolic-flux ratio analysis (Fischer & Sauer, 2003) using the program ratio FiatFlux software (Zamboni *et al.*, 2005).

6. Constraint-based genome-scale metabolic models and flux balance analysis

Flux balance analysis (FBA) was used to predict the distribution of metabolic fluxes based on the mathematical representation of different metabolic reactions. A numerical matrix was built, representing the stoichiometric coefficients for the enzymes in the upper catabolism of strain KT2440 (Edwards *et al.*, 2002; Orth *et al.*, 2010). The metabolic network employed by FBA can be represented as a stoichiometry matrix (S), in which each row represents a unique metabolite and each column represent a biochemical reaction. The values in the columns of the matrix indicate the stoichiometric coefficients of the metabolites in the reaction in such a way that if the metabolite is produced it has a positive value and, when the metabolite is consumed, the value is negative. The size of S is $m \times n$ for a network based on m metabolites and n reactions. The vector x with length m then can be defined as the concentrations of all the metabolites and the vector v with length n contains the fluxes through each reaction. A mass balance can be represented: $\frac{dx}{dt} = Sv$ or at steady state: $0 = Sv$. This equation was used to define the space of possible solutions for the flux distribution (v) in the network. An objective function was obtained as $c^T v$, where c are the objective concentrations of the metabolites. Finally, the canonical notation for such linear problem is $c^T v$ subject to $Sv = 0$ ($lowerbound < v < upperbound$). The FBA algorithm solves this objective function defining a maximum growth parameter. The COBRA toolkit (Schellenberger *et al.*, 2011) employed linear programming to obtain v , based on the constraints of the model. In the present Thesis, the *P. putida* model *i*JN746 was used as a backbone (Nogales *et al.*, 2008), to simulate the Pgi mutation by adopting information from the literature (Burgard *et al.*, 2003). The aerobic growth was modeled with an *in silico* M9 minimal medium (*i*M9) following data from the literature for external metabolites and oxygen uptake rate (Nogales *et al.*, 2008). To construct condition-specific metabolic models, the glucose uptake rates experimentally determined (q_S) for each strain were used as extra constraints. In addition, several reactions were constrained using ^{13}C-based metabolic flux analysis from *P. putida* KT2440 (Nikel *et al.*, 2015a). The units indicated in the fluxes are represented as $mmol_{glucose}\ g_{CDW}^{-1}\ h^{-1}$.

IV. RESULTS

«*There is no success without hardship*»
Sophocles
(496 BC-406 BC)

CHAPTER 1

The GlucoBrick system: A genetic tool for *à la carte* engineering of glycolytic activities in Gram-negative bacteria*

* The contents of this chapter have been published as:

Alberto Sánchez-Pascuala, Víctor de Lorenzo & Pablo I. Nikel (2017) Refactoring the Embden-Meyerhof-Parnas Pathway as a whole of portable GlucoBricks for implantation of glycolytic modules in Gram-negative bacteria. *ACS Synth. Bio*., 2017, 6 (5), pp 793–805. DOI: 10.1021/acssynbio.6b00230.

Background

The EMP pathway is widely accepted to be the biochemical standard of glucose catabolism. The well-characterized glycolytic route of *Escherichia coli*, based on the EMP catabolism, is an example of a very intricate pathway in terms of genomic organization and patterns of gene expression and regulation (Papenfort *et al.*, 2013). This intrinsic metabolic complexity renders it difficult to engineer glycolytic activities and transfer them to other microorganisms, thus limiting the enormous biotechnological potential of this pathway in bacterial hosts that lack the route. Taking into account the potential applications of such a portable tool for targeted pathway engineering, the genes encoding all the enzymes of the linear EMP route have been individually recruited from the genome of *E. coli* K-12, edited *in silico* to remove their endogenous regulatory signals, and synthesized *de novo* following a standard (*i.e.*, *GlucoBrick*) that facilitates their grouping in the form of functional modules that can be combine at the user's will. A useful tool to implement novel metabolic capabilities into different Gram-negative bacteria (including, but not limited to, *P. putida* KT2440) was tested in a practical application: glucose-dependent accumulation of poly(3-hydroxybutyrate), a biodegradable polymer, in recombinant *E. coli* strains.

1.1. Benchmarking the components of the EMP pathway as a guiding principle for the design of GlucoBricks

The first step in this research was to design a set of genes to introduce (or, in some cases, increase), glycolytic capacities in different bacteria. The EMP pathway of *E. coli*, the main route for the transformation of glucose into Pyr through the sequential activity of 10 individual enzymes (**Fig. 4a**), was taken as the model

biochemical sequence for hexose breakdown. In their native context, these 10 genes are spread out along the bacterial genome or arranged in two operons (*e.g.*, *fbaA* and *pgk*) under the transcriptional control of at least five regulators (Cra, SoxS, Crp, Fur, and FnrS) and an important number of post-transcriptional control devices (Papenfort *et al.*, 2013). Considering such complex regulatory scenario, the minimal enzyme complement of the route was selected for the design to prevent carrying host-specific regulatory connections that may compromise the portability of the tool. Under these circumstances, the distribution of what is considered a *GlucoBrick* is sketched in **Fig. 4b**.

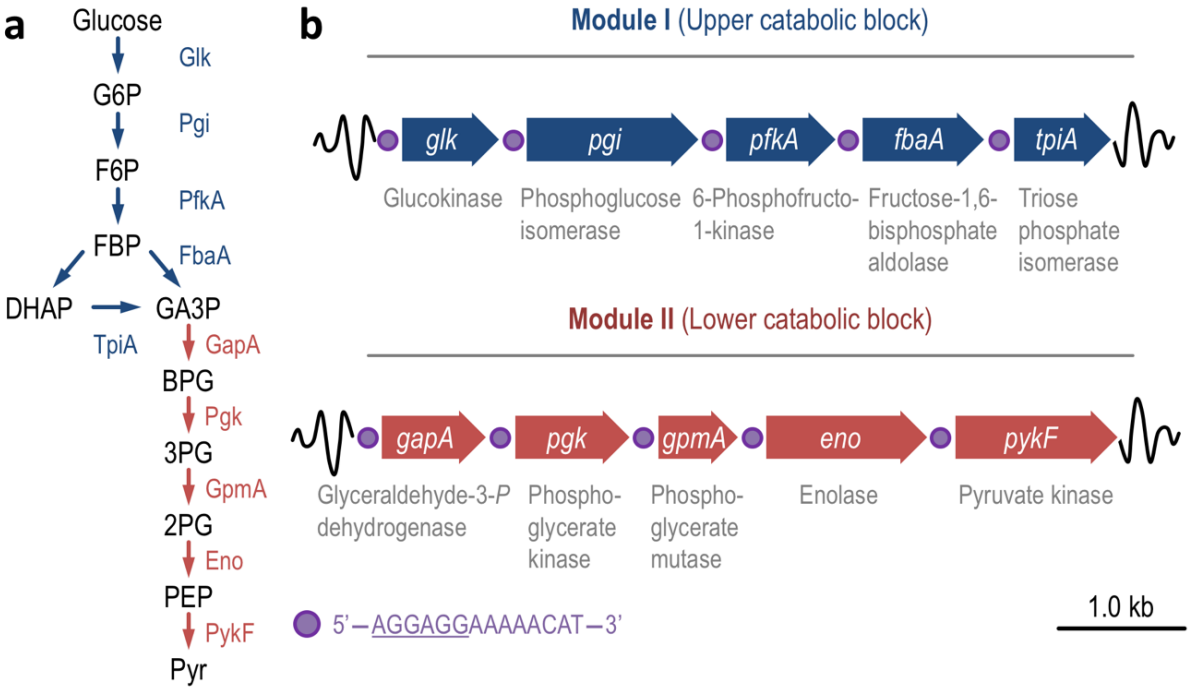

Figure 4 | **Schematic representation of the GlucoBrick platform layout and biochemical reactions thereof.** (**a**) Linear glycolytic pathway encoded by the GlucoBrick platform. The genes from *Module I* encode the necessary genes to transform glucose into glyceraldehyde-3-*P* (GA3P); in a similar way, *Module II* encodes the genes needed to transform GA3P into pyruvate (Pyr). The two sets of glycolytic activities are indicated with blue and red arrows, representing the activities within Modules I and II, respectively. Other abbreviations used in this outline are as follows: G6P, glucose-6-*P*; F6P, fructose-6-*P*; FBP, fructose-1,6-P_2; DHAP, dihydroxyacetone-*P*; BPG, glycerate-1,3-P_2; 3PG, glycerate-3-*P*; 2PG, glycerate-2-*P*; and PEP, phosphoenolpyruvate. (**b**) The genes from *E. coli* K-12 deemed necessary to activate a functional and linear Embden-Meyerhof-Parnas pathway were edited following the *Standard European Vector Architecture Vector* rules and assembled into two synthetic operons. The first operon (Module I) encodes the genes for the *upper catabolic block* of the pathway, which comprises the *preparatory phase* of the glycolysis. The second operon (Module II) encodes the genes for the *lower catabolic block* of the pathway, which comprises the *pay-off phase* of glycolysis. Glycolytic reactions are shown below the gene encoding them. All genes are preceded by a synthetic regulatory element, indicated by a purple circle, composed of a ribosome binding site (sequence underlined) and a spacer sequence.

The individual components of the route were standardized according to some basic principles. For example, there are some reactions in the naturally-occurring EMP pathway encoded by more than one gene (*i.e.*, *pfkA*/*pfkB*, *fbaA*/*fbaB*, *gpmA*/*gpmM*, and *pykA*/*pykF*). This redundancy was overcome by selecting the component reported to display the highest activity according to the information available in the literature. Once these candidates were selected, all the glycolytic genes of the system were assembled by following the same structure, starting with a leading *ATG* signal and finishing with an *STOP* codon. The whole DNA sequence was edited to eliminate restriction sites incompatible with the assembly standard, and any internal transcriptional signal was erased. As indicated in **Fig. 4b**, each open reading frame (ORF) was preceded by a standardized synthetic ribosome binding site (RBS) sequence and a short DNA spacer, and the whole segment was flanked upstream and downstream by restriction sites that match given positions of the default multiple cloning site of the SEVA format (Martínez-García *et al.*, 2014b; Silva-Rocha *et al.*, 2013); *i.e.*, following the standard format *Restriction Enzyme 1*–RBS–glycolytic gene–*Restriction Enzyme 2*. SEVA vectors comprise a selection of plasmids with four compatible broad-host-range origins of replication (*i.e.*, RK2, pBBR1, pRO1600/ColE1, and RSF1010) and six independent antibiotic markers [*i.e.*, Ap, Km, chloramphenicol (Cm), Sm, tetracyclin (Tc), and Gm]. The adoption of this standard enables the effective propagation and maintenance of up to four plasmids in any given Gram-negative bacterial host, and it also allows for the simultaneous expression of several genes. The strategy adopted for the edition of glycolytic genes would allow for the direct sub-cloning or swapping of any gene combination by a simple digestion and ligation step. Moreover, the order of insertion of each of the ten GlucoBricks in the SEVA's multiple cloning site reflects the biochemical sequence of operation in the EMP pathway, thereby allowing for whatever the combination of the parts within the route at stake (**Fig. 5**).

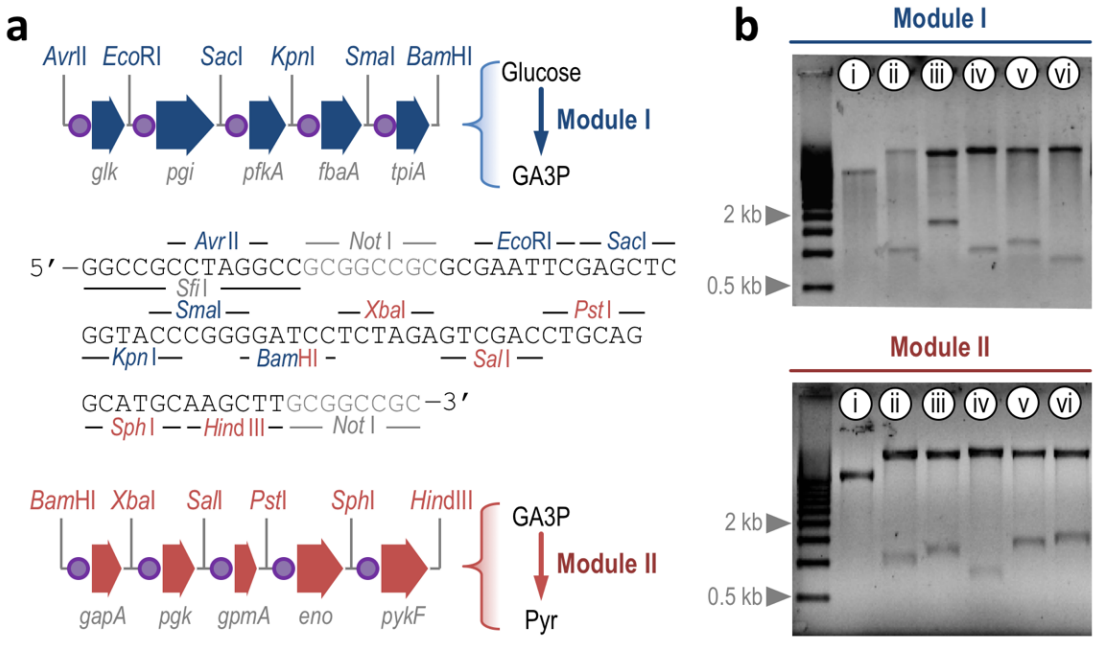

Figure 5 | **Genetic architecture of the GlucoBrick platform.** (**a**) Physical maps of Modules I and II, indicating the topology of the different restriction enzyme sites. The enzyme targets are colored in the sequence of the multiple cloning site of all the plasmids belonging to the *Standard European Architecture Vector* to identify the DNA block they belong to (*i.e.*, blue, Module I; and red, Module II). Other restriction targets that could be useful to implement different regulatory or structural elements are shown in gray. The abbreviations used in this outline are GA3P, glyceraldehyde-3-*P*; and Pyr, pyruvate. (**b**) Restriction analysis of Modules I and II. Plasmids pS224·GBI (upper panel) and pS224·GBII (lower panel) were digested with the appropriate enzymes indicated in the outline in order to individually release all the genes from the GlucoBrick system, and the products were separated by electrophoresis in a 0.7% (w/v) agarose gel. Plasmid pS224·GBI was digested with *Avr*II-*Bam*HI (i, releases the whole Module I segment); *Avr*II-*Eco*RI (ii, releases *glk*); *Eco*RI-*Sac*I (iii, releases *pgi*); *Sac*I-*Kpn*I (iv, releases *pfkA*); *Kpn*I-*Sma*I (v, releases *fba*A); and *Sma*I-*Bam*HI (vi, releases *tpiA*). Plasmid pS224·GBII was digested with *Bam*HI-*Hind*III (i, releases the whole Module II segment); *BamH*I-*Xba*I (ii, releases *gapA*); *Xba*I-*Sal*I (iii, releases *pgk*); *Sal*I-*Pst*I (iv, releases *gpmA*); *Pst*I-*Sph*I (v, releases *eno*); and *Sph*I-*Hind*III (vi, releases *pykF*).

Two DNA modules were designed to encode all the necessary enzymes for the activation of a linear glycolysis based on the EMP pathway. This synthetic EMP pathway was divided into two different catabolic blocks: the *upper catabolic block* (Module I), comprising the activities of the *preparatory* phase; and the *lower catabolic block* (Module II), spans the activities of the *pay-off* phase (**Fig. 4a**). Module I thus encodes the enzymes necessary for glucose phosphorylation and conversion into trioses-*P*. Module II encodes the enzymes necessary to transform these trioses-*P* (more specifically, GA3P) into Pyr (**Fig. 4b**). A detailed physical map of the DNA architecture of this platform (**Fig. 5a**) indicates that the two DNA blocks can be also combined sequentially in a single SEVA vector if desired, and even in transposon vectors designed for chromosomal integration of large DNA segments (Martínez-García *et al.*, 2014a), a feature that will be exploited further on in this Thesis. At the same time, the adoption of the SEVA architecture is not only useful to deliver the GlucoBrick system into target bacteria, but it also represents a pratical method to express the genes encoded in this system under the control of different constitutive and effector-responsive transcriptional devices (Calero *et al.*, 2016; Kim *et al.*, 2016b; Martínez-García *et al.*, 2014b; 2015). As a preliminary experiment to test the modularity of the GlucoBrick system, Modules I and II were separately cloned in vector pSEVA224 (RK2, Km^R), obtaining plasmids pS224·GBI and pS224·GBII, respectively. These low-copy-number plasmids were digested with the appropriate enzymes following the information of **Fig. 5a** to recover all the elements present in the GlucoBrick system (**Fig. 5b**). Every individual gene could be retrieved by following this procedure, indicating that the strategy used for the assembly of this standard tool enables the combination of all the functional elements within the system at the user's will.

1.2. Testing the GlucoBrick system: activities encoded in the platform restore or enhance glucose-dependent growth of glycolytic *E. coli* mutants

Once the GlucoBrick system was generated, its functionality was tested under *in vivo* conditions. The first attempt in order to test the system was implemented in *E. coli*. The functional characterization of the

GlucoBrick system was carried out by assessing their phenotypic impact when the corresponding plasmids were introduced in different glycolytic *E. coli* mutants defective in either single or several activities of the EMP pathway (**Table 5**). *E. coli* BW25113, a WT K-12 strain (Datsenko & Wanner, 2000), was used as the positive control, and the final cell density and the specific growth rate was obtained for each strain in cultures supplemented with Km and IPTG.

Table 5 | **Functional validation of Module I and II in glycolytic mutants of *E. coli* BW25113.**

E. coli strain[a]	Plasmid[b]	Growth parameters[c] in:			
		M9GCM semi-synthetic medium		M9 minimal medium + 20 mM glucose	
		CDW (g l^{-1})	Growth coefficient	CDW (g l^{-1})	Growth coefficient
BW25113 (wild-type strain)	None	2.7 ± 0.3	–	1.7 ± 0.1	–
Δ*glk* Δ*ptsI*	pSEVA224	1.1 ± 0.2	1.2 ± 0.1	N.G.	G.R.
	pS224·GBI	1.3 ± 0.3		1.3 ± 0.2	
Δ*pfkA* Δ*pfkB*	pSEVA224	0.4 ± 0.1	2.3 ± 0.3	N.G.	G.R.
	pS224·GBI	1.4 ± 0.2		1.9 ± 0.1	
Δ*tpiA*	pSEVA224	0.6 ± 0.1	1.4 ± 0.2	N.G.	G.R.
	pS224·GBI	1.7 ± 0.3		1.2 ± 0.3	
Δ*gapA* Δ*epd* Δ*ptsI*	pSEVA224	0.5 ± 0.1	6.1 ± 0.5	N.G.	G.R.
	pS224·GBII	1.2 ± 0.1		0.9 ± 0.1	
Δ*pgk*	pSEVA224	0.3 ± 0.1	2.9 ± 0.1	N.G.	G.R.
	pS224·GBII	1.4 ± 0.5		1.6 ± 0.4	
Δ*eno*	pSEVA224	0.8 ± 0.2	3.1 ± 0.4	N.G.	G.R.
	pS224·GBII	1.5 ± 0.2		0.9 ± 0.1	

[a] The relevant genotype of the strains is described in the *Materials and Methods* section (**Table 2**).

[b] Plasmid pSEVA224 was used as the control vector; plasmids pS224·GBI and pS224·GBII are pSEVA224 derivatives carrying either Module I or II, respectively. IPTG was added to all cultures at 1 mM at the onset of the cultivation.

[c] M9GCM semi-synthetic medium contains the same salts as M9 minimal medium, casein hydrolyzate, glycerol, and sodium malate. CDW, cell dry weight after 48 h of aerobic incubation at 37ºC. N.G., no growth (defined as a change in the CDW < 0.05 g l^{-1}). The growth coefficient is the ratio between the specific growth rate of a strain carrying either Module I or II and the specific growth rate of the same strain carrying pSEVA224; the cases in which the mutant did not grow (and hence, the growth coefficient could not be calculated) are indicated as G.R., growth restored. Results represent the mean value ± standard deviation from triplicate measurements in at least two independent experiments. All the differences in growth coefficients for the strains grown in M9GCM semi-synthetic medium were significant ($P < 0.05$, as evaluated by means of the Student's *t* test) in the pair-wise comparison of a given recombinant to the control strain carrying the empty pSEVA224 vector.

The participation of the GlucoBrick system at the level of **Glk** (*i.e.*, glucokinase) and **PtsI** [*i.e.*, the EI component of the PEP:carbohydrate phosphotransferase (PTS) system] served as the first experimental validation of the whole system. No glucose phosphorylation is possible in a double Δ*glk* Δ*ptsI* mutant of *E.*

coli, as both Glk and the PTS-dependent transport of the hexose coupled to phosphorylation are blocked (Nikel & de Lorenzo, 2013b). Note, however, that glucose transport into the cytoplasm should not be totally blocked in this genetic background, since alternative transporters (*e.g.*, the low-affinity galactose:H^+ GalP symporter and the ATP-dependent MglABC system) are known to internalize non-phosphorylated hexoses when the PTS system is not active (Jahreis *et al.*, 2008). The Δ*glk* Δ*ptsI* strain was able to grow in M9GCM semi-synthetic medium (formulated in such a way that all the glycolytic mutants tested could grow, albeit some of them grew poorly) but not in M9 minimal medium with glucose as the only carbon source. However, the addition of Module I restored the growth of the double mutant on glucose back to the levels observed in the semi-synthetic medium (**Table 5**).

In the case of the **Pfk** (*i.e.*, 6-phosphofructo-1-kinase) activity, which transforms F6P into FBP, the strain under study was a double Δ*pfkA* Δ*pfkB* mutant. This strain was unable to grow on glucose as the sole carbon source and its growth was severely affected when inoculated in M9GCM medium. The implementation of Module I in Pfk-deficient bacteria was enough to restore the growth deficiency in both culture media, and it also lead to a 2.3-fold increase in the specific growth rate of the recombinant in M9GCM medium (**Table 5**). Pfk was considered to be one of the most important metabolic nodes in the evaluation of the GlucoBrick platform as this is the activity missing in many *Pseudomonas* species (and thus a relevant target for manipulation within the overall objective of activating a linear glycolysis in *P. putida* KT2440).

Another crucial step in the EMP pathway is the **TpiA** (*i.e.*, triose-*P* isomerase) activity, which catalyzes the isomerization between GA3P and DHAP. This activity plays a central role not only in glycolysis but also in gluconeogenesis, especially in environmental bacteria (Fraenkel, 1986). Expectedly, and taking into account its physiological relevance, the growth of a Δ*tpiA* mutant was impaired among all the culture conditions tested, probably because of the build-up of methylglyoxal as a toxic intermediate (Velur Selvamani *et al.*, 2014). The implementation of Module I in a TpiA-deficient metabolic background mitigated this phenomenon, restoring the growth of the mentioned strain on glucose. At the same time, the presence of Module I also enhanced the growth in the semi-synthetic medium tested (**Table 5**).

Once the functionality of Module I was demonstrated with the practical examples discussed above, Module II was submitted to the same battery of experiments. This block carries the EMP activities from the *pay-off* phase, which comprises the reactions to transform GA3P into Pyr. The first biochemical step assayed in this case was GA3P dehydrogenase [represented by **GapA**, and possibly the GapB isozyme (Boschi-Muller *et al.*, 1997)], which catalyzes the transformation of GA3P into glycerate-1,3-P_2 (BPG). Note that a simple Δ*gapA* mutant would not reveal if GapA encoded in Module I is enough to fulfil the cognate biochemical step, due to the capacity of the PTS system to transform PEP into Pyr. Considering this complex metabolic scenario (and in order to ensure that there is no Pyr formation), a triple *E. coli* mutant was constructed by eliminating *gapA* (encoding a NAD^+-dependent GA3P dehydrogenase, and also the major

GA3P dehydrogenase prevalent in Enterobacteria), *epd* (known as *gapB*, encoding a NAD^+-dependent erythrose-4-*P* dehydrogenase), and also *ptsI*. This strain is totally unable to grow on glucose as a carbon source and, at the same time, it only reaches a modest cell density in M9GCM medium. Once again, the implementation of Module II, and the GapA activity thereof, improved or even restored the growth phenotype in the triple mutant. Interestingly, this strain had a >6-fold increase in the specific growth rate when grown in semi-synthetic medium, obtaining the highest value among the conditions and strains analyzed in this part of the study (**Table 5**).

Finally, **Δ*pgk*** and **Δ*eno*** mutants were analyzed to functionally complement missing activities by Module II, obtaining similar results as the ones described thus far. In both cases, the growth obtained in semi-synthetic medium was very poor, and no growth was detected in M9 minimal medium with glucose. In accordance with the results obtained with other glycolytic mutants, the implementation of Module II was enough to restore the growth phenotype in glucose in both strains, while the specific growth rate in M9GCM medium increased by *ca*. 3-fold in either case (**Table 5**). Despite the single complementation analyzed in this set of experiments, all the strains under study are provided with additional copies of the rest of glycolytic genes in each GlucoBrick module, boosting the channeling of hexoses though the linear EMP pathway. In all the cases here, the final cell densities in M9 minimal medium with glucose attained by the recombinants carrying either Module I or II of the GlucoBrick platform were comparable to that of WT *E. coli* BW25113.

Additionally, and in order to corroborate that the changes in the glucose-dependent growth phenotype correlated with the enzyme activities encoded in the GlucoBrick platform, the specific activities of some enzymes involved in glucose processing were evaluated *in vitro* in cell-free extracts. Two key steps in the EMP pathway, the Glk and Pkf activities, were targeted for this purpose. In the first case, the activity of Glk in the glucose-grown Δ*glk* Δ*ptsI* mutant expressing Module I was 1,370 ± 120 nmol min^{-1} $mg_{protein}^{-1}$ upon induction of gene expression with IPTG, representing a *ca*. 23- and 10-fold increase as compared with the same strain carrying the empty vector and WT BW25113 carrying the empty vector, respectively [note that some residual Glk activity was observed in the knock-out strain, possibly arising from some other non-specific hexose kinases (Meyer *et al.*, 1997)]. On the other hand, the implementation and induction of the activities encoded in Module I in the Δ*pfkA* Δ*pfkB* strain resulted in a 10-fold increase in the specific Pfk activity (1,080 ± 70 nmol min^{-1} $mg_{protein}^{-1}$) as compared with the same strain carrying the empty pSEVA224 vector. In contrast, the Pfk activity in WT BW25113 was 751 ± 36 nmol min^{-1} $mg_{protein}^{-1}$. Interestingly, there was some residual Pfk activity detected *in vitro* in the *E. coli* Δ*pfkA* Δ*pfkB* mutant (<100 nmol min^{-1} $mg_{protein}^{-1}$), that could originate from a side activity of an enzyme belonging to the PfkB family of phosphosugar kinases [a subset of the large ribokinase superfamily (Park & Gupta, 2008)]. Ribokinase (or another enzyme belonging to this family) can possibly phosphorylate F6P to FBP *in vitro*, which in turn may be due to the dilution of an allosteric inhibitor in the assay, as previously described (Chin & Cirino, 2011).

As a summary of the results obtained thus far, it can be safely assumed that the GlucoBrick system is a useful tool for the implementation of different glycolytic activities in *E. coli* strains. The next standing question to be answered is how portable this system is, and for the sake of this Thesis, checking its usability in different, unrelated bacterial species (*i.e.*, *Pseudomonas*).

1.3. Portability of the GlucoBrick system: using Modules I and II to engineer glycolysis in two different *Pseudomonas* species

The last few years have witnessed an increase in the development of dedicated genetic tools to manipulate Gram-negative bacteria, specifically *P. putida* (Benedetti *et al.*, 2016; Calero *et al.*, 2016; Martínez-García *et al.*, 2011; 2014a,b; Martínez-García & de Lorenzo, 2011; Silva-Rocha *et al.*, 2013). Along this line, the GlucoBrick system represents a new standard to implement novel metabolic capabilities in different Gram-negative bacteria, nested in the main, overarching objective of this Thesis: the rational implementation of a linear EMP pathway in *P. putida* KT2440. In order to elucidate the viability of the GlucoBrick system to bring about the activities needed for such task, and also for evaluating the portability of the system in *Pseudomonas* species, the present section describes the use of the platform in *P. putida* KT2440 and *P. aeruginosa* PAO1.

P. putida and *P. aeruginosa* are representative members of the genus, with several environmental and medical implications, respectively. Both strains use the ED pathway for hexoses breakdown as part of a most intricate glucose metabolism (Belda *et al.*, 2016; Berger *et al.*, 2014; Sudarsan *et al.*, 2014; Vicente & Cánovas, 1973a,b). Recently, this metabolic complexity was shown to run in a particular architecture in *P. putida* KT2440 (Nikel *et al.*, 2015a), which operates a combination of enzymes belonging to the EMP pathway, the ED pathway, and the PP pathway to catabolize glucose *via* a metabolic device termed EDEMP cycle (**Fig. 6a**). Such metabolic scenario is probably present in other members of the *Pseudomonas* group as well, such as *P. aeruginosa*. The high degree of metabolic complexity in the glycolysis of these bacteria makes it difficult to implement biotechnological approaches based on glucose breakdown. This is the main reason for which both *P. putida* KT2440 and *P. aeruginosa* PAO1 were adopted as heterologous hosts for testing the GlucoBrick platform. Physiological and growth parameters as well as the *in vitro* activity of key glycolytic enzymes were systematically assessed in the resulting strains as indicated below.

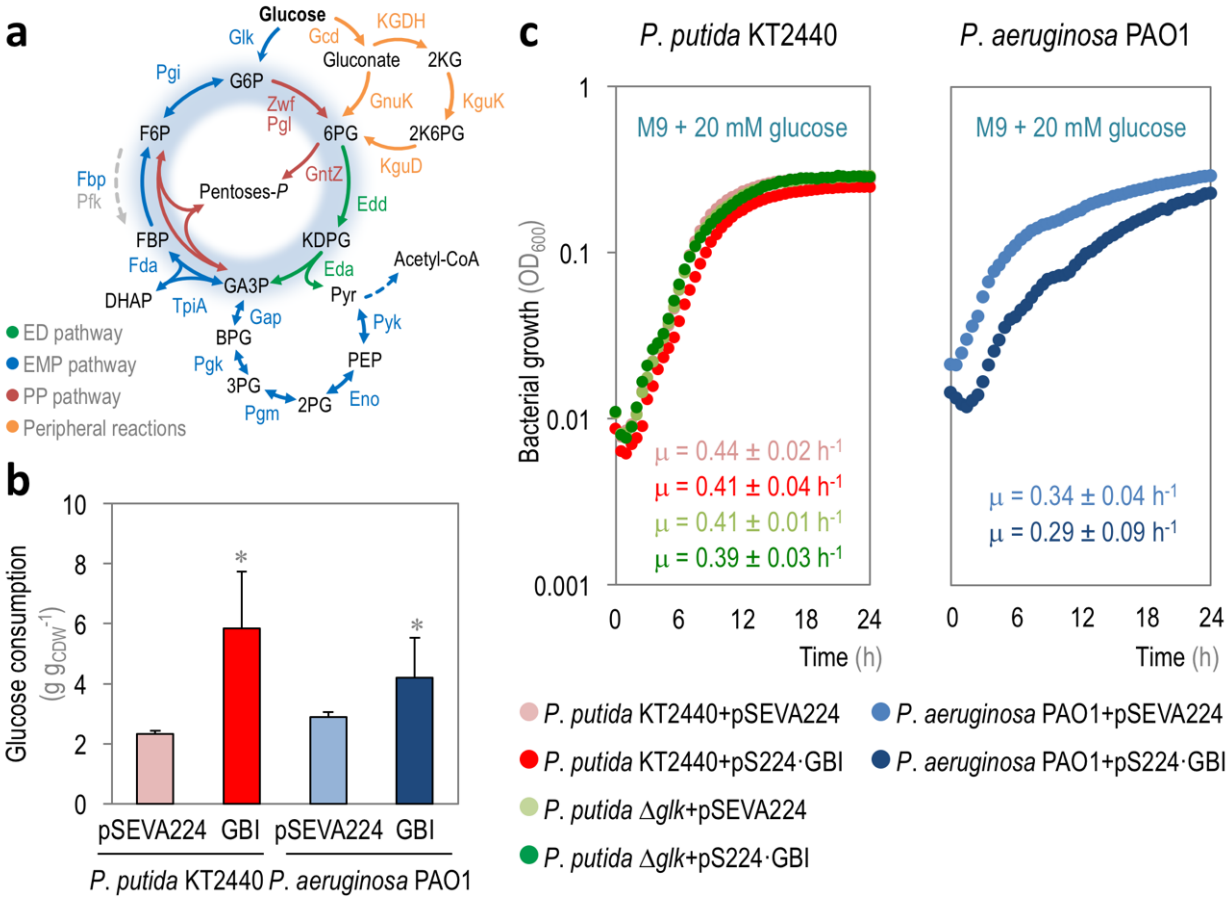

Figure 6 | **Characterization of physiological parameters in recombinant *Pseudomonas putida* and *P. aeruginosa* strains carrying Module I.** (**a**) Schematic representation of central carbon metabolism in *Pseudomonas* species. Glucose catabolism occurs mainly through the activity of the Entner-Doudoroff (ED) pathway, but part of the trioses-*P* thereby generated are recycled back to hexoses-*P* by means of the *EDEMP cycle*, that also encompasses activities from the partial Embden-Meyerhof-Parnas (EMP) and pentose phosphate (PP) pathways. A set of *peripheral reactions* can also oxidize glucose to gluconate and/or 2-ketogluconate (2KG) before any phosphorylation of the intermediates occurs. Each metabolic block is indicated with a different color along with the relevant enzymes catalyzing each step, and the EDEMP cycle is shaded in blue in this diagram. The 6-phosphofructo-1-kinase (Pfk) activity, missing in most *Pseudomonas* species, is highlighted with a dashed gray arrow. The abbreviations used for the metabolic intermediates are as indicated in the legend to **Fig. 4**; other abbreviations are as follows: 6PG, 6-phosphogluconate; KDPG, 2-keto-3-deoxy-6-phosphogluconate; acetyl-CoA, acetyl-coenzyme A; and 2K6PG, 2-ketogluconate-6-*P*. (**b**) Glucose consumption profile and (**c**) growth curves of *P. putida* KT2440, its Δ*glk* derivative, and *P. aeruginosa* PAO1, carrying either the control vector (pSEVA224) or pS224·GBI (Module I). Glucose consumption is reported as the mean value ± standard deviation from duplicate measurements in at least three independent experiments. CDW, cell dry weight. Significant differences ($P < 0.05$, as evaluated by means of the Student's *t* test) in the pair-wise comparison of a given recombinant to the control strain, carrying the empty pSEVA224 vector, are indicated by an asterisk. In the growth curves, each data point represents the mean value of the optical density measured at 600 nm (OD_{600}) of quadruplicate measurements from at least three independent experiments. The specific growth rates (μ) were calculated from these data during exponential growth, and the inset shows the mean values ± standard deviations for each strain.

The implementation of Module I should boost the extant, partially active EMP pathway in *Pseudomonas* due to the addition of the missing step catalyzed by Pfk. In order to corroborate the consequences of such scenario, the overall glucose consumption was evaluated in recombinant *P. putida* and *P. aeruginosa* strains carrying either an empty pSEVA224 vector or the pS224·GBI plasmid, bearing Module I (**Fig. 6b**). In both cases, the overall rate of glucose consumption was significantly increased by expressing the genes of Module I (*i.e.*, 2.5- and 1.5-fold in *P. putida* KT2440 and *P. aeruginosa* PAO1, respectively, as compared to the strains bearing the pSEVA224 vector). In addition, no major growth deficiencies in terms of final biomass densities and specific growth rates (as determined in microtiter-plate cultures) were observed in the strains carrying Module I (**Fig. 6c**). *P. aeruginosa* PAO1 had a slight reduction in the specific growth rate when expressing Module I, but the difference in this parameter as compared to that in the same strain carrying an empty vector was not significant.

All the information provided in the previous paragraph indicates that the GlucoBrick system influences the metabolic state of the two *Pseudomonas* species analyzed. In order to clarify if this impact is due to the action of the activities encoded by the Module I, the *in vitro* activities of the enzymes of the *preparatory phase* were evaluated in cell-free extracts obtained from the different *Pseudomonas* recombinants (**Fig. 7**). First, the specific Glk activity was assessed in strains KT2440 and PAO1 carrying pS224·GBI (Module I) and growing on glucose as the sole carbon source, with Km and IPTG added as needed (**Fig. 7a**). In contrast with the situation in *E. coli*, *Pseudomonas* species do not possess a PTS system for glucose uptake, and the phosphorylation of hexoses is directly catalyzed by Glk (*i.e.*, PP_1011 in *P. putida* and PA_3193 in *P. aeruginosa*) in the cytoplasm. The native Glk activity in both *Pseudomonas* species ranged from *ca*. 89 to 184 nmol min^{-1} $mg_{protein}^{-1}$ in *P. aeruginosa* PAO1 and *P. putida* KT2440, respectively, and this kinase activity was boosted by expression of *E. coli glk* from plasmid pS224·GBI (*i.e.*, a 1.4-fold increase in strain KT2440 and a remarkable 6.2-fold increase in strain PAO1). Simultaneously, a *P. putida* Δ*glk* strain was constructed, in which the *in vitro* Glk activity resulted below the detection limit of the assays (and thus, considered negligible). However, transforming this *glk* mutant strain with plasmid pS224·GBI, followed by induction of gene expression by adding IPTG, increased the specific kinase activity up to 45 nmol min^{-1} $mg_{protein}^{-1}$ (*i.e.*, a 100-fold increase in Glk activity) (**Fig. 7a**).

As indicated before, the missing Pfk activity in several *Pseudomonas* species (*i.e.*, strains KT2440 and PAO1) generates a gap in the EMP pathway, blocking the transformation of F6P into FBP. The introduction of Module I was explored in both *Pseudomonas* species transformed with plasmid pS224·GBI and grown in M9 minimal medium containing glucose, Km, and IPTG (**Fig. 7b**). The *in vitro* Pfk activity was firstly evaluated on both *Pseudomonas* species transformed with the empty pSEVA224 vector, and the results expectedly corroborate the absence of this key glycolytic enzyme in the native biochemical networks (**Fig. 7b**). On the other hand, the expression of the genes borne by plasmid pS224·GBI resulted in increased levels of Pfk activity, which were similarly high in both *P. putida* KT2440 and *P. aeruginosa* PAO1 (*i.e.*, *ca*.

272 and 550 nmol min^{-1} $mg_{protein}^{-1}$, respectively) (**Fig. 7b**). The change in the Pfk activity brought about by heterologous expression of *pfkA* in *P. putida* Δ*glk* was somewhat low, but it still represents a 23-fold increase as compared to the control strain transformed with an empty vector (**Fig. 7b**). The differences in terms of Pfk activities detected in the WT strain and its Δ*glk* derivative could stem from alterations in the intracellular metabolite pools, which may have an influence in the regulation of the PfkA enzyme of *E. coli*.

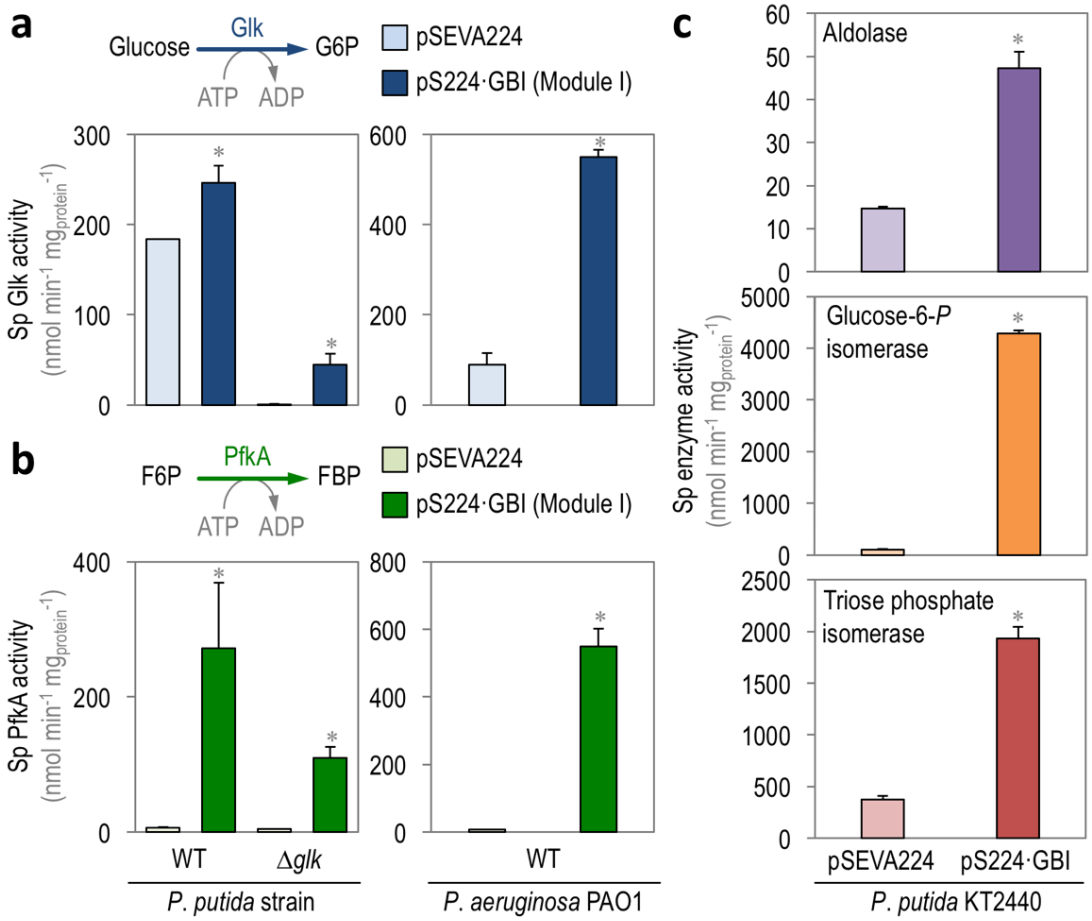

Figure 7 | **Biochemical characterization of native and implanted enzyme activities in *Pseudomonas* species.** (**a**) *In vitro* quantification of the specific (Sp) glucokinase (Glk) activity, which phosphorylates glucose to glucose-6-*P* (G6P) in wild-type (WT) *P. putida* KT2440 and its Δ*glk* derivative (*left panel*), and WT *P. aeruginosa* PAO1 (*right panel*) carrying either the empty pSEVA224 vector or Module I. (**b**) *In vitro* quantification of the specific (Sp) 6-phosphofructo-1-kinase (PfkA) activity, which converts fructose-6-*P* (F6P) into fructose-1,6-P_2 (FBP) in WT *P. putida* KT2440 and its Δ*glk* derivative (*left panel*), and WT *P. aeruginosa* PAO1 (*right panel*) carrying either the empty pSEVA224 vector or Module I. (**c**) *In vitro* quantification of the specific (Sp) activities of aldolase, glucose-6-*P* isomerase, and triose phosphate isomerase in *P. putida* KT2440 carrying either the empty pSEVA224 vector or Module I. These three activities, combined with Glk and PfkA, constitute the *preparatory phase* of the Embden-Meyerhof-Parnas pathway (*i.e.*, from glucose to glyceraldehyde-3-*P*). All the strains tested were grown on M9 minimal medium added with glucose at 20 mM and cells were harvested in mid-exponential phase for these *in vitro* enzymatic assays. Each bar represents the mean value of the corresponding enzyme activity ± standard deviation of quadruplicate measurements from at least two independent experiments. Significant differences ($P < 0.05$, as evaluated by means of the Student's *t* test) in the pair-wise comparison of a given recombinant to the control strain, carrying the empty pSEVA224 vector, are indicated by an asterisk.

Additionally, the three remaining activities within the *preparatory* phase of the EMP pathway (*i.e.*, aldolase, glucose-6-*P* isomerase, and triose phosphate isomerase) were evaluated *in vitro* in glucose-grown *P. putida* KT2440 carrying either pSEVA224 or pS224·GBI (**Fig. 7c**). In all cases, the recombinant strains carrying Module I presented a significant increase in each enzyme activity. The total aldolase and triose phosphate isomerase activities had a 3- and 5-fold increase, respectively, in *P. putida* KT2440 expressing Module I. Under the same conditions, the activity of glucose-6-*P* isomerase augmented a surprising 43-fold with respect to the control experiment.

In light of the results of this part of the study, it is possible to conclude that all the enzymes that comprise the *preparatory phase* of the EMP pathway are active in recombinant *P. putida* due to the presence of Module I of the GlucoBrick platform. This biochemical scenario is expected to trigger a modification of the intracellular metabolome of this bacterium. In order to resolve this question, the **impact of the GlucoBrick platform in the intracellular metabolome of *P. putida* KT2440** was evaluated under the same growth conditions used to analyze *in vitro* enzyme activities. The intracellular concentration of some critical metabolic intermediates was thus measured in glucose-grown *P. putida* KT2440 carrying either pSEVA224 or pS224·GBI during exponential growth. The concentration of the first metabolic intermediary after glucose phosphorylation (*i.e.*, G6P) and the last intermediate of the *preparatory phase* of the EMP pathway (*i.e.*, GA3P) was assessed by LC-MS (**Table 6**). According to the hypothesis, both metabolites were observed to have an increased abundance in the strains expressing the genes of Module I (*i.e.*, 1.7-fold in the case of the hexose-*P* and 3.2-fold in the case of the triose-*P*), a further experimental indication that the EMP pathway is active in this recombinant strain. Additionally, and a general proxy of the redox status of the cells, the concentration of the key redox cofactor NADPH was included in the same set of measurements. The *P. putida* KT2440 derivative expressing Module I showed a 26% reduction in the intracellular content of NADPH (**Table 6**). Although the intracellular concentration of redox cofactors is known to be tightly regulated by several biochemical mechanisms, the diminution observed under the experimental conditions evaluated here prompts the hypothesis that the recombinant *P. putida* strain carrying Module I is redirecting glucose from the EDEMP cycle to the newly implemented linear glycolytic pathway. This assumption is based in that the activity of Zwf reduces $NADP^+$ coupled to the oxidation of G6P into 6PG (**Fig. 6a**). If *P. putida* has an active EMP pathway, G6P would be channeled into this metabolic route at the expense of Zwf, and the level of NADPH stemming from this metabolic conversion would be smaller. Taken together, these targeted metabolomic determinations (along with the direct *in vitro* measurement of enzyme activities) indicate that glucose is probably funneled into a linear glycolysis of sorts in *P. putida* KT2440 when expressing the genes within Module I.

Table 6 | **Metabolomic determinations[a] in glucose-grown *Pseudomonas putida* KT2440 carrying the glycolytic genes borne by Module I.**

P. putida KT2440 carrying plasmid	Intracellular content (nmol mg_{CDW}^{-1}) of		
	Glucose-6-*P*	Glyceraldehyde-3-*P*	NADPH
pSEVA224 (empty vector)	52 ± 9	0.39 ± 0.08	43 ± 5
pS224·GBI (Module I)	89 ± 4	1.23 ± 0.07	32 ± 9

[a] Cells were grown aerobically in M9 minimal medium added with glucose at 20 mM, harvested during exponential growth, and rapidly quenched in liquid N_2. Intracellular metabolites were extracted and their concentration determined by means of liquid chromatography coupled to mass spectrometry as indicated in *Materials and Methods*. Each parameter is reported as the mean value ± standard deviation from duplicate measurements in at least two independent experiments.

Thus far, the results shown expose the ability of the GlucoBrick system to both (i) boost existing glycolytic activities and (ii) introduce new metabolic steps in different Gram-negative bacteria. As such, this tool looks promising to refactor the central carbon metabolism of *P. putida* KT2440, the main goal in this Thesis. However, this application, which will be fully exploited as indicated in **Chapter 4**, does not preclude the usability of the GlucoBrick platform in other Metabolic Engineering manipulations. In order to evaluate the potential of the tool in a production process, the capacity of the GlucoBrick system to enhance the production of added-value metabolites (*i.e.*, PHB) from hexoses was analyzed in recombinant strains of *E. coli*.

1.4. Enhancing heterologous PHB production by increasing glycolytic fluxes in recombinant *E. coli*

Polyhydroxyalkanoates are a structurally complex group of biopolymers produced by different bacteria (Cabrera Gomez *et al.*, 2012; López *et al.*, 2015; Ruiz *et al.*, 2006). The simplest bacterial polyhydroxyalkanoate is PHB, an isotactic polyester composed by 3-hydroxybutyrate units (Anderson & Dawes, 1990). PHB is an interesting biopolymer due to its *ecofriendly* features, such as its easy biodegradation by a large number of bacteria, and the oil-independent nature of the industrial production process (Suriyamongkol *et al.*, 2007). This biopolymer is synthesized by *Cupriavidus necator* (formerly known as *Ralstonia eutropha*) using three enzymes (**Fig. 8a**). The first step in this pathway is catalyzed by PhaA (*i.e.*, 3-ketoacyl-coenzyme A thiolase), which condense two acetyl-CoA moieties, yielding 3-acetoacetyl-CoA. This intermediate is the substrate for PhaB, a NADPH-dependent 3-acetoacetyl-CoA reductase (encoded by *phaB1*). In the final step of this biosynthetic pathway, (*R*)-(–)-3-hydroxybutyryl-CoA units are polymerized to PHB by PhaC, a PHA synthase (encoded by *phaC1*).

E. coli has been traditionally used as a microbial host of the PHB biosynthetic pathway (Leong *et al.*, 2014), since this microorganism lacks the metabolic machinery for the synthesis and degradation of polyhydroxyalkanoates (which makes pathway engineering easier, and the polymer accumulated by the recombinants does not get degraded). A problem recursively encountered when attempting to improve the yield and productivity of biopolymer in recombinant *E. coli* strains is that the PHB biosynthetic pathway is nested in the *core* biochemical network of the bacterium (Nikel *et al.*, 2010), not only drawing acetyl-CoA coming from the EMP pathway, but also using NADPH as a cofactor (Ruiz *et al.*, 2012), and the PHB biosynthetic route also competes with native fermentation pathways (**Fig. 8a**), *e.g.*, acetate formation from acetyl-CoA (Chang *et al.*, 1999). Taking into account this complex metabolic situation, the availability of biosynthetic precursors is assumed to be the main bottleneck compromising not only PHB accumulation but also bacterial growth in recombinant *E. coli*.

In order to elucidate if the GlucoBrick system can help mitigating these metabolic bottlenecks, a PHB-producing *E. coli* strain was firstly constructed by transforming plasmid pAeT41 (carrying the *phaC1AB1* gene cluster from *C. necator*) into WT *E. coli* BW25113. Plasmids pSEVA224 (Km^R, empty vector), pS438·GBI (Sm^R, carrying Module I), and/or pS224·GBII (Km^R, carrying Module II) were introduced in this strain, and growth, polymer accumulation, and acetate excretion were evaluated in LB medium cultures added with glucose and the corresponding antibiotics and inducers after 24 h of aerobic growth (**Table 7** and **Fig. 8b** and **c**). The separate introduction of Module I and II stimulated both glucose consumption and polymer accumulation with respect to the control strain. On the other hand, the glucose consumption increased by 4- and 3-fold upon induction of the genes encoded by Module I and II, respectively (**Fig. 8b**). When the two GlucoBricks modules were simultaneously present in the same strain, a 6-fold increment in the specific glucose consumption was observed with respect to the control strain. This result points to a synergistic effect of the two modules in promoting glucose metabolism through the entire EMP pathway. In addition, the increase in the total glucose consumption in this recombinant strain, accompanied with a decrease in residual biomass formation (*i.e.*, non-PHB cell material), indicates that the metabolic intermediates generated through the EMP pathway are channeled into PHB accumulation (rather than biomass formation). As an additional observation, the overexpression of either *gapA* or *glk·pfkA·gapA* did not perturb the specific growth rates of the recombinants strains. However, the presence of Module I and II reduced this parameter by *ca*. 30%, indicating some sort of metabolic burden due to plasmid maintenance (Dvořák *et al.*, 2015).

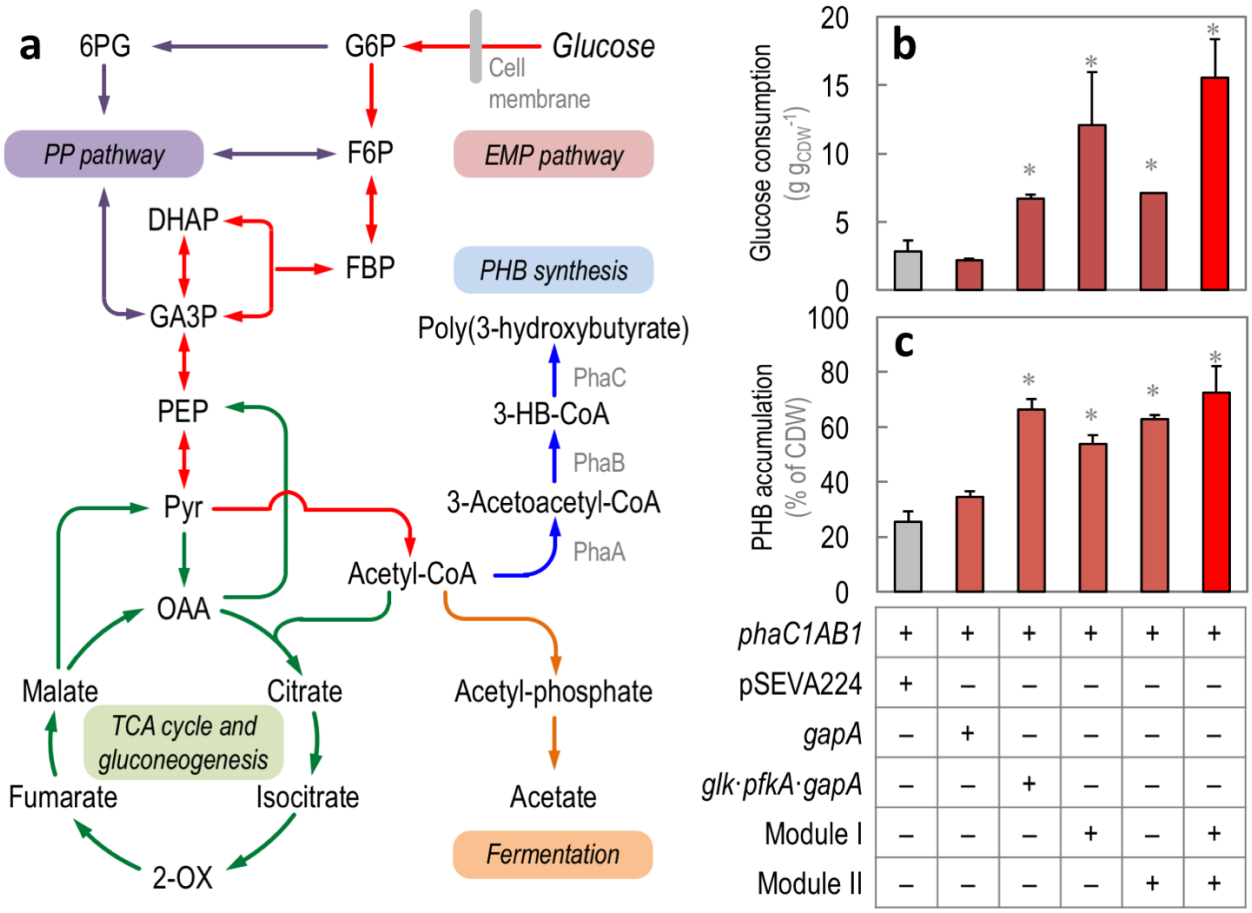

Figure 8 | **Enhanced poly(3-hydroxybutyrate) synthesis in recombinant *Escherichia coli* carrying Modules I and II.** (**a**) Three enzymes are necessary for *de novo* synthesis of poly(3-hydroxybutyrate) (PHB). In *Cupriavidus necator*, from which the cognate genes were harnessed in this study, PHB accumulation depends on the sequential activity of a 3-ketoacyl-coenzyme A (CoA) thiolase (PhaA), a NADPH-dependent 3-acetoacetyl-CoA reductase (PhaB1), and a PHB synthase (PhaC1). PhaA and PhaB1 catalyze the condensation of two molecules of acetyl-CoA to 3-acetoacetyl-CoA and the reduction of this intermediate to *R*-(–)-3-hydroxybutyryl-CoA (3-HB-CoA), respectively. PhaC1 polymerizes 3-HB-CoA monomers to PHB by releasing one CoA-SH molecule per monomer added. Note that acetyl-CoA can also be used in the major fermentation pathway of *E. coli*, that produces acetate. The main metabolic blocks within the biochemical network are identified with different colors in the outline: the Embden-Meyerhof-Parnas (EMP) pathway, *red*; the pentose phosphate (PP) pathway, *purple*; and the tricarboxylic acid (TCA) cycle and gluconeogenesis, *green*. Abbreviations of metabolic intermediates are as shown in the caption to **Fig. 4**; other abbreviations are as follows: 6PG, 6-phosphogluconate; acetyl-CoA, acetyl-coenzyme A; OAA, oxaloacetate; and 2-OX, 2-oxoglutarate. (**b**) Glucose consumption profile and (**c**) PHB accumulation by *E. coli* BW25113 carrying plasmid pAeT41 (*i.e.*, constitutively expressing the *phaC1AB1* gene cluster from *C. necator*) transformed with plasmids carrying the genes or modules indicated (see **Table 3** for further details). Cells were grown aerobically in LB medium added with glucose at 10 g l^{-1} for 24 h. Each parameter is reported as the mean value ± standard deviation from duplicate measurements in at least three independent experiments. CDW, cell dry weight. Significant differences ($P < 0.05$, as evaluated by means of the Student's *t* test) in the pair-wise comparison of a given recombinant to the control strain, carrying the empty pSEVA224 vector, are indicated by an asterisk.

Table 7 | **Growth parameters and polymer synthesis of a PHB-accumulating *Escherichia coli* strain[a] carrying different combinations of glycolytic genes.**

Plasmid[b]	*r*CDW[c] (g l^{-1})	PHB (g l^{-1})	μ (h^{-1})	Specific rate of acetate formation (mmol g_{CDW}^{-1} h^{-1})	Acetyl-coenzyme A content (nmol mg_{rCDW}^{-1})
pSEVA224 (empty vector)	0.54 ± 0.06	0.21 ± 0.04	0.46 ± 0.03	3.3 ± 0.4	0.43 ± 0.09
pS438·GBI (Module I)	0.35 ± 0.02	0.43 ± 0.02	0.29 ± 0.03	1.1 ± 0.2	0.75 ± 0.03
pS224·GBII (Module II)	0.37 ± 0.01	0.61 ± 0.01	0.29 ± 0.01	1.8 ± 0.2	0.59 ± 0.04
pS438·GBI + pS224·GBII	0.11 ± 0.01	0.35 ± 0.01	0.21 ± 0.02	1.3 ± 0.1	N.D.
pS424·*gapA*	0.45 ± 0.02	0.24 ± 0.02	0.44 ± 0.01	2.8 ± 0.3	N.D.
pS224·GPG (*glk·pfkA·gapA*)	0.32 ± 0.01	0.72 ± 0.01	0.42 ± 0.02	1.5 ± 0.1	N.D.

[a] *E. coli* BW25113 carrying plasmid pAeT41 (*i.e.*, constitutively expressing the *phaC1AB1* gene cluster from *C. necator*) was transformed with the plasmids indicated, and grown aerobically in LB medium added with glucose at 10 g l^{-1} for 24 h. Each parameter is reported as the mean value ± standard deviation from duplicate measurements in at least three independent experiments. N.D., not determined.

[b] The full description of each plasmid can be found in *Materials and Methods* section (**Table 3**).

[c] The residual cell dry weight (*r*CDW) was calculated as the difference between the total CDW and the PHB concentration.

A key issue to be considered when designing *E. coli*-based microbial cell platforms is the so-called *overflow metabolism*, *i.e.*, the spillage of metabolic intermediates into the formation of (often, undesired) by-products (Han *et al.*, 1992; Nakano *et al.*, 1997). In order to evaluate this phenomenon in the recombinant strains constructed here, the specific rate of acetate formation was measured in all recombinant strains (**Table 7**), since this metabolite is known to be the main by-product of aerobic glucose catabolism (Bernal *et al.*, 2016). The control strain, *E. coli* BW25113 carrying pSEVA224, excreted acetate at a rate of 4.8 ± 0.2 mmol g_{CDW}^{-1} h^{-1} when cultured in LB medium containing glucose. All the strains expressing the *phaC1AB1* gene cluster had a reduced rate of acetate formation (*e.g.*, the strain transformed with both Modules I and II had a 73% reduction in this parameter). This is a finding in line with previous observations, indicating that the synthesis of PHB overcomes acetate formation in recombinant *E. coli* (Chang *et al.*, 1999). As an additional experimental validation, the intracellular concentration of acetyl-CoA was also analyzed in these strains (**Table 7**), obtaining a positive correlation between PHB formation and the concentration of this metabolite. In particular, the expression of the glycolytic genes encoded by Module I or Module II significantly increased the availability of this metabolic precursor by 1.7- and 1.4-fold, respectively, as compared to *E. coli* BW25113/pAeT41 + pSEVA224. Since acetyl-CoA is the substrate of the PHB synthesis

pathway, the accumulation of polymer can be correlated with the increase in precursor availability, assuming that all strains express the *phaC1AB1* gene cluster at similar levels. PHB accumulation in the control strain reached 25.6 ± 3.7% of the CDW, while the same strain transformed with either Module I or Module II attained 53.9 ± 3.1% and 62.9 ± 1.3% of the CDW, respectively (**Fig. 8c**). The residual CDW of either strain under PHB accumulation conditions was similar (**Table 7**), indicating that neither Module I nor II affected biomass formation significantly. Predictably, the expression in the same strain of the Module I and II from two independent plasmids resulted in the highest value of PHB accumulation. Such strain accumulated up to 72.5 ± 9.8% of the CDW in the form of PHB, representing an increase of *ca*. 3-fold as compared to *E. coli* BW25113/pAeT41 + pSEVA224. Interestingly, the overexpression of the glycolytic modules did not increase the overflow metabolism from acetyl-CoA (*i.e.*, synthesis of acetate). This result indicates that the recombinant strains probably rerouted this metabolite to produce PHB at the expense of acetate formation. Furthermore, this example of pathway engineering illustrates how the availability of key precursors in central carbon metabolism can be channeled into the formation of an added-value product while minimally affecting the physiology of the bacterial host.

In an attempt to determine which glycolytic fluxes were determinant in increasing PHB accumulation by these recombinants, two extra SEVA plasmids were constructed, in which individual GlucoBrick parts, belonging to either Module I or II, are expressed under the transcriptional control of a $LacI^Q/P_{trc}$ regulatory element. Plasmids pS424·*gapA* and pS224·GPG, carrying *glk*, *pfkA*, and *gapA* [see *Materials and Methods* section (**Table 3**) for details on the construction] were separately introduced into *E. coli* BW25113/pAeT41, and growth, glucose consumption, and PHB accumulation were tested under the same culture conditions indicated in the previous section. While an increase in the flux through GA3P dehydrogenase (*i.e.*, GapA) did not result in a significant increase of either glucose consumption or polymer synthesis, the expression of the *glk·pfkA·gapA* synthetic cluster from plasmid pS224·GPG significantly enhanced both parameters with respect to the control strain (**Fig. 8b** and **c**). PHB accumulation in this recombinant peaked at 66.4 ± 3.7% of the CDW (although there were no differences in the actual PHB concentration, see **Table 7**). Yet, boosting the glycolytic flux by means of Glk, Pfk, and GapA alone was not enough to reach the highest accumulation of PHB observed in the strain bearing both Modules I and II (*i.e.*, the whole complement of EMP enzymes). This result may in turn suggest that an appropriate *channeling* of metabolic intermediates from glucose all the way down to acetyl-CoA is only possible if an adequate balance of all the individual enzyme activities involved is met.

In summary, the GlucoBrick system has been systematically proved to be a useful tool for the targeted implementation of glycolytic capacities in different Gram-negative bacteria. In the context of this Thesis, this platform represents the first step to achieve the main objective of the whole project: to refactor central carbon metabolism in *P. putida* KT2440, transforming the native glucose catabolism into a synthetic, predictable linear EMP pathway. The next chapters explain in detail the steps followed to complete this ambitious

objective that comprises the generation of a suitable *P. putida* KT2440 *glycolytic chassis* to accommodate the grafted metabolic pathway, while dissecting the biochemical principles coordinating the intricate metabolism of this bacterium.

CHAPTER 2

Design and construction of *P. putida* GC (*Glycolytic Chassis*): The starting point for deep refactoring of central carbon metabolism in environmental bacteria

Background

P. putida KT2440 is an environmental Gram-negative bacterium with a large number of interesting features for biotechnological processes. These characteristics include its generally recognized as safe (*GRAS*) status classification (Federal Register. Appendix E, 1982), the high resistance to oxidative stress (Poblete-Castro *et al.*, 2012; 2017; Regenhardt *et al.*, 2002), its amenability to genetic manipulations (Lieder *et al.*, 2015; Martínez-García *et al.*, 2014a,b; Silva-Rocha *et al.*, 2013), and the availability of different metabolic models (Belda *et al.*, 2016; Nogales *et al.*, 2008; Puchałka *et al.*, 2008; Sohn *et al.*, 2010). Accordingly, this bacterium is an appealing starting point for a deep metabolic refactoring, such as the simplification of its genetic components as an approach to generate a useful metabolic *chassis* for different applications. Glucose metabolism in *P. putida* (which is based on the ED pathway and the EDEMP cycle) is a remarkable example of adaptation to the natural environment, wiring the formation of reducing power (in the form of NADPH) and the specific adaptation to environments characterized by harsh conditions. The formation of NADPH comes, however, at the cost of ATP synthesis, as the ED pathway yields half the amount of ATP as compared to the EMP pathway (Ng *et al.*, 2015). An important number of bioprocesses mediated by cell factories in the industry have been described to be dependent on ATP availability (Hara & Kondo, 2015; Schuster, 2000). Therefore, the implementation of a linear EMP pathway (where the ATP yield per molecule of glucose is higher than that mediated by the ED pathway) could be an interesting approach to improve the energy balance in *P. putida* KT2440. Before considering the actual Metabolic Engineering manipulations needed to enable a linear glycolysis in *P. putida* KT2440, it was necessary to design a genetic *chassis* to host these heterologous enzyme activities. This *chassis*, named *P. putida* GC (***g***lycolytic ***c***hassis), is based in a *P. putida* KT2440, freed of several native glycolytic activities. The present chapter describes the set of deletions introduced in *P. putida* GC to improve glucose uptake and permit implementation of a linear EMP glycolysis.

2.1. Streamlining glucose uptake to avoid ATP consumption through the native system of *P. putida* KT2440

2.1.1. Glucose uptake system in *P. putida* KT2440. *P. putida* KT2440 can introduce glucose in its central carbon metabolism by two different routes (**Fig. 9a**): (i) phosphorylation in the cytoplasm by Glk, or (ii) oxidation in the periplasm to gluconate and/or 2KG through the activity of Gcd and/or Gad (del Castillo *et al.*, 2007; 2008; Fuhrer *et al.*, 2005; Latrach-Tlemçani *et al.*, 2008). Glucose uptake into the cytoplasm, where Glk is able to phosphorylate glucose, is based on an ABC transport system coupled to OprB porins (**Fig. 9a**). More precisely, the OprB porins [OprB-1 (PP_1019) and OprB-2 (PP_1445)] facilitate the diffusion of glucose across the outer membrane (del Castillo *et al.*, 2007; Wylie & Worobec, 1995). Subsequently, the ABC transport system captures the glucose from the periplasmic space with the aid of the periplasmic sugar-binding protein encoded by the gene *gtsA* (*PP_1015*). This complex, composed by the sugar and the periplasmic-binding protein (**Fig. 9b**), interacts with the *core* of the ABC transporter system encoded by the genes *gtsB* (*PP_1016*), *gtsC* (*PP_1017*), and *gtsD* (*PP_1018*) to introduce the carbohydrate into the cytoplasm (Schneider, 2001). Taking into account our main goal (*i.e.*, to implement a functional EMP pathway with a high ATP yield), it is necessary to have a suitable glucose transport system where energy consumption is avoided. This is certainly not the case of the native system to uptake glucose in *P. putida* KT2440, based in an ABC transport system directly correlated with the hydrolysis of ATP. In this chapter, removal of the native glucose uptake in *P. putida* KT2440 is described as the first step to reach the goal of generating a *P. putida* GC strain.

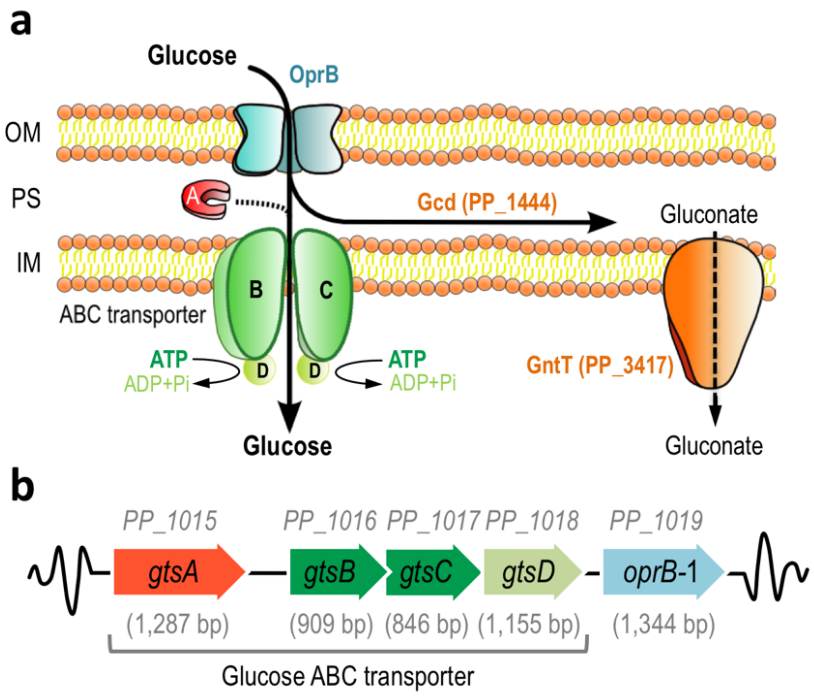

Figure 9 | **Glucose uptake in *P. putida* KT2440.** (**a**) The scheme depicts the ways that glucose follows to enter the central carbon metabolism of *P. putida* KT2440. The capital letters shown in the picture indicate the genes that encode each subunit of the ABC transporter. Abbreviations are as follows: GntT, gluconate transporter from the periplasmic space to the cytoplasm; OM, outer membrane; PS, periplasmic space; and IM, inner membrane. (**b**) Genomic context of the genes involved in glucose uptake. The adjacent location of the genes with respect to each other is an example of the functional organization within a genomic region with a specific role (in this case, glucose uptake); the transcriptional activity of which becomes relevant when the bacteria are grown in the presence of glucose (del Castillo *et al.*, 2007).

The elimination of the native glucose uptake activity in *P. putida* KT2440 is based on two different deletion processes: (i) removing the Gcd activity, and (ii) blocking the participation of the glucose ABC transporter in hexose uptake. In order to better understand the functional relevance of each element in hexose uptake and processing, a set of different mutants was generated in this study. In first place, a Δ*gcd* and Δ*gts* mutant strains were separately constructed as indicated in the *Materials and Methods* section. In the case of the Δ*gts* strain, the mutant was generated by a single deletion event that simultaneously removed the *gtsA*, *gtsB*, *gtsC*, and *gtsD* genes. At the same time, a Δ*gts* Δ*gcd* double mutant derivative of strain KT2440 was constructed by consecutively entering both deletions **(Figs. 10a and b)**.

a

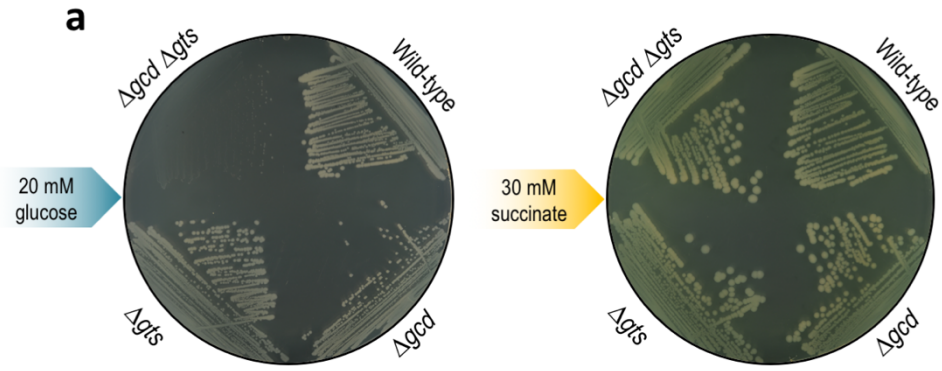

b

Strain	M9 minimal medium +	
	20 mM glucose	30 mM succinate
P. putida KT2440	✓	✓
P. putida Δ*gcd*	✓	✓
P. putida Δ*gts*	✓	✓
P. putida Δ*gcd* Δ*gts*	✗	✓

Figure 10 | **Growth phenotype characterization of glucose transport mutants.** (**a**) M9 minimal medium plates, containing either 20 mM glucose (top panel, plate shown in the left) or 30 mM succinate (top panel, plate shown in the right), were seeded with *P. putida* KT2440 (wild-type), and the mutants Δ*gcd* (*PP_1444*, encoding glucose dehydrogenase), Δ*gts* [Δ*gtsA* (*PP_1015*), Δ*gtsB* (*PP_1016*), Δ*gtsC* (*PP_1017*), and Δ*gtsD* (*PP_1018*)], and Δ*gcd* Δ*gts*. (**b**) Summary of the growth phenotypes of the strains under study (" ✓ " indicates growth, and " ✗ " indicates that the strain could not grow under the specific conditions tested in each case).

As indicated in **Fig. 9a**, *P. putida* KT2440 is able to introduce glucose in the central carbon metabolism by two different ways: oxidation (mediated by Gcd/Gad in the periplasmic space) and/or by phosphorylation (mediated by Glk in the cytoplasm). The literature indicates that less than 10% of the hexose enters into glucose catabolism *via* Glk, while the remaining 90% is oxidized by Gcd in the periplasmic space to enter into the central carbon metabolism as gluconate (Nikel *et al.*, 2015a). In full accordance with these figures, the results displayed in **Fig. 10a** and **b** indicate the capacity of *P. putida* KT2440 to grow in glucose in spite of the individual absence of Gcd activity or ABC-mediated transport. The results in this section also demonstrate that the only way to obtain a *P. putida* mutant where glucose uptake is altogether interrupted is through the simultaneous elimination of the Gcd activity *and* the glucose ABC transporter. This strain (Δ*gcd* Δ*gts*) constitutes the point of departure to analyze the functionality of an orthogonal glucose transport system in *P. putida* GC, thereby bypassing the intrinsic ATP consumption of the native system.

2.1.2. Recruitment of the glucose facilitator (*glf*) from *Zymomonas mobilis* as an alternative transport system for *P. putida* KT2440. Glucose can be introduced into the bacterial cytoplasm by means of different transport systems. As previously mentioned, ATP saving is an important principle in various industrial bioprocess (Hara & Kondo, 2015). However, glucose transport is generally regulated following a *no pain-no gain* scheme in terms of energy. The cost of glucose uptake in terms of energy expenditure is reflected by the three main different models of hexose intake: (i) the PTS system, predominant in Enterobacteria, (ii) cation- or proton- linked permeases, and (iii) ABC transporters (Baldwin & Henderson, 1989; Postma *et al.*, 1993). All these systems use metabolic energy in the form of phosphoenolpyruvate or proton-motive force. An interesting exception in terms of mechanism of hexose transport is exemplified by the system of the strictly fermentative, Gram-negative bacterium *Zymomonas mobilis*, where glucose uptake is fulfilled by the Glf glucose facilitator encoded by the *glf* gene (Dimarco & Romano, 1985). Briefly, Glf is an ATP-independent, low-affinity, and high velocity carrier protein that is able to transport glucose, fructose, and xylose (Dimarco & Romano, 1985; Schoberth & de Graaf, 1993). Glf belongs to the group of GLUT proteins that comprise members of the major facilitator superfamily of membrane transporters from both prokaryotes and eukaryotes (Baldwin, 1993).

Taking into account all the features described above, and assuming the functionality of the Glf-mediated glucose transport in other Gram-negative bacteria, *e.g.*, *E. coli* (Nikel & de Lorenzo, 2013b; Weisser *et al.*, 1995), this system was selected as a candidate transporter for *P. putida* GC. As a first step, the DNA sequence encoding the Glf transporter (*glf*, *ZMO0366*) was edited *in silico* to eliminate the restriction sites incompatible with the sites present in plasmids belonging to the SEVA platform (Martínez-García *et al.*, 2014a; Silva-Rocha *et al.*, 2013). The Glf module comprises a synthetic RBS followed by the *glf* edited sequence and flanked by *Eco*RI and *Kpn*I sites. This synthetic DNA cassette was cloned in the pSEVA438 vector (pBBR1, Sm^R/Sp^R), generating plasmid pS438·*glf*. This plasmid was used to check

whether Glf is able to restore the growth of *P. putida* KT2440 Δ*gts* Δ*gcd* on glucose as the sole carbon source. This plasmid was introduced in the mentioned mutant, and the growth phenotype was tested in M9 minimal medium plates with 20 mM glucose and proper induction (3-*m*B at 1 mM). The resulting strain was able to grow on glucose, a suitable control to check for the Glf functionality in *P. putida* KT2440.

Once this experiment was carried out as a *proof-of-concept* of the heterologous Glf function, the next step was the stable insertion of the Glf module the chromosome of *P. putida* GC. A pBAMD transposon vector was designed to deploy the Glf module described above. The Glf-encoding DNA fragment was transferred into the mini-Tn*5*–based vector pBAMD1-2 (giving rise to pBAMD1-2·*glf*, Km^R). After the transposon delivery plasmid was amplified in an appropriate *E. coli* host (*E. coli* CC118 λ*pir)*, a tripartite conjugative mating was employed to enter the transposon into the recipient strain (*P. putida* KT2440 Δ*gts* Δ*gcd*). Note that this approach, in which the DNA cargo (devoid of any promoter region) borne by the transposon is randomly inserted in the target chromosome, not only enables the stable insertion of the module, but it also results in a library of independent insertions expected to display different levels of transcription (thereby resulting in different amounts of Glf activity). In this case, the screening of successful insertion events was simplified by the fact that, after the exconjugants were plated in M9 minimal medium with Km and 0.2% (w/v) citrate (to select *P. putida* over *E. coli*), only the clones displaying an adequate level of Glf activity are able to grow in M9 medium plates containing glucose as the sole carbon source. In all these cases, the successful exconjugants were inoculated in 96-well microtiter plates in M9 minimal medium containing 20 mM glucose, and bacterial growth was assessed by measuring the OD_{600} over time in a microtiter plate reader in order to select the exconjugant(s) with the highest specific growth rate (**Fig. 11a**).

The single-copy insertion of *glf* from *Z. mobilis* is able to rescue the growth phenotype of *P. putida* KT2440 Δ*gcd* Δ*gts* in M9 minimal medium with glucose as the sole carbon source (**Fig. 11b**). Interestingly, the specific growth rate of one of the exconjugants selected (*i.e.*, *P. putida* KT2440 Δ*gcd* Δ*gts*·T) reached a similar value to that of the WT strain grown in the same conditions (**Fig. 11c**). The final cell density was likewise similar in the two strains under comparison. Randomly-amplified PCR was used to locate the site of insertion of the mini-Tn*5* module containing *glf* in this exconjugant. The insertion mapped in the 120-bp-long *PP_5SE* gene. This gene is one out of seven 5S ribosomal RNA genes encoded in the chromosome, and an insertion in this position is expected to result in a high rate of gene expression (Ammons *et al.*, 1999). In summary, the implementation of a single-copy insertion of *glf* in the chromosome allows a glucose transport-deficient derivative of *P. putida* to uptake enough glucose to support bacterial growth up to the level of the WT strain.

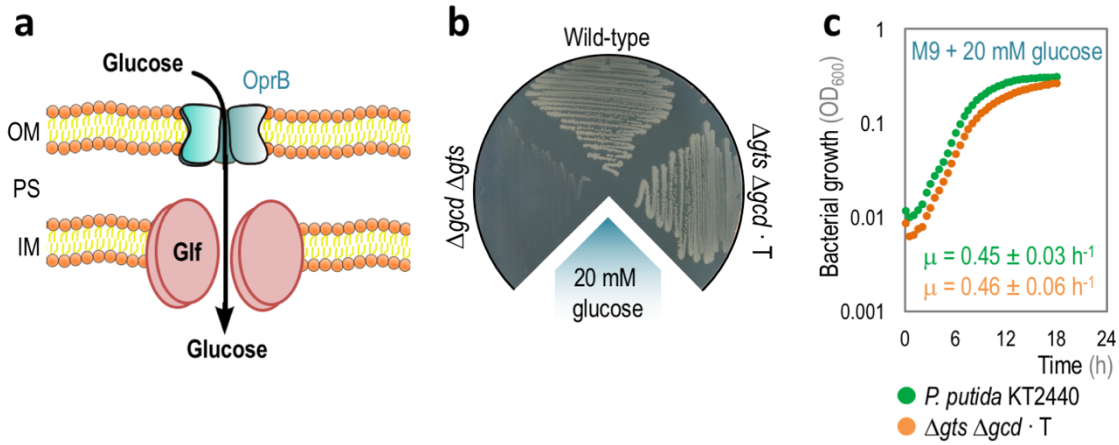

Figure 11 | **Glf functionality in a glucose transport-deficient derivative of *P. putida* KT2440.** (**a**) The scheme depicts the role that Glf plays in glucose uptake of *P. putida* KT2440 Δ*gcd* Δ*gts* mutant. Abbreviations are as follows: OM, outer membrane; PS, periplasmic space; and IM, inner membrane. (**b**) Growth phenotypes of the different strains under study. M9 minimal medium plates containing 20 mM glucose were seeded with *P. putida* KT2440 (wild-type), and the mutants Δ*gcd* Δ*gts*, and Δ*gcd* Δ*gts*·T [*i.e.*, Δ*gcd* Δ*gts* with a mini-Tn*5* transposon module inserted in the chromosome, carrying the *glf* gene (Transporter)]. (**c**) Growth curves of *P. putida* KT2440 and the exconjugant Δ*gcd* Δ*gts*·T on M9 minimal medium with 20 mM glucose. Each data point in the growth curve represents the mean value of the OD_{600} in quadruplicate measurements from at least three independent experiments. The specific growth rates (μ) were calculated from these data during exponential growth, and the inset shows the mean value ± standard deviations for each strain.

2.2. The metabolic fate of glucose in *P. putida* KT2440: A key issue to solve in order to implement a functional EMP pathway

High rates of reducing power (*i.e.*, NADPH) regeneration per molecule of glucose are relevant in order to counteract different types of environmental stress (Kim & Park, 2014). This evolutive necessity seems to have been addressed by the metabolic connectivities of the EDEMP cycle (encompassing activities from the ED, EMP, and PP pathways; **Fig. 12**), where the ED pathway serves as the main glycolytic route while the (incomplete) EMP assumes the role of regenerating hexoses-*P* from trioses-*P* (Nikel *et al.*, 2015a). On top of this metabolic versatility in the *core* metabolism, many environmental bacteria have branched pathways to introduce glucose (del Castillo *et al.*, 2007; 2008; Lessie & Phibbs, 1984). Taking into account all these features, the native metabolism of *P. putida* KT2440 needs to be streamlined and simplified in order to implement a linear glycolysis based on the EMP pathway carried by the GlucoBrick system. For this reason, one of the main goals in this Thesis was the generation of a set of mutants in which to avoid glucose misrouting, a necessary principle to funnel the hexose into a linear glycolysis. More particularly, the target metabolic nodes to remove from the central carbon metabolism of *P. putida* are both hexose phosphorylation and oxidation: (i) Glk, (ii) Gcd, and (iii) Gad activities **(Fig. 12)**.

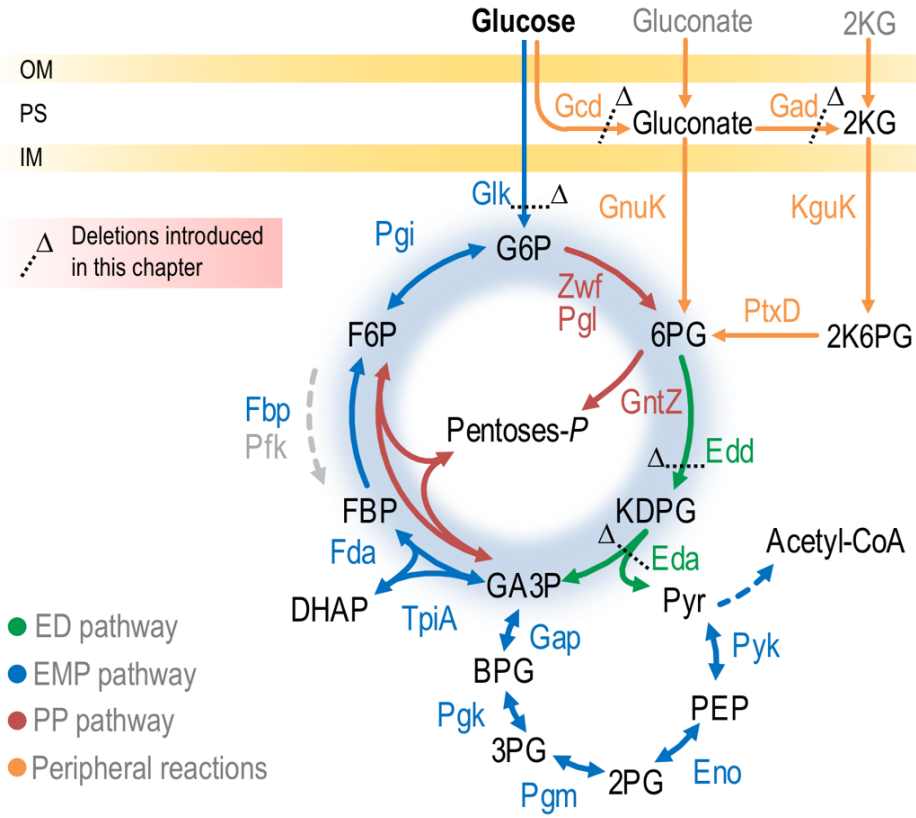

Figure 12 | **Schematic representation of central carbon metabolism in *P. putida* KT2440.** Glucose catabolism occurs mainly through the activity of the Entner-Doudoroff (ED) pathway, but part of the trioses-*P* thereby generated are recycled back to hexoses-*P* by means of the *EDEMP cycle*, that also encompasses activities from the Embden-Meyerhof-Parnas (EMP) and pentose phosphate (PP) pathways. Note that a set of *peripheral reactions* can also oxidize glucose to gluconate and/or 2-ketogluconate (2KG) before any phosphorylation of the intermediates occurs. Each metabolism block is indicated with different color and the EDEMP cycle is shaded in blue in the diagram. Note that 6-phosphofructo-1-kinase (Pfk) activity is absent and is indicated as a dashed grey row. The deletions introduced in genes encoding metabolic enzymes targeted in this chapter are indicated by a Δ symbol. The abbreviations used in this picture are as follows: G6P, glucose-6-*P*; F6P, fructose-6-*P*; FBP, fructose-1,6-P_2; DHAP, dihydroxyacetone-*P*; GA3P, glyceraldehyde-3-*P*; BPG, glycerate-1,3-P_2; 3PG, glycerate-3-*P*; 2PG, glycerate-2-*P*; PEP, phosphoenolpyruvate; Pyr, pyruvate; 6PG, 6-phosphogluconate; KDPG, 2-keto-3-deoxy-6-phosphogluconate; acetyl-CoA, acetyl-coenzyme A; 2K6PG, 2-ketogluconate-6-*P*; OM, outer membrane; PS, periplasmic space; and IM, inner membrane.

Glucokinase (Glk). The main hexose kinase activity in *P. putida* KT2440 is encoded by the *glk* gene, *i.e.*, *PP_1011* (del Castillo *et al.*, 2007). This enzyme allows *P. putida* KT2440 to phosphorylate glucose into G6P in the cytoplasm. Then, G6P can be transformed into 6PG by the action of the Zwf, the required intermediary to introduce glucose in the ED pathway *via* phosphorylation (**Fig. 12**). In spite of the fact that only 10% of the glucose entering the network is phosphorylated to G6P (Nikel *et al.*, 2015a), we planned to remove this native activity from *P. putida* in or order to facilitate the subsequent implantation of the Glk activity from the GlucoBrick system. As indicated in **Fig. 13a**, this operation avoids any potential interaction between such unrelated enzymes [*i.e.*, cellular machinery *vs.* implanted genetic constructs (Kim & Copley, 2012)].

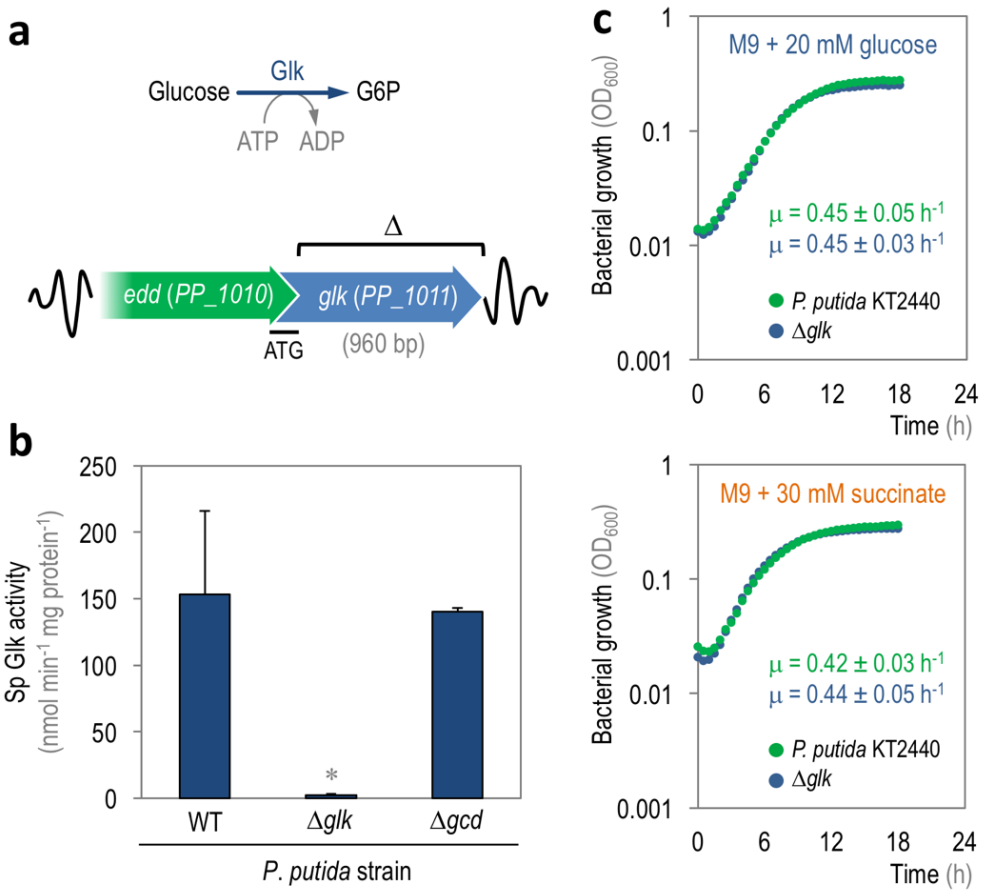

Figure 13 | **Characterization of the *glk* deletion in *P. putida* KT2440.** (**a**) The scheme depicts the location of the *glk* gene in the chromosome of *P. putida* KT2440, and the ATP-dependent reaction catalyzed by Glk. Note that the *STOP* codon of the *edd* gene overlaps with the beginning of the *glk* coding region. As detailed in the *Materials and Methods* section, the deletion introduced in this locus (indicated with a Δ symbol in the outline) eliminates most of the *glk* gene without affecting *edd*. (**b**) *In vitro* quantification of the specific (Sp) Glk activity in wild-type (WT) *P. putida* KT2440, and its Δ*glk* and Δ*gcd* mutant derivatives. All the strains employed for the *in vitro* enzymatic assays were grown on M9 minimal medium added with glucose at 20 mM and cells were harvested in mid-exponential phase to obtain the cell-free extracts. Each bar represents the mean value of the corresponding enzyme activity ± standard deviation of quadruplicate measurements from at least two independent experiments. Significant differences ($P < 0.05$, as evaluated by means of the Student's *t* test) in the pair-wise comparison of a given recombinant to the control WT strain are indicated by an asterisk. (**c**) Growth curves of *P. putida* KT2440 and its Δ*glk* derivative under glycolytic (M9 minimal medium with 20 mM glucose) or gluconeogenic (M9 minimal medium with 30 mM succinate) conditions. Each data point represents the mean value of the optical density measured at 600 nm (OD_{600}) of quadruplicate measurements from at least three independent experiments. The specific growth rates (μ) were calculated from these data during exponential growth, and the inset shows the mean values ± standard deviations for each strain.

The results shown in **Fig. 13b** indicate that the deletion of the *glk* (*PP_1011*) gene results in the loss of any detectable Glk activity in *P. putida* KT2440 (del Castillo *et al.*, 2007). At the same time, the deletion of *gcd* gene does not seem to affect the Glk activity in *P. putida* KT2440. The growth phenotype of the Δ*glk* mutant was also analyzed in order to elucidate its importance in the bacterial fitness in liquid cultures (**Fig. 13c**) and in plates (**Figs. 17a** and **b**). The results suggest that the absence of the Glk activity is not critically important for the overall fitness of the bacterium, maintaining similar values for the specific growth rate (**Fig. 13c**), under either glycolytic or gluconeogenic conditions (*i.e.*, growing on M9 minimal medium with 20 mM glucose or 30 mM succinate, respectively).

Glucose dehydrogenase (Gcd). The Gcd activity in *P. putida* KT2440 is executed by the protein encoded by the *gcd* gene, *i.e.*, *PP_1444* (del Castillo *et al.*, 2007). This enzyme is an example of inner membrane-bound glucose dehydrogenase (An & Moe, 2016), that requires the redox cofactor pyrroloquinoline quinone (PQQ). Gcd allows *P. putida* KT2440 to transform glucose into gluconate in the periplasmic space, a rather relevant role if one considers that almost 90% of the glucose that enters the central carbon metabolism of this bacterium gets oxidized (Nikel *et al.*, 2015a). This transformation of glucose into oxidized products is counterproductive for our purposes, as the use of hexoses in peripheral reactions is a competing pathway for the intended linear glycolysis (**Fig. 12**). Elimination of the Gcd activity, the first committed step in the oxidation peripheral pathway, was thus of capital importance for the construction of *P. putida* GC (**Fig. 14a**).

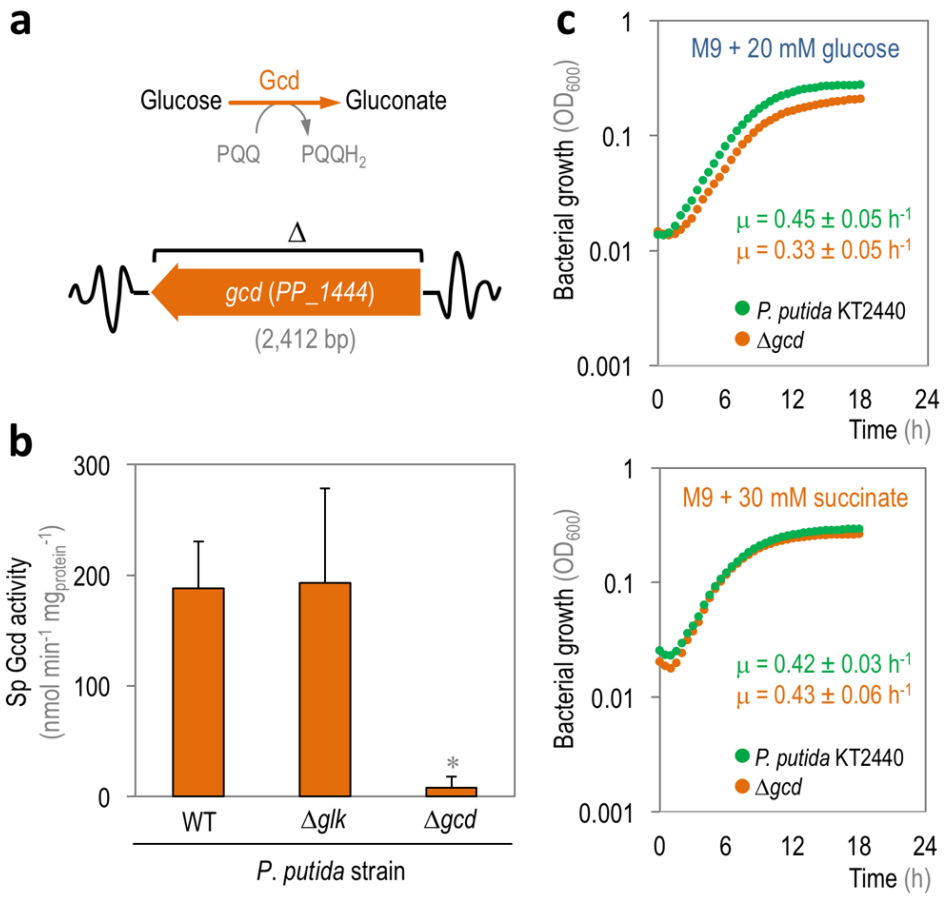

Figure 14 | **Characterization of the *gcd* deletion in *P. putida* KT2440.** (**a**) The scheme depicts the location of the *gcd* gene in the chromosome of *P. putida* KT2440, and the deletion introduced in this locus (indicated with a Δ symbol in the outline). The relative orientation of *gcd* (*i.e.*, in the reverse strand) is also indicated in the diagram. Note that the oxidation of glucose into gluconate proceeds *via* the reduction of the redox cofactor pyrroloquinoline quinone (PQQ). (**b**) *In vitro* quantification of the specific (Sp) Gcd activity in wild-type (WT) *P. putida* KT2440, and its Δ*glk* and Δ*gcd* mutant derivatives. All the strains employed for the *in vitro* enzymatic assays were grown on M9 minimal medium added with glucose at 20 mM and cells were harvested in mid-exponential phase to obtain the cell-free extracts. Each bar represents the mean value of the corresponding enzyme activity ± standard deviation of quadruplicate measurements from at least two independent experiments. Significant differences ($P < 0.05$, as evaluated by means of the Student's *t* test) in the pair-wise comparison of a given recombinant to the control WT strain are indicated by an asterisk. (**c**) Growth curves of *P. putida* KT2440 and its Δ*gcd* derivative under glycolytic (M9 minimal medium with 20 mM glucose) or gluconeogenic (M9 minimal medium with 30 mM succinate) conditions. Each data point represents the mean value of the optical density measured at 600 nm (OD_{600}) of quadruplicate measurements from at least three independent experiments. The specific growth rates (μ) were calculated from these data during exponential growth, and the inset shows the mean values ± standard deviations for each strain.

The *gcd* deletion altogether eliminated the Gcd activity in the *P. putida* KT2440, in contrast with the WT and Δ*glk* controls, which displayed similar levels of specific Gcd activity (**Fig. 14b**). In terms of growth phenotype (**Fig. 14c**), the Δ*gcd* mutant was more affected than the previously analyzed Δ*glk* strain (μ = 0.33 h^{-1} *vs.* μ = 0.45 h^{-1}, respectively) when the bacteria were growing in M9 minimal medium with 20 mM glucose. This phenotype does not involve a dramatic effect in terms of overall fitness, but it could reflect the preference that this bacterium has to metabolize glucose mainly by the oxidative branch (Nikel *et al.*, 2015a). Additionally, the results indicated in **Fig. 14c** demonstrate that the absence of Gcd activity is not revelant for growth under gluconeogenic conditions (*i.e.*, in M9 minimal medium with 30 mM succinate). It should be noted that, as expected, the accumulation of the Δ*glk* and Δ*gcd* deletions in the same strain prevented *P. putida* KT2440 to grow in glucose (**Figs. 17a** and **b**). This phenotype is in accordance with the hypothesis that hexose consumption can be blocked by limiting the entrance of glucose into central catabolism through both phosphorylation (*i.e.*, Glk) and oxidation (*i.e.*, Gcd).

Gluconate 2-dehydrogenase (Gad). The Gad activity in *P. putida* KT2440 is carried out by an enzymatic complex comprising three different gene products: PP_3382, PP_3383, and PP_3384. More precisely, Gad activity is driven by a membrane-bound flavin adenine dinucleotide (FAD)-containing gluconate 2-dehydrogenase (FAD-GADH). Such FAD-GADH activity has been characterized to some extent in *P. aeruginosa* (Matsushita *et al.*, 1982), allowing us to identify the orthologues in *P. putida* KT2440. These regions have the following features: (i) the largest subunit of the complex is encoded by the *PP_3383* gene (with a product of 594 amino acids) and comprises the dehydrogenase subunit that contains FAD as the prosthetic group, which is covalently bound to the histidine residue of the subunit (McIntire *et al.*, 1985); (ii) the middle subunit (with a product of 417 amino acids) is encoded by the *PP_3382* gene and contains the heme *c* cofactor, which probably allows the electron transfer from the FAD in the dehydrogenase subunit to

the ubiquinone carrier placed in the inner membrane, connecting the oxidation of the substrate with the respiratory chain (Matsushita *et al.*, 1994); and (iii) the small subunit (with a product of 246 amino acids) is encoded by the *PP_3384* gene and it was annotated *in silico*, only in the case of *P. aeruginosa*, as a γ subunit of the FAD-GADH complex.

In this work, the complete removal of the group of genes *PP_3382-4* was done by a single deletion event. The pair of genes *PP_3382* and *PP_3383* have a properly annotated function in the *Pseudomonas* database (Winsor *et al.*, 2016) and in the recent resequencing of the genome of strain KT2440 (Belda *et al.*, 2016). *PP_3384* does not present a clear function in strain KT2440, and it was removed since studies in other species support a key role of the product encoded by this gene in sugar oxidation (Arellano *et al.*, 2010). Additionally, the role of the products encoded by *PP_3623* and *PP_4232* in the overall Gad activity was also evaluated by eliminating the corresponding coding sequences. In the case of *PP_3623* (encoding a product of 447 amino acids), the *in silico* annotation describes the product of this gene as the cytochrome *c* subunit of an alcohol dehydrogenase (and likely a sugar dehydrogenase, too). At the same time, *PP_3623* is considered to be a duplication of the *PP_3382* gene with a high level of statistical significance. The *PP_4232* gene (encoding a product of 403 amino acids) has not been assigned any function but is also considered to be a duplication of the *PP_3382* gene with a high level of statistical significance. For these reasons, the deletion of both *PP_3623* and *PP_4232* was implemented along the elimination of *PP_3382-PP_3384* in order to completely remove the Gad activity in *P. putida* KT2440 (**Fig. 15a**).

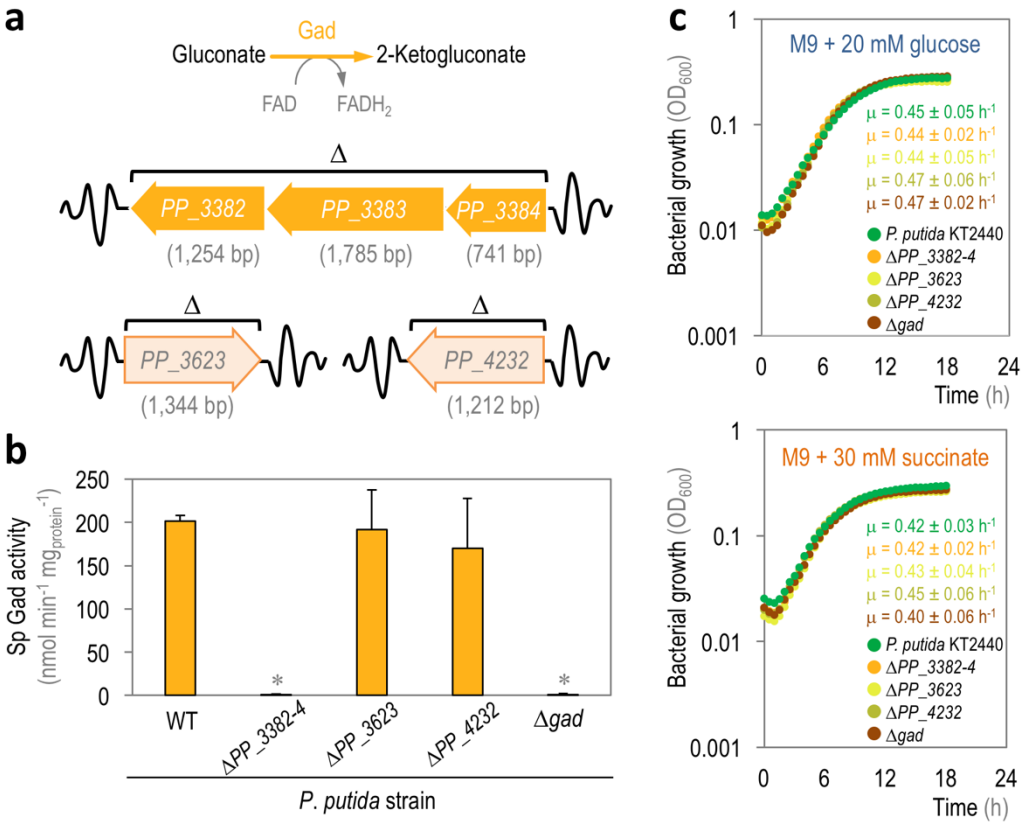

Figure 15 | **Characterization of the Gad activity removal in *P. putida* KT2440.** (**a**) The scheme depicts the distribution of the hypothetical genes involved in the Gad activity in the chromosome of *P. putida* KT2440, and the biochemical reaction they encode. The relative orientation of the genes in the chromosome is likewise indicated. (**b**) *In vitro* quantification of the specific (Sp) gluconate 2-dehydrogenase (Gad) activity in wild-type (WT) *P. putida* KT2440, and the mutant strains Δ*PP_3382-4* (which comprises the deletions of *PP_3382*, *PP_3383*, and *PP_3384*), Δ*PP_3623*, Δ*PP_4232*, and Δ*gad* (which comprises the deletions from Δ*PP_3382-4*, Δ*PP_3623*, and Δ*PP_4232*). All the strains employed for the *in vitro* enzymatic assays were grown on M9 minimal medium added with glucose at 20 mM and cells were harvested in mid-exponential phase to obtain the cell-free extracts. Each bar represents the mean value of the corresponding enzyme activity ± standard deviation of quadruplicate measurements from at least two independent experiments. Significant differences ($P < 0.05$, as evaluated by means of the Student's *t* test) in the pair-wise comparison of a given recombinant to the control WT strain are indicated by an asterisk. (**c**) Growth curves of *P. putida* KT2440 and partial and full mutants blocked in the Gad activity under glycolytic (M9 minimal medium with 20 mM glucose) or gluconeogenic (M9 minimal medium with 30 mM succinate) conditions. Each data point represents the mean value of the optical density measured at 600 nm (OD_{600}) of quadruplicate measurements from at least three independent experiments. The specific growth rates (μ) were calculated from these data during exponential growth, and the inset shows the mean values ± standard deviations for each strain.

The results shown in **Fig. 15** shed light on the genotype-to-phenotype wiring of the Gad activity in *P. putida* KT2440. Firstly, the pool of genes involved in the oxidation of gluconate into 2KG could be unambiguously identified (**Fig. 15b**). More precisely, the bulk Gad activity could be traced to the products of the *PP3382-4* operon; the products encoded by *PP_3623* and *PP_4232* displaying a marginal influence in the Gad activity with a non-statistical significance. On the other hand, the growth phenotype evaluated in both liquid medium (**Fig. 15c**) and plates (**Figs. 17a** and **b**) indicated that the Gad activity is largely irrelevant in terms of bacterial fitness, since very similar values of specific growth rates were observed in all the mutants evaluated under glycolytic (M9 minimal medium with 20 mM glucose) or gluconeogenic (M9 minimal medium with 30 mM succinate) conditions (**Fig. 15c**). In the light of the aforementioned results, the complete set of deletions for Gad activity (Δ*PP_3382-4*, Δ*PP_3623*, and Δ*PP_4232*) was introduced in the KT2440 genetic background in order to avoid glucose misrouting into oxidation pathways in *P. putida* GC.

2.3. Removing the ED pathway of *P. putida* KT2440 to establish a linear glycolysis

The ED pathway is the fundamental pillar for glucose catabolism in *P. putida* KT2440 (**Fig. 12**), and the only way that this bacterium has to consume this hexose due to the absence of a complete, catabolic EMP pathway, which is blocked at the level of Pfk (del Castillo *et al.*, 2007; Fuhrer *et al.*, 2005; Latrach-Tlemçani *et al.*, 2008; Nikel *et al.*, 2015a; Vicente & Cánovas, 1973a,b). The ED pathway enables *P. putida* KT2440 to obtain Pyr and GA3P from glucose, key intermediates in order to regenerate hexoses-*P* through the EDEMP cycle, and also to obtain energy and reducing power by means of the TCA cycle (Nikel *et al.*, 2015a). Basically, the ED pathway in strain KT2440 is composed by the sequential activity of Edd encoded by the *edd* gene (*PP_1010*), which transforms 6PG into KDPG; and Eda encoded by the *eda* gene

(*PP_1024*), which transforms KDPG into Pyr and GA3P. The next step in the stepwise construction of *P. putida* GC was to remove the components of the extant ED pathway (**Fig. 16a** and **b**).

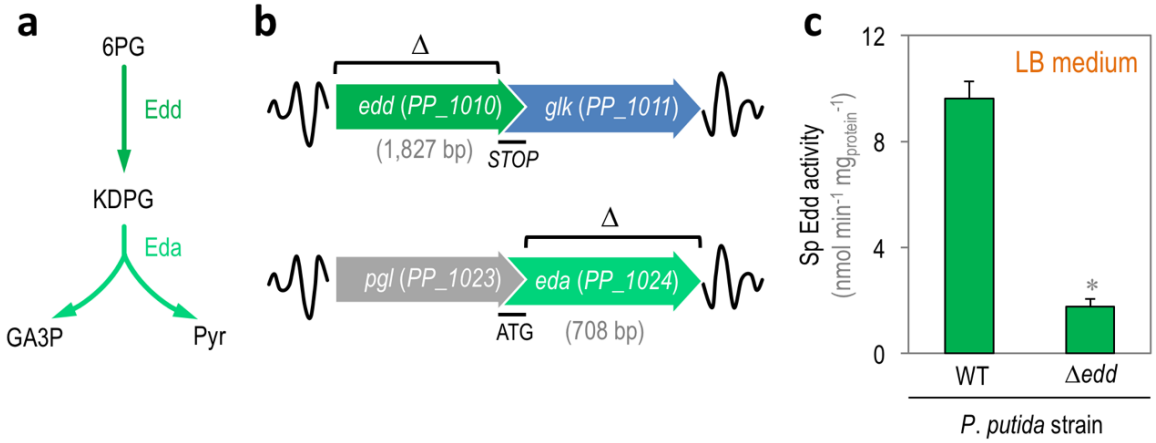

Figure 16 | **Interrupting the Entner-Doudoroff (ED) pathway of *P. putida* KT2440.** (**a**) The two-step ED pathway in *P. putida* KT2440. Abbreviations are as follows: 6PG, 6-phosphogluconate; KDPG, 2-keto-3-deoxy-6-phosphogluconate; GA3P, glyceraldehyde-3-*P*; Pyr, pyruvate; Edd, 6-phosphogluconate dehydratase; and Eda, 2-keto-3-deoxy-6-phosphogluconate aldolase. (**b**) The scheme indicates the distribution of the genes involved in the ED pathway in the chromosome of *P. putida* KT2440. Note that for both *edd* and *eda* there is an overlapping of the corresponding coding regions with adjoining genes (likely indicating co-regulation of the members in the gene cluster). The deletions implemented in this study (indicated with a Δ symbol in the outline) are shown in the outline, and do not affect the expression of the genes in the vicinity of the target loci. (**c**) *In vitro* quantification of the specific (Sp) Edd activity in wild-type (WT) *P. putida* KT2440 and its Δ*edd* mutant derivative. All the strains employed for the *in vitro* enzymatic assays were grown on LB medium and cells were harvested in mid-exponential phase to obtain the cell-free extracts. Each bar represents the mean value of the corresponding enzyme activity ± standard deviation of quadruplicate measurements from at least two independent experiments. Significant differences ($P < 0.05$, as evaluated by means of the Student's *t* test) in the pair-wise comparison of a given recombinant to the control WT strain are indicated by an asterisk.

Fig. 16a indicates that it is possible to block the ED pathway by eliminating the first committed step (*i.e.*, Edd). In this case, the deletion of the *edd* gene prevents *P. putida* KT2440 to transform 6PG into KDPG, as reflected in the *in vitro* enzymatic assay (**Fig. 16c**). Given that the Δ*edd* mutant cannot grow on glucose as the only carbon source (**Figs. 17a** and **b**), the *in vitro* enzymatic assay of the Edd activity was performed in cell-free extracts obtained from LB medium cultures. The Edd activity in *P. putida* KT2440 grown in LB medium was low (approximately 3%) as compared with that in cells grown under strictly glycolytic conditions (Nikel *et al.*, 2015a). Even when blocking the Edd step of the ED pathway was enough to prevent the glucose-dependent growth of strain KT2440, both Δ*edd* and Δ*eda* deletions were introduced in *P. putida* GC to avoid any potential misrouting of central metabolic intermediates. **Figs. 17a** and **b** summarize the growth phenotypes of all the *P. putida* KT2440 mutants constructed and described in this chapter under both glycolytic and gluconeogenic conditions.

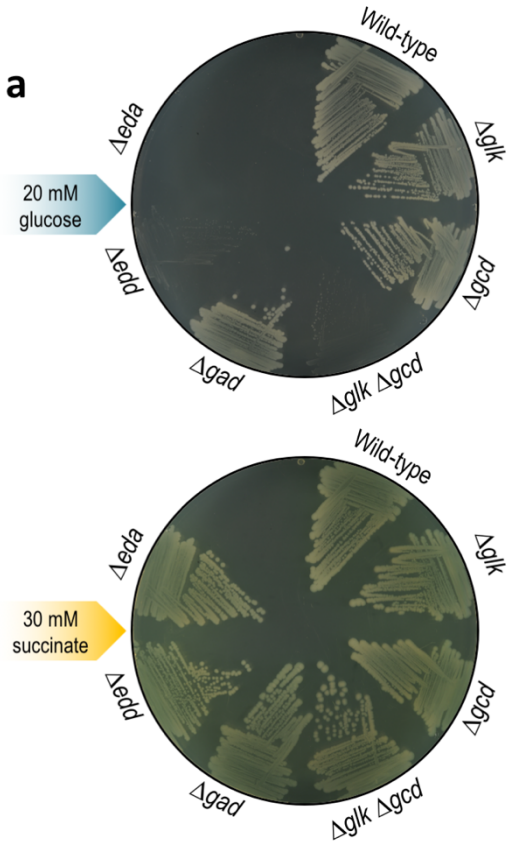

Strain	M9 minimal medium +	
	20 mM glucose	30 mM succinate
P. putida KT2440	✓	✓
P. putida Δ*glk*	✓	✓
P. putida Δ*gcd*	✓	✓
P. putida Δ*glk* Δ*gcd*	✗	✓
P. putida Δ*gad*	✓	✓
P. putida Δ*edd*	✗	✓
P. putida Δ*eda*	✗	✓

Figure 17 | **Growth phenotype characterization of different glucose catabolism mutants of *P. putida* KT2440.** (**a**) M9 minimal medium plates, containing either 20 mM glucose (top plate) or 30 mM succinate (bottom plate), were seeded with *P. putida* KT2440 (wild-type), and the mutants Δ*glk* (PP_1011, glucokinase), Δ*gcd* (PP_1444, glucose dehydrogenase), Δ*glk* Δ*gcd*, Δ*gad* (which comprises the deletions of Δ*PP_3382*, Δ*PP_3383*, Δ*PP_3384*, Δ*PP_3623* and Δ*PP_4232*, encoding gluconate 2-dehydrogenase), Δ*edd* (PP_1010, 6-phosphogluconate dehydratase), and Δ*eda* (PP_1024, 2-keto-3-deoxy-6-phosphogluconate aldolase). (**b**) Summary of the growth phenotypes of the strains under study ("✓" indicates growth, and "✗" indicates that the strain could not grow under the specific conditions tested in each case).

In summary, the gene deletions described above have been considered to construct *P. putida* GC. In all cases, the mutations studied in this chapter are correlated with the assumed loss of function in key metabolic steps of the biochemical network of strain KT2440, certifying their functionality in the *glycolytic chassis*.

CHAPTER 3

Exploring the role of glucose-6-*P* isomerase in central carbon metabolism of *P. putida* KT2440

Background

As explained previously, the regeneration of hexoses-*P* from trioses-*P* is a key feature of the normal metabolic operation of *P. putida* KT2440. A pivotal player influencing the formation of hexoses-*P* is glucose-6-*P* isomerase (Pgi). In *P. putida* KT2440, Pgi functions in the direction of G6P formation, unlike the *traditional* role of this enzyme in other bacteria, *i.e.*, catalyzing the conversion of G6P into F6P. Since the functioning of this enzyme would oppose the expected carbon flow in the intended EMP-based *P. putida* derivative, this chapter explores the phenotypic and metabolic consequences of blocking the reaction catalyzed by Pgi in *P. putida* KT2440.

3.1. Removing the Pgi activity from *P. putida* KT2440: a single step to block the EDEMP cycle

As mentioned along this Thesis, *P. putida* KT2440 bases its central carbon metabolism in the biochemical EDEMP cycle. An important role of this metabolic architecture to this end is the recycling of trioses-*P* into hexoses-*P* employing the (incomplete) EMP pathway as a gluconeogenic route. Pgi participates in such cycle as a key point in the whole metabolic sequence, catalyzing the transformation of F6P into G6P (**Fig. 18**). The *in vivo* distribution of metabolic fluxes in glucose-grown *P. putida* KT2440, analyzed by using substrates containing ^{13}C, indicated a significant participation of the Pgi activity in central carbon metabolism (Nikel *et al.*, 2015a). The biochemical role of Pgi has been investigated in many bacterial species (Hua *et al.*, 2003; Lindner *et al.*, 2013; Sanfélix-Haywood *et al.*, 2011; Toya *et al.*, 2010; Usui *et al.*, 2012), and this metabolic node has been targeted for Metabolic Engineering purposes, such as PHB production in recombinant *E. coli* (Kabir & Shimizu, 2003; Shi *et al.*, 1999). In *E. coli*, the Pgi activity mediates the formation of F6P from G6P – a situation that would be considered as the *canonical* reaction, and Pgi is considered to be the key enzyme activity controlling the fate of carbon skeletons, that can be further channeled through the EMP pathway or the PP pathway. Considering that Pgi catalyzes the *reverse* reaction in *P. putida*, and as part of the design of a suitable *chassis* for deep engineering of central carbon metabolism, the relevance of the Pgi-catalyzed step and the effects of removing the enzyme activity thereof on the overall cell physiology and metabolism was investigated by adopting a multi-omic approach.

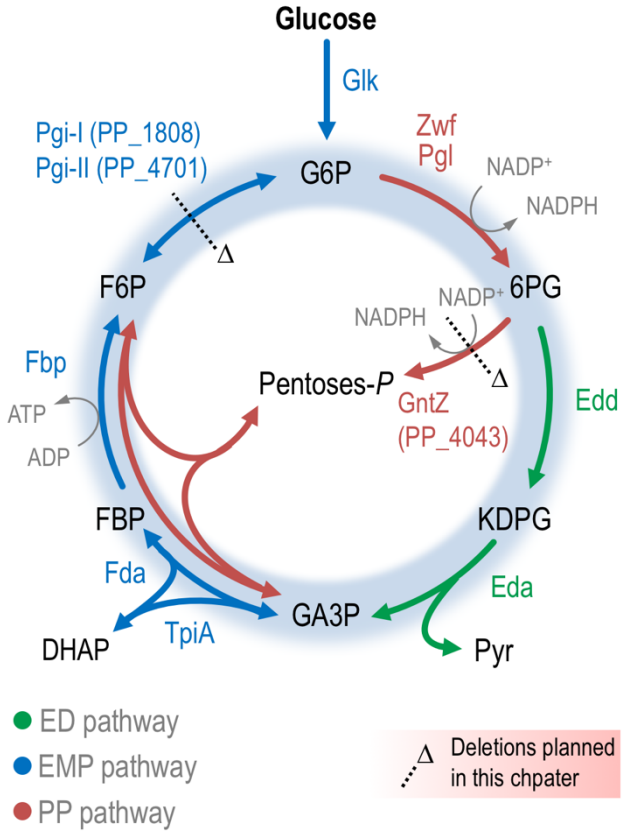

Figure 18 | **Schematic representation of the EDEMP cycle in *P. putida* KT2440.** Glucose catabolism occurs mainly through the activity of the Entner-Doudoroff (ED) pathway, but part of the trioses-*P* thereby generated are recycled back to hexoses-*P* by means of the *EDEMP cycle*, that also encompasses activities from the Entner-Doudoroff (ED) pathway, the (incomplete) Embden-Meyerhof-Parnas (EMP), and the pentose phosphate (PP) pathways. Each metabolic block is indicated with different colors and the EDEMP cycle is shaded in blue in the diagram. The deletions introduced in genes encoding metabolic enzymes targeted in this chapter are indicated by a Δ symbol. The abbreviations used in this picture are as follows: G6P, glucose-6-*P*; F6P, fructose-6-*P*; FBP, fructose-1,6-P_2; DHAP, dihydroxyacetone-*P*; GA3P, glyceraldehyde-3-*P*; Pyr, pyruvate; 6PG, 6-phosphogluconate; and KDPG, 2-keto-3-deoxy-6-phosphogluconate.

The Pgi activity is encoded in *P. putida* KT2440 by two different genes: *pgi-I* (*PP_1808*) and *pgi-II* (*PP_4701*). These two genes are annotated as to be a duplication event, and their lengths are exactly the same (1,665 nucleotides), each one encoding a protein composed of 554 amino acids. There are minor differences in the amino acid sequence of the corresponding polypeptides, which otherwise share an identity of 98% (*i.e.*, they contain only 9 amino acid differences). Considering the high degree of homology between Pgi-I and Pgi-II, the approach adopted in this chapter was based on the sequential elimination of both genes in order to completely remove the participation of Pgi in central carbon metabolism in *P. putida* KT2440 – but also revealing the individual contribution of the two *pgi* genes in the overall enzyme activity (**Fig. 19**). **Fig. 19a** indicates the in-frame deletions introduced in the two genomic loci annotated to encode Pgi activities in strain KT2440.

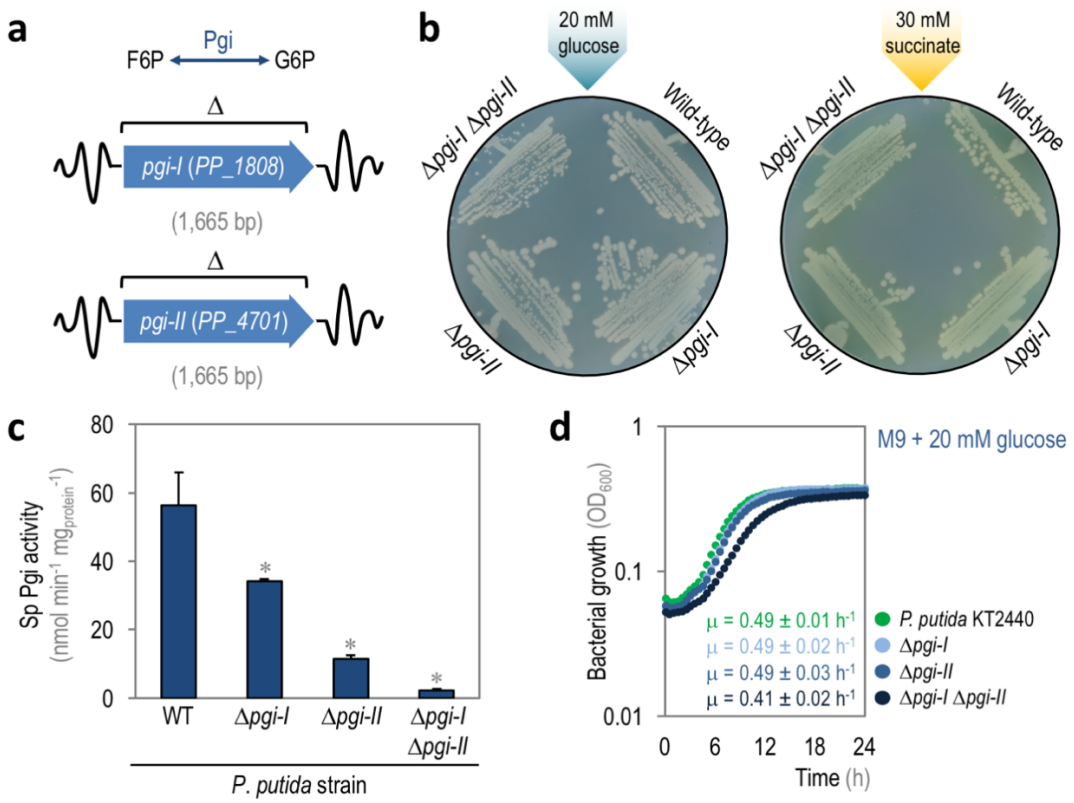

Figure 19 | **Characterization of the Pgi deletions in *P. putida* KT2440.** (**a**) The scheme depicts the location of the *pgi* genes in the chromosome of *P. putida* KT2440, and the isomerization catalyzed by glucose-6-*P* isomerase (Pgi). The targeted deletions introduced in these loci (showed with a Δ symbol in the outline) are also indicated. (**b**) M9 minimal medium plates, containing either 20 mM glucose (plate shown in the left) or 30 mM succinate (plate shown in the right), were seeded with *P. putida* KT2440 (wild-type), and the single and double mutants Δ*pgi-I*, Δ*pgi-II,* and Δ*pgi-I* Δ*pgi-II*. (**c**) *In vitro* quantification of the specific (Sp) Pgi activity in wild-type (WT) *P. putida* KT2440, and its Δ*pgi-I,* Δ*pgi-II*, and Δ*pgi-I* Δ*pgi-II* mutant derivatives. All the strains employed for the *in vitro* enzymatic assays were grown on M9 minimal medium added with glucose at 20 mM and cells were harvested in mid-exponential phase to obtain the cell-free extracts. Each bar represents the mean value of the corresponding enzyme activity ± standard deviation of quadruplicate measurements from at least two independent experiments. Significant differences ($P < 0.05$, as evaluated by means of the Student's *t* test) in the pair-wise comparison of a given recombinant to the control WT strain are indicated by an asterisk. (**d**) Growth curves of *P. putida* KT2440 and partial and full mutants blocked in the Pgi activity under glycolytic (M9 minimal medium with 20 mM glucose) conditions. Each data point represents the mean value of the optical density measured at 600 nm (OD_{600}) of quadruplicate measurements from at least three independent experiments. The specific growth rates (μ) were calculated from these data during exponential growth, and the inset shows the mean values ± standard deviations for each strain.

As a first step in the phenotypic characterization of the mutant strains, all the strains under study where streaked onto M9 minimal medium plates containing two different carbon substrates. **Fig. 19b** exposes the gross growth phenotype for the different combination of Pgi mutations under glycolytic (M9 minimal medium with 20 mM glucose) or gluconeogenic (M9 minimal medium with 30 mM succinate) conditions in solid culture. No dramatic effect was appreciated in terms of the overall fitness of single or double *pgi* mutants as compared to the WT strain. Nevertheless, the Δ*pgi-I* Δ*pgi-II* double mutant seemed to be more affected than the rest of the strains, as it formed smaller colonies on glucose-containing M9 minimal medium (**Fig. 19b**).

The next relevant question was the connection between biochemical activity and macroscopic growth effects brought about by eliminating the *pgi* genes in *P. putida*. The results shown in **Fig. 19c** indicate that the deletion of a single copy of the *pgi* gene (either *pgi-I* or *pgi-II*) is not enough to completely remove the Pgi activity in *P. putida* KT2440. This result would indicate that the redundancy of Pgi-encoding genes ensures functional complementation of the enzyme activity in absence of either gene. Therefore, the only way to completely block this reaction is the accumulation of both the Δ*pgi-I* and the Δ*pgi-II* deletions in the same strain. At the same time, the results suggest that the participation of Pgi-I in the bulk of the activity is smaller than that of Pgi-II. In particular, the simultaneous elimination of Pgi-I and Pgi-II resulted in a 40% and an 80% reduction of the total *in vitro* Pgi activity, respectively. The deletion of both isozymes expectedly resulted in a significant (*i.e.*, 96%) reduction of the overall Pgi activity in comparison with the WT strain.

The connection between the *in vitro* Pgi activity and the bacterial growth phenotypes was quantitatively explored by growing the different strains under study in liquid cultures in microtiter-plate cultures (**Fig. 19d**). Glycolytic conditions were adopted for this experiment, as glucose is the key nutrient to evaluate the process of hexoses-*P* regeneration, in which Pgi is expected to play a significant role. The results show that the partial Pgi mutants (*i.e.*, Δ*pgi-I* or Δ*pgi-II*) preserved similar specific growth rate values as compared to the WT strain. Nevertheless, in the case of the double Δ*pgi-I* Δ*pgi-II* mutant, there was a slight reduction on this growth parameter (*i.e.*, 16%) as compared with the WT strain. Interestingly, a significantly protracted lag phase was observed for the double mutant, although the final cell densities were almost identical for all the strains assayed under glycolytic conditions.

As an additional information, the growth parameters in batchwise, shaken-flask cultures of *P. putida* KT2440 and the double Δ*pgi-I* Δ*pgi-II* mutant were calculated in quantitative physiology experiments, as indicated in **Table 8**. Remarkable differences were observed between the two strains in these experiments. In the first place, and similarly to the growth patterns determined in microtiter-plate cultures, the specific growth rate value for the Δ*pgi-I* Δ*pgi-II* mutant growing under glycolytic conditions was significantly smaller (*i.e.*, 24%) than that of the WT strain. On the other hand, a 1.4-fold higher specific rate of carbon uptake (q_s) was determined for the Δ*pgi-I* Δ*pgi-II* strain as compared to the WT counterpart. Additionally, the yield of biomass on substrate ($Y_{X/S}$) showed the opposite trend, and the Δ*pgi-I* Δ*pgi-II* strain produced almost half the amount of biomass per gram of consumed glucose than the WT did. Considering the results of quantitative physiology experiments, together with the data shown in **Fig. 19**, it can be concluded that the depletion of the bulk Pgi activity in *P. putida* K2440 mediates a relevant effect on glucose utilization – both in terms of the specific substrate consumption and the fate of the carbon intermediates thereof. At the light of the results obtained in this part of the physiological characterization, further experiments were planned to unveil the biological function of Pgi in *P. putida* KT2440.

Table 8 | **Growth parameters of *P. putida* KT2440 and its Δ*pgi-I* and Δ*pgi-II* mutant derivatives in shaken-flask cultures under glycolytic growth conditions[a].**

P. putida strain	μ (h^{-1})[b]	q_S ($mmol_{glucose}$ g_{CDW}^{-1} h^{-1})[b]	$Y_{X/S}$ (g_{CDW} $g_{glucose}^{-1}$)[c]
KT2440 (WT)	0.49 ± 0.01	5.93 ± 0.04	0.46 ± 0.03
Δ*pgi-I* Δ*pgi-II*	0.37 ± 0.02	8.12 ± 0.05	0.25 ± 0.02

[a] Cells were grown in M9 minimal medium containing 20 mM glucose as the sole carbon source. All the values shown in this Table represent the mean of the corresponding parameter ± standard deviation of quadruplicate measurements from at least three independent experiments.

[b] The specific growth rate (μ) and the specific rate of carbon uptake (q_s) were obtained during exponential growth by linear regression. WT, wild-type; CDW, cell dry weight.

[c] The yield of biomass on substrate ($Y_{X/S}$) was obtained during exponential growth by correlating μ and q_s.

3.2. Phenotypic MicroArray™: Global view of the phenotypic consequences of eliminating the Pgi activity in *P. putida* KT2440

Once a suitable full Pgi mutant (*i.e.*, Δ*pgi-I* Δ*pgi-II*) of strain KT2440 was obtained, and its growth patterns were thoroughly explored, it was necessary to implement a more general screening method to understand what are the biological functions impacted by blocking this activity in *P. putida* KT2440. As indicated in **Section 3.1**, the full Pgi mutant presents a slight deficiency in the kinetic growth parameters when compared with the WT strain, and we explored the overall phenotypic features of such mutant. The use of a high-throughput screening method was considered to be a useful strategy to simultaneously explore the space of possible metabolic, stress resistance, and other phenotypic effects correlated with the absence of the Pgi activity. In particular, the BioLog Phenotypic MicroArray™ (PM) technology was employed to this end (Bochner, 2009; Bochner *et al.*, 2001). The set-up for this PM analysis was the so-called *full array*, which simultaneously evaluates a set of 20 different plates (*i.e.*, PM1-PM20) to examine diverse carbon, nitrogen, phosphorous and sulfur sources, and also to identify the effect of nutrient supplements, osmolytes, different pH values, and a large set of chemical compounds (*e.g.*, stressors). The complete report of phenotypes observed in the PM assay is presented in **Annex 1**. The majority of changes involved loss of functions (*i.e.*, 122 phenotypes were lost, and only 4 phenotypes were gained as compared to the WT strain KT2440), and the most conspicuous cases are displayed in **Fig. 20**.

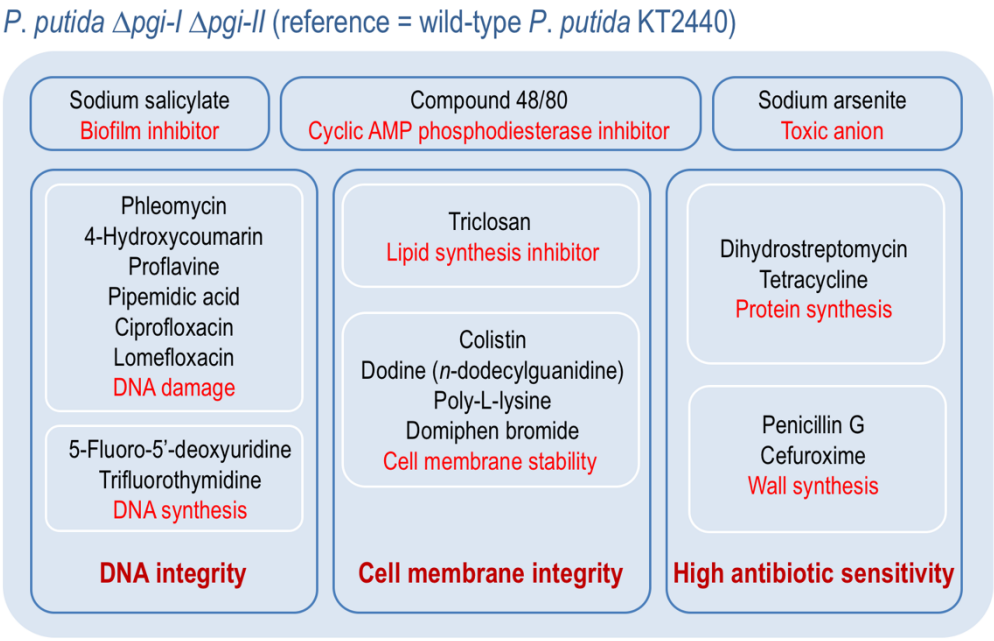

Figure 20 | **Phenomic analysis of the Pgi mutation in *P. putida* KT2440.** Selected loss-of-function phenotypes of the Pgi (Δ*pgi-I* Δ*pgi-II*) mutant strain as compared to wild-type *P. putida* KT2440. The different compounds (black) are grouped according to their effect (red). In the most relevant cases these effects are pooled by their characteristic biological role (bold red).

The results shown in **Fig. 20** indicate that the full Pgi mutant is comparatively sensitive to (i) cyclic AMP phosphodiesterase inhibitors, (ii) sodium arsenite (a toxic anion), (iii) different types of antibiotics, (iv) biofilm inhibitors, and (v) a set of compounds that disrupt the integrity of DNA and the cell membrane. The large variety of effects brought about by eliminating Pgi reflects the relevance of this activity in maintaining the overall bacterial fitness. In particular, the increased sensitivity to sub-inhibitory concentrations of antibiotics and compounds that compromise the cell membrane stability suggested, *a priori*, a link between some of the phenotypes observed for the mutant and the redox status of the cells (*e.g.*, altered NADPH availability). The potential link between the redox status of the cells in the absence of Pgi and the PM patterns described in **Fig. 20** was further explored by taking a closer look at central carbon metabolism in *P. putida* KT2440 (**Fig. 18**). The perusal of the biochemical network indicates that the elimination of Pgi-I and Pgi-II could result in (i) a reduction in the pool of NADPH (since the EDEMP cycle would be blocked, and the $NADP^+$-dependent Zwf activity would run short of G6P), and (ii) an increase in the accumulation of intracellular F6P (since the EMP pathway would continue feeding this metabolic node from trioses-*P*). Taking into account these hypotheses, and considering the phenomic analysis described above for the Pgi mutant, it was possible to sketch a cause-effect relationship as entertained in the next two sections.

3.2.1. Decrease of NADPH availability. The EDEMP cycle is a *core* feature of glucose metabolism in *P. putida* KT2440. The data available in the literature, based on the *in vivo* carbon flux distribution under glycolytic growth conditions, pointed to the Zwf activity as a key step for NADPH regeneration (Nikel *et al.*, 2015a). In particular, this reaction allows for the reduction of $NADP^+$ into NADPH by means of the oxidation of G6P into 6PG. All the attempts to remove the Zwf activity in our laboratory [comprised by three isozymes (Zwf, ZwfA, and ZwfB) in strain KT2440] altogether failed, suggesting an important role of this metabolic step in central carbon metabolism irrespective of the carbon source used. Note that, in contrast, Zwf (represented by a single enzyme) can be removed from bacteria that run a linear glycolysis, such as *E. coli* (Fischer & Sauer, 2003), without significantly affecting growth on glucose. In addition to this background information, and in direct connection with the basis of this chapter, the mentioned *in vivo* carbon flux distribution indicated that approximately 47% of the G6P converted to 6PG stems from the Pgi activity *via* cycling. The absence of any Pgi activity would reduce the generation of the carbon substrate for Zwf, thereby decreasing the reduction of $NADP^+$ into NADPH (Spaans *et al.*, 2015). As suggested by the phenomic analysis in the preceding section, there are several indications that indicate an alteration of the redox state in the double Pgi mutant. For example, the mutant showed sensitivity to sodium arsenite, a toxic anion that is counteracted by *P. putida* KT2440 via the products of the *ars* gene cluster, which includes a NADPH-dependent quinone reductase encoded by the *arsH* gene, *PP_2715* (Fernández *et al.*, 2014; Páez-Espino *et al.*, 2015). On the other hand, the Pgi mutant presented high sensitivity to different DNA harmful agents, that could possibly correlate with the shortage of NADPH and a sub-optimal operation of different DNA repair and synthesis systems, *e.g.*, the rate of $NADP^+$/NAD^+ regeneration are known to indirectly regulate DNA repair systems (Mandsberg *et al.*, 2009; Spaans *et al.*, 2015). Other interesting result is the sensitivity of the full Pgi mutant to agents that compromise the integrity of cell membranes, especially triclosan [5-chloro-2-(2,4-dichlorophenoxy)phenol, an inhibitor of lipid synthesis]. Such phenotype exposes the likely impairment of cell membrane synthesis and assembly in the Pgi mutant. This phenomenon is supported by the necessary oxidation of NADPH in different steps of the fatty acid biosynthesis pathway, *e.g.*, the NADPH-dependent β-ketoacyl-acyl carrier protein reductase encoded by the *fabG* gene, *PP_1914*, in *P. putida* KT2440 (Lai & Cronan, 2004; Yuan *et al.*, 2012). The third line of evidence indicating a redox imbalance in the mutant is the high sensitivity of this strain to different types of antibiotics, as observed in other bacterial species (Dwyer *et al.*, 2014; Dwyer *et al.*, 2015). From a more general perspective, these phenotypes can be also explained in terms of the cell membrane instability discussed above; however, the most relevant effects were associated with the treatment with antibiotics that affect the wall synthesis. In this biological process, there is an essential participation of the lipid II (a peptidoglycan motif linked to an undecaprenyl phosphate), which is considered to be the carrier to transport the peptidoglycan blocks from the cytoplasm to the cell wall (Sham *et al.*, 2014). Undecaprenyl phosphate is synthetized by most bacteria using isopentenyl as a metabolic precursor (Bouhss *et al.*, 2008). In the case of *P. putida* KT2440, isopentenyl is obtained from Pyr and GA3P following the non-mevalonate (*i.e.*, 2-*C*-methyl-D-erythritol-4-*P*/1-deoxy-D-

xylulose-5-*P*) pathway, in which various steps actively oxidize NADPH. Finally, many antibiotics are known to produce an oxidative burst in the cells in a similar fashion as compounds that damage cell membranes and would produce uncoupling of the respiratory chain (Belenky *et al.*, 2015; Dwyer *et al.*, 2014). Since most of the biochemical mechanisms that the cells use for the detoxification of reactive oxygen species ultimately depend in the intracellular availability of reducing power (Kim & Park, 2014), some of the phenotypes in the Δ*pgi-I* Δ*pgi-II* strain would also correlate with a shortage in the availability of reducing power besides the specific mechanisms discussed above. In order to experimentally validate these metabolic scenarios, where the regeneration of NADPH is compromised in the Δ*pgi-I* Δ*pgi-II* mutant, a set of experiments were designed to explore the redox state of the strains under study. These approaches combine physiology experiments, based on the effect of an oxidative stressor, with targeted genetic manipulations meant to intensify the redox-deficient phenotype, and are discussed in **Section 3.3**.

3.2.2. F6P accumulation. The absence of any Pgi activity would compromise the ability of *P. putida* KT2440 to transform F6P into G6P in a biochemical reaction that, in principle, could occur in both directions. The literature describes that the prevalent direction in strain KT2440 is F6P → G6P, as part of the characteristic EDEMP cycle (Nikel *et al.*, 2015a). Assuming that the PP pathway cannot absorb the bulk of the remaining F6P generated by the (now incomplete) EDEMP cycle, deleting *pgi-I* and *pgi-II* would probably result in the buildup of F6P in the cell. The phenomic analysis indicated a remarkable sensitivity of the Pgi mutant to sodium salicylate, a compound known to inhibit biofilm formation in some bacteria. For instance, salicylate has been associated with the inhibition of biofilm formation by *P. aeruginosa* (Prithiviraj *et al.*, 2005). In addition, F6P is the metabolic precursor employed by *P. aeruginosa* PAO1 (and other pseudomonads) to synthesize the polysaccharide alginate (Banerjee *et al.*, 1983; Ertesvåg *et al.*, 2017; Franklin *et al.*, 2011; Hentzer *et al.*, 2001). The cluster of genes that encode the activities needed to transform F6P in alginate is well conserved among pseudomonads, and in the chromosome of *P. putida* KT2440 it compromises the genes *algA* (*PP_1277*), *algF* (*PP_1278*), *algJ* (*PP_1279*), *algI* (*PP_1280*), *algL* (*PP_1282*), *algX* (*PP_1282*), *algG* (*PP_1283*), *algE* (*PP_1284*), *algK* (*PP_1285*), *alg44* (*PP_1286*), *alg8* (*PP_1287*), *algD* (*PP_1288*), and *algC* (*PP_5288*). Taking all this information together, it is possible that, in the absence of any Pgi activity, the accumulation of F6P may boost alginate formation, a polysaccharide proposed to be synthesized by strain KT2440 (Gulez *et al.*, 2014; Nilsson *et al.*, 2011). In order to evaluate this possibility, a simple phenotypic test was designed to explore biofilm formation by the Pgi mutants, as indicated in **Section 3.4**.

3.3. Genetic and metabolic perturbations to explore NADPH availability and its relationship with oxidative stress resistance in strain KT2440

3.3.1. Role of GntZ in NADPH formation upon the functional interruption of the EDEMP cycle in a Δ*pgi* genetic background. From a broad perspective, the experiments discussed so far disclose the relationship between central carbon metabolism and the intrinsic adaptation to natural environments by *P. putida* KT2440. In the quest of a suitable metabolic *chassis* for the implantation of a linear glycolysis (the *raison d'être* of the entire study), the role of Pgi was assessed by eliminating the two genes encoding this activity in strain KT2440. The PM analysis of the double mutant pointed to a shortage in the availability of NADPH as a possible cause of the many phenotypes observed in this strain. Previous work in our laboratory indicates that, besides Zwf, there is another relevant dehydrogenase in central carbon metabolism that can support NADPH formation under glycolytic growth conditions (Nikel & Chavarría, 2016; Nikel *et al.*, 2015a). 6-Phosphogluconate dehydrogenase (GntZ) is considered to be the second most important source of NADPH in the upper domain of carbon catabolism after Zwf (**Fig. 18**). The GntZ activity in *P. putida* KT2440 is encoded by the *gntZ* (*PP_4043*) gene, and catalyzes the decarboxylating reaction transforming 6PG into Ri5P (the first key intermediate of the PP pathway) using $NADP^+$ as the cofactor, thereby obtaining NADPH (**Fig. 21a**). It was then hypothesized that the already compromised redox status of the full Pgi mutant of strain KT2440 could be further perturbed by eliminating the GntZ-dependent generation of NADPH. As it is the case with other redox regulation processes (Blank *et al.*, 2008; 2010; Nikel *et al.*, 2016b), GntZ is to be considered as a *metabolic safety valve* in strain KT2440, as it does not usually participate in carbon catabolism during growth on glucose (*i.e.*, the PP pathway channels <10% of the carbon source under normal growth conditions). As a first step in the characterization of the role of this dehydrogenase in a full Pgi mutant, an in-frame deletion of *gntZ* was firstly introduced in strain KT2440 by allelic replacement (considering that this gene partially overlaps with *zwfB*, likely as a part of the same transcriptional unit, **Fig. 21a**), and the growth parameters and biochemical features of the mutant were characterized under different growth conditions.

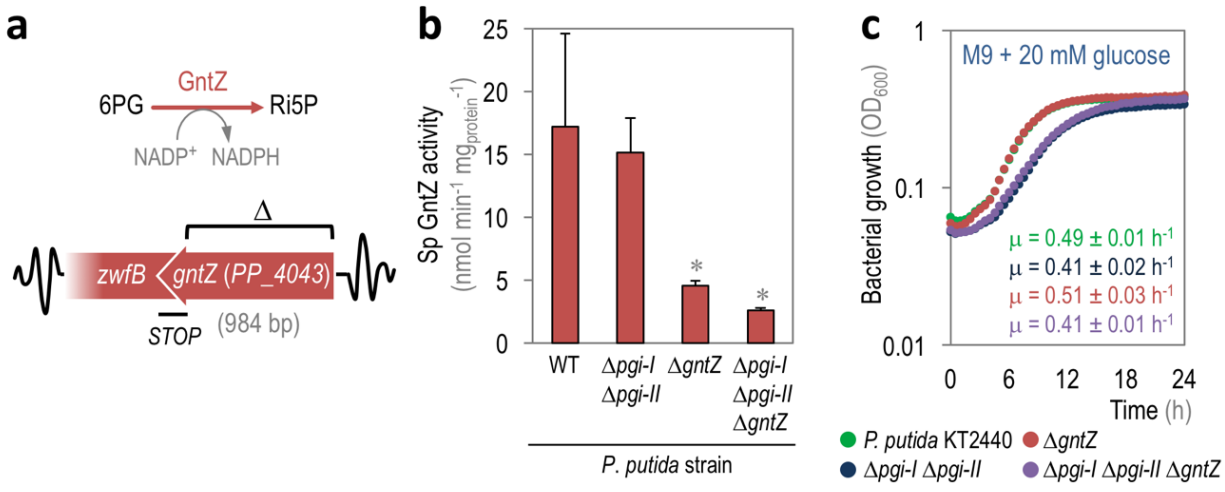

Figure 21 | **Characterization of the *gntZ* deletion in *P. putida* KT2440**. (**a**) The scheme depicts the location of the *gntZ* gene in the chromosome of *P. putida* KT2440. Note that there is an overlapping of the *gntZ* coding sequence and the *zwfB* gene (*PP_4042*), likely indicating co-regulation of the two genes. The deletion implemented in this chapter (indicated with a Δ symbol in the outline) is shown in the diagram, and does not affect the expression of the gene in the vicinity of the target locus. The relative orientation of *gntZ* (*i.e.*, in the reverse strand) is also indicated in the scheme. GntZ catalyzes the decarboxylation of 6PG into ribulose-5-*P* with the concomitant reduction of $NADP^+$. (**b**) *In vitro* quantification of the specific (Sp) GntZ activity in wild-type (WT) *P. putida* KT2440 and its Δ*gntZ*, Δ*pgi-I* Δ*pgi-II,* and Δ*gntZ* Δ*pgi-I* Δ*pgi-II* mutant derivatives. All the strains employed for the *in vitro* enzymatic assays were grown on M9 minimal medium added with glucose at 20 mM and cells were harvested in mid-exponential phase to obtain the cell-free extracts. Each bar represents the mean value of the corresponding enzyme activity ± standard deviation of quadruplicate measurements from at least two independent experiments. Significant differences ($P < 0.05$, as evaluated by means of the Student's *t* test) in the pair-wise comparison of a given recombinant to the control WT strain are indicated by an asterisk. (**c**) Growth curves of *P. putida* KT2440 and its Δ*gntZ* derivative combined (or not) with the Δ*pgi-I* Δ*pgi-II* mutations under glycolytic (M9 minimal medium with 20 mM glucose) conditions. Each data point represents the mean value of the optical density measured at 600 nm (OD_{600}) of quadruplicate measurements from at least three independent experiments. The specific growth rates (μ) were calculated from these data during exponential growth, and the inset shows the mean values ± standard deviations for each strain.

The *gntZ* deletion altogether abolished the GntZ activity in *P. putida* KT2440, in contrast with the WT counterpart and the Δ*pgi-I* Δ*pgi-II* controls, which displayed very similar levels of specific GntZ activity (**Fig. 21b**). On the other hand, the growth phenotype was not affected by the elimination of the GntZ activity (**Fig. 21c**), and the growth curve of the Δ*gntZ* mutant was essentially identical to that of the WT strain in microtiter-plate cultures. The growth curves expose that the most relevant influence in the growth pattern of the strains under study is brought about by the elimination of the Pgi activity (as indicated in **Figs. 19d** and **21c**), in which a significant decrease in the specific growth rate values can be appreciated in all the strains carrying the Δ*pgi-I* and Δ*pgi-II* deletions – irrespective of the Δ*gntZ* mutation. The final cell density was not affected by any of the mutations tested, which can be taken as an evidence of a *transient* metabolic imbalance that the cells ultimately manage to deal with. This piece of evidence indicates that GntZ seems to offer no extra role in boosting NADPH regeneration in the absence of Pgi. In any case, the still standing question is whether the redox phenotype is affected in the Pgi mutant, and this question was tackled by externally imposing oxidative stress conditions and evaluating how all the strains under study endure such conditions, as indicated in **Section 3.3.2**.

3.3.2. The metabolic imbalance of the Pgi mutant correlates with a high sensitivity to oxidative stress.

Taking into account all the experimental observations accumulated thus far, and in order to determine if the absence of Pgi activity impacts the intracellular redox state, a set of experiments was designed using paraquat (*N*,*N*'-dimethyl-4,4'-bipyridinium dichloride) as an oxidative stressor agent. Briefly, this molecule, that belongs to the *viologen* family of redox-active heterocycles, catalyzes the formation of reactive oxygen species and has been described to decrease the pool of NADPH (Bus & Gibson, 1984; Shen *et al.*, 2013).

The level of resistance to the treatment with paraquat can therefore be adopted as a proxy of the intracellular redox status in the cells. As a first attempt, the sensitivity of the strains described in this chapter was measured using the top-agar diffusion approach. In this experiment, the different mutants were grown onto solid M9 minimal medium with glucose as the carbon source, and a filter paper disc (soaked with 10 μl of 100 μM paraquat) was placed in the middle of the Petri dish. The growth inhibition zones were determined after 24 h of incubation, based on the distance from the filter paper disc to the border of the inhibition halo (**Figs. 22a** and **b**).

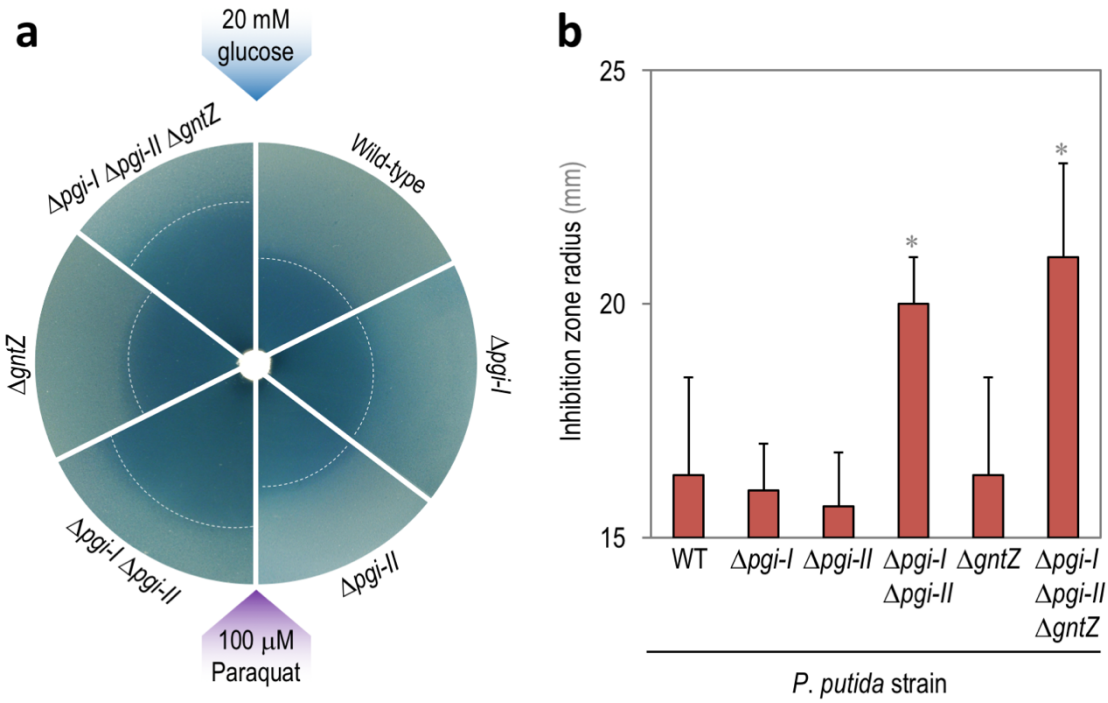

Figure 22 | **Paraquat as an oxidative stressor agent: qualitative characterization of tolerance by Pgi and GntZ mutants of *P. putida* KT2440.** (**a**) M9 minimal medium plates containing 20 mM glucose were seeded with *P. putida* KT2440 (wild-type strain), and the mutants Δ*pgi-I*, Δ*pgi-II,* Δ*pgi-I* Δ*pgi-II*, Δ*gntZ*, and Δ*pgi-I* Δ*pgi-II* Δ*gntZ*. A filter paper disc soaked with 10 μl of 100 μM paraquat was placed in the center of the Petri dishes, and the plates were incubated upwards during 24 h. (**b**) Quantification of the inhibition zone radius in wild-type (WT) *P. putida* KT2440, and its Δ*pgi-I*, Δ*pgi-II,* Δ*pgi-I* Δ*pgi-II*, Δ*gntZ*, and Δ*pgi-I* Δ*pgi-II* Δ*gntZ* mutant derivatives. All the strains employed for this assay were grown on plates of M9 minimal medium added with glucose at 20 mM with the paraquat test shown. Each bar represents the mean value of the corresponding inhibition zones (mm) ± standard deviation from at least three independent experiments. Significant differences ($P < 0.05$, as evaluated by means of the Student's *t* test) in the pair-wise comparison of a given recombinant to the control WT strain, are indicated by an asterisk.

The results shown in **Figs. 22a** and **b** indicate the qualitative effect associated to paraquat treatment in strains carrying different combinations of *pgi* and *gntZ* deletions. The most relevant result, also supported by quantitative statistical analysis (**Fig. 22b**), suggests an association of the absence of Pgi activity with a high sensitivity to paraquat. More precisely, the highest inhibition zone radii were observed in the *P. putida* mutant strains in which the Pgi activity has been completely eliminated (*i.e.*, Δ*pgi-I* Δ*pgi-II*, and Δ*pgi-I* Δ*pgi-II* Δ*gntZ*). At the same time, and in accordance with the physiological experiments reported in **Section 3.3.1**, it was noted that the Δ*gntZ* deletion did not influence the oxidative stress resistance profile of the corresponding mutant strains, obtaining similar values for the inhibition zones as compared to the WT strain. Finally, the highest value of inhibition was associated with the Δ*pgi-I* Δ*pgi-II* Δ*gntZ* strain, which would be the most compromised strain in terms of NADPH regeneration. With these results in hand, it is possible to assume that the bulk of NADPH regeneration in the upper domain of carbon metabolism could be traced to the $NADP^+$-dependent Zwf dehydrogenase activity, partially fed by Pgi. In order to contrast the results obtained in top-agar tests, the survival ratio of the Δ*pgi-I* Δ*pgi-II*, Δ*gntZ*, and Δ*pgi-I* Δ*pgi-II* Δ*gntZ* strains was evaluated in liquid cultures in the presence of paraquat as indicated in previously published methods (Martínez-García *et al.*, 2014d). *Survival ratios* were expressed as the OD_{600} values in cultures containing paraquat divided by the OD_{600} value in cultures without the stressor (**Fig. 23**).

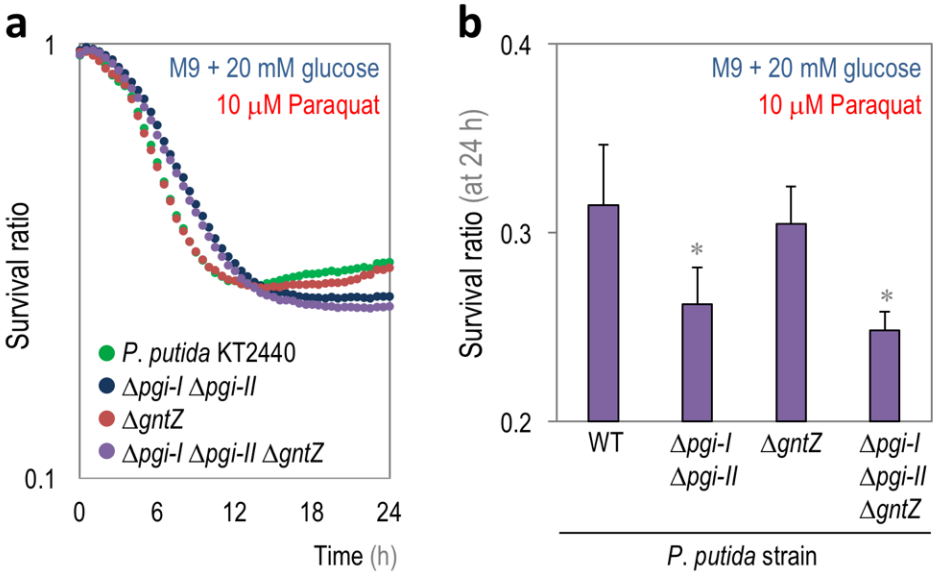

Figure 23 | **Stress resistance to paraquat in liquid cultures of *P. putida* KT2440 carrying different combinations of Pgi and GntZ mutations.** (**a**) Survival ratios for *P. putida* KT2440 (WT) and the mutants Δ*pgi-I* Δ*pgi-II*, Δ*gntZ*, and Δ*pgi-I* Δ*pgi-II* Δ*gntZ* exposed to paraquat at 10 μM and grown under glycolytic (M9 minimal medium with 20 mM glucose) conditions. Each data point represents the *survival ratio*, calculated as the optical density measured at 600 nm (OD_{600}) in cultures containing paraquat divided by the OD_{600} in cultures without the stressor of quadruplicate measurements from at least four independent experiments. (**b**) Survival ratio values at 24 h for wild-type (WT) *P. putida* KT2440, and its Δ*pgi-I* Δ*pgi-II*, Δ*gntZ*, and Δ*pgi-I* Δ*pgi-II* Δ*gntZ* mutant derivatives. Each bar represents the mean value of the survival ratio ± standard deviation of quadruplicate measurement from at least four independent experiments. Significant differences ($P < 0.05$, as evaluated by means of the Student's *t* test) in the pair-wise comparison of a given recombinant to the control WT strain, are indicated by an asterisk.

The results shown in **Fig. 23a** supported previous observations in top-agar experiments. Mutants with the double Pgi mutation (*i.e.*, Δ*pgi-I* Δ*pgi-II*) were specially affected by the presence of paraquat, giving raise to the lowest survival ratios at the end of the cultivation (**Fig. 23b**). Interestingly, the WT strain and the Δ*gntZ* mutant had almost identical curves of survival ratios over time. The rate of decrease in survival ratios was comparable among all the strains within the first 5 h of incubation, and from that point onwards, the WT strain and the Δ*gntZ* mutant reached a minimum value in this parameter at approximately 12.5 h. Both strains started to recover afterwards, while the survival ratios for the double Pgi mutant continued to decrease attaining a plateau after 18 h, at which point no further changes in survival patterns were observed. The final values for the survival ratios were statistically analyzed (**Fig. 23b**), corroborating that the changes were significant in the Δ*pgi-I* Δ*pgi-II* strains. Again, the Δ*gntZ* mutant did not suffer a heavy impact in terms of survival ratio when treated with paraquat. In summary, and taking into account the data obtained in both experiments, it is possible to conclude that the elimination of the Pgi activity compromises NADPH regeneration in *P. putida* KT2440 under glycolytic growth conditions. As indicated in previous sections, the other metabolic scenario to be tested in this mutant strain is the availability of F6P.

3.3.3. F6P accumulation and its correlation with biofilm formation in Pgi mutants. The number of phenotypic features possibly affected when a key metabolic enzyme activity is removed is rather large – all the more if such activity belongs to central carbon metabolism. Apart from suffering a defect in redox balance, Pgi mutants of *P. putida* are expected to be affected in the intracellular availability of metabolic precursors. Pgi interconverts F6P into G6P, in principle in either direction (**Fig. 18**). Previous work from our laboratory indicates that the prevalent direction in strain KT2440 is from F6P to G6P (Nikel *et al.*, 2015a). For this reason, a possible scenario in the mutant comprises the buildup of F6P since bacteria could not complete the gluconeogenic transformation of F6P into G6P catalyzed by Pgi. F6P is involved in a large number of cellular functions, and one of them is to be the metabolic precursor for alginate synthesis (Narbad *et al.*, 1988). This biopolymer is one of the most studied extracellular polymeric substances (EPS) present in the biofilm structure of some *Pseudomonas* species (Flemming *et al.*, 2007). The synthesis of alginate was also described in *P. putida* KT2440, and it was identified as a useful defense mechanism under desiccation stress imposed by mild water limitation (Gulez *et al.*, 2014). Alginate is also proposed to help maintaining biofilm stability (Nilsson *et al.*, 2011). With this evidence from the literature, it was possible to hypothesize that the buildup of the key precursor F6P in Pgi mutants could correlate with an increase in biofilm formation under glycolytic conditions. In order to contrast this hypothesis, an experiment was designed to evaluate biofilm formation in different strains of *P. putida* KT2440 (**Fig. 24**).

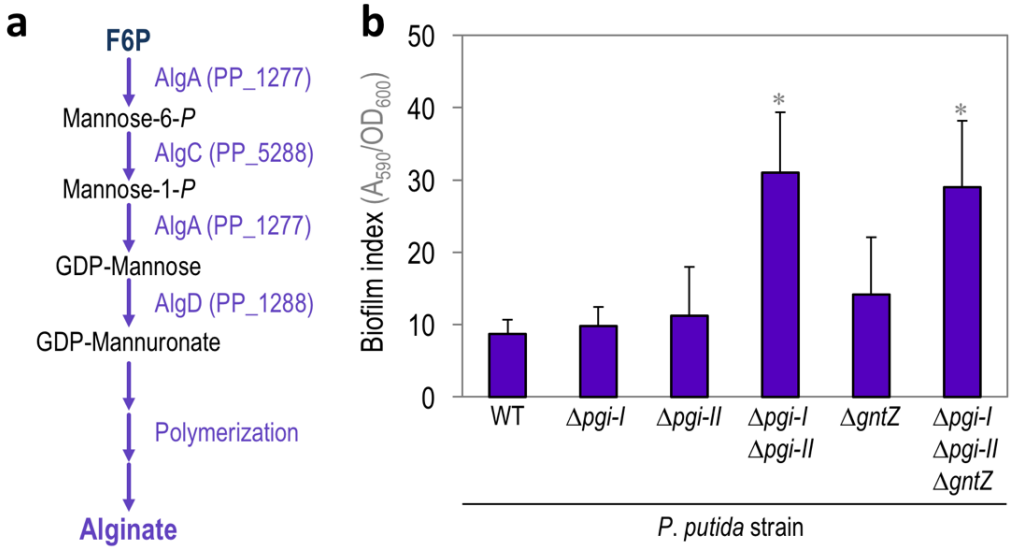

Figure 24 | **Biofilm formation in *P. putida* mutants devoid of the Pgi and GntZ activity.** (**a**) The scheme depicts the alginate biosynthesis pathway in *P. putida* KT2440. The genes involved in the formation of the building blocks are indicated in the route, and the large number of reactions that participate in polymerization of the basic monomer, *i.e.*, guanosine diphosphate (GDP)-mannuronate, have been lumped for the sake of clarity. (**b**) Biofilm formation by wild-type (WT) *P. putida* KT2440, and its Δ*pgi-I,* Δ*pgi-II,* Δ*pgi-I* Δ*pgi-II*, Δ*gntZ*, and Δ*pgi-I* Δ*pgi-II* Δ*gntZ* mutant derivatives. Cells were grown in M9 minimal medium with 20 mM glucose in static cultures for 24 h at 30°C, after which the culture broth was removed and biofilms were visualized by staining the cells attached to the microtiter plate wells with crystal violet as detailed in the *Materials and Methods* section. The biofilm index values were obtained by normalizing the absorbance of crystal violet suspensions at 590 nm (A_{590}) to the bacterial growth in each well, evaluated as the optical density measured at 600 nm (OD_{600}). Each bar represents the mean value of the corresponding biofilm index ± standard deviation of eight measurements from at least three independent experiments. Significant differences ($P < 0.05$, as evaluated by means of the Student's *t* test) in the pair-wise comparison of a given recombinant to the control WT strain, are indicated by an asterisk.

Fig. 24a depicts the alginate synthesis pathway in *P. putida* KT2440, starting with F6P as the metabolic precursor. The first steps within this metabolic route transform F6P into the nucleotide sugar guanosine diphosphate (GDP)-mannuronate. This part of the pathway comprises the activities encoded by three genes, namely, *algA* (*PP_1277*, phosphomannose isomerase and GDP-mannose pyrophosphorylase activity), *algC* (*PP_5288*, phosphomannomutase), and *algD* (*PP_1288*, GDP-mannose dehydrogenase). Subsequently, GDP-mannuronate is used as the precursor that is polymerized by the products of the rest of *alg* genes to produce the alginate polymer (Franklin *et al.*, 2011). The results indicated in **Fig. 24b** support the hypothesis correlating the accumulation of F6P with the increment of biofilm formation in a strain devoid of the Pgi activity. After 24 h of static incubation, the biofilm formation index increased by *ca*. 3.5-fold in the strains in which the Pgi activity was completely removed (*i.e.*, carrying both the Δ*pgi-I* and Δ*pgi-II* deletions) as compared to the parental strain. In the case of partial mutants (either Δ*pgi-I* or Δ*pgi-II*), no differences were

appreciated in biofilm formation in comparison with the WT strain. On the other hand, and in accordance with the results discussed in previous sections in this chapter, the Δ*gntZ* strain had no significant increase in biofilm formation when compared with the rest of the strains under evaluation. As a final remark, it should be noted that the addition of the Δ*gntZ* deletion to the Pgi mutant did not generate any differences in biofilm formation in comparison with that in the Δ*pgi-I* Δ*pgi-II* strain. In summary, the standing hypothesis that can be drawn from these data is compatible with a metabolic scenario, brought about by eliminating the Pgi activity in *P. putida* KT2440, that promotes the buildup of F6P. Among other phenotypes, this situation correlates with an increment in biofilm formation.

3.4. Constraint-based flux analysis as an additional approach to verify substrate availability for the $NADP^+$-dependent dehydrogenation catalyzed by Zwf

Flux balance analysis (FBA) is a useful mathematical approach to analyze the flow of different metabolites through a metabolic network. *P. putida* KT2440 is supported by a metabolic model, termed *i*JN746 (Nogales *et al.*, 2008), which can be adopted to predict the fluxes around specific metabolic nodes (La Rosa *et al.*, 2015). As described in the *Materials and Methods* section, these genome-scale metabolic models can be used to study the absence of different enzyme activities *in silico*. In our case, the elimination of the Pgi activity was simulated paying especial attention to its influence on redox balance. The objective of this analysis was to add consistency to the hypothesis developed in the previous sections, in which the absence of Pgi activity would result in a decrease of the G6P pool. This scenario would, in turn, lower substrate availability for the Zwf activity, decreasing the availability of reducing power (*i.e.*, NADPH). In order to corroborate this possibility, the model *i*JN746 was interrogated to simulate glucose metabolism in WT *P. putida* KT2440 (**Fig. 25a**) and in the double Δ*pgi-I* Δ*pgi-II* mutant (**Fig. 25b**). Additionally, the genome-scale metabolic model was constrained in order to represent: (i) the *in vivo* ^{13}C-based metabolic flux analysis for glucose-grown *P. putida* KT2440 (Nikel *et al.*, 2015a), and (ii) the real specific rate of carbon uptake (q_S) obtained in this Thesis (**Table 8**).

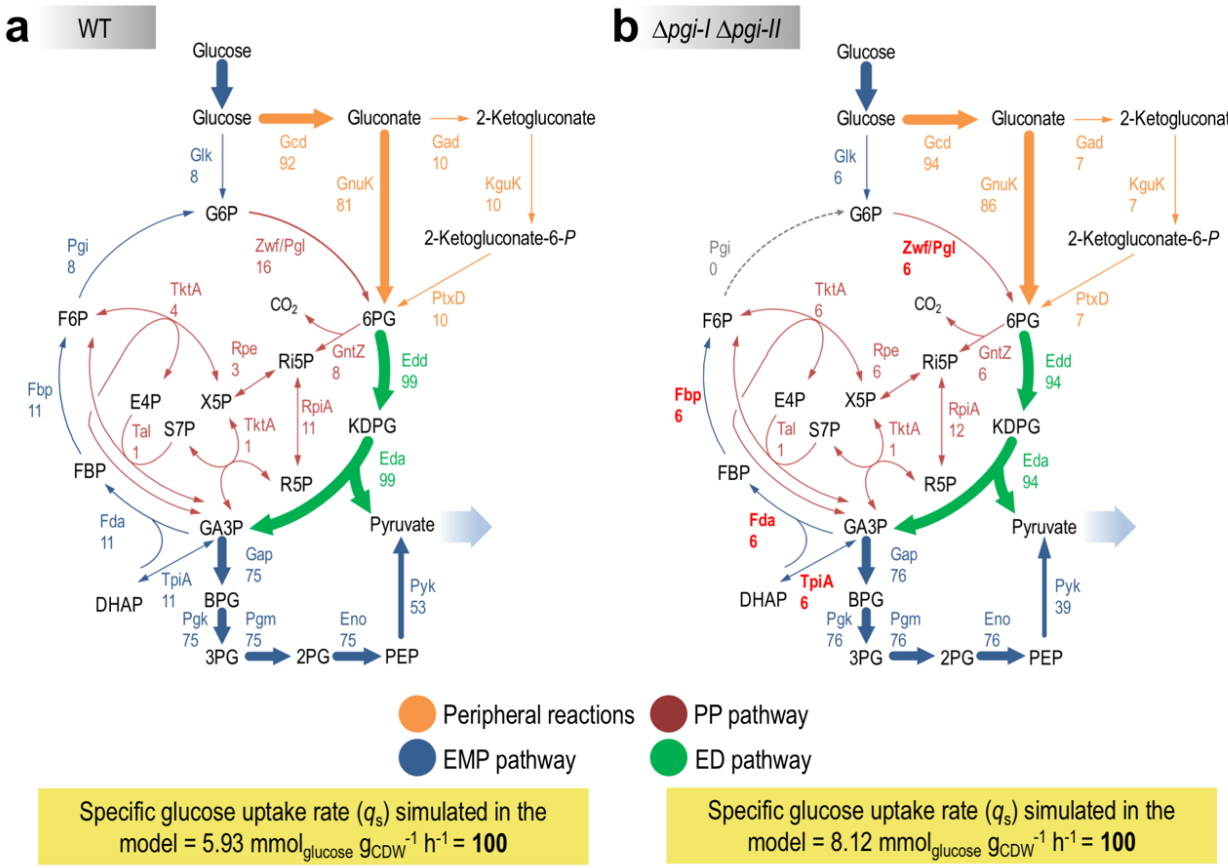

Figure 25 | **Influence of eliminating the Pgi activity on the distribution of central metabolic fluxes evaluated by constraint-based analysis.** The scheme depicts the reaction networks in *P. putida* KT2440 (WT, left panel) and the Pgi mutant (Δ*pgi-I* Δ*pgi-II*, right panel) during exponential phase in a modelled synthetic M9 minimal medium containing glucose as the sole carbon source. The orientation of the arrows indicates the assumed direction of the reactions. Significant changes (*ca*. 2-fold higher) between the Pgi strain and WT are indicated in red. Reactions downwards pyruvate are highlighted with a dashed gray arrow. All the values for individual fluxes in the diagram were normalized to the specific glucose uptake rate (q_S, arbitrarily set to 100). The abbreviations used in this picture are as follows: EMP pathway, Embden-Meyerhof-Parnas pathway; ED pathway, Entner-Doudoroff pathway; PP pathway, pentose phosphate pathway; G6P, glucose-6-*P*; F6P, fructose-6-*P*; FBP, fructose-1,6-P_2; DHAP, dihydroxyacetone-*P*; GA3P, glyceraldehyde-3-*P*; 6PG, 6-phosphogluconate; KDPG, 2-keto-3-deoxy-6-phosphogluconate; Ri5P, ribulose-5-*P*; R5P, ribose-5-*P*; X5P, xylulose-5-*P*; S7P, sedoheptulose-7-*P*; E4P, erythrose-4-*P*; BPG, glycerate-1,3-P_2; 3PG, glycerate-3-*P*; 2PG, glycerate-2-*P*; and PEP, phosphoenolpyruvate.

Fig. 25 summarizes the results obtained in the constraint-based analysis adopted to simulate the absence of Pgi activity in the central carbon metabolism of *P. putida* KT2440. It can be assumed that the bulk of the influence brought about by the Δ*pgi-I* Δ*pgi-II* deletions is focused on the EDEMP cycle, revealing a reduced impact in the carbon fluxes thorugh peripheral reactions. Elimination of Pgi activity results in a significant decrease in the flux through Zwf, correlated with a limitation in the availability of G6P. The model described a 2.7-fold lower traffic from G6P to 6PG *via* Zwf. Under these circumstances, the activity of Zwf decreases by *ca*. 63%, affecting the NADPH pool in the cell. Finally, and linked to a lower participation of

G6P in the EDEMP cycle, a significant, *ca*. 2-fold decrease in the fluxes that comprise the gluconeogenic arm of the EMP pathway [*i.e.*, fructose-1,6-bisphospatase (Fbp) and fructose-1,6-P_2 aldolase (Fda)] can be appreciated. Taking into account these results, it can be concluded that NADPH formation (and thus, optimal bacterial fitness) is correlated with a proper functioning of the EDEMP cycle. These data substantiate the particularity of the *P. putida* KT2440 metabolism, in contrast with publications that indicate an increase in the NADPH balance when the Pgi activity is removed from the biochemical network of *E. coli* (Canonaco *et al.*, 2001; Hua *et al.*, 2003; Kabir & Shimizu, 2003; Shi *et al.*, 1999).

CHAPTER 4

Functional replacement of the *core* carbon metabolism in *P. putida*: establishing a flawless linear glycolysis in strain GC2

Background

The EDEMP cycle-based central carbon metabolism of *P. putida* KT2440 has probably evolved alongside the capability of this bacterium to survive and thrive in the (often adverse) natural environments it inhabits (Chavarría *et al.*, 2013; Nikel *et al.*, 2015a). There is no doubt that these capabilities allow *P. putida* KT2440 to execute reactions of industrial interest requiring a high redox demand, thanks to the high NADPH yield per molecule of glucose stemming from the extant metabolism (Blank *et al.*, 2008; Nikel *et al.*, 2016a; Sudarsan *et al.*, 2014). The operation of such metabolic architecture has, however, a downside for the application of *P. putida* as a cell platform in a bioindustry context, which can potentially compromise its wide use in biotechnological processes. The metabolic wiring of *P. putida*, dependent on the ED pathway, leads to an intrinsically low ATP yield per molecule of glucose, which can be considered a hindrance in a large number of hexose-fueled bioprocess (Hara & Kondo, 2015; Schuster, 2000). Therefore, a deep refactoring of the central glucose metabolism was implemented in *P. putida* KT2440 to boost ATP formation from glucose. The strategy adopted in this chapter seeks to completely transform the native *core* glycolytic operation of this bacterium by combining two main approaches: (i) the targeted deletion of genes encoding the extant set of glycolytic reactions in order to generate a *chassis*, termed *P. putida* GC (***g***lycolytic ***c***hassis), and (ii) the rational, Synthetic Biology-guided design and implementation of a functional EMP pathway (a canonical example of a glycolytic route endowed with high ATP yield) *via* the GlucoBrick system.

4.1. Implementation of the GlucoBrick system in *P. putida* GC1: *beta-testing* phase to allow a linear EMP glycolysis

The very idea of completely transforming the identity of central carbon metabolism in whatever living entity is not an easy task to accomplish, and there are very few examples of such a systematic endeavor in bacteria (Papagianni, 2012). Hexose catabolism is considered to be a vital component of central carbon metabolism in many bacterial species, and it could be considered as the *metabolic heart* of the whole cell biochemistry (Nielsen & Keasling, 2016; Raab *et al.*, 2005; Romano & Conway, 1996; Siedler *et al.*, 2012). A *beta-testing* phase was considered as the starting point to successfully achieve the stable implementation of a functional EMP pathway in *P. putida* KT2440. The overall strategy adopted for testing a linear glycolysis in *P. putida*

is summarized in **Fig. 26**. Against this background, and by following the *beta-testing* engineering principle, the first attempt encompassed the construction of a preliminary version of *P. putida* GC (termed *P. putida* GC1), with all the essential genetic modifications needed to evaluate the gross consequences of introducing an EMP-based glycolysis in *Pseudomonas*. A similar type of preliminary testing involved the use of the GlucoBrick system in a plasmid-based format, as explained below.

4.1.1. Streamlining the central carbon metabolism of *P. putida* KT2440: design and construction of a suitable *chassis* for the implementation of a linear, EMP-based glycolytic pathway. The first step considered in the quest to implement novel metabolic capacities in *P. putida* was the removal of the relevant competing pathways. In other words, it was necessary to functionally block the native system that *P. putida* KT2440 employs to metabolize glucose. In particular, two metabolic and genetic nodes were targeted: (i) the competition of pathways for the very hexose substrate (*i.e.*, draining metabolic intermediates away from the glycolytic route of interest), and (ii) the interactions between the cellular machinery and the implanted genetic construct, *i.e.*, the modules of the GlucoBrick platform (Kim & Copley, 2012). The first of these approaches was focused in eliminating the preparatory steps in the consumption of glucose by *P. putida* KT2440, that can occur either *via* the Glk-dependent phosphorylation of the substrate in the phosphorylative branch, or the oxidation of the hexose to organic acids in the periplasmic space in the oxidative branch (**Fig. 26a**). Note that this task comprises the in-frame deletions explained in **Chapter 2**, finally resulting in the accumulation of the Δ*glk*, Δ*gcd*, and Δ*gad* (Δ*PP_3382-4*, Δ*PP_3623*, and Δ*PP_4232*) mutations in the same *P. putida* strain. In addition, the ED pathway was blocked by deleting the *edd* gene (*PP_1010*, 6-phosphogluconate dehydratase), encoding the first committed step in the route. The accumulation of all these mutations in the WT *P. putida* KT2440 background resulted in strain *P. putida* GC1.

4.1.2. Introduction of the genes needed to activate a linear glycolysis in *P. putida* GC1. The results described in **Chapter 1**, which demonstrated the functional versatility of the GlucoBrick system in different *Pseudomonas* species, set the basis for the activation of an EMP pathway in *P. putida* GC1. It should be mentioned that previous works in our laboratory aimed at restoring a linear glycolytic pathway in *P. putida* KT2440. This objective looks in principle simple, in that the only obvious limitation for this bacterium to employ such linear pathway is the absence of a Pfk activity. However, the implementation of this single activity in *P. putida* KT2440 lead to a severely impaired glucose-dependent growth and low resistance to oxidative stress (Chavarría *et al.*, 2013). For this reason, and following the reasoning described in **Chapter 1** for the WT strain, the first attempt was the introduction of Module I by transforming plasmid pS224·GBI in *P. putida* GC1 strain (**Fig. 26b**), in which the genes encoding the enzymes of the *preparatory phase* within the EMP pathway are under transcriptional control of an inducible $LacI^{Q}/P_{trc}$ element. The introduction of the entire metabolic block allows the circulation of carbon from glucose down to GA3P by connecting the corresponding reactions (**Fig. 26c**), improving metabolic channeling and reducing the creation of potential bottlenecks in the biochemical network (Hollinshead *et al.*, 2016).

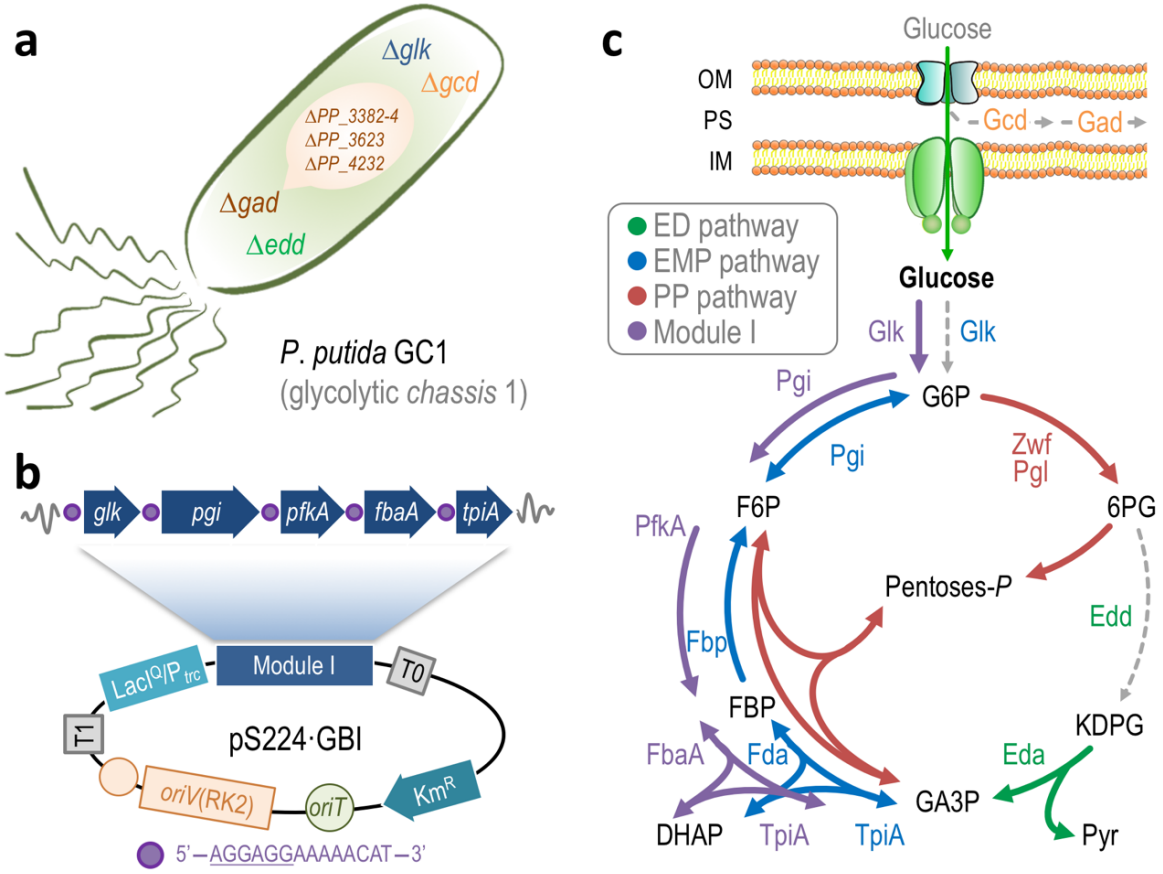

Figure 26 | **Outline for the *beta-testing* of a linear glycolysis in *P. putida*.** (**a**) Genetic profile of the *P. putida* GC1 strain. Note that Δ*gad* represents the accumulation of the individual Δ*PP_3382*, Δ*PP_3383*, Δ*PP_3384*, Δ*PP_3623*, and Δ*PP_4232* in-frame deletions. (**b**) Structure of the pS224·GBI plasmid, a derivative of vector pSEVA224 bearing Module I from the GlucoBrick system (*i.e.*, encoding the enzymes needed for the conversion of glucose into glyceraldehyde-3-*P*). T0 and T1 indicate transcriptional terminators. The IPTG-inducible $LacI^{Q}/P_{trc}$ expression system is also indicated in the plasmid map. The origin of transfer compatible with the RP4 conjugation machinery is termed *oriT*. The low-copy-number origin of replication compatible with *P. putida* KT2440 is indicated as *oriV*(RK2). Note that each gene is preceded by a synthetic regulatory element, indicated by a purple circle, composed of a ribosome binding site (sequence underlined) and a spacer sequence. The antibiotic-resistance marker, based on kanamycin, is shown as Km^{R}. The elements in this scheme are not drawn to scale. (**c**) Simplified representation of central carbon metabolism in *P. putida* GC1. The activities eliminated in this strain are represented by a dashed gray arrow. The biochemical reactions encoded by the genes from the Module I are indicated in purple. The abbreviations used in this picture are as follows: G6P, glucose-6-*P*; F6P, fructose-6-*P*; FBP, fructose-1,6-P_2; DHAP, dihydroxyacetone-*P*; GA3P, glyceraldehyde-3-*P*; Pyr, pyruvate; 6PG, 6-phosphogluconate; KDPG, 2-keto-3-deoxy-6-phosphogluconate; OM, outer membrane; PS, periplasmic space; and IM, inner membrane.

P. putida GC1 transformed with the pS224·GBI plasmid has the full enzymatic complement needed to metabolize glucose by means of the EMP pathway, thereby fulfilling the Pfk activity absent in many members of the *Pseudomonas* genus. As indicated in **Fig. 27a**, and after inducing gene expression in the recombinants with a suitable concentration of IPTG (1 mM), *P. putida* GC1 containing the empty vector (*i.e.*, pSEVA224) was unable to grow in M9 minimal medium plates using glucose as the sole carbon source. This is the expected growth phenotype for strain GC1, in light of the accumulation of several mutations that compromise glucose utilization. In contrast, *P. putida* GC1 transformed with the pS224·GBI plasmid (containing Module I from the GlucoBrick system) was able to grow on glucose under the same culture conditions. In other words, the enzyme activities encoded by the pS224·GBI plasmid allow *P. putida* GC1 to metabolize glucose *via* the EMP pathway (**Fig. 27a**). The WT strain KT2440 transformed with the empty pSEVA224 vector served as a positive control of growth under both glycolytic and gluconeogenic conditions. All the strains grew on succinate as the sole carbon source, indicating that the genetic manipulations in strain GC1 do not significantly affect bacterial growth through gluconeogenesis. Further characterization of the strains at stake in liquid cultures confirmed the growth phenotypes observed in solid media. The results shown in **Fig. 27b** indicate that the specific growth rate of *P. putida* GC1 transformed with plasmid pS224·GBI is smaller (*ca.* 4-fold decrease) than that of the WT strain containing the empty plasmid in glucose cultures. This impaired growth is somewhat expected due to the large number of modifications introduced in this strain, including several mutations in its native set of genes encoding components of the central carbon metabolism. In addition to the decrease in the specific growth rate, the final cell density was also affected in *P. putida* GC1 transformed with plasmid pS224·GBI (*i.e.*, a 40% reduction of the final OD_{600} as compared to that in cultures of *P. putida* KT2440/pSEVA224). In any case, the glucose-dependent growth of the engineered strain served as a proof-of-concept result to further develop a *P. putida* cell platform based on the functional activity of an EMP-based catabolic pathway.

In order to correlate the growth of the engineered strain on glucose with the presence of the enzymes encoded by the GlucoBrick genes, the enzyme activity of different key components in the EMP pathway was determined in *P. putida* GC1 transformed with plasmid pS224·GBI. The Glk and Pfk activities, the first enzyme in the pathway and the activity missing in *P. putida* KT2440, respectively, were determined in cell-free extracts of the relevant strains grown in minimal medium containing glucose (**Fig. 27c**). In the case of Glk, the native activity could be detected in *P. putida* KT2440 and in *E. coli* BW25113 carrying the empty vector (*i.e.*, pSEVA224), used here as an additional control, upon induction of gene expression with IPTG. The native Glk activity in strain KT2440 was almost twice that of WT *E. coli*. The specific Glk activity was also determined in *P. putida* KT2440 Δ*glk* and in *E. coli* BW25113 Δ*glk* Δ*ptsI* (*i.e.*, an *E. coli* strain completely deficient in glucose phosphorylation), carrying the empty plasmid (*i.e.*, pSEVA224) and induced with IPTG. Predictably, no significant Glk activity was detected in either mutant. Finally, this phosphorylating reaction was analyzed in *P. putida* GC1 containing plasmid pS224·GBI. The only possible way for this bacterium to grow on glucose is linked to the presence of the Glk activity encoded by Module I of the

GlucoBrick platform. Indeed, *P. putida* GC1 carrying plasmid pS224·GBI (and induced with IPTG) has a specific Glk activity 129-fold higher than that of the WT strain carrying the empty plasmid (**Fig. 27c**). This high level of enzyme activity can result from unregulated expression of the *glk* gene, alongside to the extra gene copies in the cells due to the expression of Module I in plasmid format (and also from a potentially different pattern of enzyme regulation of Glk in a heterologous context).

The specific Pfk activity was assessed in *E. coli* BW255113 and its Δ*pfkA* Δ*pfkB* double mutant derivative (termed Δ*pfk* in **Fig. 27d**) carrying the empty vector (*i.e.*, pSEVA224) in IPTG-induced glucose cultures. The Pfk activity was determined in these two *E. coli* strains as a positive and negative control, respectively, considering that *P. putida* KT2440 lacks the Pfk-dependent conversion of F6P into FBP (**Fig. 27d**). As expected, the Pfk activity test was positive in the WT *E. coli* strain in contrast to the very low level of activity detected in *E. coli* Δ*pfk* and in *P. putida* KT2440 carrying the empty vector (*i.e.*, pSEVA224). In the case of *P. putida* GC1 carrying the pS224·GBI plasmid, it was assumed that the Pfk activity must be present as this would be the only way to bestow growth on glucose. The *in vitro* biochemical determinations support this notion, and the *P. putida* GC1 transformed with the pS224·GBI plasmid (induced with a proper concentration of IPTG) had a 32-fold increase in the Pfk activity compared with WT *E. coli* BW255113 (**Fig. 27d**).

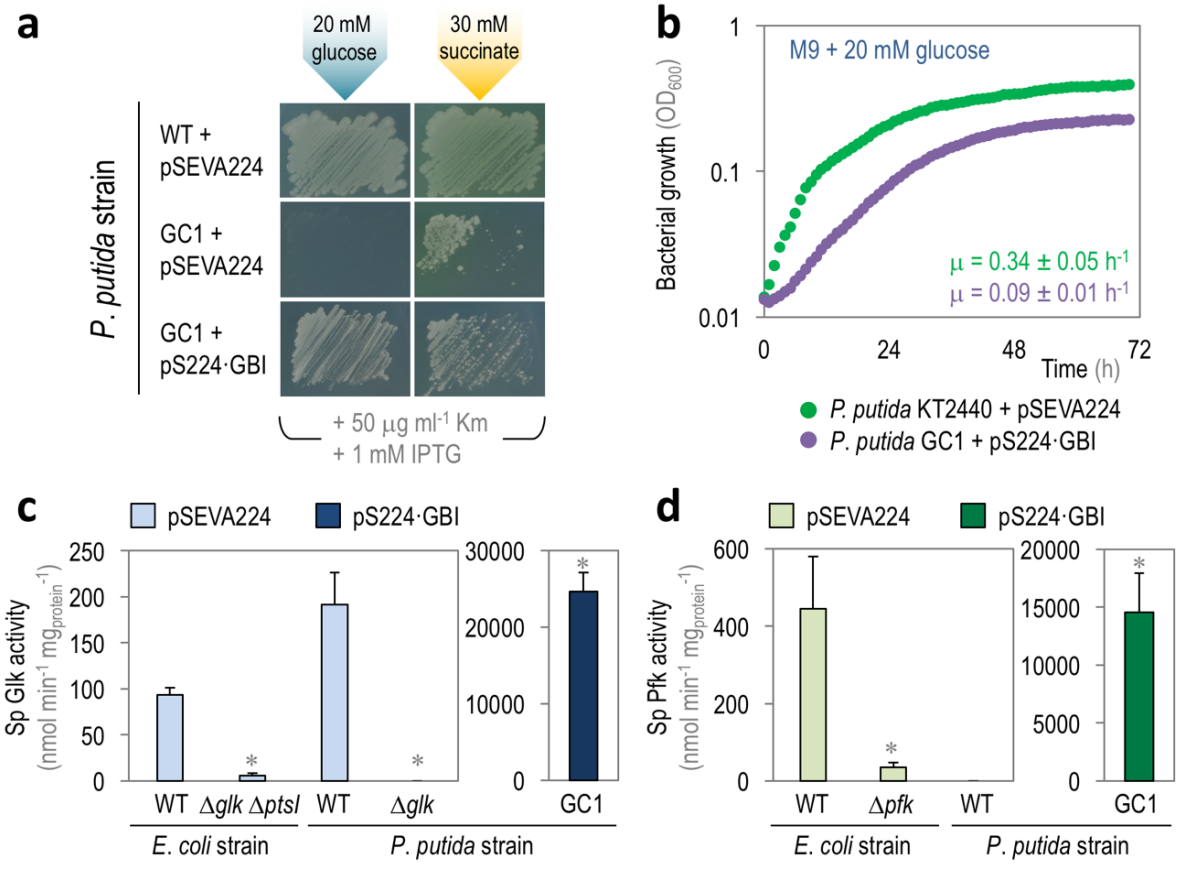

Figure 27 | **Physiological and biochemical characterization of the implanted GlucoBrick activities in *P. putida* GC1.** (**a**) M9 minimal medium plates, containing either 20 mM glucose (left column) or 30 mM succinate (right column), were inoculated with *P. putida* KT2440 (WT) carrying the empty pSEVA224 vector, and *P. putida* GC1 carrying either the empty pSEVA224 vector or Module I (pS224·GBI). (**b**) Growth curves of *P. putida* KT2440 carrying the empty pSEVA224 vector, and *P. putida* GC1 carrying plasmid pS224·GBI on M9 minimal medium with 20 mM glucose, 50 μg ml^{-1} Km, and 1 mM IPTG in microtiter-plate cultures. Each data point in the growth curves represents the mean value of the optical density measured at 600 nm (OD_{600}) in quadruplicate measurements from at least three independent experiments. The specific growth rates (μ) were calculated from these data during exponential growth, and the inset shows the mean value ± standard deviations for each strain. (**c**) *In vitro* quantification of the specific (Sp) glucokinase (Glk) activity, which phosphorylates glucose to glucose-6-P (G6P) in wild-type (WT) *E. coli* BW25113 and its Δ*glk* Δ*ptsI* derivative, and wild-type (WT) *P. putida* KT2440, and its Δ*glk* derivative (left panel) carrying the empty pSEVA224 vector. The right panel showed for the same Glk activity the results from the *P. putida* GC1 carrying plasmid pS224·GBI. (**d**) *In vitro* quantification of the specific (Sp) 6-phosphofructo-1-kinase (Pfk) activity, which converts fructose-6-*P* into fructose-1,6-P_2 in wild-type (WT) *E. coli* BW25113 and its Δ*pfkA* Δ*pkfB* (indicated as Δ*pfk*) derivative, and wild-type (WT) *P. putida* KT2440 (left panel) carrying the empty pSEVA224 vector. The right panel shows the Sp Pfk activity for *P. putida* GC1 carrying plasmid pS224·GBI. All the strains employed for the *in vitro* enzymatic assays were grown on M9 minimal medium added with glucose at 20 mM, 50 μg ml^{-1} Km, and 1 mM IPTG, and cells were harvested in mid-exponential phase to obtain the cell-free extracts. Each bar represents the mean value of the corresponding enzyme activity ± standard deviation of quadruplicate measurements from at least two independent experiments. Significant differences ($P < 0.05$, as evaluated by means of the Student's *t* test) in the pair-wise comparison of a given recombinant to the control WT strain, are indicated by an asterisk. Note that *P. putida* GC1/pS224·GBI was compared to *P. putida* Δ*glk* for the Glk activity, and to *P. putida* KT2440 for the Pfk activity.

According to the data gathered so far, the glycolytic activities encoded in Module I of the GlucoBrick system allow *P. putida* GC1 to grow in glucose using a functional EMP pathway. This *beta-testing* phase was thus useful to evaluate the feasibility of the next stage in the deep metabolic refactoring of central carbon metabolism. The goal of the second stage is to obtain an upgraded version of *P. putida* GC1 (*i.e.*, *P. putida* GC2). The construction of this second glycolytic *chassis* entails the complete elimination of the ED pathway (by removing *eda*, the second gene in the two-step route), and the substitution of the native, ATP-dependent glucose transport system of *P. putida* KT2440 by the efficient, energy-independent Glf transporter from *Z. mobilis*. *P. putida* GC2 will be thus employed as the final platform to stably introduce a linear EMP pathway *via* the GlucoBrick system. At this point of biocatalyst design, all the relevant metabolic modules (*i.e.*, the Glf transporter from *Z. mobilis*, and Modules I and II from the GlucoBrick platform) are randomly delivered into the target chromosome as a single copy *via* mini-Tn*5*–assisted transposition, as explained below.

4.2. *P. putida* GC2: implementing a stable linear glycolysis based on the EMP pathway

The results obtained in the first part of this chapter support the idea that it is possible to graft a functional EMP pathway in a *P. putida*-based genetic *chassis*. The *beta-testing* phase of the project indicated that the

engineered bacterium is able to grow on glucose as the sole carbon source by employing a combination of part of its endogenous activities and the heterologous activities encoded by Module I of the GlucoBrick platform. The second part of the overarching endeavour started with the construction of *P. putida* GC2, a genetically upgraded version of the *glycolytic chassis* under study. The construction of this multiple-mutant *P. putida* strain comprised the deletion events summarized in **Fig. 28a**.

4.2.1. Removal of the ED route. In the first place, the ED pathway was completely blocked from *P. putida* GC1, that was already unable to run the ED route due to the targeted elimination of the gene encoding the first enzymatic step of the sequence (*i.e.*, Edd). However, and in order to obtain a further reduction in the overall complexity of the biochemical network, *P. putida* GC1 was also depleted of the second (and last) activity of the ED pathway by deleting the *eda* gene (*PP_1024*, encoding 2-keto-3-deoxy-6-phosphogluconate aldolase). The experimental approach adopted for introducing this deletion was thoroughly explained in **Chapter 2**. This manipulation is expected to result in an easier-to-manipulate, more predictable bacterial host, in which the interaction between the cellular machinery and the implanted genetic constructs are reduced (Kim & Copley, 2012; Nielsen *et al.*, 2013).

4.2.2. Elimination of the native glucose transport system. The second manipulation of strain GC1 involved the native glucose transport system. As mentioned in **Chapter 2**, glucose uptake in *P. putida* KT2440 is mediated by an ABC transport system that consumes ATP as part of its normal functioning. The main goal in the project is to boost the energy balance of *P. putida* KT2440 under glucose-dependent growth conditions. For this reason, and according to the results obtained in **Chapter 2**, this wasteful native transport system was removed from *P. putida* GC1 by introducing the Δ*gts* mutation. This genetic editing step was accomplished by a single deletion event that simultaneously removed the *gtsA*, *gtsB*, *gtsC*, and *gtsD* genes.

4.3. Design of genetic elements for establishing a stable linear glycolysis in *P. putida* GC2

The accumulation of the Δ*eda* and the Δ*gts* in-frame deletions in *P. putida* GC1 gave rise to the platform strain *P. putida* GC2. The next stage to develop a set of genetic elements that will allow for an efficient expression of all the genes encoding glucose transport and catabolic processing by a linear EMP route. Mini-transposon vectors allow for the stable insertion of foreign DNA into the chromosome of many Gram-negative bacteria (Martínez-García *et al.*, 2011; 2014a; 2017; Martínez-García & de Lorenzo, 2012; Ramos *et al.*, 2000). Tn*5*-derived elements present advantages over their plasmid-based counterparts for the introduction and expression of heterologous genes. These features include (i) the maintenance of the corresponding transgenes without antibiotic selective pressure, (ii) long-term stability of the constructs and reusability of the functional DNA parts, and (iii) the fact that mini-Tn*5*–based vectors admit cloning and chromosomal delivery of considerably long DNA fragments (which would be cumbersome to manipulate in other DNA delivery tools). As the transposase-encoding gene *tnpA* is lost following each transposition event

(Reznikoff, 2008), mini-Tn*5* vectors can be recursively used in the same microbial host. Since TnpA acts in *cis* (Phadnis *et al.*, 1986), it promotes the insertion of DNA sequences borne by the plasmid irrespective of any previous DNA insertions. Martínez-García *et al*. thoroughly revisited the original mini-Tn5 transposon vector concept (Martínez-García *et al.*, 2014a). The functional modules that constitute the vector (including the mosaic elements of the Tn*5* termini) have been edited to minimize the length of the corresponding DNA fragments, improving their functionality and making them entirely modular and exchangeable. The final product was the entirely synthetic plasmid construct termed pBAM1 (*born-again mini-transposon*). This design was soon followed by a series of synthetic, modular broad-host-range mini-Tn*5* plasmids derived from pBAM1. These plasmids, termed pBAMDs vectors (Martínez-García *et al.*, 2014a; 2017), enable the possibility of easy cloning and subsequent chromosomal insertion of functional DNA cargoes with three different and interchangeable antibiotic resistance markers. Note that this approach, in which the DNA cargo borne by the transposon (devoid of any promoter region) is randomly inserted into the target chromosome, not only enables the stable insertion of the corresponding genes, but it also results in a library of independent insertions expected to display different levels of transcription (Martínez-García *et al.*, 2014a). The elements needed to engineer strain GC2 were divided in three independent transposon modules as detailed below, and the relevant parts and modules are indicated in **Fig. 28b**.

4.3.1. Implementation of the glucose facilitator (Glf) from *Z. mobilis* in strain GC2. The Glf-based glucose transporter has been demonstrated in previous sections to be a useful alternative to functionally substitute the native hexose transport system of *P. putida* KT2440. Plasmid pBAMD1-2·*glf* was designed to deliver the glucose transport activity into strain GC2. In this transposon vector, the gene encoding the Glf transporter was linked to a synthetic regulatory element that contains an efficient RBS and a short DNA spacer sequence (**Fig. 28b**). The transposition of the *glf* element also introduces a Km-resistance marker in the target chromosome.

4.3.2. Introduction of the EMP pathway activities encoded by Modules I and II of the GlucoBrick system. Once the transport of glucose into the bacterial cytoplasm was delegated to the energy-efficient Glf transporter, it was necessary to bring about the enzyme activities needed to execute the linear EMP pathway in the upgraded glycolytic *chassis*. *P. putida* GC2 is not able to use glucose as a carbon source, being completely dependent of the catabolic enzymes encoded in the GlucoBrick system. These functional elements in Modules I and II were distributed in two independent transposon vectors. Note that the *beta-testing* stage described in **Section 4.1** of this chapter indicates that Module I would be sufficient to complement the glycolytic deficiency of the mutant strains under study. However, the insertion of the second module, that contains all the reactions of the *pay-off* phase of the EMP pathway ensures a correct channelling of carbon intermediates, avoiding potential bottlenecks throughout the entire route (Hollinshead *et al.*, 2016). In this context, the design comprised the construction of plasmids pBAMD1-4·GBI (Module I) and pBAMD1-6·GBII (Module II). As indicated previously for the *glf*-containing mini-Tn*5* transposon, these

DNA constructs encompass all the relevant genes of Module I or Module II individually preceded by a synthetic regulatory element, containing a RBS and a short DNA spacer sequence (**Fig. 28b**). These regulatory motifs were the only structural feature added to the gene clusters, and no promoter element was inserted in the transposons. The insertion of the transposons borne by plasmids pBAMD1-4·GBI and pBAMD1-6·GBII also endows a Sm- and a Gm-resistance marker, respectively, in the target chromosome.

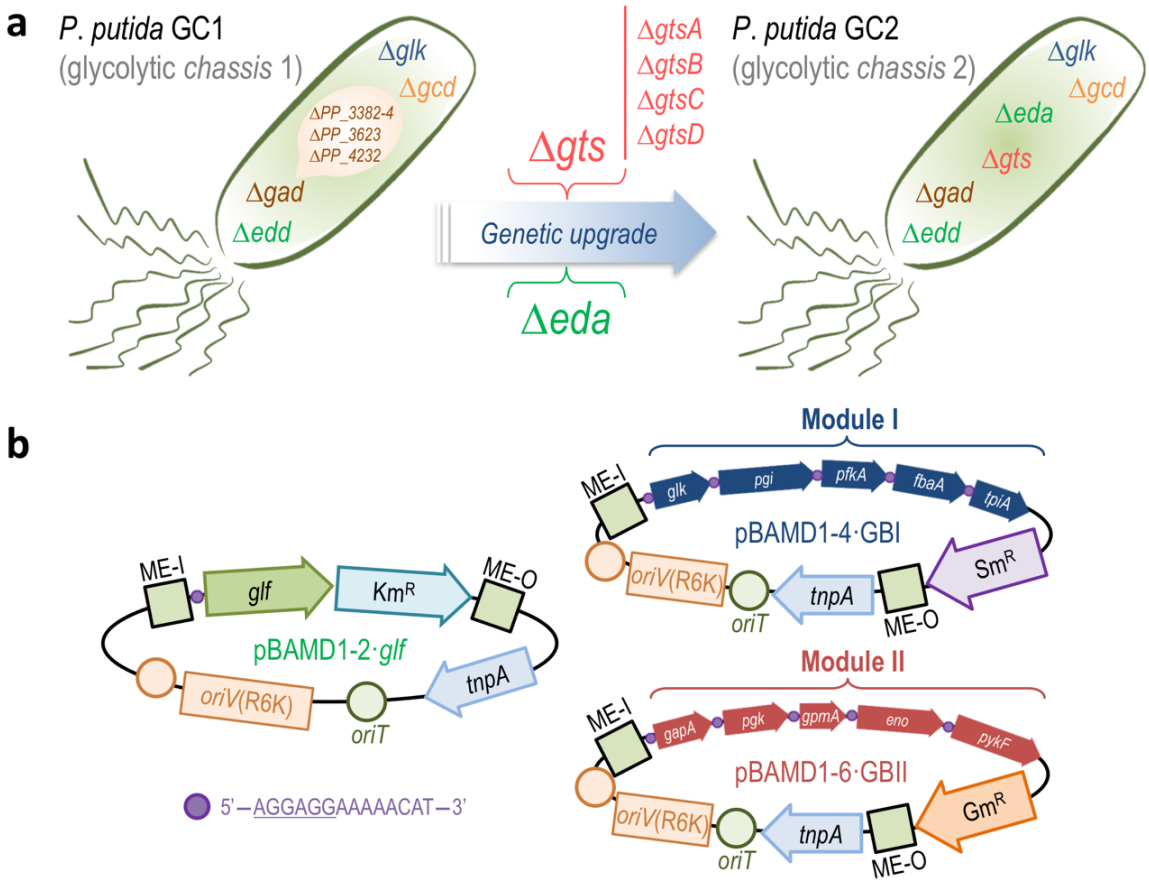

Figure 28 | **Construction of *P. putida* GC2 and transposon-based elements used for the stable implementation of a linear glycolysis.** (**a**) Genetic profile of the *P. putida* GC2 strain, indicating the deletions implemented to genetically upgrade *P. putida* GC1. Note that Δ*gts* represents the accumulation of the individual Δ*gtsA*, Δ*gtsB*, Δ*gtsC*, and Δ*gtsD* in-frame deletions. (**b**) Schematic structure of the mini-Tn*5*–based derivatives of vectors pBAMDs, employed to insert the gene encoding the Glf glucose transporter from *Z. mobilis* (pBAMD1-2·*glf*), and Module I (pBAMD1-4·GBI) and Module II (pBAMD1-6·GBII) of the GlucoBrick system in the chromosome of *P. putida* GC2. ME-I and ME-O, flanking the DNA sequence to be delivered into the target chromosome, indicate the position of the two mosaic elements recognized by the hyper-active transposase encoded by *tnpA*. A conditional origin of replication, dependent of the π protein [*oriV*(R6K)], and the origin of transfer (*oriT*) are also indicated in the outline. Note that each gene is preceded by a synthetic regulatory element, indicated by a purple circle, composed of a ribosome binding site (sequence underlined) and a short spacer sequence. The antibiotic-resistance markers follow the nomenclature: Ap^R, ampicillin; Gm^R, gentamicin; Km^R, kanamycin; and Sm^R, streptomycin. The elements in this outline are not drawn to scale.

Once all the elements needed to implement a linear EMP pathway in the final *P. putida* strain GC2 were constructed, a rational strategy was designed to bring the cognate DNA fragments into the target chromosome in the correct order. Each mini-transposon was separately delivered in the same *P. putida* GC2 strain in a sequential fashion. The correct order of these individual transposition events facilitated the subsequent phenotypic screening to isolate a triple exconjugant strain with the best growth after accumulating random insertions of all three transposons in the chromosome. The workflow followed during this experimental strategy is detailed in **Fig. 29a**.

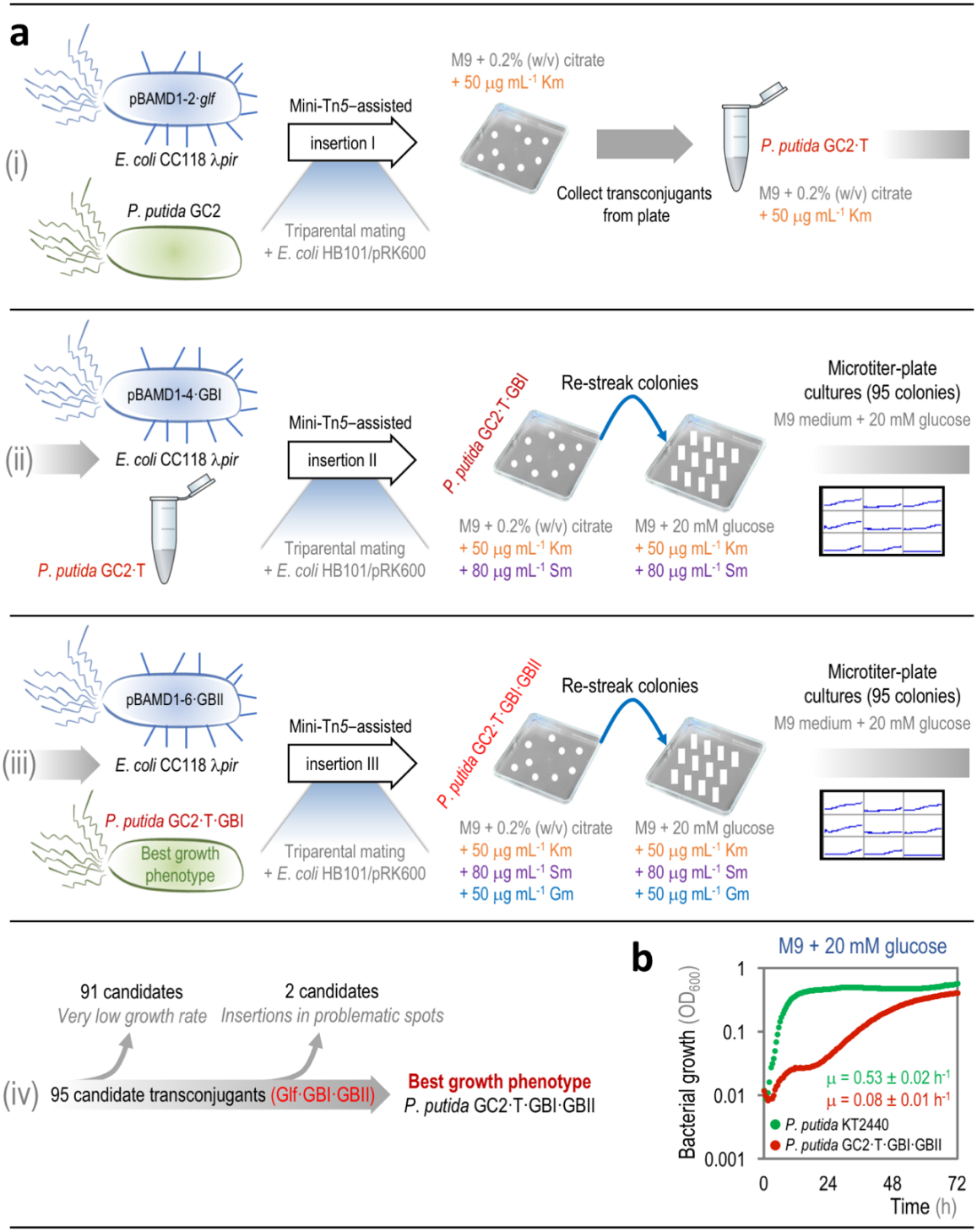

Figure 29 | **Workflow of the construction and selection of *P. putida* GC2·T·GBI·GBII.** (**a**) Sequential transposition events were executed to deliver three separate mini-Tn*5* modules carrying all the genetic parts needed for efficient glucose transport and a linear, Embden-Meyerhof-Parnas–based glycolytic pathway (*i.e.*, *glf* from *Z. mobilis* and Modules I and II of the GlucoBrick system, respectively). The relevant characteristics of the plasmids used in the construction of *P. putida* GC2·T·GBI·GBII are detailed in **Table 3** in *Materials and Methods*. The antibiotic-resistance markers follow the nomenclature: Gm, gentamicin; Km, kanamycin; and Sm, streptomycin. (**b**) Growth curves of *P. putida* KT2440 and *P. putida* GC2·T·GBI·GBII on M9 minimal medium with 20 mM glucose as the sole carbon source. Each data point in the growth curve represents the mean value of the optical density measured at 600 nm (OD_{600}) in quadruplicate measurements from at least three independent experiments. The specific growth rates (μ) were calculated from these data during exponential growth, and the inset shows the mean value ± standard deviations for each strain.

4.3.3. Insertion workflow of different glycolytic modules in *P. putida* GC2, and phenotypic analysis of glucose-using exconjugants isolates. The use of the random insertion approach was selected to obtain different levels of gene expression by taking advantage of endogenous promotor regions in the target chromosome. *P. putida* GC2 is unable to grow in glucose due to different mutations accumulated in its chromosome, which makes the screening process easier as the trait used for selection was the ability of the exconjugants to grow on glucose. In essence, the elements that this strain need to restore its glucose-dependent growth phenotype are the glucose transporter (Glf, delivered by means of plasmid pBAMD1-2·*glf*) and the Glk and Pfk activities encoded by Module I of the GlucoBrick system (borne by plasmid pBAMD1-4·GBI).

As indicated in **Fig. 29a**, the first part of the process was based on a sequential transposition of the elements in plasmids pBAMD1-2·*glf* and pBAMD1-4·GBI, introduced in the recipient strain *via* triparental mating. First, the *glf* gene was randomly introduced in the chromosome of *P. putida* GC2 [**Fig. 29a(i)**]. The mating mixture was plated onto M9 minimal medium plates containing 0.2% (w/v) citrate and Km to select a diversity of different transposition events enriched in *P. putida* GC2·T. The letter T stands for insertion of the Glf transporter in any given strain. Citrate, a gluconeogenic carbon source, was used in this first stage of selection to counterselect for *E. coli* cells from the triparental mating. The library of insertions in *P. putida* GC2·T was pooled and used in a second triparental mating associated with transposon pBAMD1-4·GBI. This transposition event generated *P. putida* GC2·T·GBI. According to the nomenclature adopted herein, GBI stands for insertion of the GlucoBrick Module I in any given strain. The triparental mating mixture was plated onto M9 minimal medium plates containing 0.2% (w/v) citrate and Km and Sm in order to select *P. putida* GC2·T·GBI exconjugants. Note that, unlike the parental *P. putida* GC2·T recipient strain, *P. putida* GC2·T·GBI exconjugants are potentially able to grow on glucose as the sole carbon source as this strain carries both *glk* and *pfkA* from *E. coli*. The resulting colonies were then patched onto M9 minimal medium plates containing 20 mM glucose, Km, and Sm to discard events that did not restore the growth phenotype

under glycolytic conditions [**Fig. 29a(ii)**]. From these plates, 95 colonies were inoculated in 96-well microtiter plates in M9 minimal medium containing 20 mM glucose, and bacterial growth was assessed by measuring the OD_{600} over time in a microtiter plate reader in order to select exconjugants displaying a high specific growth rate. Selected colonies were used as the template in randomly-amplified PCRs in order to locate the site of insertion of the mini-Tn*5* modules containing *glf* and Module I of the GlucoBrick system. A double exconjugant was singled during this screening stage. The *glf* insertion was mapped to the *PP_0841* gene (encoding the DNA-binding transcriptional regulator IscR) and Module I was located in the genome coordinate 6,005,012 bp (intergenic region between *PP_5259* and *ydcJ*).

The selected *P. putida* GC2·T·GBI exconjugant with the best growth phenotype on glucose was thus employed in a third triparental mating with the pBAMD1-6·GBII construct [**Fig. 29a(iii)**]. The triparental mating mixture was plated onto M9 minimal medium plates containing 0.2% (w/v) citrate, Km, Sm, and Gm in order to select for *P. putida* GC2·T·GBI·GBII. The positive colonies were re-streaked onto M9 minimal medium plates containing 20 mM glucose, Km, Sm, and Gm to check that the growth phenotype in glycolytic conditions was maintained. From these selection plates, 95 colonies that grew on glucose as the sole carbon source were inoculated in 96-well microtiter plates in M9 minimal medium containing 20 mM glucose, and bacterial growth was assessed by measuring the OD_{600} over time in a microtiter plate reader in order to select the exconjugant with the highest specific growth rate. In this process, 91 colonies were discarded due to very low specific growth rates, and the 4 remaining triple exconjugants that passed this quality control step were used as the template in a randomly-amplified PCR to locate the site of insertion of the mini-Tn*5* module containing Module II of the GlucoBrick system [**Fig. 29a(iv)**]. Two candidates were discarded, due to the fact that the insertions ended in potentially *problematic* genetic loci (*i.e.*, active mobile genetic elements that could bring about genetic instability). The two remaining candidates were re-inoculated in 96-well microtiter plates in M9 minimal medium containing 20 mM glucose, and bacterial growth was again assessed by measuring the OD_{600} over time in a microtiter plate reader. The final candidate, termed *P. putida* GC2·T·GBI·GBII, was selected in this experiment. This strain is a deeply genetically edited *P. putida* KT2440 derivative able to grow on glucose as the carbon source strictly using the grafted EMP pathway. The specific growth rate of *P. putida* GC2·T·GBI·GBII under glycolytic conditions represented a 15% fraction of that observed in the original WT strain KT2440 (**Fig. 29b**). The growth curve of *P. putida* GC2·T·GBI·GBII indicates a possible adaptation process during these conditions, since there were two distinct phases not observed for the WT strain, a result that was somehow expected. Apart from the fact that the final glycolytic strain has been heavily refactored and the major native pathways for hexose utilization have been removed, it should be kept in mind that the regulatory pattern of the grafted metabolic blocks (*e.g.*, temporal activation of native promoters controlling gene expression in the transposed elements) remains to be determined. In any case, the final cell density attained by the refactored strain in 72-h glucose cultures was very similar to that of the WT strain (*i.e.*, 0.41 and 0.52 units, respectively).

4.3.4. Biochemical landscape of *P. putida* GC2·T·GBI·GBII. The preceding sections described the *genetic* refactoring of whole metabolic blocks in *P. putida*. **Fig. 30** depicts the expected glucose metabolism in the thereby engineered *P. putida* GC2·T·GBI·GBII strain. In the first place, the oxidative glucose utilization pathway in the periplasm was blocked due to the absence of the Gcd activity (and the oxidations thereafter, catalyzed by Gad). On the other hand, the participation of the ED pathway in glucose catabolism was prevented by introducing the in-frame Δ*edd* and Δ*eda* mutations. In this scenario, the only way for the cells to grow in glucose would imply hexose transport by the Glf glucose transporter from *Z. mobilis* as the very first step. Once in the cytoplasm, glucose is phosphorylated into G6P by the Glk activity encoded in the inserted Module I. G6P is then transformed into GA3P through the other activities encoded in Module I. In this part of the route, the so-called *preparatory phase* of the EMP pathway, Module I share its reactions with the homologous set of endogenous enzymes in the host, with the notable exception of Pfk that is exclusively provided by the synthetic construct (**Fig. 30**). On the other hand, the so-called *pay-off phase* of the EMP pathway comprises the activities that transform GA3P into Pyr. In *P. putida* GC2·T·GBI·GBII, this part of the glycolytic pathway is likely carried out at the same time by the products of the genes encoded in Module II and the endogenous enzymes encoded in the chromosome. Finally, the pool of Pyr resulting from the linear glycolysis can continue its way to be transformed into acetyl-CoA to enter into the TCA cycle (**Fig. 30**).

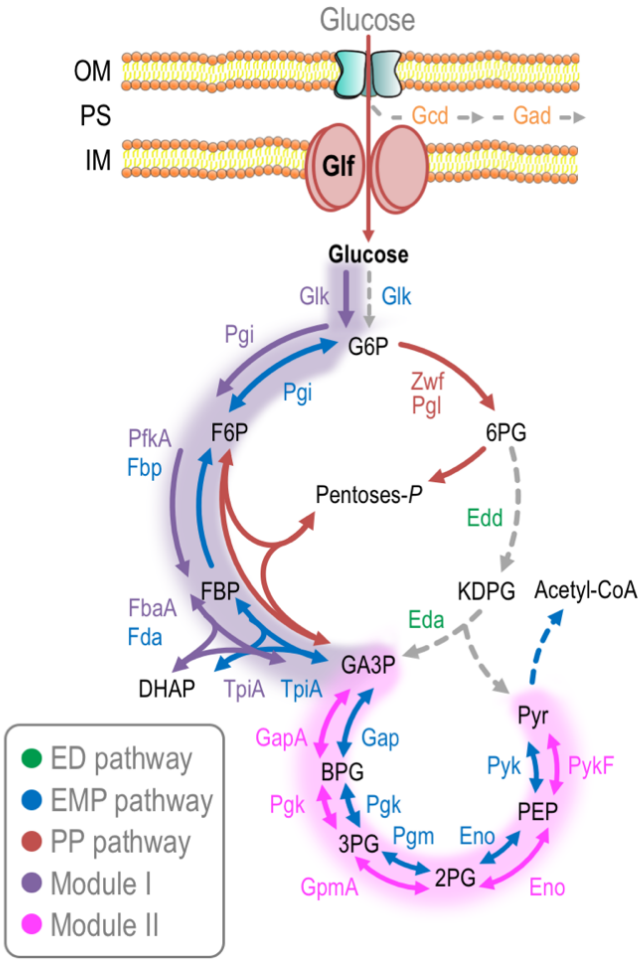

Figure 30 | **Expected glucose metabolism in *P. putida* GC2·T·GBI·GBII.** Glucose uptake in this strain takes place through the activity of the Glf transporter from *Z. mobilis*, since strain GC2 bears the Δ*gts* deletion (which erases the native, ATP-dependent transport of glucose). Glucose catabolism through the Entner-Doudoroff (ED) pathway is also blocked in this strain due to the Δ*edd* and Δ*eda* mutations. Oxidative pathways for glucose utilization were likewise suppressed due to the Δ*gcd* and Δ*gad* deletions. The non-functional Embden-Meyerhof-Parnas (EMP) pathway is completed by the Pfk activity encoded by Module I of the GlucoBrick system. As a result of the above-mentioned deletions, the *EDEMP cycle* (characteristic of the wild-type KT2440 strain) is blocked in this mutant. Each metabolic block is indicated with different colours in the scheme, and the deletions introduced in genes encoding any given enzyme activity are indicated with a dashed grey arrow. The reactions encoded by the genes from the Module I and II are indicated in purple and fuchsia, respectively. The reactions that comprise the *preparatory phase* and the *pay-off phase* of the EMP pathway are shaded in violet and pink. The abbreviations used in the biochemical network are as follows: G6P, glucose-6-*P*; F6P, fructose-6-*P*; FBP, fructose-1,6-P_2; DHAP, dihydroxyacetone-*P*; GA3P, glyceraldehyde-3-*P*; Pyr, pyruvate; BPG, glycerate-1,3-P_2; 3PG, glycerate-3-*P*; 2PG, glycerate-2-*P*; PEP, phosphoenolpyruvate; 6PG, 6-phosphogluconate; KDPG, 2-keto-3-deoxy-6-phosphogluconate; OM, outer membrane; PS, periplasmic space; and IM, inner membrane.

Since *P. putida* GC2·T·GBI·GBII was forced to employ a grafted EMP pathway operating in an entirely glycolytic regime (*i.e.*, the opposite role of the partial EMP route naturally found in strain KT2440), a mere *in vitro* characterization, based on assays of enzyme activity, is not sufficient to thoroughly explore the metabolic profile of the engineered strain. For this reason, a full ^{13}C-based metabolic flux ratio analysis, incorporating quantitative physiology data along the patterns of ^{13}C-distribution in proteinogenic amino acids, was tackled to systematically describe the operation of central carbon metabolism in strain GC2·T·GBI·GBII.

4.4. Central carbon metabolism in glucose-grown *P. putida* GC2·T·GBI·GBII: Quantitative physiology parameters and ^{13}C-based metabolic flux analysis

The biochemical pathways involved in glucose catabolism in *P. putida* (**Fig. 31**) have been studied in detail (del Castillo *et al.*, 2007; Latrach-Tlemçani *et al.*, 2008; Vicente & Cánovas, 1973a), including the description of the fate of every metabolite in the upper domain of the biochemical network of strain KT2440 (Nikel *et al.*, 2015a). *P. putida* KT2440 mostly uses the peripheral oxidation of glucose into gluconate to feed the 6PG node, the first metabolite of the ED pathway. At the same time, this bacterium uses the (partial) EMP pathway in a gluconeogenic mode of operation to recycle trioses-*P* into hexoses-*P*, with a relatively modest contribution of the PP pathway in hexose catabolism. **Fig. 31** summarizes all the activities and metabolic steps involved in this intricate metabolism and, at the same time, serves as a reference to catalog the reactions studied in the ^{13}C-based metabolic flux analysis shown below.

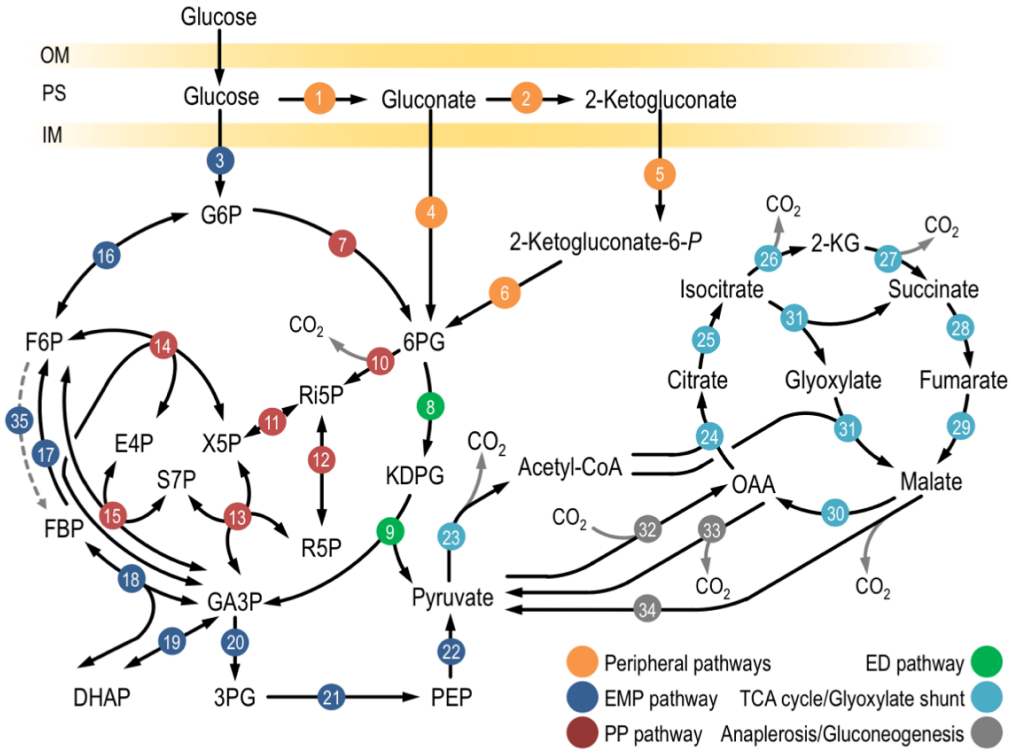

Pathway	No.	Enzyme(s)	Name(s) & locus tag
Peripheral reactions	1	Glucose dehydrogenase	Gcd (PP_1444)
	2	Gluconate 2-dehydrogenase	PP_3382-4, PP_3623, PP_4232
	4	Gluconate kinase	GnuK (PP_3416)
	5	2-Ketogluconate kinase	KguK (PP_3378)
	6	2-Ketogluconate-6-*P* reductase	PtxD (PP_3376)
Pentose phosphate pathway	7	Glucose-6-*P* 1-dehydrogenase	Zwf (PP_5351), ZwfA (PP_1022), ZwfB (PP_4042)
		6-Phosphogluconolactonase	Pgl (PP_1023)
	10	6-Phosphogluconate dehydrogenase	GntZ (PP_4043)
	11	Ribulose-5-*P* 3-epimerase	Rpe (PP_0415)
	12	Ribose-5-*P* isomerase	RpiA (PP_5150)
	13	Transketolase	TktA (PP_4965)
	14		
	15	Transaldolase B	Tal (PP_2168)
Entner-Doudoroff pathway	8	6-Phosphogluconate dehydratase	Edd (PP_1010)
	9	2-Keto-3-deoxy-6-phosphogluconate aldolase	Eda (PP_1024)
Anaplerosis / Gluconeogenesis	32	Pyruvate carboxylase	PycA (PP_5347), PycB (PP_5346)
	33	Phosphoenolpyruvate carboxylase	Ppc (PP_1505)
	34	Malic enzyme	MaeB (PP_5085)
Embden-Meyerhof-Parnas pathway	3	Glucokinase	Glk (PP_1011)
	16	Glucose-6-*P* isomerase	Pgi-I (PP_1808), Pgi-II (PP_4701)
	17	Fructose-1,6-bisphosphatase	Fbp (PP_5040)
	18	Fructose-1,6-P_2 aldolase	Fda (PP_4960), PP_2871, PP_3224
	19	Triose phosphate isomerase	TpiA (PP_4715)
	20	Glyceraldehyde-3-*P* dehydrogenase	GapA (PP_1009), GapB (PP_2149), PP_0665, PP_3443
		Phosphoglycerate kinase	Pgk (PP_4963)
	21	Phosphoglycerate mutase	GpmI (PP_5056), PP_2243, PP_3923, PP_4450
		Phosphopyruvate hydratase	Eno (PP_1612)
	22	Pyruvate kinase	PykA (PP_1362), Pyk (PP_4301)
	35	6-phosphofructo-1-kinase	Pfk (missing in *P. putida* KT2440)
Tricarboxylic acid cycle/Glyoxylate shunt	23	Pyruvate dehydrogenase	AcoA (PP_0555), AceF (PP_0338), AceE (PP_0339), Lpd (PP_5366), LdpG (PP_4187), LpdV (PP_4404)
	24	Citrate synthase	GltA (PP_4194)
	25	Aconitate hydratase	AcnA-I (PP_2112), AcnA-II (PP_2336), AcnB (PP_2339)
	26	Isocitrate dehydrogenase	Icd (PP_4011), Idh (PP_4012)
	27	2-Ketoglutarate dehydrogenase	SucA (PP_4189), SucB (PP_4188), LpdG (PP_4187), PP_2652, PP_3662
		Succinyl-coenzyme A synthetase	SucDC (PP_4185-PP_4186)
	28	Succinate dehydrogenase	SdhA (PP_4191), SdhB (PP_4190), SdhC (PP_4193), SdhD (PP_4192)
	29	Fumarate hydratase	FumC-I (PP_0944), FumC-II (PP_1755), PP_0897
	30	Malate dehydrogenase/ Malate:quinone oxidoreductase	Mdh (PP_0654), Mqo-I (PP_0751), Mqo-II (PP_1251), Mqo-III (PP_2925), DpkA (PP_3591)
	31	Isocitrate lyase	AceA (PP_4116)
		Malate synthase	GlcB (PP_0356)

Figure 31 | **Biochemical pathways for glucose catabolism in *P. putida* KT2440.** The entire metabolic network was divided in six main metabolic blocks, and they are identified with different colors in the scheme: (i) *peripheral pathways*, that comprise the oxidative transformation of glucose into gluconate and 2-ketogluconate (including the phosphorylated derivatives of these metabolites); (ii) *EMP pathway* [incomplete, due to the absence of the 6-phosphofructo-1-kinase activity (Pfk), and indicated with a dashed grey arrow]; (iii) *pentose phosphate (PP) pathway*; (iv) *ED pathway*; (v) the *tricarboxylic acid cycle* and *glyoxylate shunt*; and (vi) *anaplerotic* and *gluconeogenic bioreactions*. Some reactions have been lumped to simplify the metabolic map. The complete list of enzymes and isoenzymes catalyzing each reaction is shown in the bottom of the scheme. The information indicated in this picture was compiled by the latest update (as for June 2017) of the *Pseudomonas* Genome Database (Winsor *et al.*, 2016) and the MicroScope platform (Vallenet *et al.*, 2017). In the cases in which no gene name has been assigned to a reaction, the locus tag is indicated in the list. Abbreviations used in this diagram are as follows: G6P, glucose-6-*P*; F6P, fructose-6-*P*; FBP, fructose-1,6-P_2; DHAP, dihydroxyacetone-*P*; 6PG, 6-phosphogluconate; KDPG, 2-keto-3-deoxy-6-phosphogluconate; Ri5P, ribulose-5-*P*; R5P, ribose-5-*P*; X5P, xylulose-5-*P*; S7P, sedoheptulose-7-*P*; E4P, erythrose-4-*P*; GA3P, glyceraldehyde-3-*P*; 3PG, glycerate-3-*P*; PEP, phosphoenolpyruvate; acetyl-CoA, acetyl-coenzyme A; OAA, oxaloacetate; 2-KG, 2-ketoglutarate; OM, outer membrane; PS, periplasmic space; and IM, inner membrane.

As a requisite information for ^{13}C-based metabolic flux analysis, the growth parameters of *P. putida* KT2440 and *P. putida* GC2·T·GBI·GBII were calculated in batchwise, shaken-flask cultures in quantitative physiology experiments (**Table 9**). Important differences were observed between the two strains in these experiments. In the first place, and similarly to the growth patterns determined in microtiter-plate cultures, the specific growth rate of *P. putida* GC2·T·GBI·GBII growing under glycolytic conditions was significantly smaller (*i.e.*, around one-tenth) than that of the WT strain. The shape of the growth curve for the engineered strain in shaken-flask cultures was qualitatively similar to that of strain KT2440, which probably indicates that the results of **Fig. 29b** correlate with deficient oxygenation or agitation in microtiter-plate cultures. On the other hand, a 7.6-fold smaller specific rate of carbon uptake (q_s) was determined for *P. putida* GC2·T·GBI·GBII as compared to its WT counterpart. Additionally, the yield of biomass on substrate ($Y_{X/S}$) showed the same trend but with a smaller difference between the two strains under comparison, and *P. putida* GC2·T·GBI·GBII produced an amount of biomass per gram of glucose approximately 1.4-fold smaller than the WT. Considering the results of quantitative physiology experiments, it can be concluded that *P. putida* GC2·T·GBI·GBII is significantly affected in its glucose-dependent growth phenotype. This situation was somehow expected since, as indicated in previous sections in this chapter, the expression of the inserted gene modules (and, for that matter, any other regulatory pattern) has not been optimized in the engineered strain. In any case, the microbial platform obtained herein constituted a proof-of-principle to test the functional replacement of central glycolytic pathways, an issue that was further investigated as disclosed in the next section.

Table 9 | **Growth parameters of *P. putida* KT2440 and its *P. putida* GC2·T·GBI·GBII strain in shaken-flask cultures under glycolytic growth conditions[a].**

P. putida strain	μ (h^{-1})[b]	q_S ($mmol_{glucose}\ g_{CDW}^{-1}\ h^{-1}$)[b]	$Y_{X/S}$ ($g_{CDW}\ g_{glucose}^{-1}$)[c]
KT2440 (WT)	0.49 ± 0.01	5.93 ± 0.04	0.46 ± 0.03
GC2·T·GBI·GBII	0.048 ± 0.001	0.78 ± 0.02	0.34 ± 0.01

[a] Cells were grown in M9 minimal medium containing 20 mM glucose as the sole carbon source. In the case of *P. putida* GC2·T·GBI·GBII, the culture medium was also supplemented with Gm (50 μg ml^{-1}), Km (50 μg ml^{-1}), and Sm (80 μg ml^{-1}). All the values shown in this Table represent the mean of the corresponding parameter ± standard deviation of quadruplicate measurements from at least three independent experiments.

[b] The specific growth rate (μ) and the specific rate of carbon uptake (q_s) were obtained during exponential growth by linear regression. WT, wild-type; CDW, cell dry weight.

[c] The yield of biomass on substrate ($Y_{X/S}$) was obtained during exponential growth by correlating μ and q_s.

The ultimate experiment to characterize and ensure the intended metabolic refactoring in *P. putida* GC2·T·GBI·GBII, involved ^{13}C-based metabolic flux ratio analyses of its central carbon metabolism. In this technique, the ^{13}C-labeled carbon source (*i.e.*, glucose) is processed by the enzymes of the central carbon metabolism in a way that a significant fraction of the carbon atoms are incorporated into proteinogenic amino acids, which exhibit a characteristic labeling patterns to be analyzed by mass spectrometry methodologies (Dauner & Sauer, 2000). The labeling pattern of these individual molecules provides information about the pathway and carbon skeletons from which these amino acids originated (Sauer, 2006). Then, the fluxes through the different metabolic pathways under study can be determined by integrating the relative isotopic abundance of metabolic intermediates with stoichiometric metabolic models of the biochemical network under study and data obtained from physiological experiments (Zamboni *et al.*, 2005). The *in vivo* carbon flux distribution was thus compared in glucose-grown *P. putida* KT2440 (*i.e.*, the WT strain) and its deeply refactored *P. putida* GC2·T·GBI·GBII derivative. Mixtures of naturally labeled glucose and either uniformly ^{13}C-labeled or ^{13}C-labeled in position 1 of the hexose ([U-^{13}C]-glucose and [1-^{13}C]-glucose, respectively) were used in shaken-flask cultures of the strains, as indicated in *Materials and Methods*. Such experimental approach was adopted to elucidate the extent of manipulation that the metabolic *chassis* has been able to endure in terms of rerouting its central carbon metabolism. **Fig. 32** describes the absolute net fluxes in the glucose catabolism network for the strains under study [WT (**Fig. 32a**) and *P. putida* GC2·T·GBI·GBII (**Fig. 32b**)], in which all the values shown were normalized to the specific glucose uptake rates (**Table 9**). The different metabolic blocks of hexose catabolism and their operation in either strain are explained in the sections below.

4.4.1. Glucose transport and hexose phosphorylation/oxidation. As a starting point, it should be noted that *P. putida* GC2·T·GBI·GBII transports glucose through the activity of the Glf facilitator of *Z. mobilis*. As indicated before, and considering that the level of expression of the cognate *glf* module is unknown, the very low specific rate of carbon uptake (q_S) value of strain *P. putida* GC2·T·GBI·GBII could stem from a limitation in the Glf-mediated internalization of the substrate. According to the data discussed in **Chapter 2**, the accumulation of the Δ*gcd* and Δ*gad* deletions disabled the peripheral reactions (typically run by many bacterial members of the *Pseudomonas* genus) to oxidize glucose into gluconate and/or 2KG. Such deletions, in combination with the in-frame elimination of the endogenous *gts* genes, would completely block glucose transport. The results of **Table 9** and **Fig. 32** demonstrate that Glf is able to functionally complement these transport deficiencies in strain GC2·T·GBI·GBII. Interestingly, the WT strain channeled around 90% of the internalized glucose through the first step of the periplasmic peripheral pathways of hexose oxidation, catalyzed by Gcd. A small fraction (12%) of the thereby generated gluconate was then transformed into 2KG by a further oxidation catalyzed by Gad. This finding is consistent with the results recently published for glucose-grown strain KT2440 (Nikel *et al.*, 2015a). On the other hand, the inability of *P. putida* GC2·T·GBI·GBII to oxidize or phosphorylate glucose using the native pathways must be compensated by the Glk activity brought about by Module I from the GlucoBrick system. As expected, 100% of the substrate transported by the engineered bacterium was directly phosphorylated into G6P. This flux was approximately 10-fold higher than the native glucose phosphorylation flux in *P. putida* KT2440.

4.4.2. Metabolic origin and fate of G6P and pathways leading to Pyr formation. *P. putida* KT2440 phosphorylated approximately 10% of the total transported glucose into G6P, and the G6P node was also fed by the Pgi activity (*i.e.*, operating in the gluconeogenic direction), which added an extra 9% fraction to the G6P pool with respect to the specific rate of carbon uptake (q_S) value. G6P was then transformed into 6PG by the action of the Zwf activity. The Zwf-catalyzed conversion of G6P into 6PG had similar values in both strains, although the metabolic origin of G6P was different in either case. While all the 6PG pool in the engineered strain originated from Zwf, in strain KT2440 the 6PG node was also fed by the phosphorylation of two oxidized metabolites from the upper peripheral oxidative pathways [*i.e.*, 72% from the phosphorylation of gluconate *via* gluconate kinase (GnuK) and 11% from the reduction of 2-ketogluconate-6-*P* (2K6PG) *via* 2-ketogluconate-6-*P* reductase (PtxD)]. No G6P formation from F6P was detected in *P. putida* GC2·T·GBI·GBII, and the prevailing direction of the Pgi-catalyzed biochemical step in this strain was entirely glycolytic. Furthermore, the biochemical network in the glycolytic *chassis* mimics the native metabolism of *E. coli*, in that the G6P pool was split in a 22% being channeled into 6PG and the remaining 77% funneled into F6P (Fuhrer *et al.*, 2005). This is an additional piece of information that demonstrates that the metabolic situation of *P. putida* GC2·T·GBI·GBII is characterized by a linear glycolytic flux from G6P downwards.

As expected, the ED route was completely removed from *P. putida* GC2·T·GBI·GBII due to the introduced Δ*edd* and Δ*eda* in-frame deletions. However, the flux values for this pathway were very high in the WT strain, and 92% of the total 6PG was channeled downwards through the ED-dependent catabolism. The elimination of the ED pathway in the glycolytic *chassis* lead to a 2.4-fold increase in the traffic *via* the GntZ activity when compared with the WT strain. This result is again very similar to the flux distribution expected in glucose-grown WT *E. coli* (Fuhrer *et al.*, 2005). GntZ catalyzes the conversion 6PG + $NADP^+$ → Ri5P + CO_2 + NADPH. The GntZ activity is considered to be the main entry point into the oxidative branch of the PP pathway, and usually limits the overall carbon flux through the entire route. Interestingly, the carbon fluxes *via* the PP pathway in *P. putida* GC2·T·GBI·GBII had very similar values to those reported for *E. coli*, including the non-oxidative branch of the pathway, *i.e.*, TktA and Tal (Fuhrer *et al.*, 2005).

Metabolic fluxes through the EMP pathway were carefully analyzed in *P. putida* GC2·T·GBI·GBII and the WT strain. Consistent with previous findings in our laboratory, the WT strain deployed the (partial) EMP route as a gluconeogenic pathway to recycle trioses-*P* into hexoses-*P*. However, *P. putida* GC2·T·GBI·GBII channeled 77% of the glucose entering the network *via* the linear glycolytic EMP pathway encoded by Module I and II of the GlucoBrick system. In the glycolytic *chassis*, 73% of the generated Pyr was obtained from the EMP pathway, in contrast with a 49% in the WT strain. In both strains, the so-called *pay-off phase* of the EMP pathway transformed GA3P into Pyr to different extents. In *P. putida* GC2·T·GBI·GBII, the flux through pyruvate kinase (*i.e.*, PEP + ADP + H^+ → Pyr + ATP) was 2.5-fold higher than that in the WT counterpart. Pyruvate kinase is a key allosteric enzyme of the EMP route, and, since it catalyzes one of the two substrate-level phosphorylation steps that generate ATP, it mediates an important metabolic step in the overall objective of the refactoring of *P. putida* (Emmerling *et al.*, 2002; Zhao *et al.*, 2017).

4.4.3. Anaplerotic pathways, TCA cycle, and glyoxylate shunt. The anaplerotic fluxes from PEP and Pyr to oxaloacetate, the fluxes through the TCA cycle, and the fluxes in the glyoxylate shunt (almost zero) were very similar in *P. putida* GC2·T·GBI·GBII and the WT strain. The small differences observed in anaplerosis and TCA cycle operativity were not statistically significant, although an increase in the activity of anaplerotic pathways would be expected as this is a feature typical of *E. coli*. Additionally, these routes had similar values when they are compared with the information available in the literature not only for *P. putida* KT2440 but also other *Pseudomonas* species, such as *P. fluorescens* (Chavarría *et al.*, 2012; Fuhrer *et al.*, 2005; Nikel *et al.*, 2015a). As expected in *P. putida*, neither strain had active fermentation pathways, and the breakdown of hexoses was entirely oxidative (Fuhrer *et al.*, 2005).

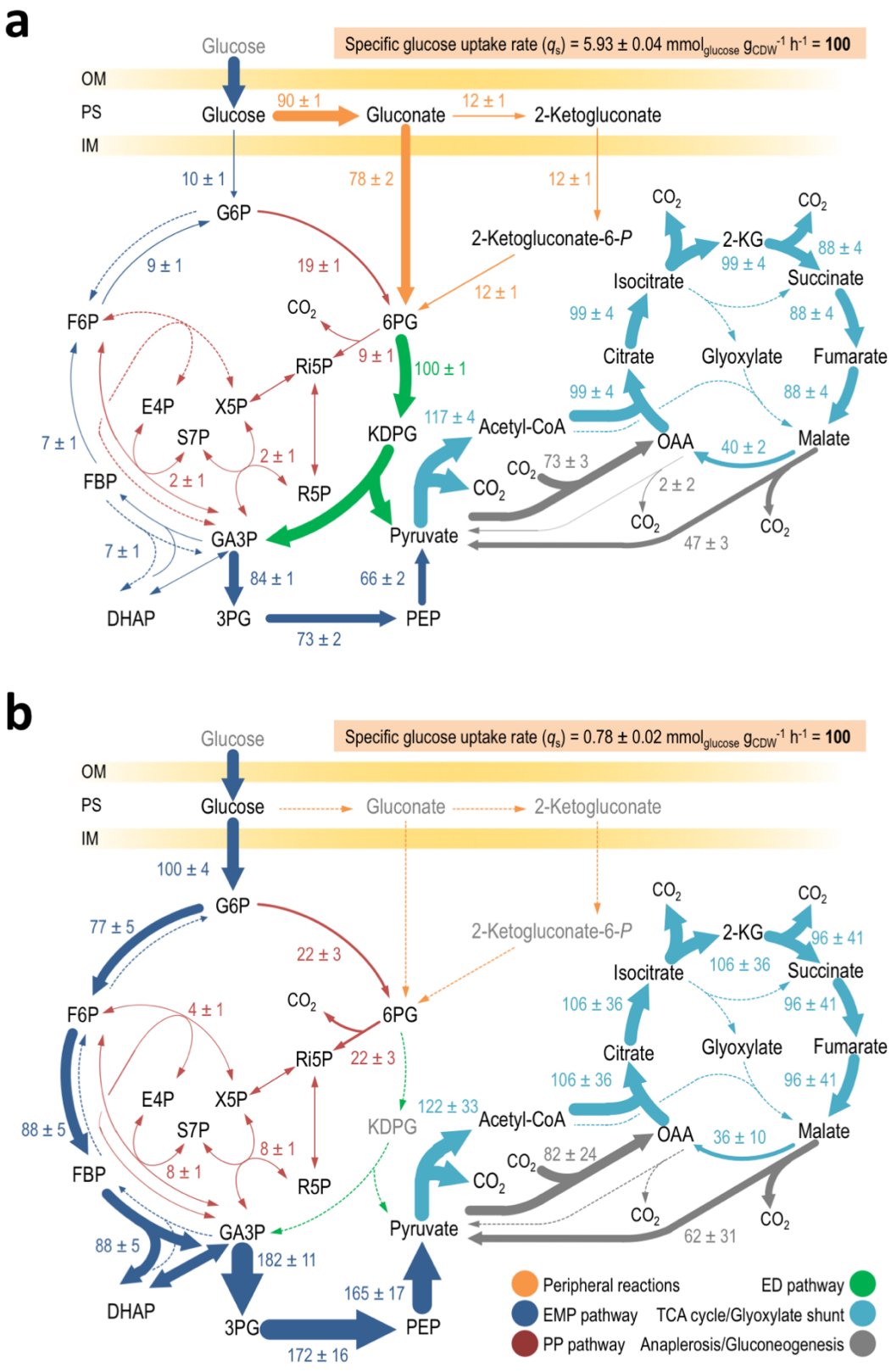
a
Glucose
Specific glucose uptake rate (q_s) = 5.93 ± 0.04 $mmol_{glucose}$ g_{CDW}^{-1} h^{-1} = 100
OM
PS
IM
Glucose
Gluconate
2-Ketogluconate
90 ± 1
12 ± 1
10 ± 1
78 ± 2
12 ± 1
G6P
2-Ketogluconate-6-P
2-KG
Isocitrate
Succinate
Citrate
Glyoxylate
Fumarate
Malate
OAA
Acetyl-CoA
KDPG
6PG
Ri5P
E4P
X5P
S7P
R5P
F6P
FBP
GA3P
DHAP
3PG
PEP
Pyruvate
CO2
9 ± 1
19 ± 1
12 ± 1
100 ± 1
117 ± 4
99 ± 4
88 ± 4
40 ± 2
73 ± 3
2 ± 2
47 ± 3
7 ± 1
2 ± 1
84 ± 1
66 ± 2
73 ± 2
b
Glucose
Specific glucose uptake rate (q_s) = 0.78 ± 0.02 $mmol_{glucose}$ g_{CDW}^{-1} h^{-1} = 100
OM
PS
IM
Glucose
Gluconate
2-Ketogluconate
100 ± 4
G6P
2-Ketogluconate-6-P
2-KG
Isocitrate
Succinate
Citrate
Glyoxylate
Fumarate
Malate
OAA
Acetyl-CoA
KDPG
6PG
Ri5P
E4P
X5P
S7P
R5P
F6P
FBP
GA3P
DHAP
3PG
PEP
Pyruvate
CO2
77 ± 5
22 ± 3
4 ± 1
22 ± 3
122 ± 33
106 ± 36
96 ± 41
82 ± 24
36 ± 10
62 ± 31
88 ± 5
8 ± 1
182 ± 11
165 ± 17
172 ± 16
Peripheral reactions
EMP pathway
PP pathway
ED pathway
TCA cycle/Glyoxylate shunt
Anaplerosis/Gluconeogenesis

Figure 32 | ***In vivo* distribution of carbon fluxes under glycolytic growth conditions for *P. putida* KT2440 and *P. putida* GC2·T·GBI·GBII.** *In vivo* distribution of carbon fluxes obtained from ratio-constrained flux balance analysis in cells grown on ^{13}C-labelled glucose. The scheme depicts the flux distribution through the biochemical network of (**a**) *P. putida* KT2440 (wild-type strain) and (**b**) *P. putida* GC2·T·GBI·GBII. All the values for individual fluxes in the diagram were normalized to the specific glucose uptake rate (arbitrarily set to 100). The ± standard deviations of duplicate measurements from at least three independent experiments were calculated using the Gaussian law of error propagation. The arrow line width in each biochemical step has been scaled to represent the relative flux percentage. Dashed lines indicate that no significant flux was detected in that particular biochemical step under the experimental conditions. The abbreviations employed for the different metabolites in the biochemical network and the distribution of the main metabolic blocks follow the same principles indicated in **Fig. 31**.

4.4.4. Impact of the engineered EMP route in the energy and redox balances of *P. putida*. The ^{13}C-based metabolic flux analysis allowed us to determine the net fluxes around three key metabolic cofactors (ATP, NADH, and NADPH) in order to evaluate the energy and redox state in the strains under study (**Fig. 33**). These net fluxes encompass all the reactions generating each of the cofactors and all the reactions at which they are consumed. The overall stoichiometry of the ED pathway is glucose + NAD^+ + $NADP^+$ + ADP + Pi → 2Pyr + NADH + NADPH + $2H^+$ + ATP; whereas the stoichiometry of the EMP pathway is glucose + $2NAD^+$ + 2ADP + 2Pi → 2Pyr + 2NADH + $2H^+$ + 2ATP. Considering these overall balances, the proper implementation of an EMP pathway in *P. putida* GC2·T·GBI·GBII should result in an increase in ATP and NADH production and, eventually, in a decrease of NADPH generation (due to the elimination of the EDEMP cycle). The former hypothesis was already proven correct by the results indicated in **Fig. 33**, in which the ATP formation has increased by approximately 20% in the *P. putida* GC2·T·GBI·GBII strain as compared with the WT counterpart. Even more striking was the value obtained for NADH formation in the engineered *chassis*, representing an increase of 2.5-fold as compared to the WT strain. This result is in line with the prediction, since NADH formation (at the expense of NADPH generation) is a key feature of the linear glycolysis over the ED pathway. Finally, a small reduction in NADPH formation was observed in *P. putida* GC2·T·GBI·GBII, although the difference with the WT strain was not statistically significant.

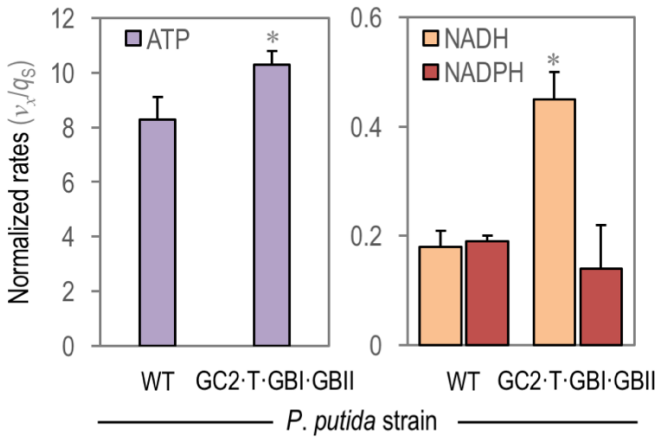

Figure 33 | **Net ATP, NADH, and NADPH formation under glycolytic growth conditions for *P. putida* KT2440 and *P. putida* GC2·T·GBI·GBII.** ATP (left panel), NADH and NADPH (right panel) rates of formation normalized by the specific rate of glucose uptake (v_x/q_S) of *P. putida* KT2440 (WT) and *P. putida* GC2·T·GBI·GBII. Cells were grown aerobically in M9 minimal medium added with glucose at 20 mM, harvested during exponential growth, and rapidly quenched with liquid N_2. Fluxes were calculated as indicated in *Materials and Methods*. The experimentally determined relative flux ratios (v_x) were used to obtain net rates as $v_x = \Sigma v_{formation} - \Sigma v_{consumption}$. Each bar represents the mean value of the corresponding normalized rates (v_x/q_S) ± standard deviation of duplicate measurements from at least three independent experiments. Significant differences ($P < 0.05$, as evaluated by means of the Student's *t* test) in the pair-wise comparison of a *P. putida* GC2·T·GBI·GBII to the control WT strain are indicated by an asterisk.

As a summary, it was possible to confirm the correct implementation of a functional, linear EMP pathway in *P. putida* KT2440, not only by supplying the activities absent in the extant biochemical network (*i.e.*, Pfk), but also by modifying the very structure of central carbon metabolism and the cofactor balance thereof. In all, the experimental approach adopted resulted in a heavily refactored derivative of *P. putida* in which the native EDEMP cycle operation was blocked and functionally replaced by a *linear glycolytic route*.

V. DISCUSSION

«*It is better to debate a question without settling it than to settle a question without debating it*»
Joseph Joubert
(1754 AC-1824 AC)

DISCUSSION

1. Metabolic Engineering meets Synthetic Biology standards: the GlucoBrick system as a tool to implement glycolytic capacities in Gram-negative bacteria

Recombinant DNA technologies have accumulated a considerable history, which resulted in a vast number of genetic constructs without a clear classification and structure (Novick *et al.*, 1976). Fortunately, during the contemporary era of *Systems and Synthetic Biology* this situation has been revisited through the promotion of the *standardization* philosophy (Canton *et al.*, 2008). One example of this rationalization is the creation of the SEVA plasmid collection, a modular set of standardized plasmid structured for an easy combinations of different antibiotics, cargoes (to introduce different genetic modules, such as expression systems), and origins of replication (Martínez-García *et al.*, 2014a,b; 2015; 2017; Silva-Rocha *et al.*, 2013). Taking inspiration on this standard, and incorporating its rules as a basis for the work discussed in this Thesis, part of this study was dedicated to design the GlucoBrick system (**Chapter 1**). This Metabolic Engineering tool comprises a set of glycolytic modules that facilitate the user-friendly implementation of EMP pathway activities in different Gram-negative bacteria.

Metabolic Engineering is presented as a key field for different research projects (King *et al.*, 2016; Raab *et al.*, 2005; Stafford & Stephanopoulos, 2001; Stephanopoulos, 2012). This burgeoning field is considered as the discipline occupied with the directed modification of metabolic pathways for the microbial-based synthesis of various products (Stephanopoulos, 2012). Usually, the most common scenario for these modifications has been focused in *peripheral aspects*, *e.g.*, the elimination of competing endogenous pathways, the optimization of uptake and secretion systems, and the rerouting of small molecules at given nodes of the target biochemical network. In contrast, the biochemical *core* (*i.e.*, central carbon metabolism) that fuels the bacterial cell factory is generally taken for granted, and hardly ever touched; *i.e.*, few efforts have tackled the refactoring of central enzymatic process in its entirety. Relevant examples of this sort include auxotrophic CO_2 fixation (Antonovsky *et al.*, 2016) and CH_3OH assimilation (Müller *et al.*, 2015) by engineered strains of *E. coli*. Faced with this caveat in the field, and considering that a large number of bioprocess are directly connected with the *core* carbon metabolism [*e.g.*, PHB production and its dependency on acetyl-CoA availability (Sharma *et al.*, 2016)], **Chapter 1** of this Thesis explored the development of the GlucoBrick system. This tool was designed to make the implantation of glycolytic modules derived from the EMP pathway in different Gram-negative bacteria easy. All in all, this system allows to the user to implement, in a driven-by-demand fashion, the combination of elements (or the entire pathway) needed to activate a synthetic EMP pathway inspired in the central carbon metabolism of *E. coli*. In other words, the potential manipulation of the central metabolism is facilitated in a large number of Gram-negative bacteria in a setup entirely compatible with the SEVA standard.

The standardization of a central metabolic process, such as the EMP pathway, cannot be considered as a simple *copy and paste* DNA procedure. The intrinsic regulation of any given metabolic pathway increases in complexity at the same time that its connectivity with other regulatory and structural elements of the cells increases (Li *et al.*, 2014). This scenario is completely applicable to the EMP pathway, which is the main catabolic route in glucose-grown *E. coli*. For this reason, one fundamental step in the process of designing the GlucoBrick system was the elimination of any regulatory elements, in order to make the system as independent as possible in terms of regulation when the modules are implanted in the bacterial host (*i.e.*, orthogonality). The work developed in order to solve this issue is indicated in the first section of **Chapter 1** of this Thesis. In this part of the manuscript, the design followed in the assembly of the GlucoBrick system, to allow the modular arrangement of its elements to make it compatible with the SEVA standard (Silva-Rocha *et al.*, 2013), is also thoroughly described. This structure will facilitate the adaptation of the genetic constructs to the necessities of future users, simplifying the tedious task of cloning multiple DNA fragments into the proper vector(s). Additionally, the compatibility with the SEVA standard allows this system to be cloned in a large number of SEVA-like systems, one of them being the pBAMDs collection of transposon vectors (Martínez-García *et al.*, 2014a). This synthetic transposon tool allows for the stable insertion of foreign DNA (in our case, the modules of the GlucoBrick system), in the chromosome of the desired Gram-negative bacteria. At the same time, the vectors, modules, and elements of the SEVA collection are continually evolving and they are regularly updated, conferring new features to the standards associated with the platform (Martínez-García *et al.*, 2014b).

The second section of **Chapter 1** is focused on demonstrating the functionality of the GlucoBrick system in the most widespread model Gram-negative bacterial host, *E. coli*. Despite the fact that the enzyme design brought about by this system was inspired on the glycolytic machinery of this Enterobacterium, the large number of modifications introduced in the DNA sequence during the standardization process resulted in a different physical and regulatory layout that differs from the original distribution of genes in *E. coli*. Such approach is reminiscent of previous attempts to decompress the regulatory complexity of different biological phenomena; *e.g.*, the refactoring of the lytic bacteriophage T7 [resulting in a decrease of *ca*. 20% of infectivity with respect to the WT virus (Chan *et al.*, 2005)], or the refactoring of the nitrogen fixation gene cluster from *Klebsiella oxytoca* [resulting in *ca*. 57% of N_2 fixation as compared to the naturally occurring system (Temme *et al.*, 2012)]. The biochemical integrity of the GlucoBrick platform was thus evaluated to assess if the different glycolytic elements, after edition and rearrangement, could bring about (or boost) an EMP route in the native context from which the genes were taken. The results indicate that the ten genes coming from the EMP route in *E. coli* can be excised from their original environment and still deliver their biochemical input in a fashion that equals (and, in some cases, improves) the natural physiology and metabolic wiring of the microbial cells; *i.e.*, in a large collection of *E. coli* glycolytic mutants.

Another feature of the GlucoBrick system is its portability. Once the viability of the system was analyzed in different *E. coli* mutants, the capability to boost the efficiency of carbon consumption and distribution was tested in other bacterial species. The third section of **Chapter 1** thus evaluated this portability in two of the most relevant *Pseudomonas* species, the *P. putida* KT2440 and *P. aeruginosa* PAO1. In both cases, it was demonstrated that the GlucoBrick system increased glucose catabolism of these bacteria by increasing the total glucose consumption. Additionally, the introduction of the Pfk activity in these two *Pseudomonas* strains resulted in actual enzyme activity, taking into account that these bacteria are defective for the Pfk glycolytic step. The results showed in this Thesis demonstrate that bridging this glycolytic gap is feasible with the introduction of Module I of the GlucoBrick system, and, more importantly, that this manipulation does not result in strains with compromised fitness as observed upon introduction of PfkA alone (Chavarría *et al.*, 2013).

In addition to the results mentioned above, the next step considered in this Thesis was to apply the GlucoBrick system in an actual test case in terms of Metabolic Engineering. To this end, the fourth section of **Chapter 1** illustrated the potential of this glycolytic tool to enhance the production of added-value metabolites, with PHB production by recombinant *E. coli* as an example. Our results showed that the presence of the GlucoBrick platform increased the glycolytic activities in a PHB-accumulating recombinant *E. coli* carrying the PHB biosynthetic genes from *Cupriavidus necator*. As a result of this test, this strain accumulated up to *ca.* 73% of the CDW in the form of PHB (**Fig. 8c**), and this polymer yield on biomass ranks among the highest reported in the literature for batch cultures using glucose as a carbon source (Leong *et al.*, 2014; Li *et al.*, 2007).

All these features reveal that the GlucoBrick system is a promising tool to implement novel EMP capacities in *P. putida* KT2440. At the same time, a new standard was made available to the Synthetic Biology community (Heinemann & Panke, 2006). This platform constitutes the basic toolbox needed to carry out the main goal of this Thesis, *i.e.*, the refactoring of the *P. putida* KT2440 central carbon metabolism into a linear EMP-based glycolytic pathway.

2. Preparing *P. putida* KT2440 to host a linear EMP pathway: upgrading the potential of environmental bacteria as a useful Synthetic Biology *chassis*

The large number of strategies and tools derived from Synthetic Biology are enabling the rational design of genetic circuits, that results in an easy application of metabolic pathways *à la carte* (Stephanopoulos, 2012). The implementation of such circuits must be displayed in the appropriate recipient, thereby providing the molecular machinery to make them functional. These biological hosts (or *chassis*) are based, for instance, on bacteria that display a set of useful characteristics in order to be employed in different biotechnological purposes (Danchin, 2012). *P. putida* KT2440 is considered a suitable frame for a robust metabolic *chassis*

(Nikel *et al.*, 2016a; Poblete-Castro *et al.*, 2012; 2017). The complete set of attractive features that support this notion was described in detail in the *Introduction* of this Thesis. *P. putida* exhibits a remarkable capacity to prevent oxidative stress due to an increased NADPH synthesis by the EDEMP cycle (Nikel *et al.*, 2015a). Certainly, this is a relevant capacity in different industrial scenarios, such as biofuels production (Liao *et al.*, 2016), but the native metabolic architecture decreases the capacity of *P. putida* to be employed in other biotechnological activities. In particular, *P. putida* KT2440 would not excel in processes for which the ATP yield on substrate could be the limiting factor [*e.g.*, glutathione (Hara *et al.*, 2009) and succinate biosynthesis (Zhao *et al.*, 2016)], as this strain produces half the ATP from glucose molecule as that of a linear glycolysis. For this reason, the present Thesis has laid the bases to revert this situation, by functionally replacing the native EDEMP cycle with a linear EMP pathway (*i.e.*, bestowing an ATP yield twice as high as the ED pathway) empowered by the GlucoBrick platform.

The deep metabolic refactoring in *P. putida* KT2440 has been made possible through the construction of a suitable *P. putida* GC (***g***lycolytic ***c***hassis). This metabolic *chassis* consists of a *P. putida* KT2440 derivative depleted of the most relevant native glycolytic activities. This genomic edition was not designed at random, instead, specific metabolic nodes were targeted, thus trying to prepare this bacterium to accommodate the implanted EMP activities. **Chapter 2** of this Thesis describes the approaches developed for the implementation of such genome editing. Basically, the guiding principles followed in this process encompassed: (i) improving the glucose uptake system, and (ii) preventing *P. putida* KT2440 to employ its native glycolytic machinery (in particular, the preparatory steps of either phosphorylation or oxidation of the hexose).

The result shown in the first section of **Chapter 2** analyze the possibility of replacing the native ATP-dependent ABC glucose transporter of *P. putida* KT2440 by the energy-efficient Glf transporter from *Z. mobilis*. Firstly, a *P. putida* mutant (Δ*gts* Δ*gcd*), unable to transport glucose to the cytoplasm and at with the oxidative glucose utilization pathway blocked, was generated. This platform strain was employed to evaluate if the Glf transporter of *Z. mobilis* can substitute for the function of the native system in *P. putida* KT2440. The results shown in **Fig. 11c** of **Chapter 2** corroborated this hypothesis, indicating that the Glf facilitator, expressed from a single copy in the chromosome, can carry out uptake of glucose into the cytoplasm of *P. putida* KT2440, maintaining the specific growth rate value and the final cell density of the resulting strain at similar levels as for the WT strain. These results are in agreement with different publications that employed the Glf transporter in different microorganisms to improve the glucose utilization in various biotechnological processes, such as biomass production in the cyanobacterium *Synechocystis* (Ranade *et al.*, 2015) and succinate generation in *E. coli* (Tang *et al.*, 2013). As a conclusion of this part of the Thesis, the Glf transport system can be safely added to the set of tools existing to improve the glucose metabolism of *P. putida* KT2440.

Once the glucose uptake issue was clarified, the rest of **Chapter 2** (sections 2 and 3) detail the deletions that comprise the biochemical adaptation of *P. putida* KT2440 in order to host the implanted linear EMP pathway. To address such challenge, *P. putida* KT2440 must be erased of its native way to metabolize glucose, based in the phosphorylation or peripheral oxidation of glucose to be subsequently processed by the ED pathway and EDEMP cycle. This approach is useful in order to prevent the interaction between the cellular machinery and the genetic constructs to be grafted into *P. putida* (Kim & Copley, 2012; Nielsen *et al.*, 2013), and to avoid the competition for the same substrate by different pathways, *i.e.*, native *vs.* engineered pathway (Tepper & Shlomi, 2010). This sort of biochemical competition is a recurrent problem in different Metabolic Engineering approaches. Examples of this issue in the literature include the conditional [to optimize isopropanol production (Soma *et al.*, 2014)] or total knock-out [to increment succinate production (Kim *et al.*, 2004)] of different central metabolism activities in *E. coli*, needed to attain an optimal bioprocess in terms of carbon distribution.

Taking into account these principles, section 2 of **Chapter 2** tackled the elimination of the two entry points that *P. putida* KT2440 employs to metabolize glucose. The objective of this section was the elimination of the Glk and Gcd activities in *P. putida* KT2440 in order to completely erase the first steps of hexose processing (del Castillo *et al.*, 2007; Nikel *et al.*, 2015a), delimiting the entering of glucose in the central carbon metabolism *via* phosphorylation mediated by Glk or oxidation mediated by Gcd. The results shown in **Figs. 17a** and **b** corroborate this hypothesis, displaying the inability of the Δ*glk* Δ*gcd* mutant to grow on glucose as a sole carbon source. At the same time, the growth curves on different carbon sources indicated that the mutant bacteria can grow without any dramatic consequence. The literature supported the information described previously, reporting similar growth characteristics in the same type of *P. putida* KT2440 mutants (Borrero de Acuña *et al.*, 2014; del Castillo *et al.*, 2007), and also in the close relative species *P. fluorescens* (Maleki *et al.*, 2015). Apart from that, the elimination of the Gad activity was analyzed as an additional mutation of the oxidative glucose utilization pathway, experimentally tracing the bulk of this activity to the *PP_3382-PP_3384* gene cluster. This result reveals that the *chassis* construction process can be simultaneously used to increase the knowledge on central carbon metabolism of *P. putida* KT2440.

With the mutations described in the paragraph above, it was possible to avoid the introduction of the bulk of glucose in the central carbon metabolism of *P. putida* KT2440, consisting of the peripheral oxidation of the substrate. However, the results displayed in section 2 of **Chapter 2** demonstrated the capacity of this bacterium to reroute glucose when this oxidation step was disabled in the presence of a Glk activity in the cell, a biochemical scenario that will be found in the glycolytic *chassis* complemented with the GlucoBrick system. For this reason, as an additional control point to generate a more predictable *chassis*, the elimination of the genes involved in the ED pathway was also analyzed. Despite the fact that this pathway is compromised to generate precursors due to the mutations described previously, the removal of the Edd and Edd activities (the two metabolic elements of the ED pathway in *P. putida* KT2440) was also considered for

the construction of the glycolytic *chassis*. Through this approach, it was possible to eradicate completely the main route for glucose catabolism in this bacterium (Wang *et al.*, 1959). This experimental scenario, in which the entire route was removed and not just the first element (*i.e.*, Edd), generated a streamlined strain while avoiding unexpected interactions due to the potential presence of *latent* enzyme activities (*i.e.*, Eda). This kind of latent activities, without a potential substrate, can evolve in biological systems generating emergent properties that are in turn able to disrupt *chassis* stability (Miller & Raines, 2004). Taking into account this information, the third section of **Chapter 2** of this Thesis described the process to remove these activities from *P. putida* KT2440. Predictably, the elimination of either activity (Δ*edd* or Δ*eda*) blocked the glucose utilization by *P. putida* KT2440 (**Figs. 17a** and **b**), a result in line with the data in the literature for *P. putida* KT2440 (del Castillo *et al.*, 2007; Nikel *et al.*, 2015a) and its close relative *P. aeruginosa* (Blevins *et al.*, 1975; Cuskey *et al.*, 1985; Temple *et al.*, 1990).

All the mutations explained in **Chapter 2** worked as expected, generating the phenotypes predicted, which was demonstrated with the use of different enzymatic assays to expose the successful elimination of the activities. This verification process supported the decision of accumulating these mutations in the *P. putida* GC strain with the explicit certainty of removing properly these elements.

3. Understanding *P. putida* KT2440 glucose metabolism as a key principle to the flawless design of *P. putida* GC: the relevance of blocking the EDEMP cycle

The generation of an appealing *chassis* is closely related to the level of knowledge of its biological and biochemical identity. The metabolism of *P. putida* KT2440 was revisited from different angles during the last few years. Relevant events in this context include the recent revision that received its genome data upon resequencing (Belda *et al.*, 2016), the availability of four genome-scale constraint-based metabolic models for *in silico* studies (Belda *et al.*, 2016; Nogales *et al.*, 2008; Puchałka *et al.*, 2008; Sohn *et al.*, 2010), and the complete carbon fluxes analysis in glucose cultures of this bacterium by using ^{13}C-labeled substrates (Nikel *et al.*, 2015a). All these information sources allow us to predict the capacity of this bacterium to suffer different manipulations in its central carbon metabolism, the main goal of the present Thesis. However, despite the fact that these studies can draw a general description of this issue, their resolution is not enough precise to evaluate a complex biochemical scenario with several simultaneous modifications. For this reason, **Chapter 3** of this Thesis attempted to shine some light on the possible situation that can emerge upon the implementation of a linear EMP route in *P. putida* KT2440.

Glucose metabolism of *P. putida* KT2440 has been large explained during this study. As it was mentioned before, the native incomplete EMP pathway displayed in this bacterium has a key role in terms of recycling trioses-*P* into hexoses-*P*. The implementation of a linear EMP pathway in *P. putida* GC (as it was shown in **Chapter 4**) modified completely the extant biochemical scenario, transforming the native

gluconeogenic EMP pathway in a completely glycolytic route. In order to evaluate the consequences of this phenomenon, **Chapter 3** of this Thesis studied the influence of the Pgi activity in *P. putida* KT2440. This mutation is useful in order to understand the physiological impact that can emerge from the blocking of the EDEMP cycle avoiding the transformation of F6P into G6P. As it was described in the first section of **Chapter 3**, the Pgi activity is comprised by the addition of the products encoded by the *pgi-I* and *pgi-II* genes. Additionally, it was demonstrated that the individual contribution of both genes is enough to maintain a normal phenotype, just detecting relevant differences in terms of specific growth rate value and specific Pgi enzyme activity in the Δ*pgi-I* Δ*pgi-II* double mutant in microtiter-plate cultures with glucose as the carbon source (**Figs. 19c** and **d**). In the same section, the growth parameters of *P. putida* KT2440 and its Δ*pgi-I* Δ*pgi-II* mutant derivatives in shaken-flask cultures under glycolytic growth conditions identified significant differences between both strains (**Table 8**). First of all, the specific growth rate value decreased (*i.e.*, 24%) in the Δ*pgi-I* Δ*pgi-II* mutant compared to the WT strain. At the same time, the utilization of glucose was remarkably different between the same strains, with a higher specific rate of carbon uptake (q_S) for the Δ*pgi-I* Δ*pgi-II* mutant. However, the opposite situation was observed in terms of the yield of biomass on substrate, indicating that the Δ*pgi-I* Δ*pgi-II* mutant has an impaired ability to transform the consumed glucose into biomass.

Once a full Pgi mutant (*i.e.*, Δ*pgi-I* Δ*pgi-II*) of strain KT2440 was analyzed in terms of growth patterns, it was necessary to explore the biological consequences of removing the Pgi activity with a more general screening method. As it was explained in the second section of **Chapter 3**, the BioLog Phenotypic MicroArray™ (PM) technology was employed to obtain a phenomic analysis of the Pgi deletion in *P. putida* KT2440. Briefly, the results obtained with this high-throughput screening method indicated two scenarios where the elimination of Pgi could play a critical role: (i) decreasing the overall NADPH availability, and (ii) build-up of F6P. The first one suggests that the blocking of the EDEMP cycle decreases the NADPH production. This hypothesis is largely correlated with the results obtained by the PM technology in **Chapter 3**. In summary, it was hypothesized that the Pgi mutation reduces the G6P availability coming from the isomerization of F6P *via* the EDEMP pathway (Nikel *et al.*, 2015a). G6P is the substrate of the Zwf activity, which concomitantly reduces $NADP^+$ into NADPH. Under this metabolic configuration, the Zwf activity cannot obtain enough G6P as the substrate, which lead to decreased levels of NADPH in the mutant. This hypothesis was also supported by the results shown in the fourth section of **Chapter 3**. In this case, the *in silico* simulation obtained for the Pgi mutant by constraint-based flux analysis indicated that the flux *via* Zwf decreased by *ca*. 63%, compromising the availability of NADPH in the cell. Finally, in order to obtain an experimental validation for this scenario, section 3 of **Chapter 3** displayed a set of experiments that correlated the absence of Pgi activity with a high sensitivity to oxidative stress, and more specifically to the presence of the redox stressor paraquat. This compound catalyzes the formation of reactive oxygen species and has been described to decrease the pool of NADPH (Bus & Gibson, 1984). For this reason, the results

mentioned so far are in agreement with the hypothesis that correlates the Pgi mutation with a diminution in the overall NADPH availability (**Figs. 22** and **23**).

Along with Pgi, we evaluated the role of the GntZ activity in the NADPH regeneration process. As it was indicated in the third section of **Chapter 3**, GntZ is considered to be the second most important source of NADPH in the upper domain of carbon catabolism after Zwf. In spite of this situation, the elimination of this activity in strain KT2440 had not impact in the redox state of the cells with the same intensity as the Pgi mutation did (third section of **Chapter 3** and **Figs. 22** and **23**).

The results discussed previously add consistence to the important physiological role of the EDEMP cycle in *P. putida* KT2440 (Nikel *et al.*, 2015a). The disruption of this pathway involves consequences that alter the fitness of this environmental bacterium. Curiously, this scenario has an opposite meaning when it applied to the well-known Enterobacterium *E. coli*. Numerous works have appreciated that the elimination of the Pgi activity in *E. coli* (*i.e.*, Δ*pgi* deletion, since in *E. coli* there is only one gene encoding Pgi) substantially increases the NADPH availability for this bacterial species (Canonaco *et al.*, 2001; Charusanti *et al.*, 2010; Hua *et al.*, 2003; Usui *et al.*, 2012). This is possible because *E. coli* employs mainly a linear glycolytic EMP pathway, and when it is disrupted, the bacterium is able to redirect the carbon flux *via* the PP pathway. At the same time, this mutation was employed in order to improve various Metabolic Engineering approaches in *E. coli*, such as PHB synthesis (Shi *et al.*, 1999) and riboflavin production (Lin *et al.*, 2014). On the other hand, it is important to appreciate the metabolic context of the *pgi* genes when their role is analyzed in *P. putida* KT2440 and *E. coli*. *P. putida* KT2440 presents a clear duplication of the *pgi* gene. This duplication event can be correlated with the importance of maintaining a suitable level of NADPH in strain KT2440, since this cofactor is known to be critical to counteract the oxidative stress conditions that environmental bacteria are usually confronted with (Bratlie *et al.*, 2010). The cited example exposed the close correlation that exists between the adaptation to the environment and the strategy adopted in central carbon metabolism in bacteria thriving in completely different environmental niches.

Finally, the second hypothesis associated to the elimination of Pgi activity is the accumulation of F6P. The ^{13}C-based metabolic flux analysis previously performed in glucose-grown *P. putida* KT2440, as it was mentioned before, indicated that this bacterium employed the EMP pathway in a gluconeogenic setup (Nikel *et al.*, 2015a). According to this information, the elimination of the Pgi activity can trigger the accumulation of F6P coming from the FBP *via* Fbp, assuming that the PP pathway cannot absorb the bulk of this metabolite. The phenomic analysis discussed in the second section of **Chapter 3** indicated sensitivity of the Pgi mutant to a biofilm-inhibiting compound (*i.e.*, sodium salicylate). In addition to this information, F6P has been described as the metabolic precursor employed in different *Pseudomonas* species to synthesize the polysaccharide alginate (Franklin *et al.*, 2011), a component of biofilm formation in some bacteria (Boyd & Chakrabarty, 1995; Flemming *et al.*, 2007). At the same time, *P. putida* KT2440 encodes in its chromosome

all the necessary elements to transform F6P into alginate, the *alg* genes (Gulez *et al.*, 2014; Nilsson *et al.*, 2011). Additionally, a simple synteny test for the mentioned group of genes showed solid results in comparison with the target region of the well-characterized alginate producer *P. aeruginosa* PAO1 (Vallenet *et al.*, 2017). Taking all this information together, it was hypothesized that the presence of the Pgi mutation in *P. putida* KT2440 can result in an increased capacity to produce biofilm. As it was suspected, the absence of Pgi activity (*i.e.*, Δ*pgi-I* Δ*pgi-II* strain) conferred a higher capacity (*ca.* 3.5-fold) to generate biofilm to this mutant as compared to the WT strain (third section of **Chapter 3** and **Fig. 24**). As an additional negative control, the biofilm formation was evaluated in the Δ*gntZ* strain (unrelated to F6P accumulation), obtaining similar results compared with the WT strain. Such situation, in which the levels of F6P may have an impact on the alginate production, was also described in different *Pseudomonas* species, such as *P. aeruginosa* (Banerjee, 1989; Banerjee *et al.*, 1983) and recently in *P. fluorescens* (Ertesvåg *et al.*, 2017; Maleki *et al.*, 2015). Accumulation of this metabolite is associated with pathogenesis in Gram-positive microorganisms (Richardson *et al.*, 2015), and it also correlates with biofilm formation in the nosocomial pathogen *Staphylococcus epidermidis* (Sadykov *et al.*, 2008). It is also relevant to mention the role that biofilm formation plays in different *P. aeruginosa* pathogenic scenarios. This bacterium displays an overproduction of alginate that results in an increment in antibiotic resistance (Hentzer *et al.*, 2001). The compendium of the information gathered so far highlights the relevant relationship between the regulation of central carbon metabolism and physiological adaptations to natural environments. The manipulation of the *core* bacterial metabolism can result in emergent characteristics (*i.e.*, biofilm formation) that can, in turn, give rise to new phenotypes during the construction of an appealing microbial *chassis*.

Blocking the EDEMP cycle *via* Pgi mutation has provided information that supports the physiological importance of this metabolic step in the normal biochemical operation of *P. putida* KT2440. The disruptions mentioned resulted in a redox imbalance condition (*i.e.*, decreasing the NADPH availability) combined with an altered biofilm formation patterns (*i.e.*, increasing the biofilm index). This kind of perturbation sets an example to predict possible scenarios that can appear during deep refactoring of the glucose central metabolism of *P. putida* KT2440, in which the direction of the carbon flow predominant in the EDEMP cycle is expected to be reversed by the implanted EMP pathway.

4. Engineering of *P. putida* to employ the linear EMP glycolytic pathway

The main goal of the whole project has been the implementation of a functional EMP pathway in *P. putida* KT2440 in order to boost ATP formation from glucose. *P. putida* KT2440 is unable to fully execute this catabolic pathway due to the absence of the Pfk activity (Latrach-Tlemçani *et al.*, 2008). Previous works developed in our laboratory attempted to bridge this gap in *P. putida* KT2440 by complementing the Pfk activity encoded by the *pfkA* gene from *E. coli* (Chavarría *et al.*, 2013). This preliminary study revealed two capital principles to take into account to confront the objectives outlined in this Thesis: (i) the implementation

of the PfkA activity alone reduces the tolerance to oxidative stress, and (ii) the addition of this biochemical step into the biochemical network of strain KT2440 cannot revert the lack of growth of an ED mutant (*i.e.*, *eda*::mini-Tn*5*) on glucose. With these notions in mind, it is not feasible to implement a functional EMP pathway in *P. putida* KT2440 through a simple strategy, entailing a simple complementation of the absence activity. The previous approach probably failed due to the influence of the EDEMP cycle (Nikel *et al.*, 2015a), which sets the EMP pathway in a gluconeogenic fashion to transform part of the trioses-*P* pool into hexoses-*P*. The introduction of the PfkA activity, that enables a glycolytic direction in the carbon flow of *E. coli* (*i.e.*, phosphorylating F6P into FBP, using ATP as the phosphodonor) in a pathway configured in the opposite direction resulted in a metabolic unbalance (Fischer & Sauer, 2003), which gives rise to the negative phenotypes previously observed (Chavarría *et al.*, 2013). For example, it is possible to correlate the effect of introducing the PfkA activity in *P. putida* KT2440, with the elimination of the Pgi activity in this strain (**Chapter 3**), that increases the sensitivity to oxidative stress due to the reduction in the NADPH pool. In both cases, the EDEMP cycle is affected, PfkA actuating as a biochemical barrier that difficult the native gluconeogenic setup, and the Pgi mutation directly blocking the assembly of a closed cycle (Portais & Delort, 2002). All the information available highlights the underlying problem of modifying the central carbon metabolism of *P. putida* KT2440, in which a clear hurdle in terms of interaction between the cellular machinery and genetic constructs is imposed by the presence of the EDEMP cycle (Kim & Copley, 2012; Nielsen *et al.*, 2013).

The experimental design followed in this Thesis to overcome this situation is summarized in **Chapter 4**. The simplification of the biological system rendered the microbial *chassis* more predictable. As it was explained before, the goal of substituting the central glucose utilization pathways presents different types of difficulties, one of them being the complex pattern of interactions between the cellular machinery and the genetic constructs. This engineering challenge can emerge from different sources, such as the competition for the same intermediaries and the cross-regulation effects between the native and implanted activities (Kim & Copley, 2012; Nielsen *et al.*, 2013). Taking into account this information, the rational generation of a suitable *chassis*, which was termed *P. putida* GC (***g***lycolytic ***c***hassis), is described in **Chapter 4** of this Thesis.

Considering the difficulties in pathway engineering identified in previous works, the first section of **Chapter 4** explains the strategy employed to construct the first version of the *P. putida* GC (termed *P. putida* GC1). This approach followed the *beta-testing* engineering principle, in which the set of essential modifications needed to check the major consequences of introducing an EMP-based glycolysis in *Pseudomonas* was evaluated. This preliminary version of the *chassis* is based on a *P. putida* KT2440 derivative that accumulated the Δ*glk*, Δ*gcd*, Δ*gad* (Δ*PP_3382-4*, Δ*PP_3623*, and Δ*PP_4232*), and Δ*edd* mutations. Briefly, a strain was constructed that (i) is unable to phosphorylate glucose, (ii) cannot employ the ED pathway for hexose catabolism, and (iii) is blocked in the use of a set of peripheral glucose utilization

reactions (*via* hexose oxidation). Due to the accumulation of the mentioned deleterious mutations, this strain cannot grow on glucose as the sole carbon source. The next step was to evaluate if our strategy of substituting the main components in the central carbon metabolism of *P. putida* KT2440 by a linear EMP pathway encoded by the GlucoBrick system was feasible. In order to check this hypothesis, Module I of the GlucoBrick system was transformed in the *P. putida* GC1 employing an inducible expression system in a plasmid vector. As it indicated in section 1 of **Chapter 4** (**Fig. 27**), the glucose-dependent growth of *P. putida* GC1 (*i.e.*, the first version of the glycolytic *chassis*) can be restored with the use of the enzyme activities encoded in Module I of the GlycoBrick platform. To the best of our knowledge, this is a first-case example of a successful attempt in which a *P. putida* strain, depleted of the native glycolytic activities used for hexose catabolism, can exclusively employ the EMP pathway as a glycolytic activity (Chavarría *et al.*, 2013). Additionally, **Figs. 27c** and **d** of this Chapter corroborate that this growth phenotype is due to the presence of the activities encoded by Module I of the GlucoBrick system through the enzyme activity assays implemented for both Glk and Pfk. It should be noted that, under this implanted metabolic scenario, *P. putida* GC1 transformed with Module I of the GlucoBrick system showed a specific growth rate value smaller (*ca.* 4-fold decrease) and a 40% reduction of the final OD_{600} than the WT strain containing the empty plasmid in glucose cultures (**Fig. 27b**). These somehow low values of kinetic and growth parameters are expected due to the large number of modifications introduced in this strain, including several mutations in its native set of genes for central carbon metabolism and possibly because of metabolic burden due to the presence of the plasmid-borne GlucoBrick platform.

The *beta-testing* protocol was useful to evaluate the feasibility of the approach adopted to construct a *chassis* to host a functional EMP pathway. The positive results previously exposed validated the second stage of the deep refactoring attempt. This subsequent step in the design was based on the construction of the second version of the *P. putida* GC, termed *P. putida* GC2, in which the deletions of the *P. putida* GC1 strain are included in addition to the Δ*gts* (Δ*gtsA*, Δ*gtsB*, Δ*gtsC*, and Δ*gtsD*) and Δ*eda* mutations. This upgraded glycolytic *chassis* was modified in order to eliminate the native ABC glucose transport system present in *P. putida* (that consumes ATP as part of its normal functioning), and also to remove completely the ED pathway participation, already blocked with the introduction of the Δ*edd* mutation (**Fig. 28a**). The first modification allowed us to substitute the energy-consuming native glucose transporter by the efficient Glf glucose facilitator from *Z. mobilis*. The validity of this modification was supported by the positive results obtained for *P. putida* KT2440 (displayed in **Fig. 11c** of **Chapter 2**), that were already explained in the second section of this *Discussion*. On the other hand, the elimination of Eda activity follows the cited principle for *good practices* in *chassis* construction, aiming at simplifying the metabolic networks and to prevent any unexpected interaction due to the presence of *latent* enzyme activities (also discussed in the second point of this section).

Once the metabolic backbone was constructed, the process of sequential stable transposition (based on a synthetic mini-Tn*5* transposon) was attempted as indicated in **Fig. 29a** in the third section of **Chapter 4**. This strategy was adopted to ensure the efficient implementation of a functional EMP pathway in *P. putida* GC2. The introduction of the Glf transporter, and Modules I and II of the GlucoBrick platform granted a linear EMP pathway as indicated in **Fig. 30** of **Chapter 4**. The random nature of the insertion process brought about by the Tn*5*-derived transposition system allowed us to obtain a strain with the desired growth phenotype. This clone, termed *P. putida* GC2·T·GBI·GBII, is the material culmination of the purpose stated at the beginning of this Thesis.

P. putida GC2·T·GBI·GBII contains all the necessary elements to employ the EMP pathway as the unique glycolytic route. The physiological parameters indicated in **Table 9** (**Chapter 4**) revealed that the specific rate of carbon uptake (q_S) and the specific growth rate value for this engineered strain were significantly smaller in comparison with the WT strain. However, it must be remarked that the high level of genetic and metabolic manipulation introduced in *P. putida* GC2·T·GBI·GBII, combined with the fact that the expression of the inserted modules has not been improved yet, results in sub-optimal growth. This microbial platform should be considered as a proof-of-principle to test the functional replacement of central glycolytic pathways in environmental bacteria. This issue cannot be analyzed with a simple set of enzyme activity assays to corroborate the presence of the EMP pathway and, for this reason, the fourth section of **Chapter 4** exposes the final (and definite) experimental test to ensure the complete metabolic refactoring carried out in *P. putida* GC2·T·GBI·GBII. In this case, the experimental approach is based on the ^{13}C-based metabolic flux ratio analysis of its central carbon metabolism. This powerful methodology is able to reconstruct a detailed map that illustrates the different pathways followed by the glucose through the entire biochemical network (Sauer, 2006).

As a key outcome of the project, **Fig. 32** of **Chapter 4** summarizes the distribution of absolute fluxes in the glucose catabolism network for the refactorized *P. putida* GC2·T·GBI·GBII strain as compared with its predecessor *P. putida* KT2440. The results obtained in this part of the Thesis have confirmed the success of the metabolic refactoring carried out in *P. putida* KT2440, breaking down the different metabolic blocks where these modifications can be fully appreciated. First, it was demonstrated that the Glf transporter has the capacity to functionally complement the hexose transport deficiencies in strain GC2·T·GBI·GBII, capturing all the glucose into Glk-dependent phosphorylation (since glucose cannot be oxidized, due to the presence of the Δ*gcd* and Δ*gad* mutations). This result is relevant when compared with the metabolic wiring in the WT strain, which channeled 90% of glucose *via* the Gcd-dependent periplasmic oxidation of the substrate according to the data obtained in our experiments and previously in the literature (Nikel *et al.*, 2015a). However, the level of expression and/or activity of Glf must be considered in the future in order to improve the general performance of the system, taking into account the low value of specific rate of carbon uptake (q_S) detected in the glycolytic *chassis*. The strategy followed in the construction of *P. putida*

GC2·T·GBI·GBII employed random transposition insertions to explore different regulation patterns of the gene modules delivered into the chromosome. This approach proved useful for the first proof-of-principle attempted in this study, and a fine-tuning regulation for all the genetic elements present in the glycolytic *chassis* is needed to harness the full potential of the EMP-operating *P. putida* strain. Second, and as a first step in the novel implemented EMP pathway, the Glk activity encoded by Module I of the GlucoBrick system was able to phosphorylate 100% of the glucose that entered in the cytoplasm employing the exogenous Glf transporter. This is the first important point engineered in *P. putida* GC2·T·GBI·GBII, in which the bulk of the glucose in the system was channeled into G6P, in a similar fashion as observed in other bacteria [*i.e.*, *E. coli* (Fuhrer *et al.*, 2005; Hua *et al.*, 2003; Usui *et al.*, 2012)], thereby reverting the natural situation of *P. putida* KT2440, in which only a 10% of the glucose gets phosphorylated by Glk (Nikel *et al.*, 2015a).

Another example of the metabolic reconfiguration in *P. putida* GC2·T·GBI·GBII as compared with *E. coli*, is the distribution of the fluxes around the G6P node. The G6P pool was split in a 22% being channeled into 6PG [a conversion catalyzed by Zwf and 6-phosphogluconolactonase (Pgl)] and the remaining 77% funneled into the formation of F6P (a reaction catalyzed by Pgi), in accordance with the values obtained in other published studies for *E. coli* growing under glycolytic conditions (Fuhrer *et al.*, 2005; Hua *et al.*, 2003; Usui *et al.*, 2012). Most remarkably, the completely elimination of the ED pathway (comprising by Δ*edd* and Δ*eda* mutations) has been reflected in the ^{13}C-based metabolic flux ratio analysis, allowing the channeling of 6PG into the PP pathway following the same quantitative distribution than in *E. coli* (Fuhrer *et al.*, 2005; Hua *et al.*, 2003; Usui *et al.*, 2012). This modification removed the glycolytic pathway that processes the bulk of hexoses in *P. putida* KT2440 (Nikel *et al.*, 2015a), demonstrating the deep metabolic reconfiguration of *P. putida* GC2·T·GBI·GBII. At the same time, the role of the implanted EMP pathway in the glycolytic *chassis* was dramatically modified, and the genes encoded by Module I of the GlucoBrick system enabled the transformation of the native gluconeogenic *preparatory* phase of *P. putida* KT2440 into an authentic glycolytic pathway.

In terms of EMP pathway implementation, *P. putida* GC2·T·GBI·GBII channeled a 77% of the glucose entering the biochemical network *via* the linear glycolytic EMP pathway encoded by Module I and II of the GlucoBrick system. To be more precise, in the glycolytic *chassis* 73% of the generated Pyr was obtained from the EMP pathway, in contrast with 49% in the WT strain. This boosted flux through the EMP pathway resulted in a 2.5-fold higher circulation *via* pyruvate kinase (*i.e.*, PEP + ADP + H^+ → Pyr + ATP). Pyruvate kinase is a key allosteric enzyme of the EMP pathway, which catalyzes one of the two substrate-level phosphorylation steps that generate ATP. For this reason, and in order to achieve the goal of improving the energy status of the glycolytic *chassis*, stabilizing this step proper is of capital importance for the present project. As it was mentioned before, the flux *via* pyruvate kinase was significantly increased in *P. putida* GC2·T·GBI·GBII. Further enhancement of this key step will comprise the fine-tuning of the activity encoded

by Module II of the GlucoBrick system (containing the *pyk*F gene from *E. coli*), at the same time that the participation of the endogenous pyruvate kinases will be thoroughly explored. In *E. coli,* there are two isoenzymes characterized to carry out this activity (*i.e.*, PykA and PykF), displaying remarkable differences in terms of absolute activity. For example, the pyruvate kinase specific activity associated to the isoform PykF has been reported to be *ca*. 16-fold higher than that of the PykA counterpart (Ponce *et al.*, 1995). When the *pykA* gene was interrupted, the enzymatic level of the remaining PykF activity increased above the levels that would be expected from the addition of both activities separately (Zhao *et al.*, 2017). *P. putida* KT2440 presents a similar scenario, containing two isoenzymes for the same pyruvate kinase activity [*i.e.*, PykA (PP_1362) and Pyk (PP_4301)] in its chromosome, and there could be a similar cross-inhibition effect as the one reported in *E. coli*. This is an example of the large number of important points that can be regulated in the glycolytic *chassis* constructed herein in order to further improve its general performance.

Once Pyr is generated in *P. putida* GC2·T·GBI·GBII, the influence of the genes encoded by Module I and II of the GlucoBrick system on downward catabolism started to be less critical. From this metabolic node downwards, the side-by-side comparison of the genetic *chassis* with *E. coli* is more difficult, due to the presence of overflow metabolism in Enterobacteria, in which acetyl-CoA is converted into acetate (Basan *et al.*, 2015; Bernal *et al.*, 2016; Fuhrer *et al.*, 2005). On the other hand, *P. putida* KT2440 and its derivative glycolytic *chassis* metabolize Pyr into acetyl-CoA and the TCA cycle, without any overflow metabolite stemming from these metabolic intermediates. The distribution of fluxes in anaplerotic pathways, TCA cycle, and glyoxylate shunt were similar in both *P. putida* GC2·T·GBI·GBII and WT strain. These routes had similar flux values when they were compared with the information available in the literature not only for *P. putida* KT2440 but also other *Pseudomonas* species, such as *P. fluorescens* (Fuhrer *et al.*, 2005; Nikel *et al.*, 2015a). As expected for *P. putida*, neither strain had active fermentation pathways (*e.g.*, formation of lactate or ethanol), and the breakdown of hexoses was entirely oxidative (Fuhrer *et al.*, 2005).

Finally, the main goal of this Thesis was evaluated using the data obtained from ^{13}C-based metabolic flux ratio analysis. This objective comprised the implementation of a complete EMP pathway in *P. putida* KT2440, as a way to improve the energy efficiency of central carbon metabolism. **Fig. 33** clarifies this issue, showing an increase in the ATP production of almost 20% for *P. putida* GC2·T·GBI·GBII compared with the WT strain. This kind of approach agrees with the current trend in order to promote metabolic capacities in different microbial *chassis* (Wu *et al.*, 2016), in which ATP generation must be improved *via* catabolic metabolism optimization. This assumption was associated to the limitation presented by the ATP synthase system (probably to most obvious target to manipulate ATP formation), which offers limited possibilities in terms of manipulation due to the constraints related to cell membrane space, interfering with the proton motive force (Eames & Kortemme, 2012). Additionally, as a collateral effect of implementing an EMP pathway, the NADH formation increased 2.5-fold as compared to WT strain, bestowing the glycolytic *chassis* with a novel stoichiometry in terms of reducing power.

5. Outlook

The metabolic refactoring of the catabolic lifestyle of *P. putida* KT2440 can be considered to be successfully achieved in this Thesis. This is a first milestone to implement not only a functional EMP pathway, but also an efficient glycolytic network in this environmental bacterium. From this point on, the possibilities to explore in order to fine-tune the central carbon metabolism of this glycolytic *chassis* are numerous. We are currently submitting this strain to an adaptive laboratory evolution process under different pressure agents in order to accumulate random mutations in the *chassis* that would enhance its growth on glucose. This procedure is being performed by using an experimental automated turbidostat device designed to avoid biofilm formation and push selection of those individual bacteria carrying beneficial variations in terms of growth phenotypes (Hansen *et al.*, 2017; Portnoy *et al.*, 2011). Our device was assembled using peristaltic pumps for pumping the required operation fluids (namely, a glucose-containing culture medium), and milli-fluidic valves to control fluid transport through the whole circuit. The whole assembly is automatically controlled by an Arduino™ automata governed by a Python-guided software program. The different parts of the whole structure were generated by demand with the use of a 3D printer. This apparatus, assembled *ad hoc*, is expected to improve the performance of the glycolytic *chassis* not only by selecting random mutants, but also by evaluating the implementation of a direct evolution experiment [*i.e.*, multiplex automated genome engineering (MAGE)] in which the desired elements are adjusted, *e.g.*, by setting the RBS and the promoters of the glycolytic genes encoded by the GlucoBrick system (Gallagher *et al.*, 2014). Even when the results of such an approach are beyond the scope of this Thesis, they are expected to bring about a completely refactored and optimized *P. putida* strain in which the central carbon metabolism is entirely based in the EMP pathway.

VI. CONCLUSIONS

«*I am turned into a sort of machine for observing facts & grinding out conclusions*»
Charles Robert Darwin
(1809 AC-1882 AC)

CONCLUSIONS

The work described throughout this Thesis has given rise to the following conclusions:

1. The development of the GlucoBrick system has enabled the *à la carte* implementation of EMP pathway-based glycolytic activities into different Gram-negative bacteria. The potential of this standardized genetic tool has been exposed by restoring absent glycolytic activities in both *E. coli* and *Pseudomonas* species. The biotechnological value of the GlucoBrick platform has also been demonstrated by boosting the glucose-dependent accumulation of the biopolymer PHB in recombinant *E. coli* strains.

2. The streamlining process conducted in the WT strain KT2440 resulted in a set of *P. putida glycolytic chassis*, specifically designed to host a functional linear EMP pathway. This task has been achieved by removing the native glucose uptake system and disabling the endogenous glycolytic routes in this bacterium.

3. The glucose facilitator (*glf*) of *Z. mobilis* has been shown to be a promising candidate to substitute the native glucose transport system of *P. putida* KT2440. The use of Glf as a hexose facilitator prevents the ATP expenditure associated to the natural glucose uptake system of strain KT2440. Yet, its activity levels need further optimization.

4. The disruption of the native glycolytic pathways, by removing the Pgi activity, compromises the overall fitness of *P. putida* KT2440 under glycolytic growth conditions. The impossibility to regenerate G6P from trioses-*P* decreases substrate availability for the Zwf activity, which is in turn reflected in an increased sensitivity to oxidative stress due to the diminution of the NADPH pool. Moreover, the elimination of the Pgi activity may result in the accumulation of F6P, the metabolic precursor of alginate, thereby increasing the biofilm formation capability of *P. putida* KT2440.

5. The *P. putida glycolytic chassis* has been used to host a functional linear EMP pathway. Fluxomic analyses have demonstrated the successful metabolic refactoring of *P. putida* KT2440, replacing the natural, ED-based catabolic lifestyle by an authentic, energy-efficient EMP glycolytic pathway.

CONCLUSIONES

El trabajo descrito a lo largo de esta Tesis ha dado lugar a las siguientes conclusiones:

1. El desarrollo del sistema GlucoBrick ha permitido la implementación *a la carta* de las actividades glicolíticas derivadas de la ruta de EMP, siendo posible su utilización en diferentes bacterias Gram-negativas. El potencial de esta herramienta genética estandarizada ha sido demostrado con el restablecimiento de diversas actividades glicolíticas ausentes tanto en *E. coli* como en diferentes especies de *Pseudomonas*. El valor biotecnológico de esta plataforma se ha demostrado gracias a la detección de una mayor acumulación de PHB dependiente de glucosa en diversas cepas recombinantes de *E. coli*.

2. La edición genética de la cepa silvestre de *P. putida* KT2440 dio lugar a la obtención de un conjunto de *chassis glicolíticos*, especialmente diseñados para albergar una ruta EMP lineal totalmente funcional. Este procedimiento fue posible gracias a la eliminación de los sistemas de transporte y metabolización nativos de glucosa en esta bacteria.

3. El transportador de glucosa (*glf*) de *Z. mobilis* ha demostrado su capacidad a la hora de sustituir las funciones desarrolladas por el sistema nativo de *P. putida* KT2440. El uso del sistema Glf como transportador de hexosas evita el gasto de ATP asociado en el sistema natural de la cepa KT2440. Sin embargo, sus niveles de actividad necesitan ser optimizados.

4. La disrupción de las rutas glicolíticas nativas, mediante la eliminación de la actividad Pgi, compromete la viabilidad de *P. putida* KT2440. La incapacidad para generar G6P a partir de triosas-*P* disminuye la cantidad de sustrato disponible para la actividad Zwf. Este escenario conduce a un incremento de la sensibilidad a estrés oxidativo, explicada en gran parte por la disminución del NADPH disponible. Además, la eliminación de la actividad Pgi podría resultar en una acumulación de F6P, un precursor metabólico de la síntesis de alginato, incrementando la formación de *biofilm* para dicho mutante en *P. putida* KT2440.

5. La creación del *chassis glicolítico* basado en *P. putida* KT2440 ha permitido su utilización como hospedador de una ruta lineal funcional de EMP. Los análisis de flujos de carbono mediante marcaje con ^{13}C han demostrado la refactorización metabólica realizada sobre *P. putida* KT2440, reemplazando la ruta natural basada en ED por una ruta de EMP, más favorable en términos de rendimiento energético.

VII. REFERENCES

«*If you don't know history, then you don't know anything.*
You are a leaf that doesn't know it is part of a tree»
John Michael Crichton
(1942 AC-2008 AC)

REFERENCES

Ajikumar PK, Xiao WH, Tyo KEJ, Wang Y, Simeon F, Leonard E, Mucha O, Phon TH, Pfeifer B, Stephanopoulos G (2010) Isoprenoid pathway optimization for taxol precursor overproduction in *Escherichia coli*. *Science* **330:** 70-74.

Ammons D, Rampersad J, Fox GE (1999) 5S rRNA gene deletions cause an unexpectedly high fitness loss in *Escherichia coli*. *Nucleic Acids Res* **27:** 637-642.

An R, Moe LA (2016) Regulation of pyrroloquinoline quinone-dependent glucose dehydrogenase activity in the model rhizosphere-dwelling bacterium *Pseudomonas putida* KT2440. *Appl Environ Microbiol* **82:** 4955-4964.

Anderson AJ, Dawes EA (1990) Occurrence, metabolism, metabolic role, and industrial uses of bacterial polyhydroxyalkanoates. *Microbiol Rev* **54:** 450-472.

Anthony JR, Anthony LC, Nowroozi F, Kwon G, Newman JD, Keasling JD (2009) Optimization of the mevalonate-based isoprenoid biosynthetic pathway in *Escherichia coli* for production of the anti-malarial drug precursor amorpha-4,11-diene. *Metab Eng* **11:** 13-19.

Antonovsky N, Gleizer S, Noor E, Zohar Y, Herz E, Barenholz U, Zelcbuch L, Amram S, Wides A, Tepper N, Davidi D, Bar-On Y, Bareia T, Wernick DG, Shani I, Malitsky S, Jona G, Bar-Even A, Milo R (2016) Sugar synthesis from CO_2 in *Escherichia coli*. *Cell* **166:** 115-125.

Arellano BH, Ortiz JD, Manzano J, Chen JC (2010) Identification of a dehydrogenase required for lactose metabolism in *Caulobacter crescentus*. *Appl Environ Microbiol* **76:** 3004-3014.

Baba T, Ara T, Hasegawa M, Takai Y, Okumura Y, Baba M, Datsenko KA, Tomita M, Wanner BL, Mori H (2006) Construction of *Escherichia coli* K-12 in-frame, single-gene knockout mutants: the Keio collection. *Mol Syst Biol* **2:** 2006.0008.

Bachmann BJ (1972) Pedigrees of some mutant strains of *Escherichia coli* K-12. *Bacteriol Rev* **36:** 525-557.

Bagdasarian M, Lurz R, Rückert B, Franklin FCH, Bagdasarian MM, Frey J, Timmis KN (1981) Specific purpose plasmid cloning vectors. II. Broad host range, high copy number, RSF1010-derived vectors, and a host-vector system for gene cloning in *Pseudomonas*. *Gene* **16:** 237-247.

Baldwin SA (1993) Mammalian passive glucose transporters: members of an ubiquitous family of active and passive transport proteins. *Biochim Biophys Acta* **1154:** 17-49.

Baldwin SA, Henderson PJ (1989) Homologies between sugar transporters from eukaryotes and prokaryotes. *Annu Rev Physiol* **51:** 459-471.

Banerjee PC (1989) Fructose-bisphosphatase-deficient mutants of mucoid *Pseudomonas aeruginosa*. *Folia Microbiol (Praha)* **34:** 81-86.

Banerjee PC, Vanags RI, Chakrabarty AM, Maitra PK (1983) Alginic acid synthesis in *Pseudomonas aeruginosa* mutants defective in carbohydrate metabolism. *J Bacteriol* **155:** 238-245.

Bar-Even A, Flamholz A, Noor E, Milo R (2012) Rethinking glycolysis: on the biochemical logic of metabolic pathways. *Nat Chem Biol* **8:** 509-517.

Basan M, Hui S, Okano H, Zhang Z, Shen Y, Williamson JR, Hwa T (2015) Overflow metabolism in *Escherichia coli* results from efficient proteome allocation. *Nature* **528:** 99-104.

Baumann P, Baumann L (1975) Catabolism of D-fructose and D-ribose by *Pseudomonas doudoroffi* - I. Physiological studies and mutant analysis. *Arch Microbiol* **105:** 225-240.

Belda E, van Heck RGA, López-Sánchez MJ, Cruveiller S, Barbe V, Fraser C, Klenk HP, Petersen J, Morgat A, Nikel PI, Vallenet D, Rouy Z, Sekowska A, Martins dos Santos VAP, de Lorenzo V, Danchin A, Médigue C (2016) The revisited genome of *Pseudomonas putida* KT2440 enlightens its value as a robust metabolic *chassis*. *Environ Microbiol* **18:** 3403-3424.

Belenky P, Ye JD, Porter CB, Cohen NR, Lobritz MA, Ferrante T, Jain S, Korry BJ, Schwarz EG, Walker GC, Collins JJ (2015) Bactericidal antibiotics induce toxic metabolic perturbations that lead to cellular damage. *Cell Rep* **13:** 968-980.

Benedetti I, Nikel PI, de Lorenzo V (2016) Data on the standardization of a cyclohexanone-responsive expression system for Gram-negative bacteria. *Data in Brief* **6:** 738-744.

Benisch F, Boles E (2014) The bacterial Entner-Doudoroff pathway does not replace glycolysis in *Saccharomyces cerevisiae* due to the lack of activity of iron-sulfur cluster enzyme 6-phosphogluconate dehydratase. *J Biotechnol* **171:** 45-55.

Bentley WE, Mirjalili N, Andersen DC, Davis RH, Kompala DS (1990) Plasmid-encoded protein: the principal factor in the "metabolic burden" associated with recombinant bacteria. *Biotechnol Bioeng* **35:** 668-681.

Berger A, Dohnt K, Tielen P, Jahn D, Becker J, Wittmann C (2014) Robustness and plasticity of metabolic pathway flux among uropathogenic isolates of *Pseudomonas aeruginosa*. *PLoS One* **9:** e88368.

Bernal V, Castaño-Cerezo S, Cánovas M (2016) Acetate metabolism regulation in *Escherichia coli*: carbon overflow, pathogenicity, and beyond. *Appl Microbiol Biotechnol* **100:** 8985-9001.

Biggs BW, De Paepe B, Santos CN, De Mey M, Kumaran Ajikumar P (2014) Multivariate modular metabolic engineering for pathway and strain optimization. *Curr Opin Biotechnol* **29:** 156-162.

Blank LM, Ebert BE, Buehler K, Bühler B (2010) Redox biocatalysis and metabolism: molecular mechanisms and metabolic network analysis. *Antiox Red Signal* **13:** 349-394.

Blank LM, Ionidis G, Ebert BE, Bühler B, Schmid A (2008) Metabolic response of *Pseudomonas putida* during redox biocatalysis in the presence of a second octanol phase. *FEBS J* **275:** 5173-5190.

Blevins WT, Feary TW, Phibbs PV (1975) 6-Phosphogluconate dehydratase deficiency in pleiotropic carbohydrate-negative mutant strains of *Pseudomonas aeruginosa*. *J Bacteriol* **121:** 942-949.

Bochner BR (2009) Global phenotypic characterization of bacteria. *FEMS Microbiol Rev* **33:** 191-205.

Bochner BR, Gadzinski P, Panomitros E (2001) Phenotype microarrays for high-throughput phenotypic testing and assay of gene function. *Genome Res* **11:** 1246-1255.

Borrero de Acuña JM, Bielecka A, Haussler S, Schobert M, Jahn M, Wittmann C, Jahn D, Poblete-Castro I (2014) Production of medium chain length polyhydroxyalkanoate in metabolic flux optimized *Pseudomonas putida*. *Microb Cell Fact* **13:** 88.

Boschi-Muller S, Azza S, Pollastro D, Corbier C, Branlant G (1997) Comparative enzymatic properties of GapB-encoded erythrose-4-phosphate dehydrogenase of *Escherichia coli* and phosphorylating glyceraldehyde-3-phosphate dehydrogenase. *J Biol Chem* **272:** 15106-15112.

Bouhss A, Trunkfield AE, Bugg TD, Mengin-Lecreulx D (2008) The biosynthesis of peptidoglycan lipid-linked intermediates. *FEMS Microbiol Rev* **32:** 208-233.

Boyd A, Chakrabarty AM (1995) *Pseudomonas aeruginosa* biofilms: role of the alginate exopolysaccharide. *J Ind Microbiol* **15:** 162-168.

Boyer HW, Roulland-Dussoix D (1969) A complementation analysis of the restriction and modification of DNA in *Escherichia coli*. *J Mol Biol* **41:** 459-472.

Bradford MM (1976) A rapid and sensitive method for the quantitation of microgram quantities of protein utilizing the principle of protein-dye binding. *Anal Biochem* **72:** 248-254.

Bratlie MS, Johansen J, Sherman BT, Huang da W, Lempicki RA, Drablos F (2010) Gene duplications in prokaryotes can be associated with environmental adaptation. *BMC Genomics* **11:** 588.

Breitling R, Takano E (2015) Synthetic biology advances for pharmaceutical production. *Curr Opin Biotechnol* **35:** 46-51.

Burgard AP, Pharkya P, Maranas CD (2003) Optknock: a bilevel programming framework for identifying gene knockout strategies for microbial strain optimization. *Biotechnol Bioeng* **84:** 647-657.

Bus JS, Gibson JE (1984) Paraquat: model for oxidant-initiated toxicity. *Environ Health Perspect* **55:** 37-46.

Calero P, Jensen SI, Nielsen AT (2016) Broad-host-range *ProUSER* vectors enable fast characterization of inducible promoters and optimization of *p*-coumaric acid production in *Pseudomonas putida* KT2440. *ACS Synth Biol* **5:** 741-753.

Canonaco F, Hess TA, Heri S, Wang T, Szyperski T, Sauer U (2001) Metabolic flux response to phosphoglucose isomerase knock-out in *Escherichia coli* and impact of overexpression of the soluble transhydrogenase UdhA. *FEMS Microbiol Lett* **204:** 247-252.

Canton B, Labno A, Endy D (2008) Refinement and standardization of synthetic biological parts and devices. *Nat Biotechnol* **26:** 787-793.

Chan LY, Kosuri S, Endy D (2005) Refactoring bacteriophage T7. *Mol Syst Biol* **1:** 2005.0018.

Chang DE, Shin S, Rhee JS, Pan JG (1999) Acetate metabolism in a *pta* mutant of *Escherichia coli* W3110: Importance of maintaining acetyl coenzyme A flux for growth and survival. *J Bacteriol* **181:** 6656-6663.

Charusanti P, Conrad TM, Knight EM, Venkataraman K, Fong NL, Xie B, Gao Y, Palsson BØ (2010) Genetic basis of growth adaptation of *Escherichia coli* after deletion of *pgi*, a major metabolic gene. *PLoS Genet* **6:** e1001186.

Chavarría M, Goñi-Moreno A, de Lorenzo V, Nikel PI (2016) A metabolic widget adjusts the phosphoenolpyruvate-dependent fructose influx in *Pseudomonas putida*. *mSystems* **1:** e00154-00116.

Chavarría M, Kleijn RJ, Sauer U, Pflüger-Grau K, de Lorenzo V (2012) Regulatory tasks of the phosphoenolpyruvate-phosphotransferase system of *Pseudomonas putida* in central carbon metabolism. *mBio* **3:** e00028-00012.

Chavarría M, Nikel PI, Pérez-Pantoja D, de Lorenzo V (2013) The Entner-Doudoroff pathway empowers *Pseudomonas putida* KT2440 with a high tolerance to oxidative stress. *Environ Microbiol* **15:** 1772-1785.

Chen RR, Agrawal M, Mao Z (2013) Impact of expression of EMP enzymes on glucose metabolism in *Zymomonas mobilis*. *Appl Biochem Biotechnol* **170:** 805-818.

Cherepanov PP, Wackernagel W (1995) Gene disruption in *Escherichia coli*: Tc^R and Km^R cassettes with the option of Flp-catalyzed excision of the antibiotic-resistance determinant. *Gene* **158:** 9-14.

Chin JW, Cirino PC (2011) Improved NADPH supply for xylitol production by engineered *Escherichia coli* with glycolytic mutations. *Biotechnol Prog* **27:** 333-341.

Choe D, Cho S, Kim SC, Cho BK (2016) Minimal genome: worthwhile or worthless efforts toward being smaller? *Biotechnol J* **11:** 199-211.

Choi KH, Kumar A, Schweizer HP (2006) A 10-min method for preparation of highly electrocompetent *Pseudomonas aeruginosa* cells: application for DNA fragment transfer between chromosomes and plasmid transformation. *J Microbiol Methods* **64:** 391-397.

Cuskey SM, Wolff JA, Phibbs PV, Olsen RH (1985) Cloning of genes specifying carbohydrate catabolism in *Pseudomonas aeruginosa* and *Pseudomonas putida*. *J Bacteriol* **162:** 865-871.

Daddaoua A, Krell T, Ramos JL (2009) Regulation of glucose metabolism in *Pseudomonas*: the phosphorylative branch and Entner-Doudoroff enzymes are regulated by a repressor containing a sugar isomerase domain. *J Biol Chem* **284:** 21360-21368.

Danchin A (2012) Scaling up synthetic biology: do not forget the *chassis*. *FEBS Lett* **586:** 2129-2137.

Datsenko KA, Wanner BL (2000) One-step inactivation of chromosomal genes in *Escherichia coli* K-12 using PCR products. *Proc Natl Acad Sci USA* **97:** 6640-6645.

Dauner M, Sauer U (2000) GC-MS analysis of amino acids rapidly provides rich information for isotopomer balancing. *Biotechnol Prog* **16:** 642-649.

Davidson AL, Chen J (2004) ATP-binding cassette transporters in bacteria. *Annu Rev Biochem* **73:** 241-268.

del Castillo T, Ramos JL, Rodríguez-Herva JJ, Fuhrer T, Sauer U, Duque E (2007) Convergent peripheral pathways catalyze initial glucose catabolism in *Pseudomonas putida*: genomic and flux analysis. *J Bacteriol* **189:** 5142-5152.

del Castillo T, Duque E, Ramos JL (2008) A set of activators and repressors control peripheral glucose pathways in *Pseudomonas putida* to yield a common central intermediate. *J Bacteriol* **190:** 2331-2339.

den Dooren de Jong LE (1926) *Bijdrage Tot de Kennis van het Mineralisatieproces*, Rotterdam, The Netherlands.

Dimarco AA, Romano AH (1985) D-Glucose transport system of *Zymomonas mobilis*. *Appl Environ Microbiol* **49:** 151-157.

Ditta G, Stanfield S, Corbin D, Helinski DR (1980) Broad host range DNA cloning system for Gram-negative bacteria: construction of a gene bank of *Rhizobium meliloti*. *Proc Natl Acad Sci USA* **77:** 7347-7351.

Doi RH, Igarashi RT (1965) Conservation of ribosomal and messenger ribonucleic acid cistrons in *Bacillus* species. *J Bacteriol* **90:** 384-390.

Durante-Rodríguez G, de Lorenzo V, Martínez-García E (2014) The *Standard European Vector Architecture* (SEVA) plasmid toolkit. *Methods Mol Biol* **1149:** 469-478.

Dvořák P, Chrást L, Nikel PI, Fedr R, Soucek K, Sedlacková M, Chaloupková R, de Lorenzo V, Prokop Z, Damborský J (2015) Exacerbation of substrate toxicity by IPTG in *Escherichia coli* BL21(DE3) carrying a synthetic metabolic pathway. *Microb Cell Fact* **14:** 201.

Dwyer DJ, Belenky PA, Yang JH, MacDonald IC, Martell JD, Takahashi N, Chan CT, Lobritz MA, Braff D, Schwarz EG, Ye JD, Pati M, Vercruysse M, Ralifo PS, Allison KR, Khalil AS, Ting AY, Walker GC, Collins JJ (2014) Antibiotics induce redox-related physiological alterations as part of their lethality. *Proc Natl Acad Sci USA* **111:** E2100-E2109.

Dwyer DJ, Collins JJ, Walker GC (2015) Unraveling the physiological complexities of antibiotic lethality. *Annu Rev Pharmacol Toxicol* **55:** 313-332.

Eames M, Kortemme T (2012) Cost-benefit tradeoffs in engineered *lac* operons. *Science* **336:** 911-915.

Ebert BE, Kurth F, Grund M, Blank LM, Schmid A (2011) Response of *Pseudomonas putida* KT2440 to increased NADH and ATP demand. *Appl Environ Microbiol* **77:** 6597-6605.

Edwards JS, Covert M, Palsson BØ (2002) Metabolic modelling of microbes: the flux-balance approach. *Environ Microbiol* **4:** 133-140.

Emmerling M, Dauner M, Ponti A, Fiaux J, Hochuli M, Szyperski T, Wüthrich K, Bailey JE, Sauer U (2002) Metabolic flux responses to pyruvate kinase knockout in *Escherichia coli*. *J Bacteriol* **184:** 152-164.

Ertesvåg H, Sletta H, Senneset M, Sun YQ, Klinkenberg G, Konradsen TA, Ellingsen TE, Valla S (2017) Identification of genes affecting alginate biosynthesis in *Pseudomonas fluorescens* by screening a transposon insertion library. *BMC Genomics* **18:** 11.

Euzeby JP (1997) List of bacterial names with standing in nomenclature: a folder available on the Internet. *Int J Syst Bacteriol* **47:** 590-592.

Federal Register. Appendix E (1982) *Certified host-vector systems* **47:** 17197.

Fernández M, Udaondo Z, Niqui JL, Duque E, Ramos JL (2014) Synergic role of the two ars operons in arsenic tolerance in *Pseudomonas putida* KT2440. *Environ Microbiol Rep* **6:** 483-489.

Fischer E, Sauer U (2003) Metabolic flux profiling of *Escherichia coli* mutants in central carbon metabolism using GC-MS. *Eur J Biochem* **270:** 880-891.

Flamholz A, Noor E, Bar-Even A, Liebermeister W, Milo R (2013) Glycolytic strategy as a tradeoff between energy yield and protein cost. *Proc Natl Acad Sci U S A* **110:** 10039-10044.

Flemming HC, Neu TR, Wozniak DJ (2007) The EPS matrix: the "house of biofilm cells". *J Bacteriol* **189:** 7945-7947.

Fraenkel DG (1986) Mutants in glucose metabolism. *Annu Rev Biochem* **55:** 317-337.

Franklin MJ, Nivens DE, Weadge JT, Howell PL (2011) Biosynthesis of the *Pseudomonas aeruginosa* extracellular polysaccharides, alginate, Pel, and Psl. *Front Microbiol* **2:** 167.

Fuhrer T, Fischer E, Sauer U (2005) Experimental identification and quantification of glucose metabolism in seven bacterial species. *J Bacteriol* **187:** 1581-1590.

Fuhrer T, Sauer U (2009) Different biochemical mechanisms ensure network-wide balancing of reducing equivalents in microbial metabolism. *J Bacteriol* **191:** 2112-2121.

Gallagher RR, Li Z, Lewis AO, Isaacs FJ (2014) Rapid editing and evolution of bacterial genomes using libraries of synthetic DNA. *Nat Protoc* **9:** 2301-2316.

Gao L, Chiou W, Tang H, Cheng X, Camp HS, Burns DJ (2007) Simultaneous quantification of malonyl-CoA and several other short-chain acyl-CoAs in animal tissues by ion-pairing reversed-phase HPLC/MS. *J Chromatogr B Analyt Technol Biomed Life Sci* **853:** 303-313.

Godoy MS, Nikel PI, Cabrera Gomez JG, Pettinari MJ (2015) The CreC regulator of *Escherichia coli*, a new target for metabolic manipulations. *Appl Environ Microbiol* **82:** 244-254.

Cabrera Gomez JG, Méndez BS, Nikel PI, Pettinari MJ, Prieto MA, Silva LF (2012) Making green polymers even greener: towards sustainable production of polyhydroxyalkanoates from agroindustrial by-products. In *Advances in Applied Biotechnology*, Petre M (ed), pp 41-62. Rijeka, Croatia: InTech.

Green MR, Sambrook J (2012) *Molecular cloning: a laboratory manual*, 4th edn. Cold Spring Harbor, NY: Cold Spring Harbor Laboratory Press.

Gulez G, Altintas A, Fazli M, Dechesne A, Workman CT, Tolker-Nielsen T, Smets BF (2014) Colony morphology and transcriptome profiling of *Pseudomonas putida* KT2440 and its mutants deficient in alginate or all EPS synthesis under controlled matric potentials. *MicrobiologyOpen* **3:** 457-469.

Hajjaj H, Blanc PJ, Goma G, François J (1998) Sampling techniques and comparative extraction procedures for quantitative determination of intra- and extracellular metabolites in filamentous fungi. *FEMS Microbiology Letters* **164:** 195-200.

Han K, Lim HC, Hong J (1992) Acetic acid formation in *Escherichia coli* fermentation. *Biotechnol Bioeng* **39:** 663-671.

Hanahan D, Meselson M (1983) Plasmid screening at high colony density. *Methods Enzymol* **100:** 333-342.

Hansen AS, Lennen RM, Sonnenschein N, Herrgård MJ (2017) Systems biology solutions for biochemical production challenges. *Curr Opin Biotechnol* **45:** 85-91.

Hara KY, Kondo A (2015) ATP regulation in bioproduction. *Microb Cell Fact* **14:** 198.

Hara KY, Shimodate N, Hirokawa Y, Ito M, Baba T, Mori H, Mori H (2009) Glutathione production by efficient ATP-regenerating *Escherichia coli* mutants. *FEMS Microbiol Lett* **297:** 217-224.

Heinemann M, Panke S (2006) Synthetic biology–Putting engineering into biology. *Bioinformatics* **22:** 2790-2799.

Hentzer M, Teitzel GM, Balzer GJ, Heydorn A, Molin S, Givskov M, Parsek MR (2001) Alginate overproduction affects *Pseudomonas aeruginosa* biofilm structure and function. *J Bacteriol* **183:** 5395-5401.

Herrero M, de Lorenzo V, Timmis KN (1990) Transposon vectors containing non-antibiotic resistance selection markers for cloning and stable chromosomal insertion of foreign genes in Gram-negative bacteria. *J Bacteriol* **172:** 6557-6567.

Hollinshead WD, Rodriguez S, García-Martín H, Wang G, Baidoo EEK, Sale KL, Keasling JD, Mukhopadhyay A, Tang YJ (2016) Examining *Escherichia coli* glycolytic pathways, catabolite repression, and metabolite channeling using Δ*pfk* mutants. *Biotechnol Biofuels* **9:** 212.

Horton RM (1995) PCR-mediated recombination and mutagenesis: *SOEing* together tailor-made genes. *Mol Biotechnol* **3:** 93-99.

Hua Q, Yang C, Baba T, Mori H, Shimizu K (2003) Responses of the central metabolism in *Escherichia coli* to phosphoglucose isomerase and glucose-6-phosphate dehydrogenase knockouts. *J Bacteriol* **185:** 7053-7067.

Jahreis K, Pimentel-Schmitt EF, Brückner R, Titgemeyer F (2008) Ins and outs of glucose transport systems in Eubacteria. *FEMS Microbiol Rev* **32:** 891-907.

Jensen JB, Peters NK, Bhuvaneswari TV (2002) Redundancy in periplasmic binding protein-dependent transport systems for trehalose, sucrose, and maltose in *Sinorhizobium meliloti*. *J Bacteriol* **184:** 2978-2986.

Jensen KF (1993) The *Escherichia coli* K-12 "wild types" W3110 and MG1655 have an *rph* frameshift mutation that leads to pyrimidine starvation due to low *pyrE* expression levels. *J Bacteriol* **175:** 3401-3407.

Jensen LJ, Skovgaard M, Sicheritz-Pontén T, Hansen NT, Johansson H, Jørgensen MK, Kiil K, Hallin PF, Ussery D (2004) Comparative genomics of four *Pseudomonas* species. In *Pseudomonas: Genomics, Life Style and Molecular Architecture*, Ramos J-L (ed), pp 139-164. Boston, MA: Springer US.

Jiménez JI, Miñambres B, García JL, Díaz E (2002) Genomic analysis of the aromatic catabolic pathways from *Pseudomonas putida* KT2440. *Environ Microbiol* **4:** 824-841.

Johnson JL, Ordal EJ (1968) Deoxyribonucleic acid homology in bacterial taxonomy: effect of incubation temperature on reaction specificity. *J Bacteriol* **95:** 893-900.

Jojima T, Inui M (2015) Engineering the glycolytic pathway: A potential approach for improvement of biocatalyst performance. *BioEngineered* **6:** 328-334.

Jones KL, Kim SW, Keasling JD (2000) Low-copy plasmids can perform as well as or better than high-copy plasmids for metabolic engineering of bacteria. *Metab Eng* **2:** 328-338.

Jullesson D, David F, Pfleger B, Nielsen J (2015) Impact of synthetic biology and metabolic engineering on industrial production of fine chemicals. *Biotechnol Adv* **33:** 1395-1402.

Kabir MM, Shimizu K (2003) Fermentation characteristics and protein expression patterns in a recombinant *Escherichia coli* mutant lacking phosphoglucose isomerase for poly(3-hydroxybutyrate) production. *Appl Microbiol Biotechnol* **62:** 244-255.

Kern A, Tilley E, Hunter IS, Legisa M, Glieder A (2007) Engineering primary metabolic pathways of industrial micro-organisms. *J Biotechnol* **129:** 6-29.

Kessler B, de Lorenzo V, Timmis KN (1992) A general system to integrate *lacZ* fusions into the chromosomes of Gram-negative eubacteria: regulation of the *Pm* promoter of the TOL plasmid studied with all controlling elements in monocopy. *Mol Gen Genet* **233:** 293-301.

Kim J, Copley SD (2012) Inhibitory cross-talk upon introduction of a new metabolic pathway into an existing metabolic network. *Proc Natl Acad Sci USA* **109:** E2856-E2864.

Kim J, Park W (2014) Oxidative stress response in *Pseudomonas putida*. *Appl Microbiol Biotechnol* **98:** 6933-6946.

Kim J, Salvador M, Saunders E, González J, Avignone-Rossa C, Jiménez JI (2016a) Properties of alternative microbial hosts used in synthetic biology: towards the design of a modular *chassis*. *Essays Biochem* **60:** 303-313.

Kim P, Laivenieks M, Vieille C, Zeikus JG (2004) Effect of overexpression of *Actinobacillus succinogenes* phosphoenolpyruvate carboxykinase on succinate production in *Escherichia coli*. *Appl Environ Microbiol* **70:** 1238-1241.

Kim SH, Cavaleiro AM, Rennig M, Nørholm MH (2016b) *SEVA Linkers*: A versatile and automatable DNA backbone exchange standard for Synthetic Biology. *ACS Synth Biol* **5:** 1177-1181.

King JR, Edgar S, Qiao K, Stephanopoulos G (2016) Accessing Nature's diversity through metabolic engineering and synthetic biology. *F1000Res* **5:** 397.

Klein AS, Domröse A, Bongen P, Brass HUC, Classen T, Loeschcke A, Drepper T, Laraia L, Sievers S, Jaeger KE, Pietruszka J (2017) New prodigiosin derivatives obtained by mutasynthesis in *Pseudomonas putida*. *ACS Synth Biol* **In press:** DOI: 10.1021/acssynbio.1027b00099.

Kojima Y, Fujisawa H, Nakazawa A, Nakazawa T, Kanetsuna F, Taniuchi H, Nozaki M, Hayaishi O (1967) Studies on pyrocatechase. I. Purification and spectral properties. *J Biol Chem* **242:** 3270-3278.

La Rosa R, Nogales J, Rojo F (2015) The Crc/CrcZ-CrcY global regulatory system helps the integration of gluconeogenic and glycolytic metabolism in *Pseudomonas putida*. *Environ Microbiol* **17:** 3362-3378.

Lai CY, Cronan JE (2004) Isolation and characterization of b-ketoacyl-acyl carrier protein reductase (*fabG*) mutants of *Escherichia coli* and *Salmonella enterica* serovar *Typhimurium*. *J Bacteriol* **186:** 1869-1878.

Latrach-Tlemçani L, Corroler D, Barillier D, Mosrati R (2008) Physiological states and energetic adaptation during growth of *Pseudomonas putida* mt-2 on glucose. *Arch Microbiol* **190:** 141-150.

Lee SY, Kim HU (2015) Systems strategies for developing industrial microbial strains. *Nat Biotechnol* **33:** 1061-1072.

Leong YK, Show PL, Ooi CW, Ling TC, Lan JC (2014) Current trends in polyhydroxyalkanoates (PHAs) biosynthesis: insights from the recombinant *Escherichia coli*. *J Biotechnol* **180:** 52-65.

Lessie TG, Phibbs PV (1984) Alternative pathways of carbohydrate utilization in pseudomonads. *Annu Rev Microbiol* **38:** 359-388.

Li R, Zhang H, Qi Q (2007) The production of polyhydroxyalkanoates in recombinant *Escherichia coli*. *Bioresour Technol* **98:** 2313-2320.

Li Z, Nimtz M, Rinas U (2014) The metabolic potential of *Escherichia coli* BL21 in defined and rich medium. *Microb Cell Fact* **13:** 45.

Liao JC, Mi L, Pontrelli S, Luo S (2016) Fuelling the future: microbial engineering for the production of sustainable biofuels. *Nat Rev Microbiol* **14:** 288-304.

Lieder S, Nikel PI, de Lorenzo V, Takors R (2015) Genome reduction boosts heterologous gene expression in *Pseudomonas putida*. *Microb Cell Fact* **14:** 23.

Lin Z, Xu Z, Li Y, Wang Z, Chen T, Zhao X (2014) Metabolic engineering of *Escherichia coli* for the production of riboflavin. *Microb Cell Fact* **13:** 104.

Lindner SN, Petrov DP, Hagmann CT, Henrich A, Krämer R, Eikmanns BJ, Wendisch VF, Seibold GM (2013) Phosphotransferase system-mediated glucose uptake is repressed in phosphoglucoisomerase-deficient *Corynebacterium glutamicum* strains. *Appl Environ Microbiol* **79:** 2588-2595.

Linger JG, Vardon DR, Guarnieri MT, Karp EM, Hunsinger GB, Franden MA, Johnson CW, Chupka G, Strathmann TJ, Pienkos PT, Beckham GT (2014) Lignin valorization through integrated biological funneling and chemical catalysis. *Proc Natl Acad Sci USA* **111:** 12013-12018.

Loeschcke A, Thies S (2015) *Pseudomonas putida*–A versatile host for the production of natural products. *Appl Microbiol Biotechnol* **99:** 6197-6214.

López NI, Pettinari MJ, Nikel PI, Méndez BS (2015) Polyhydroxyalkanoates: much more than biodegradable plastics. *Adv Appl Microbiol* **93:** 93-106.

Maleki S, Mærk M, Valla S, Ertesvåg H (2015) Mutational analyses of glucose dehydrogenase and glucose-6-phosphate dehydrogenase genes in *Pseudomonas fluorescens* reveal their effects on growth and alginate production. *Appl Environ Microbiol* **81:** 3349-3356.

Mandsberg LF, Ciofu O, Kirkby N, Christiansen LE, Poulsen HE, Høiby N (2009) Antibiotic resistance in *Pseudomonas aeruginosa* strains with increased mutation frequency due to inactivation of the DNA oxidative repair system. *Antimicrob Agents Chemother* **53:** 2483-2491.

Manoil C, Beckwith J (1985) Tn*phoA*: a transposon probe for protein export signals. *Proc Natl Acad Sci USA* **82:** 8129-8133.

Martínez-García E, de Lorenzo V (2011) Engineering multiple genomic deletions in Gram-negative bacteria: analysis of the multi-resistant antibiotic profile of *Pseudomonas putida* KT2440. *Environ Microbiol* **13:** 2702-2716.

Martínez-García E, de Lorenzo V (2012) Transposon-based and plasmid-based genetic tools for editing genomes of Gram-negative bacteria. *Methods Mol Biol* **813:** 267-283.

Martínez-García E, de Lorenzo V (2016) The quest for the minimal bacterial genome. *Curr Opin Biotechnol* **42:** 216-224.

Martínez-García E, Calles B, Arévalo-Rodríguez M, de Lorenzo V (2011) pBAM1: an all-synthetic genetic tool for analysis and construction of complex bacterial phenotypes. *BMC Microbiol* **11:** 38.

Martínez-García E, Aparicio T, de Lorenzo V, Nikel PI (2014a) New transposon tools tailored for metabolic engineering of Gram-negative microbial cell factories. *Front Bioeng Biotechnol* **2:** 46.

Martínez-García E, Aparicio T, Goñi-Moreno A, Fraile S, de Lorenzo V (2014b) SEVA 2.0: an update of the *Standard European Vector Architecture* for de-/re-construction of bacterial functionalities. *Nucleic Acids Res* **43:** D1183-D1189.

Martínez-García E, Nikel PI, Aparicio T, de Lorenzo V (2014c) *Pseudomonas* 2.0: genetic upgrading of *P. putida* KT2440 as an enhanced host for heterologous gene expression. *Microb Cell Fact* **13:** 159.

Martínez-García E, Nikel PI, Chavarría M, de Lorenzo V (2014d) The metabolic cost of flagellar motion in *Pseudomonas putida* KT2440. *Environ Microbiol* **16:** 291-303.

Martínez-García E, Benedetti I, Hueso A, de Lorenzo V (2015) Mining environmental plasmids for synthetic biology parts and devices. *Microbiol Spectr* **3:** PLAS-0033-2014.

Martínez-García E, Aparicio T, de Lorenzo V, Nikel PI (2017) Engineering Gram-negative microbial cell factories using transposon vectors. *Methods Mol Biol* **1498:** 273-293.

Martins dos Santos VAP, Heim S, Moore ER, Strätz M, Timmis KN (2004) Insights into the genomic basis of niche specificity of *Pseudomonas putida* KT2440. *Environ Microbiol* **6:** 1264-1286.

Matsushita K, Shinagawa E, Ameyama M (1982) D-Gluconate dehydrogenase from bacteria, 2-keto-D-gluconate-yielding, membrane-bound. *Methods Enzymol* **89:** 187-193.

Matsushita K, Toyama H, Adachi O (1994) Respiratory chains and bioenergetics of acetic acid bacteria. *Adv Microb Physiol* **36:** 247-301.

McIntire W, Singer TP, Ameyama M, Adachi O, Matsushita K, Shinagawa E (1985) Identification of the covalently bound flavins of D-gluconate dehydrogenases from *Pseudomonas aeruginosa* and *Pseudomonas fluorescens* and of 2-keto-D-gluconate dehydrogenase from *Gluconobacter melanogenus*. *Biochem J* **231:** 651-654.

Meyer D, Schneider-Fresenius C, Horlacher R, Peist R, Boos W (1997) Molecular characterization of glucokinase from *Escherichia coli* K-12. *J Bacteriol* **179:** 1298-1306.

Migula W (1894) *Über ein neues System der Bakterien*. *Arb Bakteriol Inst Karlsruhe* **1:** 235–328.

Migula W (1900) *System der Bakterien*, Vol. 2, Jena, Germany.

Miller BG, Raines RT (2004) Identifying latent enzyme activities: substrate ambiguity within modern bacterial sugar kinases. *Biochemistry* **43:** 6387-6392.

Müller JEN, Meyer F, Litsanov B, Kiefer P, Potthoff E, Heux S, Quax WJ, Wendisch VF, Brautaset T, Portais JC, Vorholt JA (2015) Engineering *Escherichia coli* for methanol conversion. *Metab Eng* **28:** 190-201.

Nakano K, Rischke M, Sato S, Markl H (1997) Influence of acetic acid on the growth of *Escherichia coli* K12 during high-cell-density cultivation in a dialysis reactor. *Appl Microbiol Biotechnol* **48:** 597-601.

Narbad A, Russell NJ, Gacesa P (1988) Radiolabelling patterns in alginate of *Pseudomonas aeruginosa* synthesized from specifically-labelled ^{14}C-monosaccharide precursors. *Microbios* **54:** 171-179.

Nelson KE, Weinel C, Paulsen IT, Dodson RJ, Hilbert H, Martins dos Santos VAP, Fouts DE, Gill SR, Pop M, Holmes M, Brinkac L, Beanan M, DeBoy RT, Daugherty S, Kolonay J, Madupu R, Nelson W, White O, Peterson J, Khouri H, Hance I, Chris Lee P, Holtzapple E, Scanlan D, Tran K, Moazzez A, Utterback T, Rizzo M, Lee K, Kosack D, Moestl D, Wedler H, Lauber J, Stjepandic D, Hoheisel J, Straetz M, Heim S, Kiewitz C, Eisen JA, Timmis KN, Düsterhöft A, Tümmler B, Fraser CM (2002) Complete genome sequence and comparative analysis of the metabolically versatile *Pseudomonas putida* KT2440. *Environ Microbiol* **4:** 799-808.

Ng FM, Dawes EA (1973) Chemostat studies on the regulation of glucose metabolism in *Pseudomonas aeruginosa* by citrate. *Biochem J* **132:** 129-140.

Ng CY, Farasat I, Maranas CD, Salis HM (2015) Rational design of a synthetic Entner-Doudoroff pathway for improved and controllable NADPH regeneration. *Metab Eng* **29:** 86-96.

Nielsen AA, Segall-Shapiro TH, Voigt CA (2013) Advances in genetic circuit design: novel biochemistries, deep part mining, and precision gene expression. *Curr Opin Chem Biol* **17:** 878-892.

Nielsen J, Keasling JD (2016) Engineering cellular metabolism. *Cell* **164:** 1185-1197.

Nikel PI, Chavarría M (2016) Quantitative physiology approaches to understand and optimize reducing power availability in environmental bacteria. In *Hydrocarbon and Lipid Microbiology Protocols–Synthetic and Systems Biology - Tools*, McGenity TJ, Timmis KN, Nogales-Fernández B (eds), pp 39-70. Heidelberg, Germany: Humana Press.

Nikel PI, de Lorenzo V (2013a) Engineering an anaerobic metabolic regime in *Pseudomonas putida* KT2440 for the anoxic biodegradation of 1,3-dichloroprop-1-ene. *Metab Eng* **15:** 98-112.

Nikel PI, de Lorenzo V (2013b) Implantation of unmarked regulatory and metabolic modules in Gram-negative bacteria with specialised mini-transposon delivery vectors. *J Biotechnol* **163:** 143-154.

Nikel PI, Pettinari MJ, Galvagno MA, Méndez BS (2006) Poly(3-hydroxybutyrate) synthesis by recombinant *Escherichia coli arcA* mutants in microaerobiosis. *Appl Environ Microbiol* **72:** 2614-2620.

Nikel PI, Giordano AM, de Almeida A, Godoy MS, Pettinari MJ (2010) Elimination of D-lactate synthesis increases poly(3-hydroxybutyrate) and ethanol synthesis from glycerol and affects cofactor distribution in recombinant *Escherichia coli*. *Appl Environ Microbiol* **76:** 7400-7406.

Nikel PI, Chavarría M, Martínez-García E, Taylor AC, de Lorenzo V (2013) Accumulation of inorganic polyphosphate enables stress endurance and catalytic vigour in *Pseudomonas putida* KT2440. *Microb Cell Fact* **12:** 50.

Nikel PI, Kim J, de Lorenzo V (2014a) Metabolic and regulatory rearrangements underlying glycerol metabolism in *Pseudomonas putida* KT2440. *Environ Microbiol* **16:** 239-254.

Nikel PI, Martínez-García E, de Lorenzo V (2014b) Biotechnological domestication of pseudomonads using synthetic biology. *Nat Rev Microbiol* **12:** 368-379.

Nikel PI, Chavarría M, Fuhrer T, Sauer U, de Lorenzo V (2015a) *Pseudomonas putida* KT2440 strain metabolizes glucose through a cycle formed by enzymes of the Entner-Doudoroff, Embden-Meyerhof-Parnas, and pentose phosphate pathways. *J Biol Chem* **290:** 25920-25932.

Nikel PI, Romero-Campero FJ, Zeidman JA, Goñi-Moreno A, de Lorenzo V (2015b) The glycerol-dependent metabolic persistence of *Pseudomonas putida* KT2440 reflects the regulatory logic of the GlpR repressor. *mBio* **6:** e00340-00315.

Nikel PI, Chavarría M, Danchin A, de Lorenzo V (2016a) From dirt to industrial applications: *Pseudomonas putida* as a Synthetic Biology *chassis* for hosting harsh biochemical reactions. *Curr Opin Chem Biol* **34:** 20-29.

Nikel PI, Pérez-Pantoja D, de Lorenzo V (2016b) Pyridine nucleotide transhydrogenases enable redox balance of *Pseudomonas putida* during biodegradation of aromatic compounds. *Environ Microbiol* **18:** 3565-3582.

Nilsson M, Chiang WC, Fazli M, Gjermansen M, Givskov M, Tolker-Nielsen T (2011) Influence of putative exopolysaccharide genes on *Pseudomonas putida* KT2440 biofilm stability. *Environ Microbiol* **13:** 1357-1369.

Nogales J, Palsson BØ, Thiele I (2008) A genome-scale metabolic reconstruction of *Pseudomonas putida* KT2440: *i*JN746 as a cell factory. *BMC Syst Biol* **2:** 79.

Novick RP, Clowes RC, Cohen SN, Curtiss R, 3rd, Datta N, Falkow S (1976) Uniform nomenclature for bacterial plasmids: a proposal. *Bacteriol Rev* **40:** 168-189.

O'Toole GA, Kolter R (1998) Flagellar and twitching motility are necessary for *Pseudomonas aeruginosa* biofilm development. *Mol Microbiol* **30:** 295-304.

Okamura-Abe Y, Abe T, Nishimura K, Kawata Y, Sato-Izawa K, Otsuka Y, Nakamura M, Kajita S, Masai E, Sonoki T, Katayama Y (2016) b-Ketoadipic acid and muconolactone production from a lignin-related aromatic compound through the protocatechuate 3,4-metabolic pathway. *J Biosci Bioeng* **121:** 652-658.

Orth JD, Thiele I, Palsson BØ (2010) What is flux balance analysis? *Nat Biotechnol* **28:** 245-248.

Páez-Espino AD, Durante-Rodríguez G, de Lorenzo V (2015) Functional coexistence of twin arsenic resistance systems in *Pseudomonas putida* KT2440. *Environ Microbiol* **17:** 229-238.

Palleroni NJ (2003) Prokaryote taxonomy of the 20th century and the impact of studies on the genus *Pseudomonas*: a personal view. *Microbiology* **149:** 1-7.

Palleroni NJ, Kunisawa R, Contopoulou R, Doudoroff M (1973) Nucleic acid homologies in the genus *Pseudomonas*. *Int J Syst Evol Microbiol* **23:** 333-339.

Papagianni M (2012) Recent advances in engineering the central carbon metabolism of industrially important bacteria. *Microb Cell Fact* **11:** 50.

Papenfort K, Sun Y, Miyakoshi M, Vanderpool CK, Vogel J (2013) Small RNA-mediated activation of sugar phosphatase mRNA regulates glucose homeostasis. *Cell* **153:** 426-437.

Park J, Gupta RS (2008) Adenosine kinase and ribokinase–the RK family of proteins. *Cell Mol Life Sci* **65:** 2875-2896.

Park JH, Lee SY (2008) Towards systems metabolic engineering of microorganisms for amino acid production. *Curr Opin Biotechnol* **19:** 454-460.

Peoples OP, Sinskey AJ (1989) Poly-β-hydroxybutyrate (PHB) biosynthesis in *Alcaligenes eutrophus* H16. Identification and characterization of the PHB polymerase gene (*phbC*). *J Biol Chem* **264:** 15298-15303.

Pflüger-Grau K, Chavarría M, de Lorenzo V (2011) The interplay of the $EIIA^{Ntr}$ component of the nitrogen-related phosphotransferase system (PTS^{Ntr}) of *Pseudomonas putida* with pyruvate dehydrogenase. *Biochim Biophys Acta* **1810:** 995-1005.

Phadnis SH, Sasakawa C, Berg DE (1986) Localization of action of the IS*50*-encoded transposase protein. *Genetics* **112:** 421-427.

Poblete-Castro I, Becker J, Dohnt K, Martins dos Santos VAP, Wittmann C (2012) Industrial biotechnology of *Pseudomonas putida* and related species. *Appl Microbiol Biotechnol* **93:** 2279-2290.

Poblete-Castro I, Borrero de Acuña JM, Nikel PI, Kohlstedt M, Wittmann C (2017) Host organism: *Pseudomonas putida*. In *Industrial Biotechnology: Microorganisms*, Wittmann C, Liao JC (eds). Weinheim, Germany: Wiley-VCH Verlag GmbH & Co. KGaA.

Ponce E, Flores N, Martínez A, Valle F, Bolívar F (1995) Cloning of the two pyruvate kinase isoenzyme structural genes from *Escherichia coli*: the relative roles of these enzymes in pyruvate biosynthesis. *J Bacteriol* **177:** 5719-5722.

Ponce E, García M, Muñoz ME (2005) Participation of the Entner-Doudoroff pathway in *Escherichia coli* strains with an inactive phosphotransferase system (PTS^{-} Glc^{+}) in gluconate and glucose batch cultures. *Can J Microbiol* **51:** 975-982.

Portais JC, Delort AM (2002) Carbohydrate cycling in micro-organisms: what can ^{13}C-NMR tell us? *FEMS Microbiol Rev* **26:** 375-402.

Portnoy VA, Bezdan D, Zengler K (2011) Adaptive laboratory evolution–Harnessing the power of biology for metabolic engineering. *Curr Opin Biotechnol* **22:** 590-594.

Postma PW, Lengeler JW, Jacobson GR (1993) Phosphoenolpyruvate:carbohydrate phosphotransferase systems of bacteria. *Microbiol Rev* **57:** 543-594.

Prieto MA, Escapa IF, Martínez V, Dinjaski N, Herencias C, de la Peña F, Tarazona N, Revelles O (2016) A holistic view of polyhydroxyalkanoate metabolism in *Pseudomonas putida*. *Environ Microbiol* **18:** 341-357.

Prithiviraj B, Bais HP, Weir T, Suresh B, Najarro EH, Dayakar BV, Schweizer HP, Vivanco JM (2005) Down regulation of virulence factors of *Pseudomonas aeruginosa* by salicylic acid attenuates its virulence on *Arabidopsis thaliana* and *Caenorhabditis elegans*. *Infect Immun* **73:** 5319-5328.

Puchałka J, Oberhardt MA, Godinho M, Bielecka A, Regenhardt D, Timmis KN, Papin JA, Martins dos Santos VAP (2008) Genome-scale reconstruction and analysis of the *Pseudomonas putida* KT2440 metabolic network facilitates applications in biotechnology. *PLoS Comput Biol* **4:** e1000210.

Raab RM, Tyo KEJ, Stephanopoulos G (2005) Metabolic engineering. *Adv Biochem Eng Biotechnol* **100:** 1-17.

Ramos C, Molina L, Mølbak L, Ramos JL, Molin S (2000) A bioluminescent derivative of *Pseudomonas putida* KT2440 for deliberate release into the environment. *FEMS Microbiol Ecol* **34:** 91-102.

Ramos JL, Sol Cuenca M, Molina-Santiago C, Segura A, Duque E, Gómez-García MR, Udaondo Z, Roca A (2015) Mechanisms of solvent resistance mediated by interplay of cellular factors in *Pseudomonas putida*. *FEMS Microbiol Rev* **39:** 555-566.

Ranade S, Zhang Y, Kaplan M, Majeed W, He Q (2015) Metabolic engineering and comparative performance studies of *Synechocystis* sp. PCC 6803 strains for effective utilization of xylose. *Front Microbiol* **6:** 1484.

Regenhardt D, Heuer H, Heim S, Fernández DU, Strömpl C, Moore ER, Timmis KN (2002) Pedigree and taxonomic credentials of *Pseudomonas putida* strain KT2440. *Environ Microbiol* **4:** 912-915.

Reznikoff WS (2008) Transposon Tn*5*. *Annu Rev Genet* **42:** 269-286.

Richardson AR, Somerville GA, Sonenshein AL (2015) Regulating the intersection of metabolism and pathogenesis in Gram-positive bacteria. *Microbiol Spectr* **3**

Romano AH, Conway T (1996) Evolution of carbohydrate metabolic pathways. *Res Microbiol* **147:** 448-455.

Rühl M, Le Coq D, Aymerich S, Sauer U (2012) ^{13}C-Flux analysis reveals NADPH-balancing transhydrogenation cycles in stationary phase of nitrogen-starving *Bacillus subtilis*. *J Biol Chem* **287:** 27959-27970.

Ruiz JA, de Almeida A, Godoy MS, Mezzina MP, Bidart GN, Méndez BS, Pettinari MJ, Nikel PI (2012) *Escherichia coli* redox mutants as microbial cell factories for the synthesis of reduced biochemicals. *Comput Struct Biotechnol J* **3:** e201210019.

Ruiz JA, Fernández RO, Nikel PI, Méndez BS, Pettinari MJ (2006) *dye* (*arc*) Mutants: insights into an unexplained phenotype and its suppression by the synthesis of poly(3-hydroxybutyrate) in *Escherichia coli* recombinants. *FEMS Microbiol Lett* **258:** 55-60.

Sadykov MR, Olson ME, Halouska S, Zhu Y, Fey PD, Powers R, Somerville GA (2008) Tricarboxylic acid cycle-dependent regulation of *Staphylococcus epidermidis* polysaccharide intercellular adhesin synthesis. *J Bacteriol* **190:** 7621-7632.

Sanfélix-Haywood N, Coll-Marqués JM, Yebra MJ (2011) Role of α-phosphoglucomutase and phosphoglucose isomerase activities at the branching point between sugar catabolism and anabolism in *Lactobacillus casei*. *J Appl Microbiol* **111:** 433-442.

Sauer U (2006) Metabolic networks in motion: ^{13}C-based flux analysis. *Mol Syst Biol* **2:** 62.

Schellenberger J, Que R, Fleming RM, Thiele I, Orth JD, Feist AM, Zielinski DC, Bordbar A, Lewis NE, Rahmanian S, Kang J, Hyduke DR, Palsson BØ (2011) Quantitative prediction of cellular metabolism with constraint-based models: the COBRA Toolbox v2.0. *Nat Protoc* **6:** 1290-1307.

Schneider E (2001) ABC transporters catalyzing carbohydrate uptake. *Res Microbiol* **152:** 303-310.

Schoberth SM, de Graaf AA (1993) Use of *in vivo* ^{13}C nuclear magnetic resonance spectroscopy to follow sugar uptake in *Zymomonas mobilis*. *Anal Biochem* **210:** 123-128.

Schuster KC (2000) Monitoring the physiological status in bioprocesses on the cellular level. *Adv Biochem Eng Biotechnol* **66:** 185-208.

Schuster S, Fell DA, Dandekar T (2000) A general definition of metabolic pathways useful for systematic organization and analysis of complex metabolic networks. *Nat Biotechnol* **18:** 326-332.

Seta FD, Boschi-Muller S, Vignais ML, Branlant G (1997) Characterization of *Escherichia coli* strains with *gapA* and *gapB* genes deleted. *J Bacteriol* **179:** 5218-5221.

Sham LT, Butler EK, Lebar MD, Kahne D, Bernhardt TG, Ruiz N (2014) Bacterial cell wall. MurJ is the flippase of lipid-linked precursors for peptidoglycan biogenesis. *Science* **345:** 220-222.

Sharma PK, Fu J, Spicer V, Krokhin OV, Cicek N, Sparling R, Levin DB (2016) Global changes in the proteome of *Cupriavidus necator* H16 during poly-(3-hydroxybutyrate) synthesis from various biodiesel by-product substrates. *AMB Express* **6:** 36.

Shen T, Rui B, Zhou H, Zhang X, Yi Y, Wen H, Zheng H, Wu J, Shi Y (2013) Metabolic flux ratio analysis and multi-objective optimization revealed a globally conserved and coordinated metabolic response of *E. coli* to paraquat-induced oxidative stress. *Mol BioSyst* **9:** 121-132.

Shi H, Nikawa J, Shimizu K (1999) Effect of modifying metabolic network on poly-3-hydroxybutyrate biosynthesis in recombinant *Escherichia coli*. *J Biosci Bioeng* **87:** 666-677.

Siedler S, Bringer S, Blank LM, Bott M (2012) Engineering yield and rate of reductive biotransformation in *Escherichia coli* by partial cyclization of the pentose phosphate pathway and PTS-independent glucose transport. *Appl Microbiol Biotechnol* **93:** 1459-1467.

Silva-Rocha R, Martínez-García E, Calles B, Chavarría M, Arce-Rodríguez A, de las Heras A, Páez-Espino AD, Durante-Rodríguez G, Kim J, Nikel PI, Platero R, de Lorenzo V (2013) The *Standard European Vector Architecture* (SEVA): a coherent platform for the analysis and deployment of complex prokaryotic phenotypes. *Nucleic Acids Res* **41:** D666-D675.

Singh R, Mailloux RJ, Puiseux-Dao S, Appanna VD (2007) Oxidative stress evokes a metabolic adaptation that favors increased NADPH synthesis and decreased NADH production in *Pseudomonas fluorescens*. *J Bacteriol* **189:** 6665-6675.

Sohn SB, Kim TY, Park JM, Lee SY (2010) *In silico* genome-scale metabolic analysis of *Pseudomonas putida* KT2440 for polyhydroxyalkanoate synthesis, degradation of aromatics and anaerobic survival. *Biotechnol J* **5:** 739-750.

Soma Y, Tsuruno K, Wada M, Yokota A, Hanai T (2014) Metabolic flux redirection from a central metabolic pathway toward a synthetic pathway using a metabolic toggle switch. *Metab Eng* **23:** 175-184.

Spaans SK, Weusthuis RA, van der Oost J, Kengen SW (2015) NADPH-generating systems in bacteria and archaea. *Front Microbiol* **6:** 742.

Stafford DE, Stephanopoulos G (2001) Metabolic engineering as an integrating platform for strain development. *Curr Opin Microbiol* **4:** 336-340.

Stanier RY, Palleroni NJ, Doudoroff M (1966) The aerobic pseudomonads: a taxonomic study. *J Gen Microbiol* **43:** 159-271.

Stephanopoulos G (2012) Synthetic biology and metabolic engineering. *ACS Synth Biol* **1:** 514-525.

Stettner AI, Segrè D (2013) The cost of efficiency in energy metabolism. *Proc Natl Acad Sci U S A* **110:** 9629-9630.

Stover CK, Pham XQ, Erwin AL, Mizoguchi SD, Warrener P, Hickey MJ, Brinkman FSL, Hufnagle WO, Kowalik DJ, Lagrou M, Garber RL, Goltry L, Tolentino E, Westbrock-Wadman S, Yuan Y, Brody LL, Coulter SN, Folger KR, Kas A, Larbig K, Lim R, Smith K, Spencer D, Wong GKS, Wu Z, Paulsen IT, Reizer J, Saier MH, Hancock REW, Lory S, Olson MV (2000) Complete genome sequence of *Pseudomonas aeruginosa* PAO1, an opportunistic pathogen. *Nature* **406:** 959-964.

Sudarsan S, Dethlefsen S, Blank LM, Siemann-Herzberg M, Schmid A (2014) The functional structure of central carbon metabolism in *Pseudomonas putida* KT2440. *Appl Environ Microbiol* **80:** 5292-5303.

Suriyamongkol P, Weselake R, Narine S, Moloney M, Shah S (2007) Biotechnological approaches for the production of polyhydroxyalkanoates in microorganisms and plants–A review. *Biotechnol Adv* **25:** 148-175.

Tang J, Zhu X, Lu J, Liu P, Xu H, Tan Z, Zhang X (2013) Recruiting alternative glucose utilization pathways for improving succinate production. *Appl Microbiol Biotechnol* **97:** 2513-2520.

Tang YJ, Martin HG, Deutschbauer A, Feng X, Huang R, Llora X, Arkin A, Keasling JD (2009) Invariability of central metabolic flux distribution in *Shewanella oneidensis* MR-1 under environmental or genetic perturbations. *Biotechnol Prog* **25:** 1254-1259.

Temme K, Zhao D, Voigt CA (2012) Refactoring the nitrogen fixation gene cluster from *Klebsiella oxytoca*. *Proc Natl Acad Sci USA* **109:** 7085-7090.

Temple L, Cuskey SM, Perkins RE, Bass RC, Morales NM, Christie GE, Olsen RH, Phibbs PV (1990) Analysis of cloned structural and regulatory genes for carbohydrate utilization in *Pseudomonas aeruginosa* PAO. *J Bacteriol* **172:** 6396-6402.

Tepper N, Shlomi T (2010) Predicting metabolic engineering knockout strategies for chemical production: accounting for competing pathways. *Bioinformatics* **26:** 536-543.

Thomson J, Gerstenberger PD, Goldberg DE, Gociar E, Orozco de Silva A, Fraenkel DG (1979) ColE1 hybrid plasmids for *Escherichia coli* genes of glycolysis and the hexose monophosphate shunt. *J Bacteriol* **137:** 502-506.

Timmis KN (2002) *Pseudomonas putida*: a cosmopolitan opportunist *par excellence*. *Environ Microbiol* **4:** 779-781.

Toya Y, Ishii N, Nakahigashi K, Hirasawa T, Soga T, Tomita M, Shimizu K (2010) ^{13}C-metabolic flux analysis for batch culture of *Escherichia coli* and its Pyk and Pgi gene knockout mutants based on mass isotopomer distribution of intracellular metabolites. *Biotechnol Prog* **26:** 975-992.

Tyo KE, Ajikumar PK, Stephanopoulos G (2009) Stabilized gene duplication enables long-term selection-free heterologous pathway expression. *Nat Biotechnol* **27:** 760-765.

Udaondo Z, Molina L, Segura A, Duque E, Ramos JL (2016) Analysis of the core genome and pangenome of *Pseudomonas putida*. *Environ Microbiol* **18:** 3268-3283.

Usui Y, Hirasawa T, Furusawa C, Shirai T, Yamamoto N, Mori H, Shimizu H (2012) Investigating the effects of perturbations to *pgi* and *eno* gene expression on central carbon metabolism in *Escherichia coli* using ^{13}C metabolic flux analysis. *Microb Cell Fact* **11:** 87.

Vallenet D, Calteau A, Cruveiller S, Gachet M, Lajus A, Josso A, Mercier J, Renaux A, Rollin J, Rouy Z, Roche D, Scarpelli C, Médigue C (2017) MicroScope in 2017: an expanding and evolving integrated resource for community expertise of microbial genomes. *Nucleic Acids Res* **45:** D517-D528.

van der Werf MJ, Overkamp KM, Muilwijk B, Koek MM, van der Werff-van der Vat BJ, Jellema RH, Coulier L, Hankemeier T (2008) Comprehensive analysis of the metabolome of *Pseudomonas putida* S12 grown on different carbon sources. *Mol BioSyst* **4:** 315-327.

Vardon DR, Franden MA, Johnson CW, Karp EM, Guarnieri MT, Linger JG, Salm MJ, Strathmann TJ, Beckham GT (2015) Adipic acid production from lignin. *Energy Environ Sci* **8:** 617-628.

Velur Selvamani RS, Telaar M, Friehs K, Flaschel E (2014) Antibiotic-free segregational plasmid stabilization in *Escherichia coli* owing to the knockout of triosephosphate isomerase (*tpiA*). *Microb Cell Fact* **13:** 58.

Vicente M, Cánovas JL (1973a) Glucolysis in *Pseudomonas putida*: physiological role of alternative routes from the analysis of defective mutants. *J Bacteriol* **116:** 908-914.

Vicente M, Cánovas JL (1973b) Regulation of the glucolytic enzymes in *Pseudomonas putida*. *Arch Microbiol* **93:** 53-64.

Wang CH, Stern IJ, Gilmour CM (1959) The catabolism of glucose and gluconate in *Pseudomonas* species. *Arch Biochem Biophys* **81:** 489-492.

Weisser P, Kramer R, Sahm H, Sprenger GA (1995) Functional expression of the glucose transporter of *Zymomonas mobilis* leads to restoration of glucose and fructose uptake in *Escherichia coli* mutants and provides evidence for its facilitator action. *J Bacteriol* **177:** 3351-3354.

Wendisch VF, Brito LF, Gil Lopez M, Hennig G, Pfeifenschneider J, Sgobba E, Veldmann KH (2016) The flexible feedstock concept in Industrial Biotechnology: Metabolic engineering of *Escherichia coli*, *Corynebacterium glutamicum*, *Pseudomonas*, *Bacillus* and yeast strains for access to alternative carbon sources. *J Biotechnol* **234:** 139-157.

Williams PA, Murray K (1974) Metabolism of benzoate and the methylbenzoates by *Pseudomonas putida* (*arvilla*) mt-2: evidence for the existence of a TOL plasmid. *J Bacteriol* **120:** 416-423.

Winsor GL, Griffiths EJ, Lo R, Dhillon BK, Shay JA, Brinkman FS (2016) Enhanced annotations and features for comparing thousands of *Pseudomonas* genomes in the *Pseudomonas* Genome Database. *Nucleic Acids Res* **44:** D646-D653.

Wirth R, Friesenegger A, Fiedler S (1989) Transformation of various species of Gram-negative bacteria belonging to 11 different genera by electroporation. *Mol Gen Genet* **216:** 175-177.

Wong SM, Mekalanos JJ (2000) Genetic footprinting with *mariner*-based transposition in *Pseudomonas aeruginosa*. *Proc Natl Acad Sci USA* **97:** 10191-10196.

Worsey MJ, Williams PA (1975) Metabolism of toluene and xylenes by *Pseudomonas putida* (*arvilla*) mt-2: evidence for a new function of the TOL plasmid. *J Bacteriol* **124:** 7-13.

Wu G, Yan Q, Jones JA, Tang YJ, Fong SS, Koffas MAG (2016) Metabolic burden: cornerstones in synthetic biology and metabolic engineering applications. *Trends Biotechnol* **34:** 652-664.

Wylie JL, Worobec EA (1995) The OprB porin plays a central role in carbohydrate uptake in *Pseudomonas aeruginosa*. *J Bacteriol* **177:** 3021-3026.

Xavier KB, Martins LO, Peist R, Kossmann M, Boos W, Santos H (1996) High-affinity maltose/trehalose transport system in the hyperthermophilic archaeon *Thermococcus litoralis*. *J Bacteriol* **178:** 4773-4777.

Yadav VG, De Mey M, Lim CG, Ajikumar PK, Stephanopoulos G (2012) The future of metabolic engineering and synthetic biology: towards a systematic practice. *Metab Eng* **14:** 233-241.

Yadav VG, Stephanopoulos G (2010) Reevaluating synthesis by biology. *Curr Opin Microbiol* **13:** 371-376.

Yang Y, Zhao G, Man TK, Winkler ME (1998) Involvement of the *gapA*- and *epd* (*gapB*)-encoded dehydrogenases in pyridoxal 5'-phosphate coenzyme biosynthesis in *Escherichia coli* K-12. *J Bacteriol* **180:** 4294-4299.

Yuan Y, Sachdeva M, Leeds JA, Meredith TC (2012) Fatty acid biosynthesis in *Pseudomonas aeruginosa* is initiated by the FabY class of β-ketoacyl acyl carrier protein synthases. *J Bacteriol* **194:** 5171-5184.

Zamboni N, Fischer E, Sauer U (2005) FiatFlux–A software for metabolic flux analysis from ^{13}C-glucose experiments. *BMC Bioinformatics* **6:** 209.

Zhao C, Lin Z, Dong H, Zhang Y, Li Y (2017) Reexamination of the physiological role of PykA in *Escherichia coli* revealed that it negatively regulates the intracellular ATP levels under anaerobic conditions. *Appl Environ Microbiol*

Zhao Y, Wang CS, Li FF, Liu ZN, Zhao GR (2016) Targeted optimization of central carbon metabolism for engineering succinate production in *Escherichia coli*. *BMC Biotechnol* **16:** 52.

VIII. ANNEXES

ANNEXES

Annex 1. Phenotypic MicroArray™ complete report (*P. putida* KT2440 *vs. P. putida* KT2440 Δ*pgi-1* Δ*pgi-2*)

Plate Panel	Well(s)	Respiration ratio	Chemical	Category
Phenotypes Gained				
PM07	F06	58	Trp-Ala	N-Source, peptide
PM08	E01	50	Thr-Phe	N-Source, peptide
PM04A	C02	72	Phospho-Glycolic acid	P-Source, organic
PM13B	H12	61	Tylosin	protein synthesis, 50S ribosomal subunit, macrolide
Phenotypes Lost				
PM20B	C06,C07	-105	Atropine	acetylcholine receptor, antagonist
PM20B	B02,B03,B04	-247	Orphenadrine	anti-cholinergic
PM20B	F09,F10,F11	-224	Pridinol	anti-cholinergic
PM20B	B07,B08	-135	D,L-Propanolol	beta-adrenergic blocker
PM17A	B01,B02,B03	-191	Salicylate, sodium	biofilm inhibitor, anti-capsule agent, chelator, prostaglandin syntetase inhibitor, mar inducer
PM20B	G09,G10	-190	8-Hydroxyquinoline	chelator, lipophilic
PM17A	E05,E06,E07	-310	Compound 48/80	cyclic AMP phosphodiesterase inhibitor
PM17A	H06,H07	-93	Caffeine	cyclic AMP phosphodiesterase inhibitor
PM15B	D03,D04	-114	Phleomycin	DNA damage, oxidation
PM20B	F02,F03	-118	4-Hydroxycoumarin	DNA intercalator
PM20B	D01,D02	-105	Proflavine	DNA intercalator, inhibits RNA synthesis
PM18C	B06,B07	-126	Pipemidic Acid	DNA topoisomerase
PM20B	D07,D08	-122	Ciprofloxacin	DNA topoisomerase
PM11C	B11,B12	-116	Lomefloxacin	DNA topoisomerase
PM11C	E12	-74	Nalidixic acid	DNA topoisomerase
PM17A	A01,A02	-148	D-Serine	inhibits 3PGA dehydrogenase (L-serine and pantothenate synthesis)
PM13B	A07,A08	-113	Dequalinium chloride	ion channel inhibitor, K+
PM17A	C01	-76	4-Aminopyridine	ion channel inhibitor, K+
PM18C	G01,G02,G03,G04	-302	Triclosan	lipid synthesis, fatty acid inhibitor
PM20B	E06,E07	-216	Dodine (*n*-Dodecylguanidine)	membrane permeability, guanidine, fungicide

PM15B	A07	-88	Guanidine hydrochloride	membrane, chaotropic agent
PM11C	C05,C06,C07	-279	Colistin	membrane, cyclic peptide
PM19	H09,H10	-125	Polymyxin B	membrane, cyclic peptide
PM17A	E01,E02	-116	Niaproof	membrane, detergent, anionic
PM18C	C01,C02,C03	-266	Poly-L-lysine	membrane, detergent, cationic
PM19	B03,B04	-189	Methyltrioctylammonium chloride	membrane, detergent, cationic
PM12B	H09	-71	Dodecyltrimethyl ammonium bromide	membrane, detergent, cationic
PM15B	D06,D07	-204	Domiphen bromide	membrane, detergent, cationic, fungicide
PM19	G01	-63	Lauryl sulfobetaine (*N*-Dodecyl-*N*,*N*-dimethyl-3-ammonio-1-propanesulfonate)	membrane, detergent, zwitterionic
PM20B	E09,E10,E11,E12	-216	Hexachlorophene	membrane, electron transport
PM16A	C05	-99	Protamine sulfate	membrane, nonspecific binding
PM20B	C01,C02,C03	-226	Thioridazine	membrane, phenothiazine, efflux pump inhibitor, anti-psychotic
PM17A	D11,D12	-203	Chlorpromazine	membrane, phenothiazine, efflux pump inhibitor, anti-psychotic
PM13B	G11,G12	-176	Trifluoperazine	membrane, phenothiazine, efflux pump inhibitor, anti-psychotic
PM20B	A01,A02,A03,A04	-338	Amitriptyline	membrane, transport
PM20B	H03,H04	-101	Patulin	microtubulin polymerization inhibitor, antifungal
PM03B	F11	-63	Uridine	N-Source, other
PM07	B11	-98	Met-Gly	N-Source, peptide
PM06	F03	-94	Gly-Tyr	N-Source, peptide
PM06	C11	-77	Asp-Leu	N-Source, peptide
PM06	E12	-52	Gly-Ser	N-Source, peptide
PM18C	F06,F07,F08	-198	Tinidazole	nitro compound, oxidizing agent, DNA damage
PM20B	C11,C12	-137	Ornidazole	nitro compound, oxidizing agent, DNA damage
PM18C	B09,B10,B11,B12	-205	Azathioprine	nucleic acid analog, purine
PM18C	H01,H02,H03,H04	-392	5-Fluoro-5'-deoxyuridine	nucleic acid analog, pyrimidine, DNA synthesis
PM18C	B01,B02,B03,B04	-248	Trifluorothymidine	nucleic acid analog, pyrimidine, DNA synthesis
PM09	D01	-86	3% Potassium chloride	osmotic sensitivity, KCl
PM09	D02	-75	4% Potassium chloride	osmotic sensitivity, KCl
PM09	A04	-66	4% NaCl	osmotic sensitivity, NaCl
PM09	E04	-62	4% Sodium formate	osmotic sensitivity, sodium formate
PM09	F03	-82	3% Sodium lactate	osmotic sensitivity, sodium lactate

PM09	F04	-82	4% Sodium lactate	osmotic sensitivity, sodium lactate
PM10	F05	-102	pH 9.5 + L-Threonine	pH, deaminase
PM10	F02	-93	pH 9.5 + L-Phenylalanine	pH, deaminase
PM10	E11	-65	pH 9.5 + L-Leucine	pH, deaminase
PM10	G01	-65	pH 9.5 + Anthranilic acid	pH, deaminase
PM10	D08	-131	pH 4.5 + 5-Hydroxy-L-Lysine	pH, decarboxylase
PM10	C04	-115	pH 4.5 + L-Serine	pH, decarboxylase
PM10	D04	-115	pH 4.5 + α-Amino-*N*-Butyric acid	pH, decarboxylase
PM10	C03	-106	pH 4.5 + L-Proline	pH, decarboxylase
PM10	C08	-106	pH 4.5 + L-Valine	pH, decarboxylase
PM10	C05	-101	pH 4.5 + L-Threonine	pH, decarboxylase
PM10	D07	-99	pH 4.5 + D-Lysine	pH, decarboxylase
PM10	C02	-98	pH 4.5 + L-Phenylalanine	pH, decarboxylase
PM10	D06	-92	pH 4.5 + L-Cysteic acid	pH, decarboxylase
PM10	C07	-89	pH 4.5 + L-Citrulline	pH, decarboxylase
PM10	B07	-88	pH 4.5 + L-Glutamine	pH, decarboxylase
PM10	C11	-88	pH 4.5 + L-Homoarginine	pH, decarboxylase
PM10	B04	-87	pH 4.5 + L-Asparagine	pH, decarboxylase
PM10	C01	-81	pH 4.5 + L-Methionine	pH, decarboxylase
PM10	C10	-81	pH 4.5 + L-Ornithine	pH, decarboxylase
PM10	B09	-76	pH 4.5 + L-Histidine	pH, decarboxylase
PM10	B12	-69	pH 4.5 + L-Lysine	pH, decarboxylase
PM10	D10	-66	pH 4.5 + D,L-Diamino-α,ε-pimelic acid	pH, decarboxylase
PM10	D11	-66	pH 4.5 + Trimethylamine-N-Oxide	pH, decarboxylase
PM10	D12	-66	pH 4.5 + Urea	pH, decarboxylase
PM10	B02	-62	pH 4.5 + L-Alanine	pH, decarboxylase
PM10	B01	-95	pH 4.5	pH, decarboxylase control
PM10	A03	-96	pH 4.5	pH, growth at 4.5
PM10	A04	-81	pH 5	pH, growth at 5
PM14	H07,H08	-195	Promethazine	phenothiazine, anti-cholinergic, anti-psychotic, sedative
PM19	D09,D10,D11,D12	-209	Phenyl-methylsulfonyl-fluoride (PMSF)	protease inhibitor, serine
PM19	G05,G06,G07,G08	-276	Dihydrostreptomycin	protein synthesis, 30S ribosomal subunit, aminoglycoside
PM13B	E07,E08	-166	Geneticin disulfate (G418)	protein synthesis, 30S ribosomal subunit, aminoglycoside

PM11C	F10,F11	-163	Neomycin	protein synthesis, 30S ribosomal subunit, aminoglycoside
PM12B	D02,D03	-151	Sisomicin	protein synthesis, 30S ribosomal subunit, aminoglycoside
PM12B	F01,F02	-136	Tobramycin	protein synthesis, 30S ribosomal subunit, aminoglycoside
PM11C	G07,G08	-111	Gentamicin	protein synthesis, 30S ribosomal subunit, aminoglycoside
PM12B	G01	-77	Spectinomycin	protein synthesis, 30S ribosomal subunit, aminoglycoside
PM11C	H05	-70	Kanamycin	protein synthesis, 30S ribosomal subunit, aminoglycoside
PM20B	A08	-66	Apramycin	protein synthesis, 30S ribosomal subunit, aminoglycoside
PM16A	E01	-63	Streptomycin	protein synthesis, 30S ribosomal subunit, aminoglycoside
PM12B	A05,A06,A08	-230	Tetracycline	protein synthesis, 30S ribosomal subunit, tetracycline
PM12B	H01	-74	Spiramycin	protein synthesis, 50S ribosomal subunit, macrolide
PM19	H05,H06	-97	α-Monothioglycerol	reducing agent, thiol, adenosyl methionine antagonist
PM19	E01,E02,E03,E04	-188	FCCP	respiration, ionophore, H^+
PM19	F09,F10,F11	-186	Sodium caprylate	respiration, ionophore, H^+
PM19	A05,A06,A07	-169	Gallic acid	respiration, ionophore, H^+
PM20B	G06,G07	-157	3,5-Dinitrobenzoic acid	respiration, ionophore, H^+
PM19	C11,C12	-103	*trans*-Cinnamic acid	respiration, ionophore, H^+
PM13B	E11,E12	-148	Ruthenium red	respiration, mitochondrial Ca^{2+} porter
PM17A	D01,D02	-150	Oxycarboxin	respiratory enzymes, carboxamide, fungicide
PM18C	G05,G06,G07	-285	3,5- Diamino-1,2,4-triazole (Guanazole)	ribonucleotide DP reductase inhibitor
PM15B	H05	-71	Hydroxyurea	ribonucleotide DP reductase inhibitor, antifolate (inhibits thymine and methionine synthesis)
PM18C	D01,D02,D03,D04	-253	Sodium Arsenite	toxic anion
PM16A	F01	-111	Potassium tellurite	toxic anion
PM11C	G09,G10	-109	Potassium tellurite	toxic anion
PM18C	E09,E10,E11	-204	Antimony (III) chloride	toxic cation
PM16A	G02,G03,G04	-177	Chromium (III) chloride	toxic cation
PM14	D01,D02	-117	Cadmium chloride	toxic cation
PM13B	F09	-108	Thallium (I) acetate	toxic cation
PM13B	F03,F04	-99	Cesium chloride	toxic cation
PM12B	C09	-100	D,L-Serine hydroxamate	tRNA synthetase
PM13B	F07,F08	-121	Glycine HCl	wall
PM13B	D01,D02,D03,D04	-251	Cefuroxime	wall, cephalosporin
PM17A	G11,G12	-116	Cefoperazone	wall, cephalosporin

PM15B	A11,A12	-106	Cefmetazole	wall, cephalosporin
PM11C	H01	-73	Cephalothin	wall, cephalosporin
PM12B	A01,A02,A03	-280	Penicillin G	wall, lactam
PM19	F01,F02,F03	-214	Phenethicilllin	wall, lactam
PM12B	B02,B03,B04	-171	Oxacillin	wall, lactam
PM12B	A09,A10	-108	Carbenicillin	wall, lactam

Annex 2. Permission/License

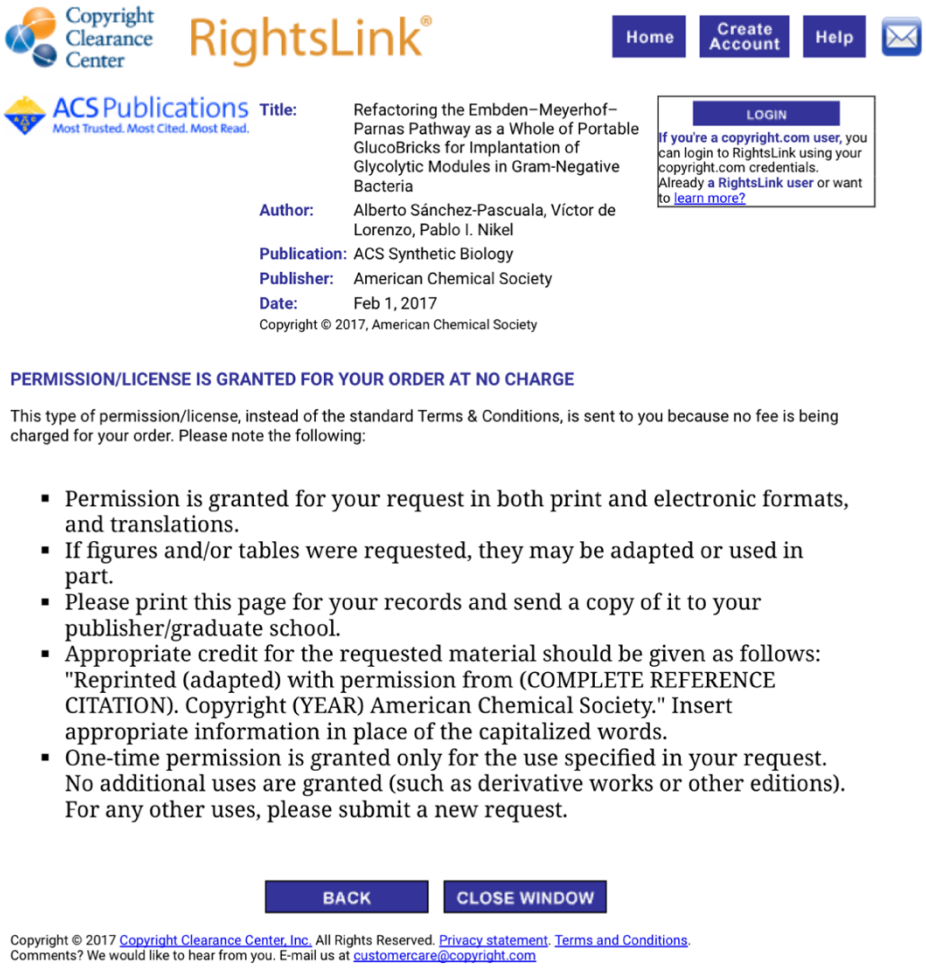

Copyright Clearance Center RightsLink®

Home | Create Account | Help

ACS Publications
Most Trusted. Most Cited. Most Read.

Title: Refactoring the Embden–Meyerhof–Parnas Pathway as a Whole of Portable GlucoBricks for Implantation of Glycolytic Modules in Gram-Negative Bacteria

Author: Alberto Sánchez-Pascuala, Víctor de Lorenzo, Pablo I. Nikel

Publication: ACS Synthetic Biology

Publisher: American Chemical Society

Date: Feb 1, 2017

Copyright © 2017, American Chemical Society

LOGIN

If you're a copyright.com user, you can login to RightsLink using your copyright.com credentials. Already a RightsLink user or want to learn more?

PERMISSION/LICENSE IS GRANTED FOR YOUR ORDER AT NO CHARGE

This type of permission/license, instead of the standard Terms & Conditions, is sent to you because no fee is being charged for your order. Please note the following:

- Permission is granted for your request in both print and electronic formats, and translations.
- If figures and/or tables were requested, they may be adapted or used in part.
- Please print this page for your records and send a copy of it to your publisher/graduate school.
- Appropriate credit for the requested material should be given as follows: "Reprinted (adapted) with permission from (COMPLETE REFERENCE CITATION). Copyright (YEAR) American Chemical Society." Insert appropriate information in place of the capitalized words.
- One-time permission is granted only for the use specified in your request. No additional uses are granted (such as derivative works or other editions). For any other uses, please submit a new request.

BACK | CLOSE WINDOW

Copyright © 2017 Copyright Clearance Center, Inc. All Rights Reserved. Privacy statement. Terms and Conditions.
Comments? We would like to hear from you. E-mail us at customercare@copyright.com